FACULTY OF SCIENCES

Unraveling the role of oceanographic forcing on a small-scale contourite drift

Onset, evolution and present-day sedimentary processes of the Belgica Mound Drift

Alice Ofélia Matossian

Supervisor: prof. dr. David Van Rooij

Academic year 2025 - 2026

A dissertation submitted to the Faculty of Sciences of Ghent University in fulfilment of the requirements for the degree of Doctor of Science in Geology

GHENT UNIVERSITY

Members of the examination committee:

prof. dr. Stephen Louwye (chair, Ghent University, Belgium)

prof. dr. Marc De Batist (Ghent University, Belgium)

prof. dr. Vera Van Lancker (RBINS & Ghent University, Belgium)

prof. dr. Martin White (University of Galway, Ireland)

prof. dr. Elda Miramontes García (University of Bremen, Germany)

This research was carried out by Alice Ofélia Matossian with the financial support of the Research Foundation – Flanders (FWO grant 3G021719) and the Ghent University Special Research Fund (BOF grant BOF23/CDV/126).

Please refer to this dissertation as: *Matossian, A.O., 2025. Unraveling the role of oceanographic forcing on a small-scale contourite drift. Onset, evolution and present-day sedimentary processes of the Belgica Mound Drift. PhD thesis, Ghent University, Ghent, Belgium.*

Table of Contents

List of Figures

List of Tables

List of abbreviations

In alphabetical order:

ADCP	Acoustic Doppler Current Profiler
AI	Asymmetry Index
AMOC	Atlantic meridional overturning circulation
AUV	Autonomous Underwater Vehicle
BMP	Belgica Mound Province
CDS	Contourite Depositional System
CTD	Conductivity, Temperature and Depth
CWC	Cold-water coral
ENAW	Eastern North Atlantic Water
ESC	European Slope Current
GEBC	Glacial Eastern Boundary Current
HF	High frequency
ID1	Internal discontinuity 1
IRD	Ice-rafted debris
LF	Low frequency
MOW	Mediterranean Outflow Water
MPT	Middle Pleistocene Transition
nm	Nautical miles
RCM7	Recording current meter 7
RCM9	Recording current meter 9
RD1	Regional discontinuity 1
RD2	Regional discontinuity 2
ROV	Remotely Operated underwater Vehicle
SBP	Sub-bottom profiler
SSS	Side-scan sonar
T-S	Temperature - Salinity
TWT	Two-way travel time
USBL	Ultra-Short Baseline
UTC	Coordinated Universal Time
VLIZ	Flanders Marine Institute

Acknowledgements

David, a huge thank you for the great opportunity you gave me in 2019 by offering me this PhD position. Thanks to you, I had the chance to continue growing in a different and enriching environment and to gain many new experiences. You always have been there for me, available when I needed it, always understanding. Without you as my supervisor, I don't think I would have managed to achieve this huge step in my life. I will always keep the image of you as the ever-optimistic Yoda and me the ever-doubtful Padawan. Bedankt!

I would like to extend my appreciation to the University of Ghent, as well as to the FWO and BOF that funded the DynaMOD project and my PhD.

I would like to acknowledge Martin White and his team, Eoghan Daly and Sheena Fennell, for providing the moorings as well as their support with the oceanographic data. Martin, you are one of the kindest people I have ever met, and I am thankful for your kind words. You gave me the motivation I truly needed during the last months of my PhD.

I would also like to thank all the jury members: Vera Van Lancker for helping with the bedform interpretation, Elda Miramontes García, Marc De Batist, and Stephen Louwye.

I am grateful to VLIZ for providing the resources necessary for this study. Thomas Vandorpe, Wieter Boone, Kobus Langedock, Fred Fourie, Leandro Ponsoni and Christophe Maier, an enormous thank you for providing the ROV *Zonnebloem*, AUV *Barabas* and glider *YOKO* datasets. I realise how fortunate I was to work with such a diverse range of high-resolution data. It is not common to have the opportunity to work with so many robots, and for an oceanographer, this has truly been a dream come true! I also greatly appreciated the humour of the famous duo Kobus and Fred, the "mother and father" of the AUV. Thank you also for providing beautiful pictures of the Belgica (see cover).

I extend my thanks to all participants who gave their time and insights to this research, among them Wenyan Zhang and Lucas Porz.

Special thanks to the Department of Geology and the fellow RCMG members, including Thomas Mestdagh, Shan, Piet, Lotte and Koen for their collaboration, discussions, moral support, and reloads of chokotoff.

Merci à mes parents de m'avoir donné la chance de pouvoir faire de longues études. Ça n'aura pas été simple, mais si j'y suis arrivée, c'est grâce à vous. Cedric, Bruna, Cat, Sarah, Seda, merci pour votre indéfectible soutient! Շնորհակալություն!

This would not have been possible without the RV Belgica (old and new one!) and its crew. Ce que le Belgica m'a apporté est inestimable, tant par l'expérience, les rencontres et bien plus encore... J'ai passé mon premier détroit avec lui et un des plus beaux et derniers moments partagés avec mon père a été grâce à lui. Mille mercis à ceux qui ont contribué à sa naissance et qui m'ont permis de voyager à son bord. Cet incroyable navire, qui a aidé et qui aidera nombre de scientifiques belges et internationaux à développer leurs recherches, mérite amplement de voguer vers de nouvelles aventures pour de nombreuses années. Je lui souhaite tout le meilleur et j'espère de tout cœur pouvoir remonter à son bord! Bon vent!

Summary

Unlike large-scale drifts that tend to reflect regional oceanographic processes, small-scale contourite drifts (≤ 100 km²) are key sedimentary features that reflect local processes and water mass interactions. These systems offer valuable high-resolution archives of both past and present bottom-current dynamics. However, accurately reconstructing past processes from the drift morphology requires a detailed understanding of the present-day sediment dynamic and oceanographic processes shaping the morphology of small-scale contourite drifts.

The Belgica Mound Drift, located in the Porcupine Seabight (NE Atlantic, offshore Ireland), is an example of small-scale contourite drifts that allows to explore the morphological evolution, hydrodynamic variability, and sediment dynamics associated with such drifts. It is a small (~36 km²), deep-water drift developed between 500 and 800 m water depth and enclosed by cold-water coral (CWC) mounds. This drift is at the same water depth as the Eastern North Atlantic Water (ENAW) and the Mediterranean Outflow Water (MOW) interface. This makes the Belgica Mound Drift one of the most distal contouritic expressions influenced by the MOW in the NE Atlantic Ocean.

High-resolution pseudo-3D seismic reflection data reveal that the Belgica Mound Drift underwent three distinct evolutionary stages, each corresponding to major shifts in paleoceanography, affecting both the bottom-current dynamic and sediment input. There was at first the pre-drift stage (Pliocene–Early Pleistocene), characterised by the RD1 regional erosive event attributed to the renewed influence of the MOW in the Porcupine Seabight. This phase created a distinct paleotopography that subsequently governed ensuing sedimentary and hydrodynamic processes. This was followed by the inception stage (Early–Middle Pleistocene), corresponding to the drift onset. It initiated in two separate centres of growth, strongly guided by local topographic obstacles, particularly the CWC mounds and RD1 paleosurface. These obstacles influenced sediment accumulation and the bottom-current strength and direction during the formation of the drift. Finally, the aggradational stage (Middle Pleistocene–Present), marked by more continuous and aggradational mounded stratification in the architecture of the drift, indicates a relatively stable and less energetic depositional environment. This stage is related to the Middle Pleistocene Transition, during which bottom currents weakened and sediment input decreased. The evolving moat morphology suggests an overall weakening of the strength of the bottom currents throughout the drift development.

To evaluate the modern hydrodynamic regime influencing the Belgica Mound Drift, a high-resolution oceanographic dataset was acquired through the deployment of moorings equipped with current meters, an AUV (*Barabas*, VLIZ; visual imagery and side-scan sonar), an ROV (*Zonnebloem*, VLIZ; visual imagery) and a glider (*YOKO*, VLIZ) equipped with CTD and ADCP sensors. These tools provided a comprehensive dataset on the present-day spatial and temporal variability of bottom currents over the drift and its moats, as well as the internal water mass structure.

The most important hydrodynamic process observed in all CTD profiles is a trapped baroclinic motion. This motion is characterised by a dominant diurnal K_1 tidal constituent. The strong bottom currents (up to 50 cm/s) extending up to 100 m above the seafloor highlight the enhancement of this motion due to its interaction with the local steep topography and the

presence of the water mass stratification related to the permanent thermocline, which coincides with the ENAW-MOW interface. The bottom Ekman transport, which weakens and deflects the bottom currents close to the seafloor (up to 20 m), was identified for the first time in this setting via glider-based ADCP data. Through the glider-mounted ADCP data, both processes can now be quantified. The glider deployment, in particular, proved effective in capturing dynamic vertical and horizontal variations, identifying the ENAW–MOW interface at depths corresponding to the drift body.

As direct measurements of bottom currents can be limited, for example from moorings, the study of deep-water bedforms, through ROV and AUV imagery, can offer fresh perspectives on spatial variability of local hydrodynamic processes. Closer to the seafloor, the analysis of sediment waves and their superimposed bedforms, including sinuous, linguoid, and washed-out ripples, revealed further insights into the spatial variability in bottom currents and how they can shape the present-day morphology of the drift. Two sediment wave fields within or adjacent to the moats were identified, with their crestline almost parallel to the contours, suggesting the presence of an across-slope tidal current, which was recorded through the mooring data. Many of the ripples are likely formed by tidally-forced currents (≤ 50 cm/s) active during every tidal cycle, while others, especially the washed-out ripples, may be relics formed under stronger, episodic peak flows not recorded by moorings. This suggests that the drift and its moats are still being influenced by a strong hydrodynamic regime. The across-slope flow likely arises from the trapped baroclinic tidal motion at the ENAW–MOW interface, located at a similar depth as the drift and sediment wave fields. Another weaker recorded current is the residual (i.e. net flow excluding periodic components, such as tides) northward bottom current, which combines both a contour current (thermohaline circulation involving the European Slope Current) and generated alongslope bottom current, related to the interaction of the trapped baroclinic motion with the continental slope. This weaker residual northward current, responsible for the formation of the drift and its moats throughout Quaternary, is currently overridden by the across-slope tidal component of the trapped baroclinic motion, which possesses enough energy to remobilise sediment previously deposited on the drift, transporting it laterally in the moats, entrapping the sediment within the moats, and forming sediment waves and their superimposed ripples in the moats.

This research presents a crucial paradigm for advancing our knowledge of elucidating the complexities of small-scale contourite drifts in diverse oceanic environments. Unlike large-scale contourite drifts that tend to reflect regional-scale oceanographic processes, small-scale drifts like the Belgica Mound Drift offer an opportunity to improve comprehension of local hydrodynamic processes and their influence on a contourite drift. This study demonstrates in the first place the value of a multi-disciplinary approach combining moorings, glider-based ADCP and CTD data, AUV and ROV imagery, and seismic data. It clearly highlights the importance of secondary hydrodynamic processes, particularly trapped baroclinic motions and Ekman transport, in controlling small-scale sediment transport and drift evolution. Also drift, moats and associated bedforms offer valuable insights into local sediment dynamics and bottom-current variability, preserving signals of both recent and paleo bottom-current dynamics.

Samenvatting

In tegenstelling tot grootschalige contouriet drifts, die de neiging hebben regionale oceanografische processen te weerspiegelen, zijn kleinschalige drifts (≤ 100 km²) belangrijke sedimentaire structuren die eerder lokale processen en interacties tussen watermassa's weerspiegelen. Deze systemen bieden waardevolle, hoog-resolutie archieven van zowel voorbije als recente stromingsdynamiek. Het nauwkeurig reconstrueren van vroegere processen op basis van de driftmorfologie vereist echter een gedetailleerd inzicht in de hedendaagse sedimentdynamiek en oceanografische processen die de morfologie van kleinschalige contourietdrifts vormgeven.

De Belgica Mound Drift, gelegen in de Porcupine Seabight (NO Atlantische Oceaan, voor de kust van Ierland), is een voorbeeld van kleinschalige contouriet drifts, die het mogelijk maakt de morfologische evolutie, hydrodynamische variabiliteit en sedimentdynamiek die met dergelijke drifts gepaard gaan, te onderzoeken. Het betreft een kleine (~36 km²) diepwaterdrift die zich heeft ontwikkeld tussen 500 en 800 m diepte, en die omringd wordt door koudwaterkoraalheuvels. Deze drift bevindt zich op dezelfde diepte als de grens tussen het Eastern North Atlantic Water (ENAW) en het Mediterranean Outflow Water (MOW). Dit maakt de Belgica Mound Drift tot een van de meest distale contouritische expressies die in de NO Atlantische Oceaan door het MOW worden beïnvloed.

Hoge-resolutie pseudo-3D seismische reflectiedata tonen aan dat de Belgica Mound Drift drie afzonderlijke evolutionaire fasen heeft doorstaan. Elke fase komt overeen met belangrijke verschuivingen in de paleo-oceanografie die zowel de bodemstroomdynamiek als de sedimenttoevoer beïnvloed hebben. De eerste fase betreft het pre-drift stadium (Plioceen–Vroeg Pleistoceen), gekarakteriseerd door de regionale erosieve RD1 gebeurtenis, toegeschreven aan de hernieuwde invloed van het MOW in de Porcupine Seabight. Deze fase creëerde een uitgesproken paleotopografie die de daaropvolgende sedimentaire en hydrodynamische processen bepaalde. Daarop volgde het initiatiefstadium (Vroeg–Midden Pleistoceen), dat overeenkomt met het begin van de driftvorming. Deze fase begon in twee afzonderlijke groeicentra, die sterk beïnvloed werden door lokale topografische obstakels, met name de koraalheuvels en de RD1 nonconformiteit. Deze obstakels beïnvloedden zowel de sedimentatie als de sterkte en richting van de bodemstromingen tijdens de vorming van de drift. Ten slotte is er het aggradationele stadium (Midden Pleistoceen–Heden), gekenmerkt door een meer continue en opwaarts bouwende gelaagde stratificatie in de driftarchitectuur. Dit stadium wijst op een relatief stabiele en minder energetische afzettingsomgeving. Deze fase is gekoppeld aan de Midden-Pleistoceen Transitie, tijdens welke de bodemstromingen verzwakten en de sedimenttoevoer afnam. De evoluerende morfologie van de "moats" suggereert een algemene verzwakking van de intensiteit van de bodemstromingen gedurende de ontwikkeling van de drift.

Om het moderne hydrodynamische regime dat de Belgica Mound Drift beïnvloedt te evalueren, werd een hoog-resolutie oceanografische dataset verzameld door het uitzetten van moorings uitgerust met stromingsmeters, een AUV (*Barabas*, VLIZ; visuele beelden en side-scan sonar), een ROV (*Zonnebloem*, VLIZ; visuele beelden) en een glider (*YOKO*, VLIZ) uitgerust met CTD- en ADCP-sensoren. Deze instrumenten leverden een uitgebreide dataset

op over de hedendaagse ruimtelijke en temporele variabiliteit van bodemstromingen over de drift en de moats, evenals over de interne structuur van de watermassa's.

Het belangrijkste hydrodynamische proces dat in alle CTD-profielen werd waargenomen, is een gevangen barocline beweging. Deze beweging wordt gekenmerkt door een dominante diurnale K_1-getijcomponent. De sterke bodemstromingen (tot 50 cm/s), die zich tot ongeveer 100 m boven de zeebodem uitstrekken, benadrukken de versterking van deze beweging door interactie met de lokale steile topografie en de aanwezigheid van watermassa-stratificatie gerelateerd aan de permanente thermocline, die samenvalt met het ENAW–MOW grensvlak. Het Ekman transport, dat de bodemstromingen nabij de zeebodem (tot 20 m) verzwakt en afbuigt, werd in deze omgeving voor het eerst geïdentificeerd via glider-gebaseerde ADCP-data. Dankzij de glider ADCP-data kunnen beide processen nu worden gekwantificeerd. De inzet van de glider bleek in het bijzonder effectief voor het vastleggen van dynamische verticale en horizontale variabiliteit, waarbij het ENAW–MOW grensvlak werd geïdentificeerd op dieptes die overeenkomen met de driftafzetting.

Aangezien directe metingen van bodemstromingen beperkt kunnen zijn, bijvoorbeeld via moorings, kan de studie van diepwater-bodemvormen, met behulp van ROV- en AUV-beelden, nieuwe inzichten bieden in de ruimtelijke variabiliteit van lokale hydrodynamische processen. Dichter bij de zeebodem onthulde de analyse van sedimentgolven en hun overlappende bodemvormen, waaronder slingerende, linguoïde en uitgespoelde ribbels, verdere inzichten in de ruimtelijke variabiliteit van bodemstromingen en hoe deze de huidige morfologie van de drift kunnen vormgeven. Twee velden van sedimentgolven, binnen of grenzend aan de moats, werden geïdentificeerd, waarvan de kamlijnen bijna parallel lopen aan de hoogtelijnen. Dit suggereert de aanwezigheid van een getijstroom dwars op het talud, die werd geregistreerd via de moorings. Veel van de ribbels zijn waarschijnlijk gevormd door getij-afgedwongen stromingen (≤ 50 cm/s) die actief zijn tijdens elke getijcyclus, terwijl andere, vooral de uitgespoelde ribbels, mogelijk relicten zijn, gevormd onder sterkere, episodische piekstromingen die niet door de moorings geregistreerd werden. Dit suggereert dat de drift en haar moats nog steeds worden beïnvloed door een krachtig hydrodynamisch regime. De hellingsparallelle stroming ontstaat waarschijnlijk uit de gevangen barocline getijbeweging op het ENAW–MOW grensvlak, dat zich op een vergelijkbare diepte bevindt als de drift en de sedimentgolfen. Een andere, zwakkere gemeten stroming is de residuele (netto stroming met uitsluiting van periodieke componenten, zoals getijden) noordwaartse bodemstroming, die zowel een contourstroom (thermohaliene circulatie die de *European Slope Current* omvat) als een hellingsparallelle bodemstroming combineert, gerelateerd aan de interactie van de gevangen barocline beweging met de continentale helling. Deze zwakkere residuele noordwaartse stroming, verantwoordelijk voor de vorming van de drift en haar moats gedurende het Quartair, wordt momenteel overheerst door de hellingsparallelle getijcomponent van de gevangen barocline beweging, die voldoende energie bezit om eerder afgezet sediment op de drift opnieuw te mobiliseren, het lateraal in de moats te transporteren, het sediment binnen de moats vast te houden, en sedimentgolven en hun overlappende ribbelstructuren in de moats te vormen.

Deze studie onderzoekt een belangrijk thema omtrent de complexiteit van kleine contourietafzettingen in diverse oceanische omgevingen. In tegenstelling tot grote contourietdrifts, die vaak een weerspiegeling zijn van regionale oceanografische processen, bieden kleine drifts, zoals de Belgica Mound Drift, de mogelijkheid om lokale hydrodynamische processen en hun invloed op een contourietdrift beter te begrijpen. In de eerste plaats

onderlijnt deze studie de waarde van een multidisciplinaire aanpak. Moorings, ADCP- en CTD-data van gliders, AUV- en ROV-beelden (en beeldvorming) worden gebruikt om de huidige oceanografische omstandigheden, evenals de morfologie van de zeebodem te karakteriseren. Aan de hand van seismische profielen werd de laterale evolutie van deze drift doorheen de tijd in kaart gebracht. Daarnaast benadrukt dit onderzoek de belangrijke rol van secundaire hydrodynamische processen, zoals “trapped diurnal baroclinic motion” en Ekman-transport. Deze spelen een cruciale rol bij kleinschalig sedimenttransport en de ontwikkeling van contourietdrifts. Evenals de relatie tussen drift, moat en bijbehorende sedimentaire structuren bieden waardevolle inzichten in de lokale sedimentdynamiek en variabiliteit van bodemstromingen, waarbij signalen van zowel recente- als paleo-stromingsdynamiek worden bewaard.

Au-dessus de nous, l'espace, au-dessous, un miroir. En se penchant vers l'épaisseur des eaux, chacun n'y verra qu'un reflet de son propre visage ; en se relevant, son regard retrouvera le cercle d'horizon. Et Vikings marche avec son cercle. N'existe sur la mer, ni passé, ni futur. La trace des sillages s'efface. Il y a l'éternelle seconde présente qui est le centre, et l'horizon poursuivi recule, et rien, jamais ne s'arrête.

Excerpt from « Le carnet Vikings » by Anita Conti, born Caracotchian, the first French female oceanographer.

Chapter 1 – Introduction

1.1 Oceanic circulation as a driver of bottom currents and contourite drift development

The large-scale circulation in the oceans is either a wind-driven circulation, happening in the upper few hundred metres and controlling surface currents, or the density-driven circulation, i.e. the thermohaline circulation (Toggweiler and Key, 2001). The giant conveyor belt is an overturning thermohaline circulation driven by differences in temperature and salinity and has an important role in the Earth's climate regulation, with heat transfers induced by the transport of water masses. This circulation is most vigorous in the Atlantic Ocean, where the upper part of the thermohaline circulation carries warm water from the tropical and subtropical North Atlantic to the north, while the deeper part transports cold and dense water towards the south, beyond the tip of Africa (Toggweiler and Key, 2001; Rahmstorf, 2006).

Persistent currents near the seafloor, i.e. **bottom currents**, can be induced by different mechanisms such as the wind and tidal forces (Shanmugam, 2008; Stow et al., 2019). The thermohaline circulation can also be responsible for their formation. The thermohaline bottom currents (Stow et al., 2019) transport deep-water masses (Faugères et al., 1993; Rebesco et al., 2014), with their speed correlated to the strength of the density gradient driving them (Rebesco et al., 2014). These thermohaline bottom currents are steered by the Earth's rotation causing them to flow along the contours, i.e. **contour currents** (Shanmugam, 2008; Rebesco et al., 2014; Stow et al., 2019). Their path and speed can be altered by topographic features such as canyons, ridges and mounds. When the speed increases beyond a certain threshold, the current can erode sediment from the seafloor and transport it away. As the flow slows down, the sediment is eventually deposited elsewhere (Stow et al., 2002; Rebesco et al., 2014). Through these processes, the currents can shape the seafloor by forming bedforms such as ripples, dunes and sediment waves, reflecting the hydrodynamic conditions and the sediment availability (Stow et al., 2009).

Sediment reworked and deposited by bottom currents, especially contour currents, are known as **contourites**, which can be interbedded with other sediment types, and the larger sedimentary accumulations they form are referred to as **contourite drifts** (Faugères et al., 1993; Stow et al., 2002; Rebesco, 2005). The contourite drifts (Fig. 1.1) are widespread and are observable from abyssal plains to continental margins (Rebesco et al., 2014). They were first identified 60 years ago through deep-sea photographs (Heezen and Hollister, 1964; Hollister, 1967). The understanding of the contourites has gradually progressed via cooperation amongst researchers from various disciplines and through the IODP (Integrated Ocean Drilling Program) expeditions. These studies allowed to define them as being deposits

formed by the predominant action of contour currents, associated with other multiple types of hydrodynamic processes (Rebesco and Camerlenghi, 2008) in the deep ocean (Campbell and Deptuck, 2012; Uenzelmann-Neben and Gohl, 2012), on continental slopes (Preu et al., 2012; Roque et al., 2012; Li et al., 2013), in shallow margins (Verdicchio and Trincardi, 2008; Vandorpe et al., 2011), in lakes (Ceramicola et al., 2001; Gilli et al., 2005; Heirman et al., 2012) and in fjords (Wils et al., 2021). Although research on contourite drifts has increased significantly in recent decades, their diagnostic sedimentological criteria remain insufficiently defined (Rebesco et al., 2014; Van Rooij et al., 2016). The hydrodynamic processes responsible for their formation, such as benthic storms, vertical eddies, internal tides, and baroclinic (internal) waves, are closely tied to deep-water circulation. Over the past decade, the integration of oceanographic measurements with numerical modelling into contourite drift studies has significantly advanced research in this field (Nicholson et al., 2024). However, these processes remain not fully understood, largely due to limitations in the resolution at which they are studied. Their spatial and temporal dynamic variabilities are thus not fully captured and their average integrated within the numerical models (Nicholson et al., 2024). As a result, the role of bottom currents in shaping the seafloor, generating diverse erosional and depositional features, and influencing the formation and evolution of contourite drifts remains insufficiently explored (Rebesco et al., 2014; Van Rooij et al., 2016; Nicholson et al., 2024).

The contourite drifts (Fig. 1.1) typically exhibit an elongated, mounded geometry that lies parallel or oblique to the continental margin contours and are often bordered by at least one adjacent concave moat. Their size varies significantly, from small-scale drifts ≤ 100 km² to giant elongated drifts exceeding 100000 km². The large-scale drifts are easily identifiable through bathymetric and seismic data (Rebesco et al., 2014). In contrast, smaller-scale drifts are often overlooked in favour of larger ones, as their limited size makes them difficult to be detected.

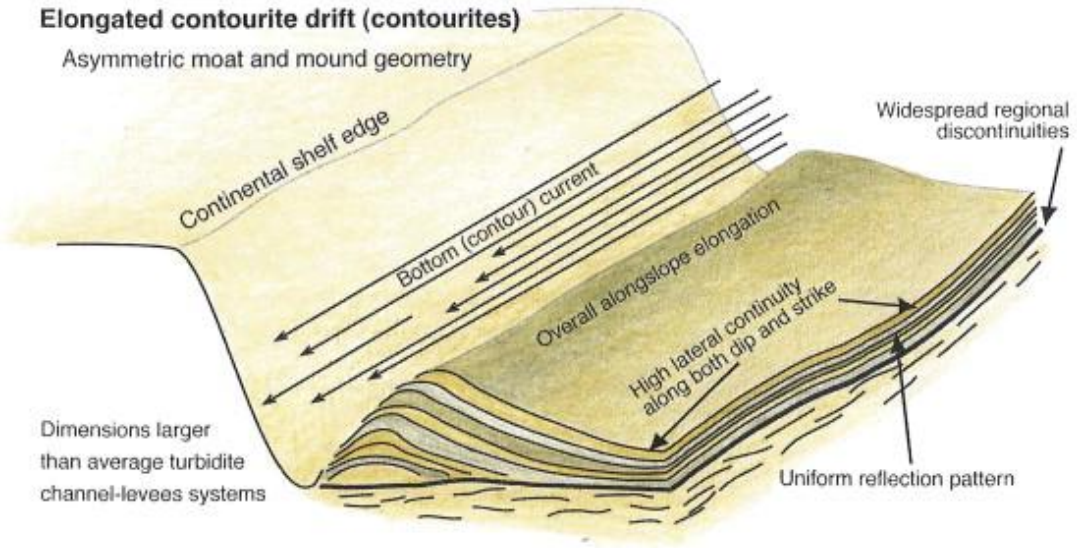

Figure 1.1. Schematic illustration highlighting the key features of an elongated contourite drift (from Rebesco et al., 2014).

Contourite drifts are classified into several types based on their morphology (Fig. 1.2), with for example *elongated mounded drifts* and *confined drifts*. The formation and type of drift are controlled by factors such as bottom-current characteristics, slope morphology and gradient, and sediment supply. These drifts can be isolated or, when aligned with dominant alongslope processes, form part of a larger **Contourite Depositional System** (CDS), a complex association of drifts and related erosive features (Hernández-Molina et al., 2003, 2009). Moats are associated features of contourite drifts and are linear depressions, or channels, that run parallel to the slope, formed primarily by erosion or non-deposition under the action of contour currents. Their development is influenced by the Coriolis force, which deflects the flow and enhances scouring along one side. The *elongated mounded drifts* (separated or detached; Fig. 1.2) develop on continental slopes, with one moat along one side of the drifts. They are stretched out in the direction of the current and develop parallel or slightly oblique to the slope (e.g. North Iberian margin, Liu et al., 2019, 2020; South Greenland margin, Hunter et al., 2007; Alboran ridge, Ercilla et al., 2016; Vandorpe et al., 2019; Hikurangi subduction margin, Bailey et al., 2021; NW Sicilian continental margin, Spatola et al., 2021). *Confined drifts*, on the other hand, develop parallel to the axis of relatively small, enclosed basins and are flanked by moats on both sides (e.g. Lake Baikal; Ceramicola et al., 2001; Hikurangi subduction margin, Bailey et al., 2021; Djibouti Ville Seamount, Palomino et al., 2011, Vandorpe et al., 2019). In practice, the boundaries between drift types are not always well-defined and a drift can fit with several types (Rebesco et al., 2014).

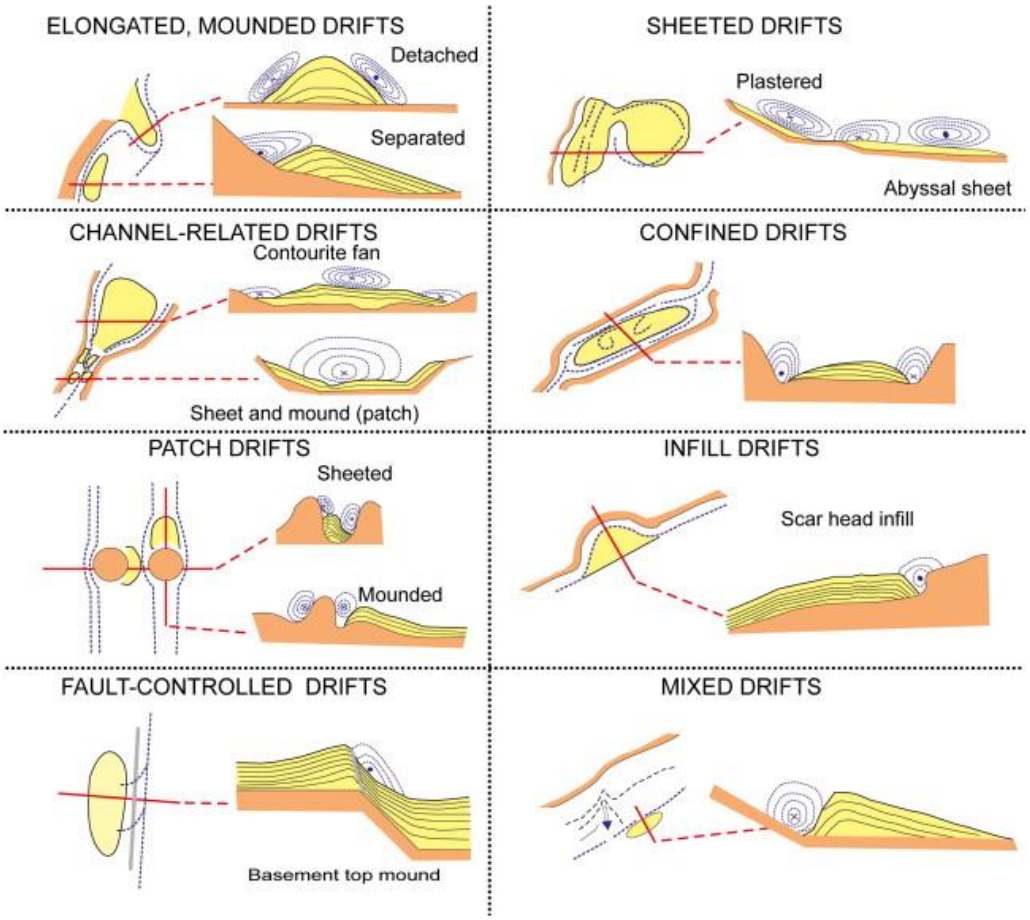

Figure 1.2. Classification of sediment drift types and reconstructed bottom-current paths (from Rebesco et al., 2014). The dots show a current towards the reader and crosses a current going away.

In addition to moats, bottom currents generate a variety of bedforms, both depositional and erosional (Stow et al., 2009). These bedforms often coexist with contourite drifts and exhibit a high variability in sediment composition, morphology, and scale, from decametric scale ripples to kilometric scale sediment waves (Wynn and Masson, 2008; Stow et al., 2013).

The geometry of these features are valuable indicators of past bottom-current velocities and directions (Stow et al., 2009). While sediment waves on continental shelves are well documented, knowledge of slope-associated sediment waves formed under the influence of contour currents remains limited (King et al., 2014). These deep-water bedforms have significant potential to improve the understanding of bottom-current behaviour, particularly in areas lacking direct, long- or short-term measurements, such as mooring data. Studying these structures can thus offer critical insights into the hydrodynamic processes shaping the seafloor (Van Rooij et al., 2016).

1.2 Relevance of the study of contourite drifts

Contourite drifts hold significant scientific value across several fundamental research fields, particularly in paleoclimatology and paleoceanography, slope stability, and hydrocarbon exploration (Rebesco, 2005; Rebesco et al., 2014). Due to their typically high sedimentation rates, driven by focused contour currents, these deposits can preserve high-resolution records of ocean circulation variability and ice-sheet dynamics (Rebesco et al., 2014). This makes contourite drifts valuable archives for reconstructing past hydrodynamic conditions. Detailed information on these conditions can be extracted from the drifts through a combination of continuous geophysical logging, discrete sediment analyses, and seismic imaging. Seismic data, in particular, allows to envision the drift morphology, with its internal structures, offering insights into paleo-current direction and strength on timescales ranging from tens of thousands to millions of years (Rebesco et al., 2014). The progress in contourite research highly depends on the technological advancements that improve the resolution seafloor observations (Rebesco et al., 2014; Van Rooij et al., 2016; Nicholson et al., 2024). The use of modelling, with enhanced integration of long- and short-term oceanographic, geological and sedimentological datasets, including coring, seismic surveys, multibeam bathymetry, Autonomous Underwater Vehicles (AUV), Remotely Operated underwater Vehicles (ROV), and moorings, is essential for understanding the complex interactions between sediment dynamic and oceanographic processes (Hernández-Molina et al., 2014; Rebesco et al., 2014; Van Rooij et al., 2016; Nicholson et al., 2024).

While most large-scale CDS have been mapped, small-scale drifts remain underexplored due to limitations in data resolution. These smaller drifts, however, offer unique potential: Unlike large drifts, which primarily reflect regional to global-scale hydrodynamics such as thermohaline circulation, small-scale drifts record more local processes (Rebesco et al., 2014). The study of small-scale contourite drifts allows for high-resolution and dense spatial coverage, enabling more precise reconstructions of sediment and hydro-dynamics. Ultimately, advancing contourite research, particularly of small-scale contourite drifts, requires closer collaboration between geologists and oceanographers, supported by continued technological innovation (Rebesco et al., 2014). Employing higher-resolution measurements, such as those obtained from Acoustic Doppler Current Profilers (ADCP), could greatly enhance the

understanding of the spatial and temporal variability of the hydrodynamic regime influencing the drifts (Nicholson et al., 2024).

For long-term interpretations, seismic and bathymetric datasets can provide information on average bottom-current characteristics. In contrast, current meter data and high-resolution seabed imagery, such as from ROV and AUV, are crucial for understanding present-day processes and bedform dynamics. A multidisciplinary approach, combining geological, oceanographic, and geophysical methods, is essential to compare and integrate observations across different temporal and spatial scales. This integrated strategy not only enhances the interpretation of contourite systems but also helps define the methodological limits and strengths of each data source.

1.3 Small-scale contourite drifts and their association with cold-water coral mounds

Several studies reveal that small-scale contourite drifts often develop in close association with deep-water obstacles such as cold-water coral (CWC) mounds, which locally modify bottom-current trajectories, amplify flow intensity, and promote sediment deposition on the drifts (Van Rooij et al., 2007; Hanebuth et al., 2015; Hebbeln et al., 2016; Hebbeln et al., 2019; Steinmann et al., 2020). The co-occurrence of CWC mounds and contourite drifts is well documented along the eastern Atlantic margin, spanning from the Moroccan margin (Vandorpe et al., 2016; Hebbeln et al., 2019) to the Irish margin (Van Rooij et al., 2007). These coral mounds are commonly composed of *Lophelia pertusa* and *Madrepora oculata* (De Mol et al., 2002) and are typically situated at the interface of intermediate water masses, particularly the Mediterranean Outflow Water (MOW) (De Mol et al., 2002). This dynamic interface fosters baroclinic waves, enhancing bottom currents and generating nepheloid layers (White, 2007) that deliver suspended sediments and planktonic food to coral communities (De Mol et al., 2002; Hebbeln et al., 2016).

Detailed investigations such as done by Van Rooij et al. (2007) and Huvenne et al. (2009) have provided valuable insights into the formation mechanisms, spatial distribution, and environmental significance of the contourite drifts associated with CWC mounds at depths between approximately 200 and 1000 m, highlighting the Porcupine Seabight, offshore Ireland, as a key natural laboratory for studying CWC ecosystems and sediment dynamics in continental margin settings.

The Porcupine Seabight (Fig. 1.3), located along the northeast Atlantic continental margin, is a complex hydrodynamic system. This system results from the combined effects of large-scale oceanic circulation, baroclinic motions, tidal forces, and complex seabed morphology. The prevailing flow regime is cyclonic (White, 2007) and is primarily influenced by the European Slope Current (ESC; Fig. 1.3), which is a boundary current flowing northward, along the continental slope, between roughly 500 and 2000 m depth (Toucanne et al., 2021). Closer to the seabed, the ESC is complemented by a poleward bottom current generated through rectification of baroclinic motions (Pingree and Le Cann, 1990; White et al., 2007). These overlapping currents are intensified especially along the eastern slope of the Seabight, where direct interactions with the seafloor topography occur (White, 2007). The presence of the CWC mounds, significantly affects the bottom-current patterns. These features redirect bottom

currents, thereby contributing to the spatial variability of the currents in the region (Dorschel et al., 2007; Van Rooij et al., 2007). In addition, baroclinic motions can become amplified near the seafloor when they resonate with the vertical density structure of the water column. The strongest density gradient is around the permanent pycnocline, which typically occurs around 700 m depth, representing the boundary between the Eastern North Atlantic Water (ENAW) and the MOW (Pingree and Le Cann, 1990; White, 2007). The maximum amplification of these motions is at a similar depth (600-800 m; White and Dorschel, 2010) as the main distribution zone of CWC mounds (White, 2007; Van Rooij et al., 2007).

The CWC mounds in the Porcupine Seabight are clustered within three distinct provinces: the Hovland, Magellan, and Belgica Mound provinces (Fig. 1.3; De Mol et al., 2002).

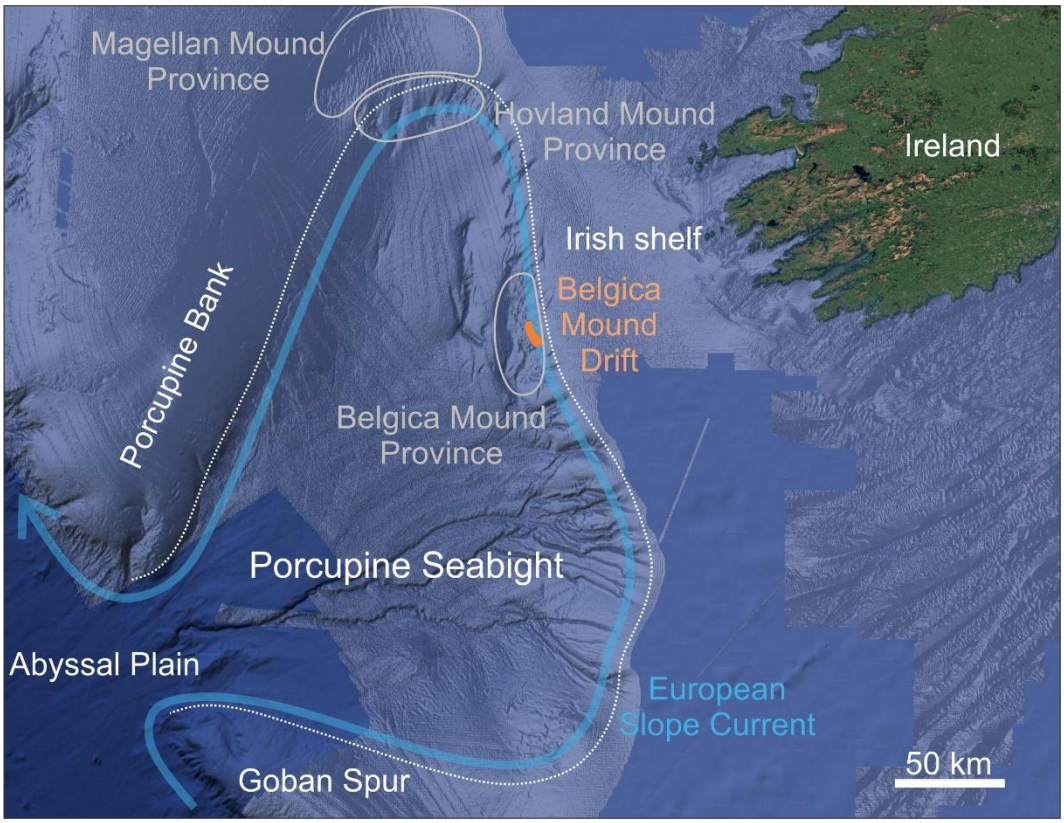

Figure 1.3. Map of the Porcupine Seabight, offshore Ireland. The pathway of the European Slope Current (based on Toucanne et al., 2021) is indicated in blue. The three cold-water coral mound provinces are in grey, while the Belgica Mound Drift is shown in orange. The shaded relief in the background is based on the 25 m resolution data from INFOMAR (2023).

The Belgica Mound Province (Fig. 1.3) is located on the eastern flank of the Porcupine Seabight, with water depths ranging from 550 to 1025 m. This area is elongated in shape, measuring approximately 45 km in length and 10 km in width. This province gathers both buried and outcropping CWC mounds (De Mol et al., 2002), such as the Challenger Mound (Fig. 1.4; Van Rooij et al., 2003, 2007; Huvenne et al., 2009). This province is designated as a Special Area of Conservation (SAC 002327) mainly because of the presence of the CWC mounds (National Parks & Wildlife Service, 2025). The Belgica Mound Province is thus protected by the Irish government and activities within the site are regulated.

Initial seismic stratigraphic investigations by Henriet et al. (1998), De Mol et al. (2002), Huvenne et al. (2003), and Van Rooij et al. (2003) laid the groundwork for drilling operations during IODP Expedition 307 (Fig. 1.4), specifically targeting the Challenger Mound and its surrounding area (Ferdelman et al., 2006). The Challenger Mound is positioned adjacent to a confined contourite drift covering approximately 36 km², first identified by Van Rooij et al. (2003, 2007) and named in the course of this work as Belgica Mound Drift (Fig. 1.4).

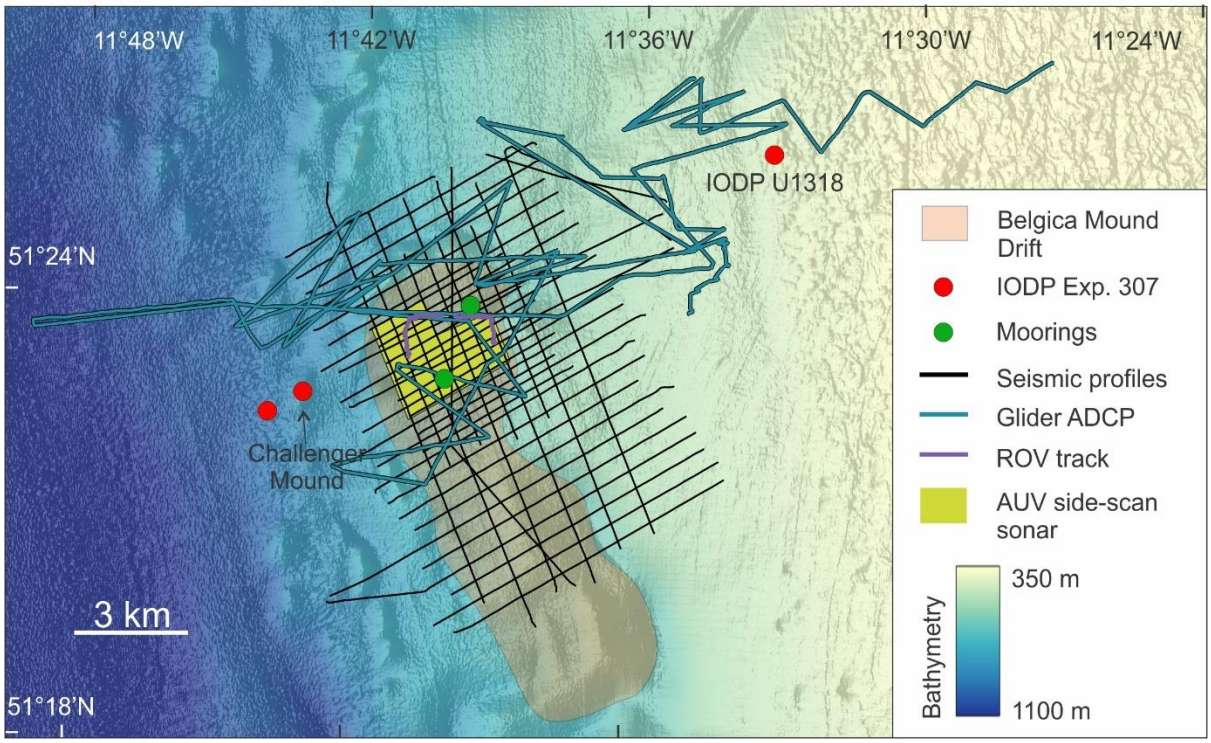

Figure 1.4. Map showing the Belgica Mound Drift (orange) and the location of the different datasets. The red dots represent the IODP Exp. 307 sites. The seismic lines, the glider and ROV tracks are shown respectively by the black, blue and purple lines. The moorings are indicated with the green dots and the AUV side-scan sonar is in yellow.

At the time, the available seismic grid was too sparse to provide a detailed understanding of the internal structure and spatial variability of the drift. The original local seismic stratigraphy, as defined by Van Rooij et al. (2003), was validated during IODP Exp. 307, establishing a robust chronostratigraphic framework (Kano et al., 2007; Louwye et al., 2008) and tying these stratigraphic markers to key phases of CWC mound formation (Huvenne et al., 2009). However, the correlation between the main body of the contourite drift and the drilled IODP sites remained limited due to insufficient seismic coverage.

1.4 Scientific context

This PhD is fully framed within the FWO-funded DynaMOD project (2019-2023), which investigated the sedimentary and oceanographic dynamics shaping confined contourite drifts. Its aim was to understand how present-day hydrodynamic processes, particularly bottom currents influenced by the MOW, affect long-term seabed evolution in areas with complex topography, such as CWC mounds. As a secondary objective, this project also seeks to

contribute to the refinement of diagnostic criteria for contourite drifts, with particular attention to the characteristics of the bottom currents responsible for their formation. The eastern slope of the Porcupine Seabight, offshore Ireland, provided an ideal natural laboratory for investigating contourite drifts due to its confined setting and active hydrodynamics. The study of one of the drifts, i.e. the Belgica Mound Drift located in the Porcupine Seabight, offered crucial insights into smaller-scale contourite systems.

Building upon previous seismic studies (Van Rooij et al., 2003, 2007, 2009; Huvenne et al., 2009), this research addresses the limitations of earlier datasets by leveraging newly acquired, densely spaced, high-resolution seismic data (Fig. 1.4). This advancement allows a revision of the previous **(objective 1) seismic stratigraphy** and an accurate **(objective 2) reconstruction of the spatial and temporal evolution** of the drift in high resolution. To achieve this, a pseudo-3D seismic view of the drift can be produced, enabling a detailed reconstruction of the architectural evolution of the drift, in parallel with the development of the adjacent CWC mounds during Quaternary. The interplay of multiple driving forces shaping contourite drift formation has proven to be challenging to disentangle (Rebesco et al., 2014) and this pseudo-3D reconstruction could help to better define them. This reconstruction requires a robust **(objective 3) chronostratigraphic framework** and reliable lithological ground-truthing, provided by IODP Expedition 307 (Ferdelman et al., 2006). By correlating seismic data with these core records, a high-resolution understanding of both the temporal and lateral sedimentological variability within the drift system could be delivered.

Another goal is to grasp more fully and quantify the temporal and spatial variability of the **(objective 4) present-day hydrodynamic regime**. While the broader regional oceanographic context of the Porcupine Seabight and the Belgica Mound Province is relatively well understood (White, 2007), local complexity increases due to the irregular seafloor topography (Dorschel et al., 2007). A particular focus is placed on resolving the detailed behaviour of baroclinic motions linked to the MOW around the Belgica Mound Drift.

Based on the present-day observations and past records, 3D numerical modelling can be used to simulate the **(objective 5) paleohydrodynamic variability**, aiming to better understand the oceanographic processes that have driven the formation of the contourite drift. This can be achieved through an integrated approach that combines a rich legacy of seismic data with high-resolution observations from oceanographic moorings, glider and AUV surveys, and ROV imagery (Fig. 1.4).

The four subsequent research chapters (Figs. 1.4, 1.5) in this thesis concentrate on one or more objectives of the DynaMOD project, with each chapter focusing on several sub-research questions.

Chapter 2 is based on high-resolution seismic dataset covering the entire drift and aims to:

- Reassess the seismic stratigraphy of the Belgica Mound Drift and to better define its seismic architecture (objective 1);
- Investigate the temporal and spatial variability of the drift near the CWC mounds (objective 2);
- Correlate the revised Quaternary evolution of the Belgica Mound Drift with the chronostratigraphy established by IODP Expedition 307 (objective 3);

- Explore the co-evolution of the drift and CWC mounds, testing the hypothesis that the mounds were fully developed before the drift deposition began (Huvenne et al., 2009) (objective 2);
- Evaluate the influence of the MOW in shaping one of its most distal contouritic expressions in the NE Atlantic Ocean (objective 5).

Chapter 3 is based on mooring data and ROV imagery from the northern sector of the drift and aims to:

- Identify seafloor features, such as bedforms;
- Assess the strength, direction, as well as the spatial and temporal variability of bottom currents on the drift and in its moats (objective 2);
- Verify whether the inferred bottom currents from seafloor features accurately reflect present-day conditions (objective 4).

Chapter 4 is based on high-resolution AUV side-scan sonar, bathymetry, and imagery from the northern sector of the drift and aims to:

- Investigate large-scale bedforms and determine the presence of sediment waves across the drift and its surrounding area;
- Analyse the geometry of these features in order to assess the spatial variability of the hydrodynamic processes that shaped them (objective 2);
- Develop an integrated understanding of the drift and its bedforms as a dynamic system and to evaluate whether present-day hydrodynamic processes had an influence on the past sedimentary evolution of the drift (objectives 4 and 5).

Chapter 5 is based on mooring data and glider-mounted ADCP and CTD data from the northern sector of the drift and aims to:

- Define the water column structure above the drift (objective 4);
- Evaluate the spatial and temporal variability of the present-day hydrodynamic regime, close to the seabed and in the water column (objective 4);
- Better investigate the enhancement of the bottom currents (objective 4).

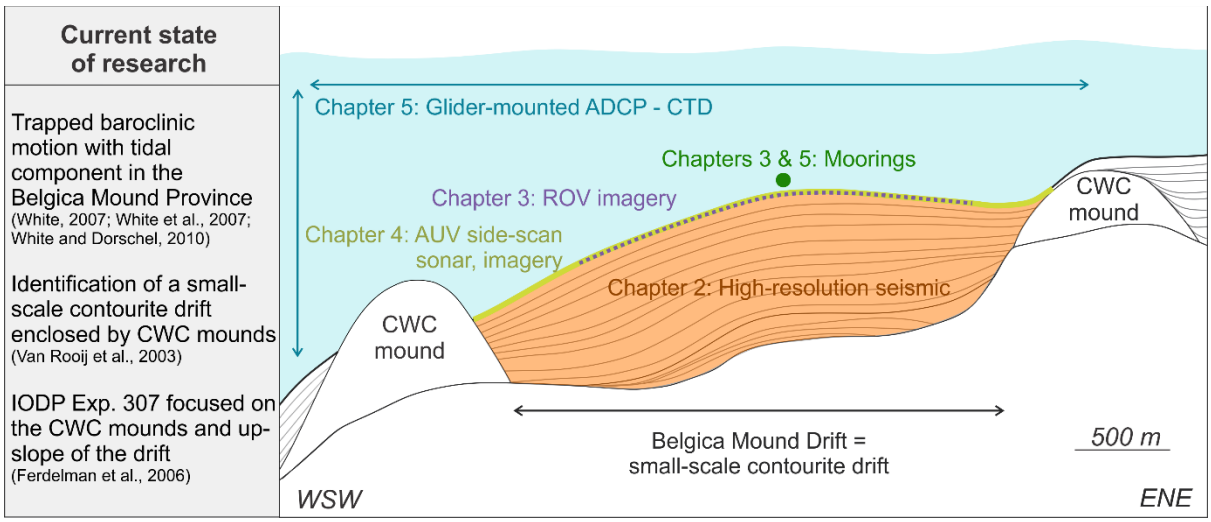

Figure 1.5. Schematic overview of the datasets used and their corresponding chapters, with previously established knowledge of the area shown on the left. CWC stands for cold-water coral.

1.5 References

Bailey, W.S., McArthur, A.D., McCaffrey, W.D., 2020. Distribution of contourite drifts on convergent margins: Examples from the Hikurangi subduction margin of New Zealand. Sedimentology 68, 294–323. https://doi.org/10.1111/sed.12779.

Campbell, D.C., Deptuck, M.E., 2012. Alternating bottom-current-dominated and gravity flow-dominated deposition in a lower slope and rise setting—insights from the seismic geomorphology of the Western Scotian Margin, Eastern Canada., in: Prather, B.E., Deptuck, M.E., Mohrig, D., Van Hoorn, B., Wynn, R.B. (Eds.), Application of the Principles of Seismic Geomorphology to Continental-slope and Base-of-slope Systems: Case Studies from Seafloor and Near-seafloor Analogues. SEPM Special Publication, 99, pp. 329–346. http://doi.org/10.2110/pec.12.99.0329.

Ceramicola, S., Rebesco, M., De Batist, M., Khlystov, O., 2001. Seismic evidence of small-scale lacustrine drifts in Lake Baikal (Russia). Mar. Geophys. Res. 22, 445–464. http://doi.org/10.1023/A:1016351700435.

De Mol, B., Van Rensbergen, P., Pillen, S., Van Herreweghe, K., Van Rooij, D., McDonnell, A., Huvenne, V., Ivanov, M., Swennen, R., Henriet, J.P., 2002. Large deep-water coral banks in the Porcupine Basin, southwest of Ireland. Mar. Geol. 188, 193–231. https://doi.org/10.1016/S0025-3227(02)00281-5.

Dorschel, B., Hebbeln, D., Foubert, A., White, M., Wheeler A.J., 2007. Hydrodynamics and cold-water coral facies distribution related to recent sedimentary processes at Galway Mound west of Ireland. Mar. Geol. 244, 184–195. https://doi.org/10.1016/j.margeo.2007.06.010.

Ercilla, G., Juan, C., Hernández-Molina, F.J., Bruno, M., Estrada, F., Alonso, B., Casas, D., Farran, M., Llave, E., García, M., Vázquez, T., D'Acremont, E., Gorini, C., Palomino, D., Valencia, J., El Moumni, B., Ammar, A., 2016. Significance of bottom currents in deep-sea morphodynamics: An example from the Alboran Sea. Mar. Geol. 378, 157–170. https://doi.org/10.1016/j.margeo.2015.09.007.

Faugères, J.C., Mézerais, M.L., Stow, D.A.V., 1993. Contourite drift types and their distribution in the North and South Atlantic Ocean basins. Sediment. Geol. 82, 189–203. https://doi.org/10.1016/0037-0738(93)90121-K.

Ferdelman, T.G., Kano, A., Williams, T., Henriet, J.-P., Expedition 307 Scientists (Eds.), 2006. Proceedings of the IODP, 307, Proceedings of the IODP. Integrated Ocean Drilling Program. https://doi.org/10.2204/iodp.proc.307.2006.

Gilli, A., Anselmetti, F.S., Ariztegui, D., Beres, M., McKenzie, J.A., Markgraf, V., 2005. Seismic stratigraphy, buried beach ridges and contourite drifts: the Late Quaternary history of the closed Lago Cardiel basin, Argentina (49 degrees S). Sedimentology 52, 1–23. https://doi.org/10.1111/j.1365-3091.2004.00677.x.

Hanebuth, T.J.J., Zhang, W., Hofmann, A.L., Löwemark, L.A., Schwenk, T., 2015. Oceanic density fronts steering bottom-current induced sedimentation deduced from a 50 ka contourite-drift record and numerical modeling (off NW Spain). Quat. Sci. Rev. 112, 207–225. https://doi.org/10.1016/j.quascirev.2015.01.027.

Hebbeln, D., Van Rooij, D., Wienberg, C., 2016. Good neighbours shaped by vigorous currents: Cold-water coral mounds and contourites in the North Atlantic. Mar. Geol. 378, 171–185. https://doi.org/10.1016/j.margeo.2016.01.014.

Hebbeln, D., Bender, M., Gaide, S., Titschack, J., Vandorpe, T., Van Rooij, D., Wintersteller, P., Wienber, C., 2019. Thousands of cold-water coral mounds along the Moroccan Atlantic continental margin: Distribution and morphometry. Mar. Geol. 411, 51–61. https://doi.org/10.1016/j.margeo.2019.02.001.

Heezen, B.C., Hollister, C.D., 1964. Deep sea current evidence from abyssal sediments. Mar. Geol. 1, 141–174.

Heirman, K., De Batist, M., Arnaud, F., De Beaulieu, J.L., 2012. Seismic stratigraphy of the late Quaternary sedimentary infill of Lac d'Armor (Kerguelen archipelago): a record of glacier retreat, sedimentary mass wasting and southern Westerly intensification. Antarct. Sci. 24, 608–618. http://doi.org/10.1017/S0954102012000466.

Henriet, J.P., De Mol, B., Pillen, S., Vanneste, M., Van Rooij, D., Versteeg, W., Croker, P.F., Shannon, P.M., Unnithan, V., Bouriak, S., Chachkine, P., Belgica 97 Shipboard Party, 1998. Gas hydrate crystals may help build reefs. Nature 391, 648–649. https://doi.org/10.1038/35530.

Hernández-Molina, F.J., Llave, E., Somoza, L., Fernández-Puga, M.C., Maestro, A., León, R., Barnolas, A., Medialdea, T., García, M., Vázquez, J.T., Díaz del Río, V., FernándezSalas, L.M., Lobo, F., Alveirinho Dias, J.M., Rodero, J., Gardner, J., 2003. Looking for clues to paleoceanographic imprints: a diagnosis of the gulf of Cadiz contourite depositional systems. Geology 31, 19–22. https://doi.org/10.1130/0091-7613(2003)031<0019:LFCTPI>2.0.CO;2.

Hernández-Molina, F.J., Paterlini, M., Violante, R., Marshall, P., de Isasi, M., Somoza, L., Rebesco, M., 2009. Contourite depositional system on the Argentine slope: an exceptional record of the influence of Antarctic water masses. Geology 37, 507–510.

Hernández-Molina, F.J., Stow, D.A.V., Alvarez-Zarikian, C.A., Acton, G., Bahr, A., Balestra, B., Ducassou, E., Flood, R., Flores, J.-A., Furota, S., Grunert, P., Hodell, D., Jimenez-Espejo, F., Kim, J.K., Krissek, L., Kuroda, J., Li, B., Llave, E., Lofi, J., Lourens, L., Miller, M., Nanayama, F., Nishida, N., Richter, C., Roque, C., Pereira, H., Sanchez Goñi, M.F., Sierro, F.J., Singh, A.D., Sloss, C., Takashimizu, Y., Tzanova, A., Voelker, A., Williams, T., Xuan, C., 2014. Onset of Mediterranean outflow into the North Atlantic. Science 344, 1244–1250. https://doi.org/10.1126/science.1251306.

Hollister, C.D., 1967. Sediment distribution and deep circulation in the western North Atlantic. (PhD thesis) Columbia University, New York.

Hunter, S.E., Wilkinson, D., Louarn, E., McCave, I.N., Rohling, E., Stow, D.A.V., Bacon, S., 2007. Deep Western Boundary Current dynamics and associated sedimentation on the Eirik Drift, Southern Greenland Margin. Deep-Sea Res. I Oceanogr. Res. Pap. 54, 2036–2066. https://doi.org/10.1016/j.dsr.2007.09.007.

Huvenne, V.A.I., De Mol, B., Henriet, J.-P., 2003. A 3D seismic study of the morphology and spatial distribution of buried coral banks in the Porcupine Basin, SW of Ireland. Mar. Geol. 198, 5–25. https://doi.org/10.1016/S0025-3227(03)00092-6.

Huvenne, V.A.I., Van Rooij, D., De Mol, B., Thierens, M., O'Donnell, R., Foubert, A., 2009. Sediment dynamics and palaeo-environmental context at key stages in the Challenger cold-water coral mound formation: Clues from sediment deposits at the mound base. Deep-Sea Res. I Oceanogr. Res. Pap. 56, 2263–2280. https://doi.org/10.1016/j.dsr.2009.08.003.

INFOMAR, 2023. INFOMAR Marine Data Download Portal [WWW Document].

Kano, A., Ferdelman, T.G., Williams, T., Henriet, J.-P., Ishikawa, T., Kawagoe, N., Takashima, C., Kakizaki, Y., Abe, K., Sakai, S., Browning, E.L., Li, X., Integrated Ocean Drilling Program Expedition 307 Scientists, 2007. Age constraints on the origin and growth history of a deep-water coral mound in the northeast Atlantic drilled during Integrated Ocean Drilling Program Expedition 307. Geology 35, 1051–1054. https://doi.org/10.1130/G23917A.1.

King, E.L., Bøe, R., Bellec, V.K., Rise, L., Skarðhamar, J., Ferré, B., Dolan, M.F.J., 2014. Contour current driven continental slope-situated sandwaves with effects from secondary current processes on the Barents Sea margin offshore Norway. Mar. Geol., 353, 108–127. https://doi.org/10.1016/j.margeo.2014.04.003.

Li, H., Wang, Y., Zhu, W., Xu, Q., He, Y., Tang, W., Zhuo, H., Wang, D., Wu, J., Li, D., 2013. Seismic characteristics and processes of the Plio-Quaternary unidirectionally migrating channels and contourites in the northern slope of the South China Sea. Mar. Petrol. Geol. 43, 370–380. https://doi.org/10.1016/j.marpetgeo.2012.12.010.

Liu, S., Van Rooij, D., Vandorpe, T., Gonzalez-Pola, C., Ercilla, G., Hernández-Molina, F.J., 2019. Morphological features and associated bottom-current dynamics in the Le Danois Bank region (southern Bay of Biscay, NE Atlantic): A model in a topographically constrained small basin. Deep-Sea Res. I: Oceanogr. Res. Pap. 149, 103054. https://doi.org/10.1016/j.dsr.2019.05.014.

Liu, S., Hernández-Molina, F.J., Ercilla, G., Van Rooij, D., 2020. Sedimentary evolution of the Le Danois contourite drift systems (southern Bay of Biscay, NE Atlantic): A reconstruction of the Atlantic Mediterranean Water circulation since the Pliocene. Mar. Geol. 427, 106217. https://doi.org/10.1016/j.margeo.2020.106217.

Louwye, S., Foubert, A., Mertens, K., Van Rooij, D., THE IODP EXPEDITION 307 SCIENTIFIC PARTY, 2008. Integrated stratigraphy and palaeoecology of the Lower and Middle Miocene of the Porcupine Basin. Geol. Mag. 145, 321–344. https://doi.org/10.1017/S0016756807004244.

National Parks & Wildlife Service, 2025. Belgica Mound Province SAC. https://www.npws.ie/protected-sites/sac/002327.

Nicholson, U., Stow, D. A. V., Brackenridge, R. E., Miramontes, E., Wåhlin, A. (2024). Introduction: Special issue on bottom currents and contourites: Processes, products and impact. Mar. Geol., 469, Article 107237. https://doi.org/10.1016/j.margeo.2024.107237.

Palomino, D., Vázquez J.-T., Ercilla, G., Alonso, B., López-González, N., Díaz-del-Río, V., 2011. Interaction between seabed morphology and water masses around the seamounts on the Motril Marginal Plateau (Alboran Sea, Western Mediterranean). Geo-Mar. Lett. 31, 465–479. https://doi.org/10.1007/s00367-011-0246-y.

Pingree, R.D., Le Cann, B., 1990. Structure, strength and seasonality of the slope currents in the Bay of Biscay region. J. Mar. Biol. Assoc. U. K. 70, 857–885. https://doi.org/10.1017/S0025315400059117.

Preu, B., Schwenk, T., Hernández-Molina, F.J., Violante, R., Paterlini, M., Krastel, S., Tomasini, J., Spieß, V., 2012. Sedimentary growth pattern on the northern Argentine slope: the impact of North Atlantic Deep Water on southern hemisphere slope architecture. Mar. Geol. 329–331, 113–125. https://doi.org/10.1016/j.margeo.2012.09.009.

Rahmstorf, S., 2006. Thermohaline Ocean Circulation, in: Elias, A. (Ed.), Encyclopedia of Quaternary Sciences. Elsevier, Amsterdam, pp. 1–10.

Rebesco, M., 2005. Sedimentary Environments: Contourites, in: Selley, R.C., Cocks, L.R.M., Plimer, I.R. (Eds.), Encyclopedia of Geology. Elsevier, Oxford, pp. 513–527. https://doi.org/10.1016/B0-12-369396-9/00497-4.

Rebesco, M., Camerlenghi, A., 2008. Contourites, Developments in Sedimentology. Elsevier, Amsterdam.

Rebesco, M., Hernández-Molina, F.J., Van Rooij, D., Wåhlin, A., 2014. Contourites and associated sediments controlled by deep-water circulation processes: State-of-the-art and future considerations. Mar. Geol. 352, 111–154. https://doi.org/10.1016/j.margeo.2014.03.011.

Roque, C., Duarte, H., Terrinha, P., Valadares, V., Noiva, J., Cachão, M., Ferreira, J., Legoinha, P., Zitellini, N., 2012. Pliocene and Quaternary depositional model ofthe Algarve margin contourite drifts (Gulf of Cadiz, SW Iberia): seismic architecture, tectonic control and paleoceanographic insights. Mar. Geol. 303–306, 42–62. https://doi.org/10.1016/j.margeo.2011.11.001.

Shanmugam, G., 2008. Deep-water bottom currents and their deposits. In: Rebesco, M., Camerlenghi, A. (Eds.), Contourites, Developments in Sedimentology. Elsevier, Amsterdam, pp. 59–81. https://doi.org/10.1016/S0070-4571(08)10005-X.

Spatola, D., Sulli, A., Casalbore, D., Chiocci, F.L., 2021. First Evidence of Contourite Drifts in the North-Western Sicilian Active Continental Margin (Southern Tyrrhenian Sea). J. Mar. Sci. Eng. 9, 1043. https://doi.org/10.3390/jmse9101043.

Steinmann, L., Baques, M., Wenau, S., Schwenk, T., Spiess, V., Piola, A.R., Bozzano, G., Violante, R., Kasten, S., 2020. Discovery of a giant cold-water coral mound province along the northern Argentine margin and its link to the regional Contourite Depositional System and oceanographic setting. Mar. Geol. 427, 106223. https://doi.org/10.1016/j.margeo.2020.106223.

Stow, D.A.V., Faugères, J.-C., Howe, J.A., Pudsey, C.J., Viana, A.R., 2002. Geol. Soc. London Mem. 22, 7–20.

Stow, D.A.V., Hernández-Molina, F.J., Llave, E., Bruno, M., García, M., Díaz del Rio, V., Somoza, L., Brackenridge, R.E., 2013. The Cadiz Contourite Channel: Sandy contourites, bedforms and dynamic current interaction. Mar. Geol. 343, 99–114. https://doi.org/10.1016/j.margeo.2013.06.013.

Stow, D., Smillie, Z., Esentia, I., 2019. Deep-Sea Bottom Currents: Their Nature and Distribution. In: Cochran, J.K., Bokuniewicz, H.J., Yager, P.L. (Eds.), Encyclopedia of Ocean Sciences. Elsevier, pp. 90–96. https://doi.org/10.1016/b978-0-12-409548-9.10878-4.

Toggweiler, JR, Key, R.M., 2001. Ocean circulation: thermohaline circulation. In: Steele, J., Thorpe, S., Turekian, K. (Eds.), Encyclopedia of ocean sciences. Academic Press, London, pp. 2941–2947.

Toucanne, S., Soulet, G., Riveiros, N.V., Boswell, S.M., Dennielou, B., Waelbroeck, C., Bayon, G., Mojtahid, M., Bosq, M., Sabine, M., Zaragosi, S., Bourillet, J.-F., Mercier, H., 2021. The North Atlantic Glacial Eastern boundary current as a key driver for ice-sheet—amoc interactions and climate instability. Paleoceanogr. Paleoclimatol., 36. https://doi.org/10.1029/2020PA004068.

Uenzelmann-Neben, G., Gohl, K., 2012. Amundsen Sea sediment drifts: archives of modifications in oceanographic and climatic conditions. Mar. Geol. 299–302, 51–62. https://doi.org/10.1016/j.margeo.2011.12.007.

Vandorpe, T., Van Rooij, D., Stow, D.A.V., Henriet, J.-P., 2011. Pliocene to recent shallowwater contourite deposits on the shelf and shelf edge off south-western Mallorca, Spain. Geo-Mar. Lett. 31, 391–403. http://doi.org/10.1007/s00367-011-0248-9.

Vandorpe, T., Collart, T., Cnudde, V., Lebreiro, S., Hernández-Molina, F.J., Alonso, B., Mena, A., Antón, L., Van Rooij, D., 2019. Quantitative characterisation of contourite deposits using medical CT. Mar. Geol. 417, 106003. https://doi.org/10.1016/j.margeo.2019.106003.

Van Rooij, D., De Mol, B., Huvenne, V., Ivanov, M., Henriet, J.-P., 2003. Seismic evidence of current-controlled sedimentation in the Belgica mound province, upper Porcupine slope, southwest of Ireland. Mar. Geol. 195, 31–53. https://doi.org/10.1016/S0025-3227(02)00681-3.

Van Rooij, D., Blamart, D., Kozachenko, M., Henriet, J.-P., 2007. Small mounded contourite drifts associated with deep-water coral banks, Porcupine Seabight, NE Atlantic Ocean. Geol. Soc. Lond. Spec. Publ. 276, 225–244. https://doi.org/10.1144/GSL.SP.2007.276.01.11.

Van Rooij, D., Campbell, C., Rueggeberg, A., Whalin, A., 2016. The Contourite Log-Book: significance for Palaeoceanography, Ecosystems and Slope Instability. Mar. Geol. 378, 1–4. https://doi.org/10.1016/j.margeo.2016.05.018.

Vandorpe, T., Martins, I., Vitorino, J., Hebbeln, D., García, M., Van Rooij, D., 2016. Bottom currents and their influence on the sedimentation pattern in the El Arraiche mud volcano province, southern Gulf of Cadiz. Mar. Geol. 378, 114–126. https://doi.org/10.1016/j.margeo.2015.11.012.

Verdicchio, G., Trincardi, F., 2008. Mediterranean shelf-edge muddy contourites: examples from the Gela and South Adriatic basins. Geo-Mar. Lett. 28, 137–151. http://doi.org/10.1007/s00367-007-0096-9.

White, M., 2007. Benthic dynamics at the carbonate mound regions of the Porcupine Sea Bight continental margin. Int. J. Earth Sci. 96, 1–9. https://doi.org/10.1007/s00531-006-0099-1.

Wils, K., Wermersche, M., Van Rooij, D., Lastras, G., Lamy, F., Arz, H.W., Siani, G., Bertrand, S., Van Daele, M., 2021. Late Holocene current patterns in the northern Patagonian fjords recorded by sediment drifts in Aysén Fjord. Mar. Geol. 441, 106604. https://doi.org/10.1016/j.margeo.2021.106604.

Wynn, R.B., Masson, D.G., 2008. Sediment waves and bedforms. In: Rebesco, M., Camerlenghi, A. (Eds.), Contourites. Developments in Sedimentology, 60. Elsevier, Amsterdam, pp. 289–300.

Chapter 2 – Morphosedimentary evolution of the Belgica Mound Drift: Controls on contourite depositional system development in association with cold-water coral mounds

---

This chapter has been slightly modified from the published version (open access):

Matossian, A.O. and **Van Rooij, D.** (2024). Morphosedimentary evolution of the Belgica Mound Drift: Controls on contourite depositional system development in association with cold-water coral mounds. *Marine Geology* 477, 107410.

Abstract: Small-scale contourite drift is an important component of continental margins that can record information about complex oceanographic processes. The Belgica Mound Drift is one example of a small-scale contourite drift. It is formed under the influence of cold-water coral (CWC) mounds and represents one of the most distal contouritic expressions influenced by the Mediterranean Outflow Water (MOW) in the NE Atlantic Ocean. Three distinct evolutionary stages have been identified from new high-resolution pseudo-3D reflection seismic data, each associated with a significant change in paleoceanography, affecting both bottom-current intensity and sediment input. The pre-drift stage (Pliocene–Early Pleistocene) corresponds to the regional RD1 erosive event, which was caused by the reintroduction of the MOW in the Porcupine Seabight, creating a distinct paleotopography that will influence all ensuing sedimentary processes. The second stage (Early Pleistocene–Middle Pleistocene) is the contourite drift inception in two distinct centres of growth, strongly steered by topographic obstacles such as the CWC mounds. During the third and final stage (Middle Pleistocene–present day), the contourite drift is developed under a more stable but less dynamic environment, characterised by more continuous and mounded aggradational stratification. The final stage of the contourite drift is related to the Middle Pleistocene Transition, with a spatially variable reduction in the MOW-related bottom currents and sediment input. The spatial and temporal evolution of this drift shows that its present-day morphology is controlled by the location of initial growth. Evolving moat morphology indicates that the intensity of the bottom currents generally decreases during the drift evolution. This research presents a crucial paradigm for advancing our knowledge of elucidating the complexities of smaller-sized contourite systems in diverse oceanic environments.

Keywords: contourite drift; bottom current; cold-water coral mounds; seismic stratigraphy; Northeast Atlantic; Porcupine Seabight; Quaternary

Author contributions: The data acquisition and conceptualisation of the 2019/16 survey were made by D. Van Rooij. The seismic data were processed and interpretated by A.O. Matossian.

Both authors were involved in the writing of this chapter. The figures were made by A.O. Matossian.

2.1 Introduction

Contourites are deep-sea sedimentary deposits formed under the influence of persistent bottom currents, i.e. contour currents, caused by numerous oceanographic processes (Stow et al., 2002; Rebesco, 2005; Rebesco et al., 2014). Their study highlights the past environmental conditions under which the sediment has been deposited and the different factors governing their formation, such as the sediment supply and bottom-current characteristics (Mulder et al., 2013; Rebesco et al., 2014). Numerous large-scale contourite drifts, with a size range from 100 to 100000 km², have been identified in the North Atlantic Ocean (Faugères et al., 1993, 1999) and especially on the western side of the Atlantic Ocean (Faugères et al., 1999; Rebesco et al., 2014). These drifts are principally related to the deep thermohaline circulation. Because of their large size and relation with large current systems, those drifts are easily identifiable on bathymetric and regional 2D seismic data and have often been closely observed and examined (Rebesco et al., 2014).

Conversely, smaller-scale drifts (~100 km²; Faugères et al., 1993, 1999) are not always easy to encounter or identify due to their size or because of poorly known regional oceanography. High- to very high-resolution seismic and bathymetric surveys already allowed the observation and identification of such smaller drifts, e.g. in fjord environments (Wils et al., 2021), in the Santaren Channel (Lüdmann et al., 2016), in the Lago Cardiel basin (Gilli et al., 2005), along the Norwegian continental slope (Rebesco et al., 2013), in the South China Sea (Li et al., 2013) and along the Moroccan margin (Vandorpe et al., 2023). Those small-scale drifts tend to reflect local processes that are more complex, such as internal waves, tides and bathymetric obstacles that can locally accentuate the bottom currents responsible for the formation of the drift (Rice et al., 1991; De Mol et al., 2002; Van Rooij et al., 2010; Rebesco et al., 2014). Even though large-scale contourite drifts are common and well-known across the world, from abyssal plains to continental margins, there are currently no unambiguous diagnostic criteria for smaller-scale contourite drifts (Rebesco et al., 2014; Van Rooij et al., 2016; Rodrigues et al., 2022). By defining those diagnostic criteria, it may be possible to distinguish small-scale contourite drifts from other deposits, which would consequently help to comprehend the origin and evolution of those drifts. Advances in investigation methods, such as very high-resolution geophysics on smaller-scale contourite drifts and the collection of high-quality data, might allow for fine-tuning their diagnostic potential in the future.

Additionally, there are several examples of small-scale contourite drifts associated with deep-water obstacles, such as cold-water coral (CWC) mounds (Van Rooij et al., 2007; Hanebuth et al., 2015; Hebbeln et al., 2016). Those obstacles (and others) locally modify the path of the bottom currents, intensifying their strength and assisting in local contourite depositional processes. The co-existence of CWC mounds and contourite drifts is widespread along the eastern Atlantic margin, ranging from the Moroccan (Vandorpe et al., 2016) to the Irish margins (Van Rooij et al., 2007), as well as in the Alborán Sea and on the Mexican margin (Hebbeln et al., 2016). Most of those CWC mounds are correlated to intermediate water masses (Henry et al., 2014), such as the Mediterranean Outflow Water (MOW), as they rely on the strong hydrodynamic regime induced by internal waves occurring at the interfaces with

other water masses (De Mol et al., 2002; Hernández-Molina et al., 2011; Hebbeln et al., 2016). This, in turn, creates nepheloid layers that facilitate the supply of sediment and food particles (Hebbeln et al., 2016). This could explain why the corals and the contourite drifts are frequently found side-by-side from 200 to 1000 m of water depth, as the distribution of the CWC mounds is more restricted, extending from shallow to intermediate water depths (1000 m) (Viana et al., 2007; Hebbeln et al., 2016).

One of the most notable examples of co-evolution between CWC mounds and contourites, triggered by the presence of the MOW, is located in the Porcupine Seabight, offshore Ireland (Hovland et al., 1994; Henriet et al., 1998; De Mol et al., 2002). Those coral communities are composed of *Lophelia pertusa* and *Madrepora oculata* (De Mol et al., 2002), which are deep-sea framework-building corals settling on hard substratum and under vigorous bottom currents (Freiwald et al., 1999; Hebbeln et al., 2016). Based upon the initial seismic stratigraphic studies by Henriet et al. (1998), De Mol et al. (2002), Huvenne et al. (2003) and Van Rooij et al. (2003), the Belgica Mound Province (BMP) and more particularly the Challenger Mound and its surroundings were drilled during IODP Exp. 307 (Ferdelman et al., 2006). The Challenger Mound is located adjacent to a confined contourite drift of around 36 km², earlier identified by Van Rooij et al. (2003, 2007) (Fig. 2.1). The contemporary seismic network was too sparsely spaced to allow any detailed insight into the architecture and evolution of this contourite drift. This necessary insight into its spatial and temporal growth is now made possible by the acquisition of a new densely spaced high-resolution seismic dataset. Due to its particular importance for this paper, this drift is referred to as the Belgica Mound Drift due to its association with the Belgica CWC mounds.

The initial local seismic stratigraphy, defined by Van Rooij et al. (2003), was ground-truthed during IODP Exp. 307, providing a reliable chronostratigraphy (Kano et al., 2007; Louwye et al., 2008), which was linked to the phases of the CWC mound growth (Huvenne et al., 2009). Nevertheless, the spatial correlation between the actual main body of this drift and the IODP sites was based on sparse seismic data (Fig. 2.2). IODP site U1318 also did not drill the full record of the contourite drift sequence; only the youngest strata were recovered (Fig. 2.2). However, the IODP results reported a hiatus of 6 My at site U1318 before the onset of the drift deposition (Kano et al., 2007; Louwye et al., 2008). Since the oldest part of the contourite sequence had not been drilled, the exact onset and extent of this hiatus required re-evaluation. However, at that time, the constraints on the MOW evolution and dynamics were not as well understood as they are now. IODP Exp. 339 in the Gulf of Cadiz (Stow et al., 2013) clearly highlighted the MOW as a key actor in the genesis of several Contourite Depositional Systems (CDS) along the eastern Atlantic continental margin. The work of Hernández-Molina et al. (2006, 2011, 2014) in the Gulf of Cadiz, Hanebuth et al. (2015) at the Galicia Bank, Hernández-Molina et al. (2011) and Collart et al. (2018) at the Ortegal CDS, Ercilla et al. (2008), Van Rooij et al. (2010) and Liu et al. (2020) at the Le Danois CDS and Delivet et al. (2016) at the Goban Spur, respectively presented from a proximal to a distal MOW, delivered new insights into the temporal and lateral variability of this intermediate water mass along the NW European margin and its effects on local bottom-current dynamics. The Cadiz CDS is directly related to the thermohaline circulation and a proximal MOW, whereas in the case of the smaller-scale CDS, located further along the NW European margin, a more distal MOW induces internal waves and tides caused by the interaction with topography, locally enhancing bottom-current intensities.

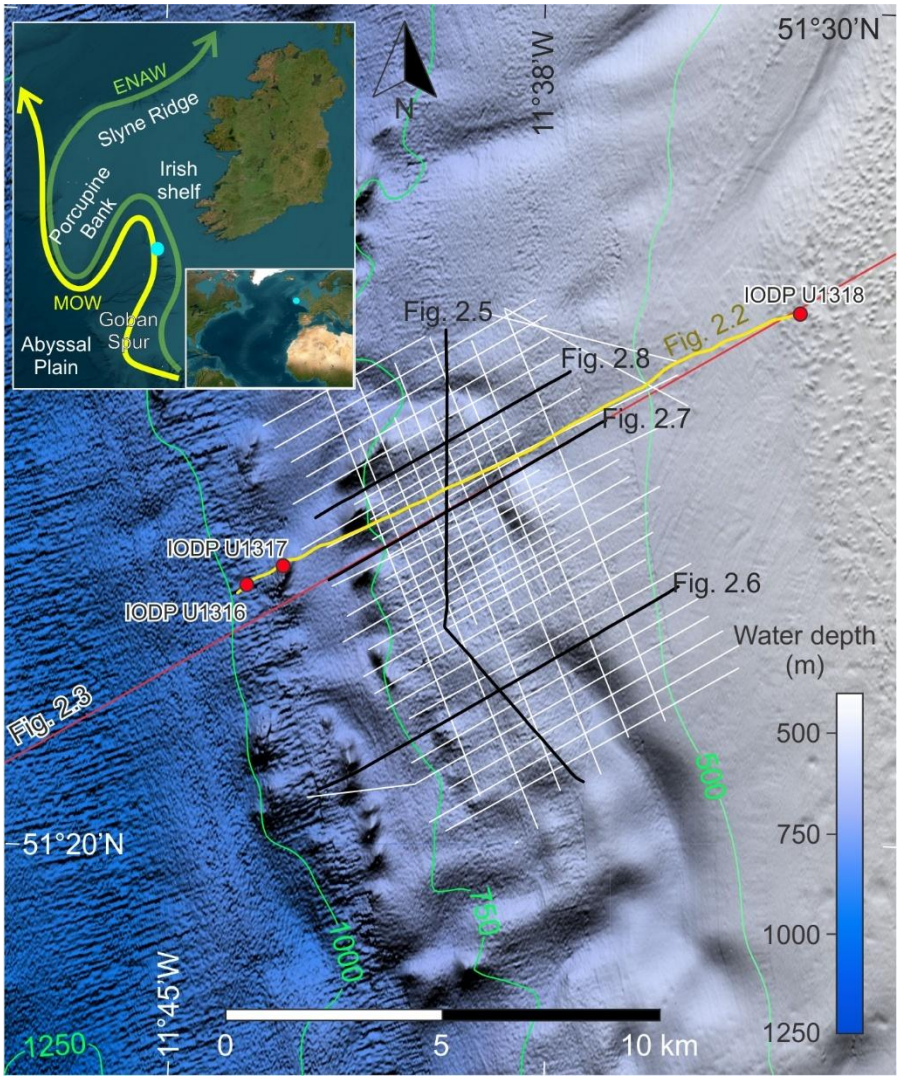

Figure 2.1. Bathymetric map of the study area (blue dot in the upper left corner inset) in the Porcupine Seabight, offshore Ireland (adapted from 25 m resolution data from INFOMAR, 2023). The green and yellow arrows represent the intermediate water mass circulation of Eastern North Atlantic Water (ENAW) and Mediterranean Outflow Water (MOW), respectively (upper left corner inset; based on Dullo et al., 2008). The white lines in the main figure represent the seismic lines, whereas the black lines represent the lines shown as figures (Figs. 2.5–2.8). The yellow line is seismic line P980521 (Fig. 2.2). The red line represents the salinity cross-section profile (Fig. 2.3). The IODP Exp. 307 coring sites (U1316, U1317 and U1318) are circled in red.

The investigation of lesser-known small-scale contourite drifts is essential for the future development of diagnostic criteria. Their study is also crucial to consider since it may record local past environmental conditions under which the sediment has been deposited and reworked in various settings, such as continental margins, lakes and fjords. Therefore, this study aims (1) to revise and investigate with greater resolution the previous seismic stratigraphy of the most recent units in the area (Van Rooij et al., 2003, 2009; Huvenne et al., 2009), i.e., the Belgica Mound Drift and the CWC mounds, and to better define the seismic architecture of this confined contourite drift; (2) to refine, in very high-resolution pseudo-3D seismic data, the temporal and spatial variability of this confined contourite drift adjacent to

the CWC mounds in order to gain more insight into the contemporary sediment dynamic regime; (3) to correlate the revised and updated Quaternary evolution of the Belgica Mound Drift to the IODP Exp. 307 chronostratigraphy; (4) to evaluate the co-evolution between the Belgica Mound Drift and CWC mounds, starting with the hypothesis of Huvenne et al. (2009) that the mounds were fully grown before the onset of the drift deposition; and (5) to assess the effects of the MOW in one of its most distal contouritic expressions within the eastern Atlantic Ocean.

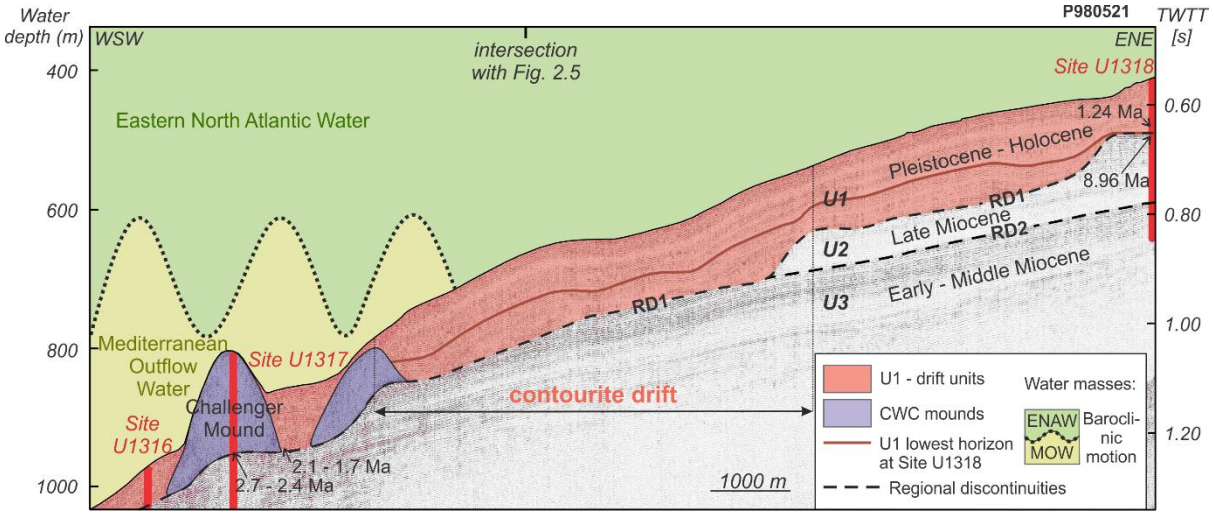

Figure 2.2. Seismic profile P980521 (location: Fig. 2.1) was already studied by Van Rooij et al. (2003, 2007) and used in the framework of IODP Exp. 307 (Ferdelman et al., 2006). The red vertical lines represent the three coring sites defined with the aim of recovering the seismic units previously identified by Van Rooij et al. (2003), including the drift unit U1 in red. The dashed lines are the boundaries (regional discontinuities RD1 and RD2) between seismic units U1, U2 and U3. Their approximative ages are based on Ferdelman et al. (2006). The geological dates around IODP site U1317 (Challenger Mound) are from Huvenne et al. (2009). The ages at IODP site U1318 are from Kano et al. (2007). This profile gives us a better view of the hiatus of missing drift deposits at IODP site U1318 (red horizon in U1). The figure also shows the position of the dynamic interface between Eastern North Atlantic Water (ENAW) and Mediterranean Outflow Water (MOW) in the study area.

2.2 Regional setting

2.2.1 Geography and geology

The Porcupine Seabight is a large basin (320 x 240 km) with a N–S trend on the western margin of the Irish Shelf, 200 km west of Ireland (Fig. 2.1). Water depths vary from 350 m in the northern part to 3000 m in the southwest (Naylor and Shannon, 1982). This basin is bounded to the north by the Slyne Ridge and Porcupine Bank, to the east by the Irish Mainland Shelf and to the west by the Porcupine Ridge (Fig. 2.1). In the southwest, it opens out into the Porcupine Abyssal Plain (4000 m of water depth) (Naylor and Shannon, 1982).

The bathymetry of the Porcupine Seabight shows the complexity of the underlying geology with a Middle to Late Jurassic failed rift and features composed of Precambrian rocks,

deformed Upper Paleozoic strata, Mesozoic strata, and a Cenozoic sediment cover on top (Naylor and Shannon, 1982). It corresponds to a deep sedimentary trough, i.e., the Porcupine Basin, fault-bounded on its western and eastern margins and filled with post-rift sediments with thicknesses of up to 10 km at their centre (Naylor and Shannon, 1982). The evolution of the basin is directly related to the opening of the North Atlantic Ocean (Johnston et al., 2001) with an episodic crustal extension during the Permo–Triassic to Early Cretaceous times (Croker and Shannon, 1995; McDonnell and Shannon, 2001), followed by an extensive phase during the Late Jurassic to Early Cretaceous (Johnston et al., 2001; McDonnell and Shannon, 2001). Thermal subsidence occurred afterwards and created an accommodation space for the Late Cretaceous and Cenozoic sediments (McDonnell and Shannon, 2001).

Several margin-wide unconformities have been identified and correlated through stratigraphic and sedimentary comparisons of the Cenozoic evolution of the Porcupine and Rockall basins (McDonnell and Shannon, 2001). Within the Neogene, two major unconformities are relevant for this study. The Early Miocene C20 unconformity was caused by a sea level fall related to the last pulses of the Alpine Orogeny (McDonnell and Shannon, 2001). This unconformity has been identified by Van Rooij et al. (2003) on high-resolution seismic profiles as a regional discontinuity RD2 occurring in the lower Middle Miocene in the BMP (Fig. 2.2). This regional discontinuity separates seismic stratigraphic units U3 and U2 (Van Rooij et al., 2003). Within unit U3, the local occurrence of upslope migrating sigmoidal deposits already suggests the presence of intensified bottom currents (Van Rooij et al., 2003). Unit U2, characterised by acoustically transparent facies, was deposited over the entire area (Van Rooij et al., 2003) and has a homogenous composition with silty clays of a Late Miocene age (Kano et al., 2007; Louwye et al., 2008).

The Early Pliocene C10 unconformity, observed by Stoker et al. (2001, 2005) along the NW European Atlantic margin, is related to the onset of global cooling and Northern European glaciation. Van Rooij et al. (2003) correlated this to a rather intra-Pliocene regional discontinuity RD1 in the Porcupine Seabight. Several provinces of the CWC coral mounds were also recognised along the northern and eastern slopes of the Porcupine Seabight (De Mol et al., 2002), all rooted upon this RD1 unconformity and associated with relatively strong bottom currents (Van Rooij et al., 2003; Huvenne et al., 2009). Especially in the BMP, along the eastern slope, this has created a typical small-scale contourite depositional system, corresponding to the youngest unit U1 (Van Rooij et al., 2003).

2.2.2 Hydrographic setting

The present-day water mass stratification related to the Belgica Mound Drift (Figs. 2.2, 2.3) shows a seasonal thermocline at a depth of 50 to 70 m (White, 2007). On average, between 0 and 600 m of water depth, the Eastern North Atlantic Water (ENAW), a warm (9.5–12°C) and saline (35.47–35.6) water mass, can be observed (Rice et al., 1991; New et al., 2001; White, 2007; Dullo et al., 2008). A permanent pycnocline separates the ENAW and the MOW at a depth of approximately 700 m (Pingree and Le Cann, 1990; Rice et al., 1991; White, 2007). A salinity maximum is observed between 800 and 1000 m of water depth (Fig. 2.3) and corresponds to the MOW, associated with salinity and temperature ranges of 35.47–35.55 and 8–9.5°C, respectively (Dullo et al., 2008). The studied seafloor section ranges from 500 to 900 m of water depth and thus correlates to the interface between the ENAW and the MOW (Figs. 2.2, 2.3). The main water mass circulation in the present and the past has thus been influenced by the MOW.

The MOW has been active since the end of the Messinian salinity crisis (Khélifi et al., 2009). Since the lower Pliocene, with the start of glacial–interglacial cycles and the onset of the present-day current circulation regime, the MOW has been engaged in the development of contourite drifts and CDSs at intermediate water depths all over the NE Atlantic margin (Khélifi et al., 2009, 2014), from the Gibraltar Strait to the north of the Porcupine Bank (Iorga and Lozier, 1999; van Aken, 2000; McCartney and Mauritzen, 2001). The glacial–interglacial cycles had an impact on the establishment of the modern North Atlantic stratification and the deep-water circulation by changing the production and pathways of water masses, including the MOW (Stow, 1982; Pearson and Jenkins, 1986). The contourite drifts deposited along the NW European margin thus form sedimentary records of the palaeoceanographic evolution of the MOW (Van Rooij et al., 2007; Ercilla et al., 2008; García et al., 2016; Hernández-Molina et al., 2016; Liu et al., 2020). Its reintroduction in the Porcupine Seabight within the course of the Pliocene is thought to be the origin of RD1 (Van Rooij et al., 2003, 2009).

According to White (2001), the general sea surface circulation in the Porcupine Seabight is cyclonic and influenced by a boundary current, the European Slope Current (ESC; Toucanne et al., 2021), with at its upper levels the Shelf-Edge Current (SEC), which is a northward-flowing slope current (Pingree and Le Cann, 1989). The SEC carries the upper part of the ENAW northwards along the NE Atlantic margin (Rice et al., 1991; New et al., 2001; White, 2007). The boundary current can be observed near the seafloor, with persistent and alongslope bottom currents that are stronger closer to the seafloor (White, 2001). In addition to this general cyclonic circulation, there are local variations in the direction and speed of those bottom currents on the eastern flank of the Porcupine Seabight and around the depth of the study area (Figs. 2.2, 2.3). These variations are caused by a number of processes, including the strong semidiurnal to diurnal tides with a seasonal response (Pingree and Le Cann, 1989, 1990; Rice et al., 1991). The local intensification of the bottom currents is related to internal wave resonance and enhanced diurnal baroclinic tides occurring at the permanent pycnocline (Pingree and Le Cann, 1989, 1990; Rice et al., 1991; White, 2007).

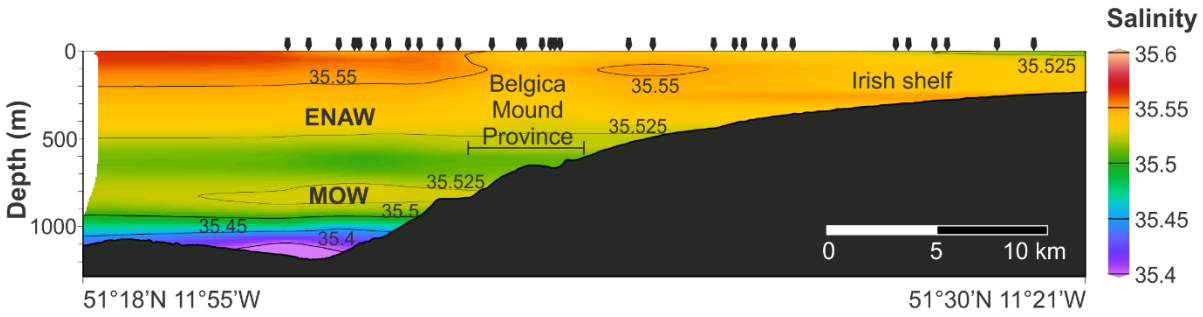

Figure 2.3. Salinity-versus-depth cross-section profile located over the study area (location: Fig. 2.1), based on CTD data (black arrows) from the World Ocean Database (Boyer et al., 2018). The profile was produced using Ocean Data View (Schlitzer, 2021). ENAW and MOW, respectively, stand for Eastern North Atlantic Water and Mediterranean Outflow Water.

2.3 Materials and methods

The Belgica Mound Drift, 10 km long and 8 km wide (Fig. 2.1), has been covered by a large network of 1500 km high-resolution single-channel seismic reflection profiles obtained

throughout several surveys with RV Belgica from 1997 to 2018 (Van Rooij et al., 2003, 2007). This “legacy” dataset was used to plan a seismic survey with higher-density line spacing covering 50 km² located at 460–900 m of water depth over the study area (Fig. 2.1). This was carried out during the RV Belgica 2019 survey using a SIG sparker source and a single-channel SIG surface streamer. This new dataset yielded 44 high-resolution seismic profiles, from 5 to 10 km in length, spaced between 0.125 and 0.25 nautical miles (nm) in the WSW–ENE direction and between 0.25 and 0.5 nm in the NNW–SSE direction, and is characterised by a vertical resolution of 1.5 m.

During this survey, the seismic source was fired every 2 s at 600 J with a record length of 2.7 s TWT, allowing a penetration depth of around 400 m under the seafloor. During the acquisition, the velocity of the ship was maintained at around 3 knots. The data were digitised with an iXblue Delph system at a sampling frequency of 8 kHz and recorded in SEGY floating-point format. The data were processed in RadExPro 2016.3. Several filters were used on all processed lines: a burst noise removal, a bandpass filter (on average, low-cut ramp of 100 to 150 Hz and high-cut ramp of 1000 to 1500 Hz) and a swell filter. The visualisation and interpretation were carried out using S&P Global Kingdom Geoscience software. The drift and the two major unconformities (RD1 and RD2) had been previously identified by Van Rooij et al. (2003, 2007) and confirmed by IODP Exp. 307 (Ferdelman et al., 2006). The basic concepts of seismic stratigraphy (Mitchum et al., 1977; Badley, 1988) were applied for the identification and description of the spatial and temporal evolution of the drift.

The 25 m resolution-processed bathymetric data (Fig. 2.1) were made available by INFOMAR (2023) and were used to realise the slope gradient map with Global Mapper software. The combined use of the bathymetry, the slope gradient and the seafloor reflections on the seismic profiles (Fig. 2.1) assisted in the morphosedimentary mapping. The salinity data (Fig. 2.3) are based on CTD data from the World Ocean Database (Boyer et al., 2018) and were used for the identification of the water masses. Fig. 2.3 was produced using Ocean Data View (Schlitzer, 2021).

2.4 Results

2.4.1 Morphosedimentary mapping

Although the eastern slope of the Porcupine Seabight has a relatively constant and gentle slope of 1 to 2° towards the west (Fig. 2.4A), the bathymetry is more variable on a smaller scale in the study area (Fig. 2.1). Fig. 2.4B is a revised map of the bathymetric data of a slope-parallel mounded, elongated (separated) and confined contourite drift (Van Rooij et al., 2003), here called the Belgica Mound Drift. It is enclosed by an escarpment, conical CWC mounds (Henriet et al., 1998; De Mol et al., 2002) and moats.

The contourite drift partly overlaps with smaller and steeper CWC mounds along its northern and western edges (Fig. 2.4B). It is 36 km² in size and is located at 600–800 m water depth. This drift is roughly elongated in the NNW–SSE direction and confined in the W–E direction. It is 10 km long and 2.5 to 4 km wide, with the widest part on average in the south of the drift. In more detail, it can be separated into a northern and a southern sector, characterised by a change from a respective N–S and NW–SE orientation halfway along the length of the drift. A crest running is visible alongside the 600 m contour line in the northern sector and at 650 m

depth in the southern sector. The slope east of the crest corresponds to the average slope in the area, between 1 and 2° (Fig. 2.4A), while towards the west, the slope is slightly steeper, up to 7°.

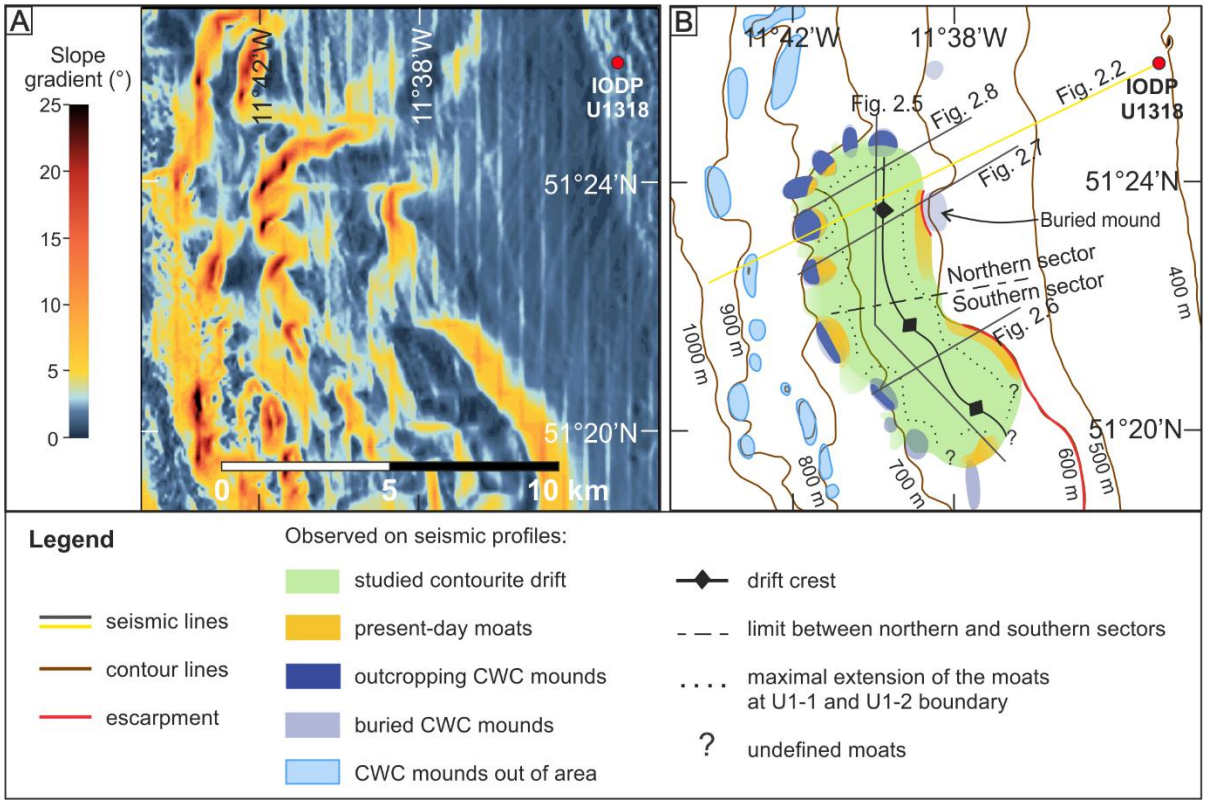

Figure 2.4. (A) Slope gradient map and (B) morphosedimentary map of the study area, based on bathymetric data (Fig. 2.1). The morphosedimentary map represents the present-day surface expression of the drift, including moats and their maximal extension according to the ID1 horizon (Fig. 2.5).

Along its eastern boundary, the southern sector of the drift, as well as its moats, terminate against an escarpment (Fig. 2.4B). This escarpment has a total length of 8 km (including 3.5 km inside the study area) with a NW–SE orientation and a slope gradient between 3 and 11° (Fig. 2.4A), bridging water depths of between 500 and 600 m.

The observed present-day moats (Fig. 2.4B) have a width between 200 and 650 m in the northern sector and 200 and 500 m in the southern sector. They are typically about 5 m deep, the height difference being measured with respect to the crest of the corresponding horizon of the drift. However, the moat connected to the main escarpment is up to 20 m deep and is significantly longer, up to 6.7 km. The second-longest moat is related to a minor escarpment (3 km long) and is 20 m deep, located at the eastern boundary of the northern sector (Fig. 2.4B). The smallest moats have a length of about 300 m along the CWC mounds in the northern sector. These moats generally feature an alongslope orientation and are located either upslope of the CWC mounds (W) or downslope of the escarpments (E). However, moats are not observed between the CWC mounds, making it difficult to clearly delimit the boundaries of the drift based on multibeam bathymetry alone, particularly on the NE side of the northern sector. Furthermore, at the transition between the northern and southern sectors, no moat has been observed on the eastern side over a length of 1 km (Fig. 2.4B). Even along

some of the CWC mounds, moats may be absent, such as in the northernmost part of the drift (Figs. 2.4B, 2.5). In the southernmost part, only one moat has been observed in the vicinity of buried CWC mounds. The location of the southern moat (Fig. 2.5) defines the southern limit of the drift.

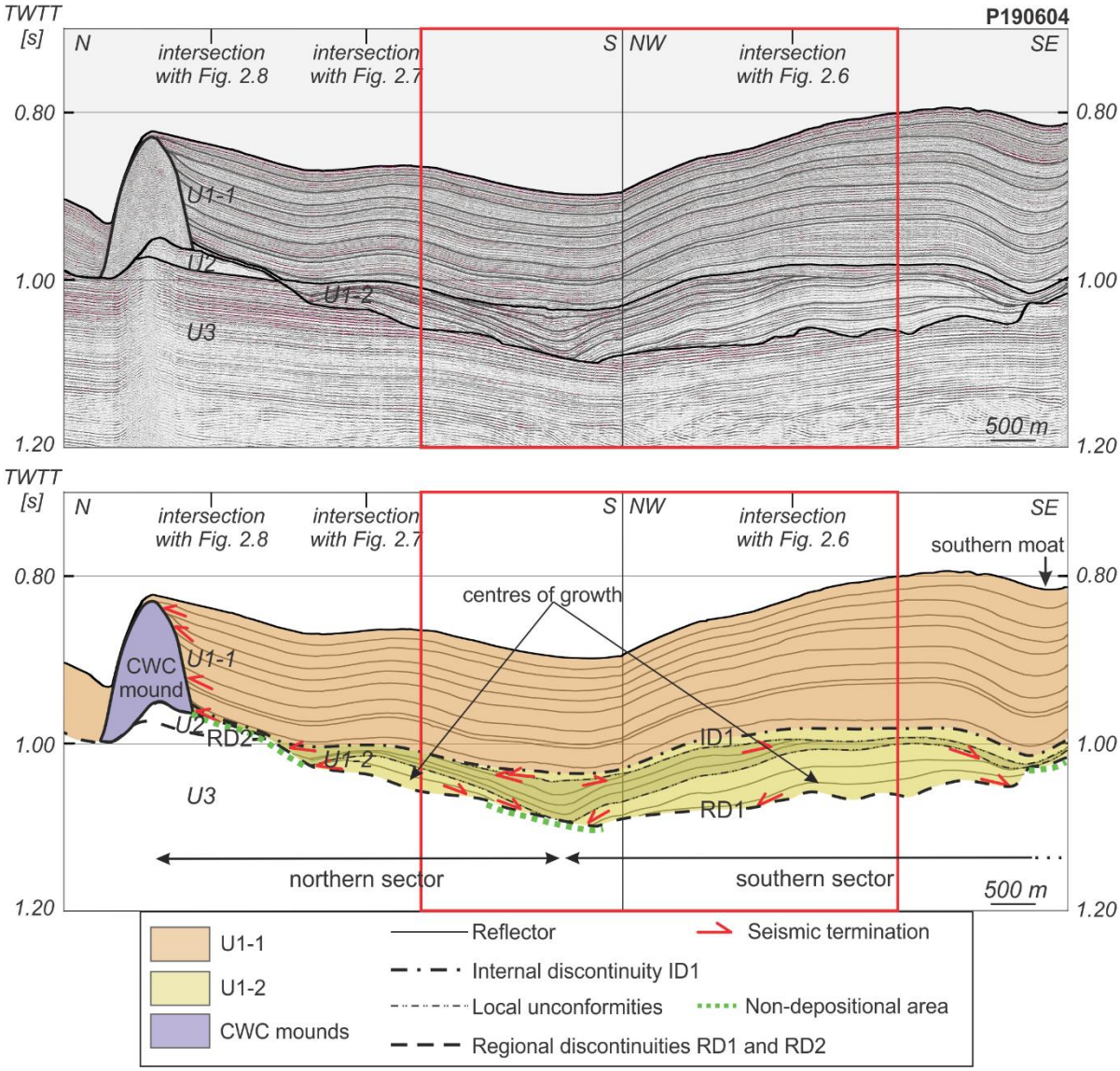

Figure 2.5. Seismic profile (location: Fig. 2.1) along the crest of the drift with the interpreted seismic stratigraphic units. The thick dashed lines represent the regional discontinuities (RD1 and RD2) and the boundary between U1-1 and U1-2 (ID1 horizon; internal discontinuity), while the thinner dashed lines are local unconformities within U1-2. The red rectangle corresponds to a part of the profile used as a reference in Fig. 2.9.

Twenty-six elongated CWC mounds are spread out over and adjacent of the study area (Fig. 2.4B). They have an elongated asymmetric elliptic footprint, mostly arranged in a SSE–NNW direction, lined up alongslope on the western edge of the contourite drift, between 600 and 900 m of water depth. More details on the general geometries were described by De Mol et al. (2002). Whereas smaller mounds (typically 10 m high) form single conical structures, larger mounds (at least 500 m wide) are seen to combine into clustered ridge structures. Twelve of

those mounds are directly spatially related to the sediment drift as they form the western (Figs. 2.6–2.8) and northern (Fig. 2.5) boundaries of the drift, with inferred slopes from 4 up to 25° (Fig. 2.4A). The steepest slopes have been observed on the NW side of the mounds. Seven of the mounds (Fig. 2.4B), especially in the northern sector, are partially outcropping downslope and are buried upslope (Figs. 2.6–2.8) along the moats of the drift, while the others are completely buried. The CWC mounds in the northern sector, with a W–E elongation, are more closely spaced (400 to 550 m between mounds), forming a tight barrier at the western side of the sediment drift. The mounds located in the southern sector are more averagely spaced (up to 1100 m between mounds) than in the northern sector and have a N–S elongation.

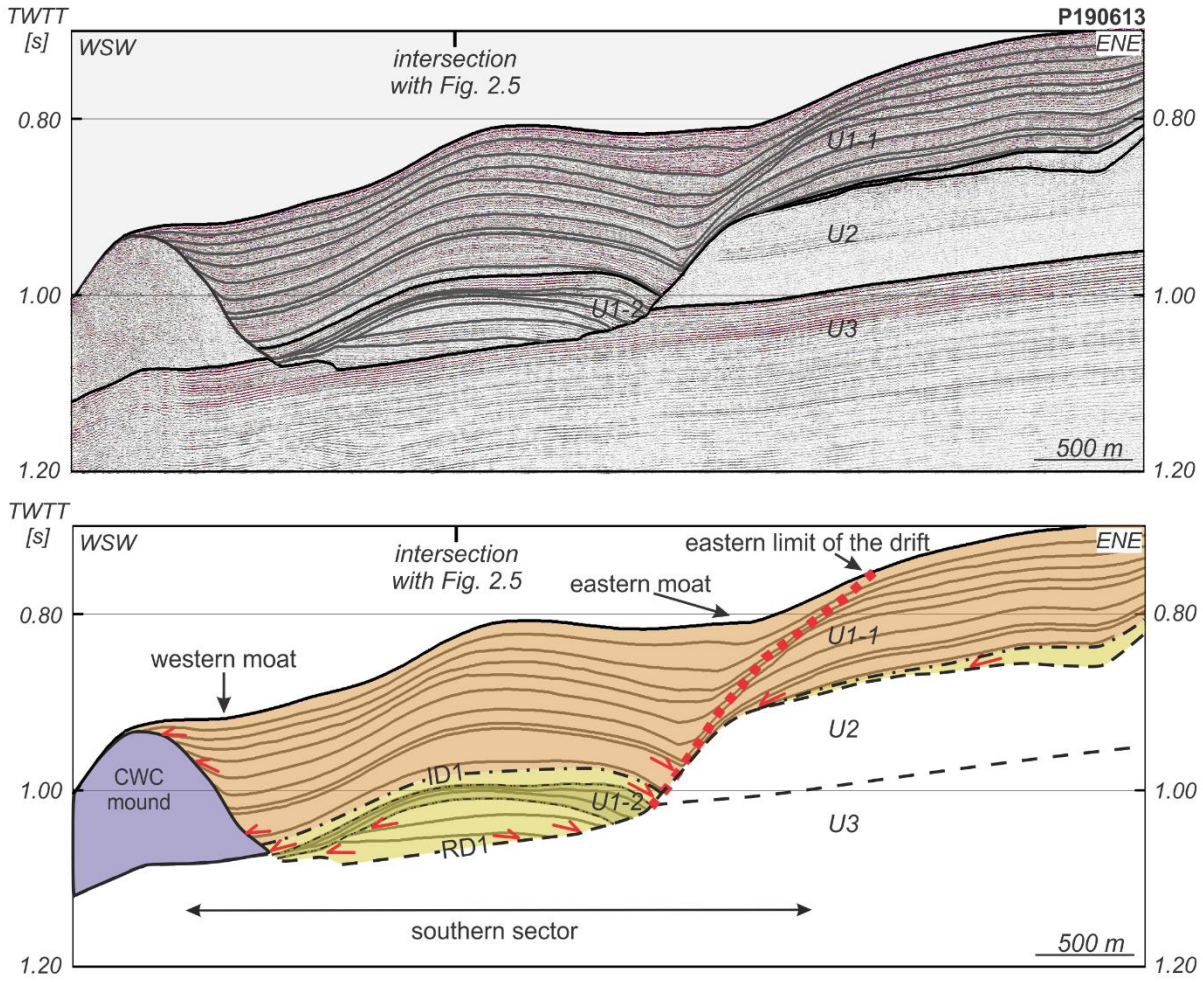

Figure 2.6. Seismic profile (location: Fig. 2.1) across the crest of the southern sector of the drift with the interpreted seismic stratigraphic units. The thick black dashed lines represent the regional unconformities (RD1 and RD2) and the boundary between U1-1 and U1-2 (ID1 horizon; internal discontinuity), while the thinner black dashed lines are local unconformities within U1-2. The red dashed line is the defined eastern limit of the drift. See legend in Fig. 2.5.

One isolated feature with a length of 850 m (Fig. 2.4B), visible on the eastern side of the northern sector of the drift, is completely buried (Fig. 2.7) and forms on its western side a seemingly small but steep escarpment, characterised by a slope of up to 16° (Fig. 2.4A) and between 580 and 660 m of water depth.

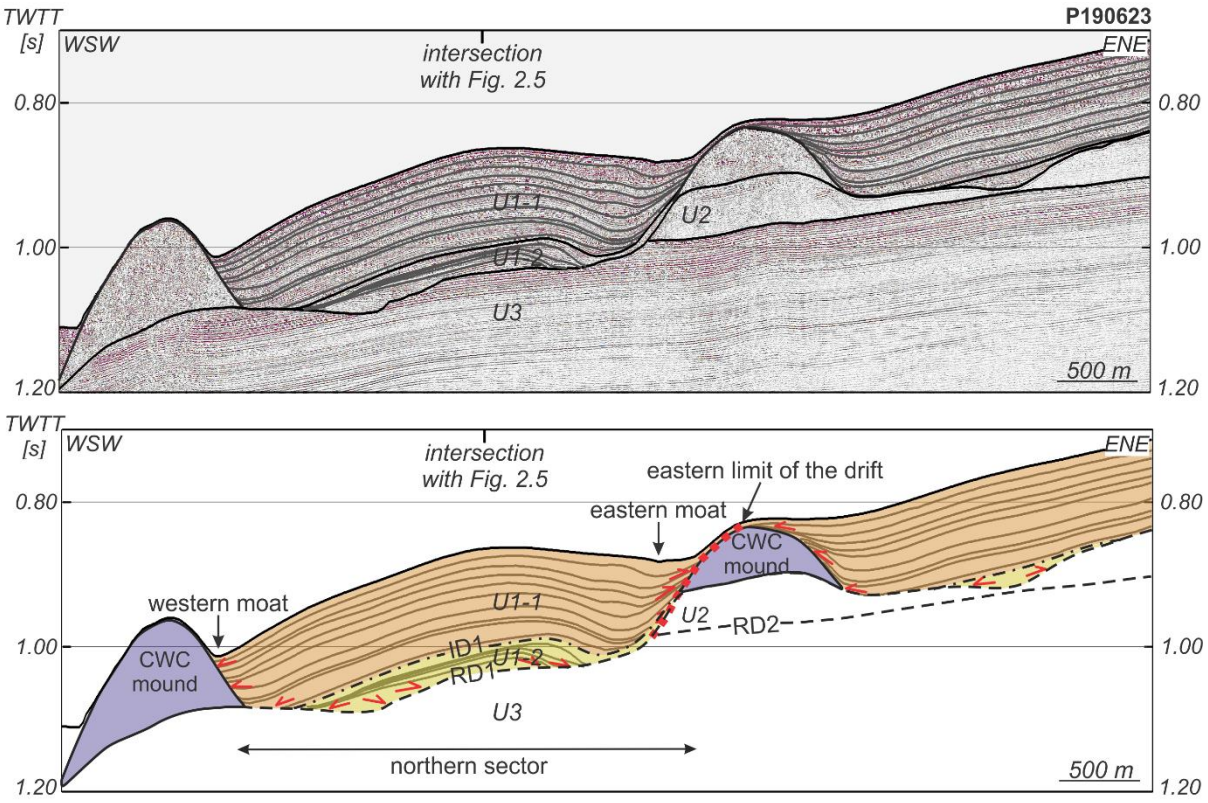

Figure 2.7. Seismic profile (location: Fig. 2.1) across the crest of the northern sector of the drift with the interpreted seismic stratigraphic units. The thick black dashed lines represent the regional unconformities (RD1 and RD2) and the boundary between U1-1 and U1-2 (ID1 horizon; internal discontinuity). The red dashed line is the defined eastern limit of the drift. See legend in Fig. 2.5.

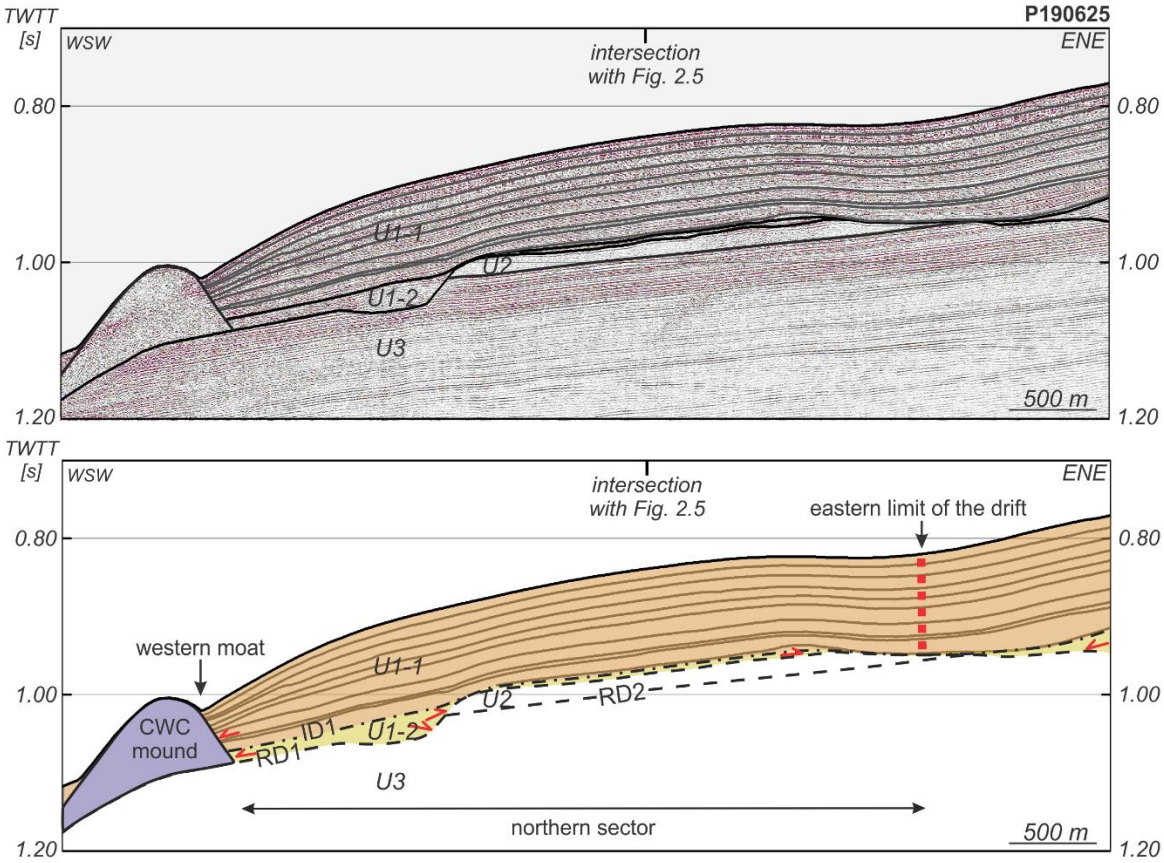

Figure 2.8. Seismic profile (location: Fig. 2.1) across the crest of the northern sector of the drift with the interpreted seismic stratigraphic units. The thick black dashed lines represent the regional discontinuities and the boundary between U1-1 and U1-2 (ID1 horizon; internal discontinuity). The red dashed line is the defined eastern limit of the drift. See legend in Fig. 2.5.

2.4.2 Seismic stratigraphy

The erosive event that created RD1 drastically changed the contemporaneous seafloor topography by deeply cutting into older strata (Fig. 2.5). It had a significant impact on the subsequent depositional and erosive processes and thus on the formation of the contourite drift, corresponding to the youngest unit U1 observed by Van Rooij et al. (2003, 2007). Therefore, the seismic stratigraphic description will be focused on the phases during and after the creation of this RD1 erosive discontinuity.

2.4.2.1 RD1 expression and morphology

The general morphology of the RD1 discontinuity in the study area, in combination with the location of CWC mounds, forms a confined “basin” paleosurface (Figs. 2.9A, E).

The RD1 discontinuity is an irregular erosive downslope-dipping surface, characterised by deep incisions of up to 200 ms TWT into the underlying units U2 and U3 (Figs. 2.5–2.8). Unit U2 is completely absent downslope in the west due to erosion. A few remnants remain at the northernmost boundary of the study area (Fig. 2.5), whereas lower U2 remains preserved upslope in the east (Figs. 2.6–2.8). Along the eastern boundary of the area, the thickness of U2 decreases from 150 to 0 ms TWT. This has created a N–S escarpment with relatively steep flanks that reach a maximum height of 200 ms TWT and a slope of approximately 15° on the

eastern side of the study area (Figs. 2.6, 2.9A). The upper part of unit U3 has also been eroded downslope, with predominant erosion in the centre of the area (Fig. 2.5). Hence, this erosion created at least the eastern flanks of the basin-shaped surface (Fig. 2.7). The northern and specifically western limits are formed by the alignment of the CWC mounds (Figs. 2.4, 2.9A).

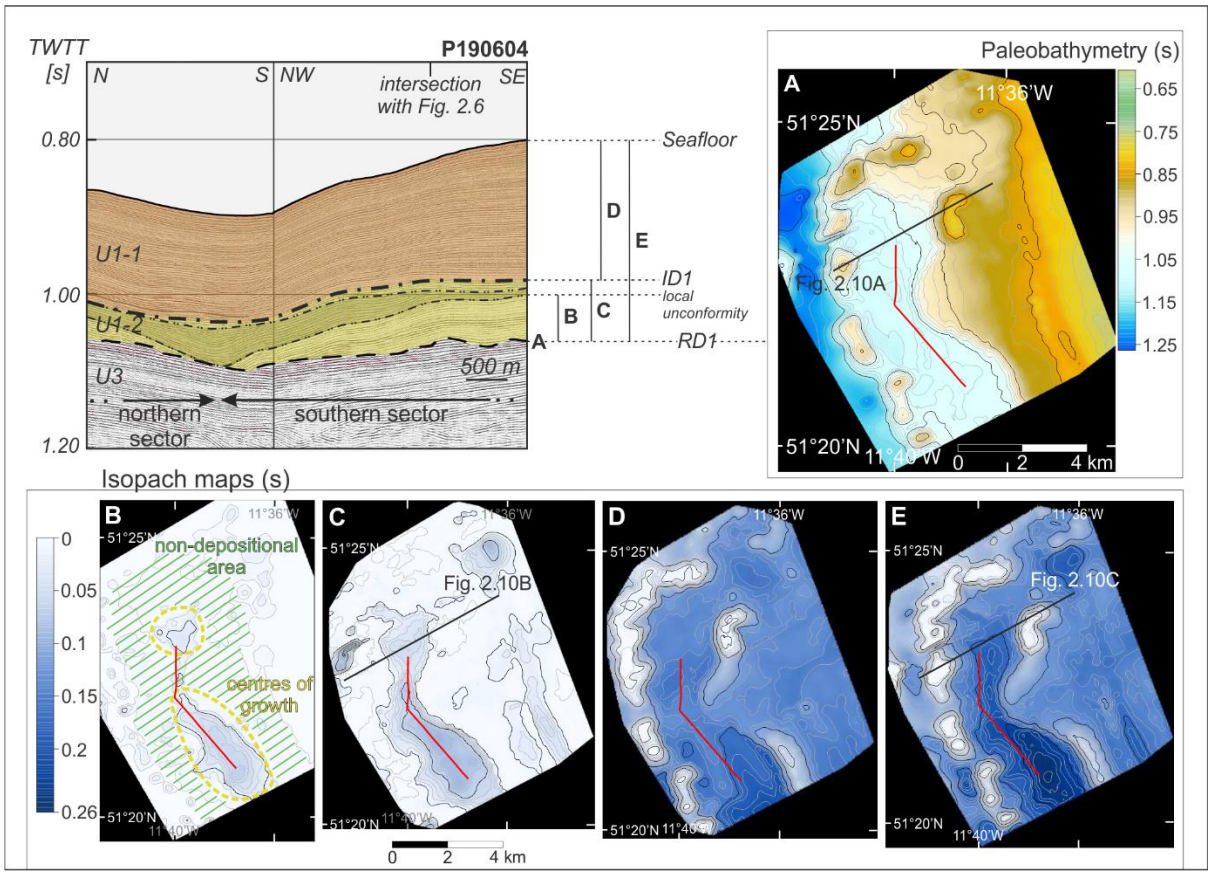

Figure 2.9. Section of Fig. 2.5 (red line in panels A, B, C, D and E), used as a reference to illustrate the drift isopachs and their corresponding reflectors. See legend in Fig. 2.5. (A) Paleobathymetry map of the RD1 surface (s TWT). The black line corresponds to Fig. 2.10A. Here, it is assumed that CWC mounds were fully grown before the start of the drift deposition. (B) Isopach map (s TWT) of the sediments deposited between RD1 and a local unconformity. The yellow dashed lines delimit the two centres of growth while the green dashed lines cover the non-depositional area. (C) Isopach map (s TWT) of the sediments deposited between RD1 and ID1 (internal discontinuity), i.e., the complete sub-unit U1-2. The black line corresponds to Fig. 2.10B. (D) Isopach map (s TWT) of the sediments deposited between ID1 and the seafloor, i.e., the complete sub-unit U1-1. (E) Isopach map (s TWT) of the sediments deposited between RD1 and the seafloor, i.e., the complete unit U1. The black line corresponds to Fig. 2.10C.

These ellipsoidal to conical asymmetric mounds have a broad base up to 1800 m wide and are rooted in alongslope trends on the RD1 unconformity on elevated topographic irregularities (Figs. 2.5, 2.7). They are acoustically transparent without any clear internal reflections. Diffraction hyperbolae conceal the true shape of the mounds, especially their base and limits (Figs. 2.5–2.8). The size of the mounds decreases from north to south, and their height above RD1 ranges between 35 and 175 ms TWT. Towards the southern part of the area, all mounds are buried under a thin sedimentary cover of up to 20 ms TWT.

The combination of the RD1 paleotopography, including the CWC mounds, is used for the construction of a paleobathymetric map from this composite surface (Fig. 2.9A). For the objectives of this paper, focusing mainly on the sediment dynamics leading to the deposition of unit U1, it is assumed that the CWC mounds were fully grown before the deposition of unit U1 (Huvenne et al., 2009). This composite paleotopography basically forms a NNW–SSE artificial channel of 2 to 3 km wide and 10 km long, with an average slope between 0 and 3°. Its flanks on the east are about 200 ms TWT high, whereas its slopes range between 13 and 25° at the escarpments and between 6 and 16° in the central area. The western flanks, delimited by CWC mounds, are, on average, 150 ms TWT high with slopes of 20 to 30°. As such, this pre-U1 paleotopography may be considered a peculiar confined basin (or trap) in which unit U1 was deposited.

2.4.2.2 Post-RD1 deposits

The contourite drift identified by Van Rooij et al. (2003) is formed by unit U1 (Figs. 2.5–2.8), covering the entire study area and a part of the CWC mounds. Its seismic facies are characterised by high-frequency, continuous, sub-parallel to mounded reflections with mainly high but variable amplitudes. On a smaller scale, there are various reflection characteristics.

In general, the drift is thinning to the north, with a maximum thickness of up to 250 ms TWT for the southern sector and 200 ms TWT for the northern sector, respectively (Figs. 2.6, 2.9E). The maximum thickness is located in the centre of the sectors. The minimum thickness is reached at the extremities of the drift, either in the vicinity of the mounds, near the escarpments, or in the northern part (from 0 to 100–150 ms TWT) (Fig. 2.9E).

Unit U1 can be subdivided into two sub-units, U1-2 and U1-1, based on a marked difference in reflector configuration (Figs. 2.5–2.9). The boundary between both sub-units has been set at the last visible minor internal discontinuity (ID1). In general, the older sub-unit U1-2 is characterised by more chaotic, irregular reflectors and several minor unconformities, whereas sub-unit U1-1 displays continuous, regular and sub-parallel reflectors. Both sub-units have an overall upward convex geometry, flanked by moats. The moats are well developed during the deposition of U1-2 and are progressively phased out within the sediments of U1-1 (Figs. 2.5–2.8).

Sub-unit U1-2

Sub-unit U1-2 has been deposited directly upon the RD1 erosional unconformity. The reflectors downlap on RD1 in the centre of the deposit (Fig. 2.5) and on the eastern border (Fig. 2.6). They also onlap on RD1 and the CWC mounds towards the edges of the drift. Sub-unit U1-2 shows both mounded continuous and irregular reflectors with high lateral variability and several minor unconformities (Fig. 2.5). The maximum thickness of sub-unit U1-2 is about 80 ms TWT. It is composed of eight different smaller units, each with an average thickness of 16 ms TWT, showing diverse acoustic facies with low, medium and high amplitudes and frequencies (Table A.2.1 in Supplementary material). The stacking and stratigraphic relationship between these smaller units allow for the three main growth phases to be distinguished.

The deposition of sub-unit U1-2 was initiated (Figs. 2.5, 2.9B) from two distinct centres of growth. One centre of growth is located in the northern sector, with a length and width of 2.8 and 1.6 km, respectively, at the end of the first phase. The other centre of growth is located

within the southern sector and has a respective length and width of 4.7 km and 2.2 km, displaying a more elongated shape in a NW–SE orientation. This is in contrast to the northern centre, which does not display a clear orientation and has a more circular shape. Both centres are separated from each other by a non-depositional flat area (Fig. 2.9B). The southern centre of growth is more developed than the northern one, with a thicker sediment deposition of a maximum of 80 ms and 48 ms TWT, respectively. This first phase mainly shows a progradational deposition with a lateral filling of the basin for the northern centre of growth and in a more dominant NW–SE direction for the southern centre of growth.

The second phase is delimited by two minor unconformities (Figs. 2.5, 2.9), which can be observed with the entire Belgica Mound Drift. They are irregular in extent, and their style of incision is complex and spatially variable. They cut 1 to 3 ms TWT deep and between 700 and 1000 m wide with the first sub-unit U1-2 deposits at the edges of the drift (Fig. 2.5). The second phase corresponds to a mixed period with progradational phases along the sides in the W–E direction. At the end of the second phase, the northern and southern centres of growth were 3.2 km long and 2.2 km wide and 4.5 km long and 2.4 km wide, respectively. This was also accompanied by aggradational phases in the middle of the centres of growth towards the N–S and NW–SE direction. The non-depositional area in between the two centres of growth and identified during the first phase has evolved into a concave-up moat. It was progressively filled by 48 ms TWT of sediment (Fig. 2.5). After that, the two centres of growth were completely connected.

The last phase is mainly progradational (Fig. 2.9C) in the southern centre of growth (4.7 km long and 2.7 km wide). It corresponds to a thin deposit delimited by two minor unconformities, the top one being the boundary between U1-2 and U1-1 (ID1), which has a conformable character. This deposit is almost absent in the northern centre of the growth, either by a lack of deposition or eroded by the ID1 event. Reflection terminations indicate that ID1 is of erosional origin, and this discontinuity can be mapped throughout the drift.

Sub-unit U1-1

Sub-unit U1-1 is a well-stratified unit with mounded continuous regular horizons inherited from the final U1-2 morphology at ID1 (Fig. 2.5). This unit has continuous seismic characteristics throughout the entire drift and is deposited over the initial two centres of growth (Fig. 2.9D). In sub-unit U1-1, the two centres of growth correspond to the northern and southern sectors. They are consequently referred to as “sectors” in the next paragraphs. The maximum thickness of sub-unit U1-1 amounts to 200 ms TWT. The difference in thickness between the two sectors (Fig. 2.9D) in sub-unit U1-1 is not as straightforward as in sub-unit U1-2 (Figs. 2.9B, C). Nevertheless, in sub-unit U1-1, the southern sector features higher accumulation rates up to 200 ms TWT, compared to the northern sector, up to 140 ms TWT, which is demonstrated by the isopach maps of sub-unit U1-1 (Fig. 2.9D) as well as of the entire unit U1 (Fig. 2.9E). Within sub-unit U1-1, up to 10 smaller cyclic sediment packages with an average thickness of 20 ms TWT can be identified, based on their variable seismic facies, varying between low, medium and high amplitudes and frequencies (Table A.2.1). At IODP site U1318, only the six top packages are present (Fig. 2.2). There, and along the edges of the study area, sub-unit U1-1 is directly deposited on top of RD1 and progressively fills the moats. This is in contrast to the centre of the basin, where sub-unit U1-1 directly covers U1-2, separated by ID1. Sub-unit U1-1 shows a downlap configuration on RD1 in the west of the drift (Fig. 2.7) and in the east (Fig. 2.6), whereas it shows an onlap on the CWC mounds and

RD1 in the west and north (Fig. 2.7). Still, within the morphology and depositional architecture of sub-unit U1-1, the two sectors of sub-unit U1-2 are reflected. Overall, sub-unit U1-1 displays a progradational depositional pattern near the moats in N–S and W–E directions and is aggradational at the centre of the drifts (Fig. 2.5).

Moats

Conversely to the complex depositional patterns of sub-unit U1-2, the rather uniform nature of the main body of sub-unit U1-1 does not hint at a chaotic depositional pattern indicating vigorous currents. Contrastingly, the evolution of its moats shows a more spatial and temporal variability. In order to better characterise this evolution, the moat classification of Wilckens et al. (2023) is used based on several key seismic profiles (Figs. 2.5–2.8).

The maximal extension of the moats at ID1 was between 150 and 1000 m wide. At the onset of sub-unit U1-2, the moats were either exclusively concave-up (western moats in Figs. 2.6, 2.8 and southern moat in Fig. 2.5) or flat-based (eastern moats in Figs. 2.6, 2.7). These moats often evolved to a concave-up shape (eastern moat in Fig. 2.6 and western moat in Fig. 2.7) during the progressive deposition of the contourite drift. In sub-unit U1-2, the moats mainly mixed depositional-erosional as demonstrated by the downlapping reflectors (both moats in Fig. 2.6 and western moat in Fig. 2.7). At the base of sub-unit U1-1, the moats mainly show a concave-up geometry and are either exclusively constructional with onlapping reflectors (southern moat in Fig. 2.5 and Fig. 2.6), or they are mixed depositional-erosional moats evolving towards constructional moats (western moat in Fig. 2.7). During the deposition of sub-unit U1-1, some moats eventually disappear at several locations of the drift (western moat in Fig. 2.6).

2.5 Discussion

2.5.1 Morphosedimentary evolution of the Belgica Mound Drift

The new pseudo-3D seismic stratigraphic analysis of the Belgica Mound Drift architecture suggests that its evolution has followed three main stages (Fig. 2.10). The conceptual model of the evolution of the drift (Fig. 2.10) is based on the model developed by Huvenne et al. (2009), which focused on the CWC mounds. The revised model presented herein focuses on the evolution of the adjacent contourite drift, taking into account the new high-resolution chronostratigraphic framework.

2.5.1.1 Pre-drift processes related to RD1 (Pliocene–Early Pleistocene)

RD1 is a regionally pronounced erosive discontinuity characterised locally by relatively steep escarpments, laying the foundations of the RD1 paleotopography (Figs. 2.9A, 2.10A). Its effects can still be observed in present-day bathymetry (Figs. 2.1, 2.4). Within the study area, the RD1 unconformity cuts into units U2 and U3 and has almost entirely removed unit U2 (Figs. 2.5–2.8). As also observed by Van Rooij et al. (2003) in the channels surrounding the study area, the irregular RD1 topography was likely created by strong and persistent S–N contour currents (Fig. 2.10A). This peculiar topography contributes to the local intensification of the bottom currents and their consequent erosive nature. Van Rooij et al. (2003) correlated this to the start of the effect of glacial–interglacial cycles on the deep-water circulation as well

as to the reintroduction of the MOW in the NE Atlantic during the Pliocene (Stow, 1982; Pearson and Jenkins, 1986). Subsequent research by Khélifi et al. (2014) indicates a reduction in the MOW flow from 2.95 Ma to 2.65 Ma, corresponding to the onset of the major Northern Hemisphere Glaciation. The corresponding sea level falls and subsequent reduction in Atlantic versus Mediterranean exchange, thus influencing the MOW production, may have caused the reduction in the bottom-current intensity in the Porcupine Seabight, bringing the RD1 event to an end. The later reintroduction of the MOW during interglacial periods will have increased the bottom-current intensity again, likely creating hydrodynamic conditions leading to the onset of CWC mound growth (Huvenne et al., 2009; Raddatz et al., 2011), around 2.7 Ma, during the Late Pliocene (Kano et al., 2007).

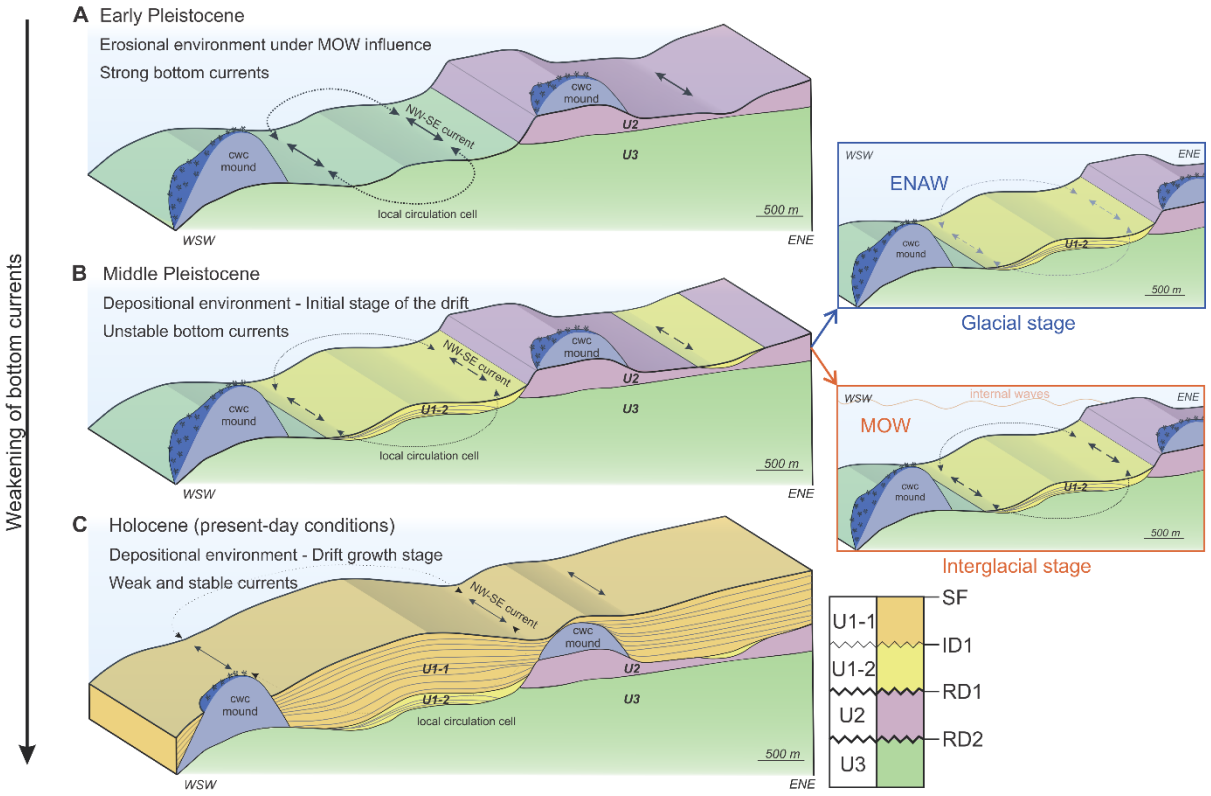

Figure 2.10. 3D sketch of the Belgica Mound Drift (northern sector) evolution from the Early Pleistocene to the present day: (A) Before the deposition of the drift (RD1 paleotopography in Fig. 2.9A); (B) during the onset of the drift (isopach map in Fig. 2.9C), with an example during the glacial (blue) and interglacial (orange) stages; and (C) during the growth stage of the drift (isopach map in Fig. 2.9E). The arrows correspond to the deduced intensity of the current in the moats, varying from strong (A), strong and unstable (B) to weaker and more stable (C).

From seismic profiles alone, it remains complicated to identify the CWC mound growth stages. Hence, it is difficult to compare the evolution of the CWC mounds to the contourite drift evolution. Therefore, it was previously assumed by Huvenne et al. (2009) and Thierens et al. (2010) that the CWC mounds were already fully developed before the deposition of unit U1 (Fig. 2.10A). The current seismic stratigraphy confirms that the CWC mound growth was initiated before the onset of the contourite drift (Figs. 2.5–2.8). As suggested by Van Rooij et al. (2003) and confirmed by the present more detailed dataset, the lower unit U1 horizons show an onlap relation with respect to the CWC mounds (Figs. 2.5–2.7), which are

asymmetrically embedded in the contourite drift (Figs. 2.5–2.8). The CWC mounds thus reached a significant size before the onset of the drift deposition, as evidenced by the basin-like area formed by the CWC mounds' alignment and the steep flanks cut into units U2 and U3 (Fig. 2.9A). They had a direct influence on the onset of the drift (Fig. 2.9) and on the evolution of the moats (Fig. 2.4) since they drove the intensification and pathways of the bottom currents (Van Rooij et al., 2003; Huvenne et al., 2009).

2.5.1.2 Contourite drift inception (Early Pleistocene–Middle Pleistocene)

The isopach map related to the onset of the contourite drift (Fig. 2.9B) shows the onset only occurred in the central area of the southern centre of growth, as the oldest sediment package can be observed there (Figs. 2.5, 2.9B). This can be interpreted by the action of locally weaker currents on the lee side of the CWC mounds and enhanced currents in the direct vicinity of the CWC mounds, as well as near the steep eastern flanks and in the northern sector. The occurrence of stratigraphically younger contourite drift deposits in the second centre of growth (Fig. 2.5), located in the central area of the northern sector, indicates the sediment was deposited later (Fig. 2.10B). As such, it is suggested that both centres of growth, both visible in the present-day bathymetry as the two sectors, started growing independently from each other, and were separated by a non-depositional area (Figs. 2.5, 2.9B). The difference in shape and elongation between both centres of growth (Fig. 2.9B) may be related to the inferred circulation pattern of the contemporary bottom currents. The elongated shape of the southern centre of growth (Fig. 2.9B) is associated with bottom currents with an inferred NW–SE orientation circulating on the western and eastern sides of the drift, represented by the moats. The more circular shape of the northern centre of growth (Fig. 2.9B) is related to a more complex environment with bottom-current deflection caused by the presence of the CWC mounds, locally accelerating the currents, preventing deposition in the northern centre of growth and between the two centres (Fig. 2.9B). As such, this may suggest the presence of a local circulation cell, stuck in the northern part of the confined basin, due to topographical deflection (Fig. 2.9B). The geometry of the moats was exclusively concave-up (western moats in Figs. 2.6, 2.8 and southern moat in Fig. 2.5) or flat-based (eastern moats in Figs. 2.6, 2.7) at the start of sub-unit U1-2. However, it evolved towards concave-up (eastern moat in Fig. 2.6 and western moat in Fig. 2.7) and mainly a mixed depositional-erosional pattern (both moats in Fig. 2.6 and western moat in Fig. 2.7) with the progressive infill of the basin. Also, the seismic stratigraphic analysis of sub-unit U1-2 infers various growing directions and several internal unconformities (Figs. 2.5–2.8, 2.10B). Its rather irregular horizons gradually build up from the central part of the northern and southern centres of growth and progressively join in a later stage of sub-unit U1-2 by the partial filling of the previously non-depositional area (Figs. 2.5, 2.9C). This suggests a decrease in the intensity of the local hydrodynamic conditions, leading to less vigorous bottom currents (Fig. 2.10C). This shows, on average, a slowing down of the NW–SE currents and the circulation cell (Fig. 2.9C), as well as a likely increase in sediment input in the vicinity of the mounds and flanks where sediment started to accumulate (Fig. 2.10C). The internal unconformities, irregular horizons, various growth directions and the mixed nature of the moats highlight unstable currents, occasionally increasing in intensity, inducing possible erosion of sub-unit U1-2, or decreasing in intensity, allowing depositional processes.

2.5.1.3 Contourite drift development (Middle Pleistocene–present day)

The two centres of growth identified in U1-2 morphologically correspond to the present-day northern and southern sectors (Fig. 2.9). This inherited morphology results in the continued evolution of the two sectors (Fig. 2.5), enclosed by the confined basin from CWC mounds and erosive escarpments.

Within sub-unit U1-1, the southern sector still shows a relatively thicker sediment accumulation compared to the northern sector (Fig. 2.9D). This may still be related to the local intensification of the bottom currents in the northern sector due to the forcing of the currents into a circulation cell by the surrounding CWC mounds. Alternatively, this may indicate proximity to sediment sources from a southern location, such as the Gollum Channels, located south of the study area. Verweirder et al. (2021, 2023) have already demonstrated that this channel system was more active during glacial periods and was the major sediment source in the Porcupine Seabight.

The mapped moats in the southern sector indicate that the bottom currents maintained a NW flow direction throughout U1-1 deposition (Fig. 2.9D). Within sub-unit U1-1, these moats are mainly concave-up and evolved from mixed depositional-erosional moats towards constructional moats (western moat in Fig. 2.7). Up to about 25% of the moats even completely disappear. According to Wilckens et al. (2023), this suggests an average weakening of the bottom currents. Although the intensity of the bottom currents seems to decrease, the moats near the escarpments and CWC mounds are still active (Figs. 2.4, 2.6–2.8). This local intensification would be due to topographic steering where gentle currents are still locally enhanced, as, for example, identified by Vandorpe et al. (2023) offshore Morocco. In contrast with the previous sub-unit, sub-unit U1-1 is characterised by one main growth style (Fig. 2.5) with continuous and mounded reflectors, prograding along the edges and aggrading along the crests of the two sectors (Figs. 2.5, 2.10C). This variation in seismic facies and geometry suggests a switch from an erosive to a depositional-dominated environment with a weakening and possible stabilisation of the bottom currents and a potentially increased sediment input throughout the entire drift (Fig. 2.10C). This has led to the progressive disappearing of the moats (Figs. 2.6–2.8) and a partial burial of the CWC mounds (Figs. 2.5–2.8). This particular switch coincides with the start of deposition at IODP site U1318 (Fig. 2.2).

2.5.2 Implications for local chronostratigraphic framework

Sub-unit U1-2 and the oldest strata of U1-1 are deposited within the confined basin created by a combined surface formed by the RD1 paleotopography and CWC mounds. However, the most recent strata of sub-unit U1-1 are also deposited outside this area, such as at IODP site U1318 (Fig. 2.2), where sub-unit U1-2 is missing (Fig. 2.2). At IODP site U1318, of the 10 identified sediment packages of sub-unit U1-1 (Table A.2.1), only the six youngest sediment packages were deposited. Consequently, the oldest contouritic deposits, being the first sediment packages not present on IODP site U1318, are only preserved in the confined drift area. This could be due to a variety of factors, such as stronger bottom currents, likely associated with the SEC, preventing local sedimentation upslope. The observation of 4 m of medium to fine sand and gravel lag interbedded with silty clay at the base of U1 at IODP site U1318 (Ferdelman et al., 2006) could corroborate the hypothesis of a long-term non-deposition (Huvenne et al., 2009). The sediment is retained by the nepheloid layer at the

boundary between the MOW and ENAW (Figs. 2.2, 2.3), as also observed by Hanebuth et al. (2015) along the Galicia margin. This may account for the lack of sediment at IODP site U1318.

Thus, the numerous observations, analyses and dating realised from IODP Exp. 307 only yielded age constraints on the most recent part of the contourite drift (Fig. 2.2). The onset of unit U1 in the confined basin, and thus of the Belgica Mound Drift, should consequently be older than what has been defined by Kano et al. (2007) at IODP site U1318, i.e., 1.24 Ma, suggesting a probable Early Pleistocene age (Van Rooij et al., 2003, 2007). This may better correspond to the proposed depositional window between 2.1 and 1.7 Ma of sandy contourites at IODP site U1316 at the foot of the Challenger Mound by Huvenne et al. (2009). This window fits with an earlier initiation of the drift, still allowing 0.6 My for the CWC mound to reach a considerable size.

The marked difference in stratigraphic architecture between sub-unit U1-1 and U1-2 was most likely influenced by glacial–interglacial paleoceanographic changes throughout the Pleistocene, influenced by corresponding decreases and rises in sea level (Van Rooij et al., 2009) with a respective absence or presence of the MOW in the Porcupine Seabight (Raddatz et al., 2011). Huvenne et al. (2009), Foubert and Henriet (2009) and Kano et al. (2007) correlated the onset of contourite sedimentation to the first phase of the Middle Pleistocene Transition (MPT). Hence, sub-unit U1-1 would correspond to the units deposited in IODP sites U1316 and U1318 during and following the MPT (1.6–0.5 Ma; Huvenne et al., 2009) (Fig. 2.2). The MPT was characterised by the initiation of full glacial eccentricity-driven conditions with long-term (100 ky) cooling (Lisiecki and Raymo, 2005), increasing of the global ice volume (Berends et al., 2021), leading to decreased bottom-current speeds due to a reduced MOW production and outflow and higher sediment input due to lowered sea levels (Van Rooij et al., 2007; Huvenne et al., 2009). Those conditions during the MPT, while favouring the sedimentation in the area, made the Porcupine Seabight a hydrodynamic less intensive area and reduced the development of CWC mounds (Kano et al., 2007). Whereas decreased bottom currents and higher sediment input are generally advantageous for drift accumulation, this also signifies less favourable conditions for CWC mound growth, leading to CWC decay and potential burial (Hebbeln et al., 2016). After the MPT, a decrease in the MOW influence was also observed in the Goban Spur (Delivet et al., 2016) in contrast with proximal areas such as the Cadiz (Hernández-Molina et al., 2006, 2011, 2014) and the Le Danois CDS (Ercilla et al., 2008; Van Rooij et al., 2010; Liu et al., 2020).

This finally allowed the relatively fast accumulation of sub-unit U1-1 (Fig. 2.9D), leading to about 200 ms TWT since the MPT. Assuming an average P-wave velocity of 1600 m/s over this unit (Van Rooij et al., 2009), this may roughly have led to an accumulation rate of 17 cm/ky. In their late stage of development, most of the CWC mounds ended up buried under the youngest deposits of sub-unit U1-1, such as the example observed with the isolated eastern CWC mound (Fig. 2.7). This observation, as well as the moat evolution (Figs. 2.6–2.8), indeed highlights a change in the sedimentary environment, evolving from an erosional environment during the initiation of the CWC mounds to a mainly depositional environment in the present day (Fig. 2.10). Nevertheless, the present-day seabed morphology of the Belgica Mound Drift (Fig. 2.4) and its moats (Figs. 2.5–2.8) testify of the local contemporary (present interglacial) intensification of the bottom currents. The footprint of the RD1 paleotopography on the present-day topography (Figs. 2.4, 2.9), as well as the CWC mounds related to internal wave resonance and enhanced diurnal baroclinic tides occurring at the permanent pycnocline (Pingree and Le Cann, 1989, 1990; Rice et al., 1991; White, 2007), which coincides with the

ENAW-MOW interface, play a key role in the enhancement of the bottom currents and on the evolution of the contourite drift.

2.6 Conclusions

This work, focusing on the small-scale Belgica Mound Drift, has shown that a high-resolution pseudo-3D dissection and detailed analysis of a contourite drift yields valuable insights into its spatial and temporal evolution, including its onset and growth patterns. It serves as a showcase of past oceanographic information, specifically for the relative intensity and circulation pattern of the bottom currents at the origin of the drift's morphology.

More specifically, the architecture of this confined contourite drift gave insight into three distinct evolutionary stages, each of which is related to a major change in paleoceanography, affecting both the bottom-current intensity and sediment input. The pseudo-3D dissection allowed for the refinement of the temporal and spatial variability of contourite depositional processes driven by the MOW in its most distal occurrence within the eastern Atlantic Ocean.

- The pre-drift stage (Pliocene–Early Pleistocene) corresponds to the regional RD1 erosive event, which was caused by the reintroduction of the MOW in the Porcupine Seabight, which allowed to shape a peculiar paleotopography, strongly influencing the ensuing sediment dynamics until the present day.
- The second stage (Early Pleistocene–Middle Pleistocene) shows the onset of actual contourite depositional processes, starting from two distinct centres of growth, strongly steered by previously defined topographic obstacles, progressively joining together. The initial deposition happened under the influence of a slightly weakened MOW compared to the first stage. This may be correlated to the general onset of glacial–interglacial cycles at the start of the Quaternary.
- During the third and final stage (Middle Pleistocene–present day), the Belgica Mound Drift development happens under a more stable but less dynamic environment, characterised by more continuous and mounded stratification. This last stage can be fully connected to the effects of the MPT, with a spatial variable reduction in the MOW-related bottom currents, as well as increasing sediment input from potentially nearby sources such as the Gollum Channels. Nevertheless, the present-day bottom currents, in an "interglacial mode", are still strong enough to allow the development of moats due to continued topographic steering (though attenuated with respect to the 2nd phase) by internal wave resonance and tidal enhancement at the MOW-ENAW interface.

During this work, the chronostratigraphic framework, previously established through IODP Exp. 307, required revision since it only provided information regarding the evolution of the most recent stage of the drift. This allowed the onset of contouritic processes to be reset to an earlier date, situated in a window around 2.1 Ma, as defined for IODP site U1316, but now expanded for the entire Belgica Mound Drift.

Finally, this study also contributed to a better insight into the co-habitation or co-evolution between the contourite drifts and the presence of framework-building ecosystems, such as CWCs. The evolution of the Belgica Mound Drift directly relates to the presence of CWC mounds. Their specific geographic occurrence on an already heavily accentuated

paleotopography locally enhanced the intensity and circulation pattern of the bottom currents, especially during the inception of contouritic sedimentation. The combined effects of the RD1 paleotopography and the CWC mounds can still be observed in the present-day bathymetry. This indicates that the mechanisms that shaped the past seabed may still be active today. Therefore, a deeper comprehension of the governing oceanographic processes taking place along the eastern slope of the Porcupine Seabight is required, especially in the drift area.

In general, the complexity of this small-scale contourite deposit is not represented by its youngest part, but it is inherited from its initiation phase. This study is a showcase of the past oceanographic information that is locked in all stages of drift growth. This observation was only possible due to the high-resolution pseudo-3D study of this contourite drift. Hence, it can be argued that valuable paleoceanographic information is only unlocked by choosing an appropriate seismic network (which does not necessarily need to be a costly 3D study), yielding valuable information on both its architectural framework and its spatial and temporal evolution.

Acknowledgements

This research was conducted in the framework of the FWO project DynaMOD (FWO grant 3G021719). Ship time on RV Belgica was provided by BELSPO and RBINS-OD Nature. We would also like to thank Koen De Rycker, Wim Versteeg and the RV Belgica crews for their help during the acquisition of the seismic data and Thomas Mestdagh for helping with the processing of the dataset. We also would like to thank the editor, Michele Rebesco, Rachel Brackenridge and the anonymous reviewers for their constructive comments, significantly improving this manuscript.

2.7 References

Badley, M.E. (1988). Practical Seismic Interpretation. Prentice Hall.

Berends, C.J., Köhler, R., Lourens, L.J., Wal, R.S.W., 2021. On the cause of the Mid-Pleistocene transition. Rev. Geophys. 59. https://doi.org/10.1029/2020RG000727.

Boyer, T.P., Baranova, O.K., Coleman, C., García, H.E., Grodsky, A., Locarnini, R.A., Mishonov, A.V., Paver, C.R., Reagan, J.R., Seidov, D., Smolyar, I.V., Weathers, K.W., Zweng, M.M., 2018. World Ocean Database 2018. A.V. Mishonov, Techincal Editor. NOAA Atlas NESDIS 87.

Collart, T., Verreydt, W., Hernández-Molina, F.J., Llave, E., León, R., Gómez-Ballesteros, M., Pons-Branchu, E., Stewart, H., Van Rooij, D., 2018. Sedimentary processes and cold-water coral mini-mounds at the Ferrol canyon head, NW Iberian margin. Prog. Oceanogr. 169, 48–65. https://doi.org/10.1016/j.pocean.2018.02.027.

Croker, P., Shannon, P., 1995. The petroleum geology of Ireland's offshore basins: Introduction. Geol. Soc. Lond. Spec. Publ. 93, 1–8. https://doi.org/10.1144/GSL.SP.1995.093.01.01.

De Mol, B., Van Rensbergen, P., Pillen, S., Van Herreweghe, K., Van Rooij, D., McDonnell, A., Huvenne, V., Ivanov, M., Swennen, R., Henriet, J.P., 2002. Large deep-water coral

banks in the Porcupine Basin, southwest of Ireland. Mar. Geol. 188, 193–231. https://doi.org/10.1016/S0025-3227(02)00281-5.

Delivet, S., Van Eetvelt, B., Monteys, X., Ribó, M., Van Rooij, D., 2016. Seismic geomorphological reconstructions of Plio-Pleistocene bottom current variability at Goban Spur. Mar. Geol. 378, 261–275. https://doi.org/10.1016/j.margeo.2016.01.001.

Dullo, W.-C., Flögel, S., Rüggeberg, A., 2008. Cold-water coral growth in relation to the hydrography of the Celtic and Nordic European continental margin. Mar. Ecol. Prog. Ser. 371, 165–176. https://doi.org/10.3354/meps07623.

Ercilla, G., García-Gil, S., Estrada, F., Gràcia, E., Vizcaino, A., Váquez, J.T., Díaz, S., Vilas, F., Casas, D., Alonso, B., Dañobeitia, J., Farran, M., 2008. High-resolution seismic stratigraphy of the Galicia Bank Region and neighbouring abyssal plains (NW Iberian continental margin). Mar. Geol. 249, 108–127. https://doi.org/10.1016/j.margeo.2007.09.009.

Faugères, J.C., Mézerais, M.L., Stow, D.A.V., 1993. Contourite drift types and their distribution in the North and South Atlantic Ocean basins. Sediment. Geol. 82, 189–203. https://doi.org/10.1016/0037-0738(93)90121-K.

Faugères, J.-C., Stow, D.A.V., Imbert, P., Viana, A., 1999. Seismic features diagnostic of contourite drifts. Mar. Geol. 162, 1–38. https://doi.org/10.1016/S0025-3227(99)00068-7.

Ferdelman, T.G., Kano, A., Williams, T., Henriet, J.-P., Expedition 307 Scientists (Eds.), 2006. Proceedings of the IODP, 307, Proceedings of the IODP. Integrated Ocean Drilling Program. https://doi.org/10.2204/iodp.proc.307.2006.

Foubert, A., Henriet, J.-P., 2009. Nature and Significance of the Recent Carbonate Mound Record: The Mound Challenger Code. Springer Berlin, Heidelberg. https://doi.org/10.1007/978-3-642-00290-8.

Freiwald, A., Wilson, J., Henrich, R., 1999. Grounding Pleistocene iceberg shape recent deep-water coral reefs. Sediment. Geol. 125, 1–8. https://doi.org/10.1016/S0037-0738(98)00142-0.

García, M., Hernández-Molina, F.J., Alonso, B., Vázquez, J.T., Ercilla, G., Llave, E., Casas, D., 2016. Erosive sub-circular depressions on the Guadalquivir Bank (Gulf of Cadiz): Interaction between bottom current, mass-wasting and tectonic processes. Mar. Geol. 378, 5–19.

Gilli, A., Anselmetti, F.S., Ariztegui, D., Beres, M., McKenzie, J.A., Markgraf, V., 2005. Seismic stratigraphy, buried beach ridges and contourite drifts: the Late Quaternary history of the closed Lago Cardiel basin, Argentina (49°S). Sedimentology 52, 1–23. https://doi.org/10.1111/j.1365-3091.2004.00677.x.

Hanebuth, T.J.J., Zhang, W., Hofmann, A.L., Löwemark, L.A., Schwenk, T., 2015. Oceanic density fronts steering bottom-current induced sedimentation deduced from a 50 ka contourite-drift record and numerical modeling (off NW Spain). Quat. Sci. Rev. 112, 207–225. https://doi.org/10.1016/j.quascirev.2015.01.027.

Hargreaves, P.M., 1984. The distribution of Decapoda (Crustacea) in the open ocean and near-bottom over an adjacent slope in the northern North-east Atlantic Ocean during autumn 1979. J. Mar. Bio. Assoc. U. K. 64, 829–857. https://doi.org/10.1017/S0025315400047275.

Hebbeln, D., Van Rooij, D., Wienberg, C., 2016. Good neighbours shaped by vigorous currents: Cold-water coral mounds and contourites in the North Atlantic. Mar. Geol. 378, 171–185. https://doi.org/10.1016/j.margeo.2016.01.014.

Henriet, J.P., De Mol, B., Pillen, S., Vanneste, M., Van Rooij, D., Versteeg, W., Croker, P.F., Shannon, P.M., Unnithan, V., Bouriak, S., Chachkine, P., Belgica 97 Shipboard Party, 1998. Gas hydrate crystals may help build reefs. Nature 391, 648–649. https://doi.org/10.1038/35530.

Henry, L.-A., Frank, N., Hebbeln, D., Wienberg, C., Robinson, L., de Flierdt, T. van, Dahl, M., Douarin, M., Morrison, C.L., Correa, M.L., Rogers, A.D., Ruckelshausen, M., Roberts, J.M., 2014. Global ocean conveyor lowers extinction risk in the deep sea. Deep-Sea Res. I Oceanogr. Res. Pap. 88, 8–16. https://doi.org/10.1016/j.dsr.2014.03.004.

Hernández-Molina, F.J., Llave, E., Stow, D.A.V., García, M., Somoza, L., Vázquez, J.T., Lobo, F.J., Maestro, A., Díaz del Río, V., León, R., Medialdea, T., Gardner, J., 2006. The contourite depositional system of the Gulf of Cádiz: A sedimentary model related to the bottom current activity of the Mediterranean outflow water and its interaction with the continental margin. Deep Sea Res. Part II Top. Stud. Oceanogr. 53, 1420–1463. https://doi.org/10.1016/j.dsr2.2006.04.016.

Hernández-Molina, F.J., Serra, N., Stow, D.A.V., Llave, E., Ercilla, G., Van Rooij, D., 2011. Along-slope oceanographic processes and sedimentary products around the Iberian margin. Geo-Mar. Lett. 31, 315–341. https://doi.org/10.1007/s00367-011-0242-2.

Hernández-Molina, F.J., Stow, D.A.V., Alvarez-Zarikian, C.A., Acton, G., Bahr, A., Balestra, B., Ducassou, E., Flood, R., Flores, J.-A., Furota, S., Grunert, P., Hodell, D., Jimenez-Espejo, F., Kim, J.K., Krissek, L., Kuroda, J., Li, B., Llave, E., Lofi, J., Lourens, L., Miller, M., Nanayama, F., Nishida, N., Richter, C., Roque, C., Pereira, H., Sanchez Goñi, M.F., Sierro, F.J., Singh, A.D., Sloss, C., Takashimizu, Y., Tzanova, A., Voelker, A., Williams, T., Xuan, C., 2014. Onset of Mediterranean outflow into the North Atlantic. Science 344, 1244–1250. https://doi.org/10.1126/science.1251306.

Hernández-Molina, F.J., Sierro, F.J., Llave, E., Roque, C., Stow, D.A.V., Williams, T., Lofi, J., Van der Schee, M., Arnáiz, A., Ledesma, S., Rosales, C., Rodríguez-Tovar, F.J., Pardo-Igúzquiza, E., Brackenridge, R.E., 2016. Evolution of the gulf of Cadiz margin and southwest Portugal contourite depositional system: Tectonic, sedimentary and paleoceanographic implications from IODP expedition 339. Mar. Geol. 377, 7–39. https://doi.org/10.1016/j.margeo.2015.09.013

Hovland, M., Croker, P.F., Martin, M., 1994. Fault-associated seabed mounds (carbonate knolls?) off western Ireland and north-west Australia. Mar. Pet. Geol. 11, 232–246. https://doi.org/10.1016/0264-8172(94)90099-X.

Huvenne, V.A.I., De Mol, B., Henriet, J.-P., 2003. A 3D seismic study of the morphology and spatial distribution of buried coral banks in the Porcupine Basin, SW of Ireland. Mar. Geol. 198, 5–25. https://doi.org/10.1016/S0025-3227(03)00092-6.

Huvenne, V.A.I., Van Rooij, D., De Mol, B., Thierens, M., O'Donnell, R., Foubert, A., 2009. Sediment dynamics and palaeo-environmental context at key stages in the Challenger cold-water coral mound formation: Clues from sediment deposits at the mound base. Deep-Sea Res. I Oceanogr. Res. Pap. 56, 2263–2280. https://doi.org/10.1016/j.dsr.2009.08.003.

INFOMAR, 2023. INFOMAR Marine Data Download Portal [WWW Document].

Iorga, M.C., Lozier, M.S., 1999. Signatures of the Mediterranean outflow from a North Atlantic climatology: 2. Diagnostic velocity fields. J. Geophys. Res. Oceans 104, 26011–26029. https://doi.org/10.1029/1999JC900204.

Johnston, S., Dore, A., Spencer, A., 2001. The Mesozoic evolution of the Southern North Atlantic region and its relationship to basin development in the South Porcupine Basin, offshore Ireland. Geol. Soc. London Spec. Publ. 188, 237–263. https://doi.org/10.1144/GSL.SP.2001.188.01.14.

Kano, A., Ferdelman, T.G., Williams, T., Henriet, J.-P., Ishikawa, T., Kawagoe, N., Takashima, C., Kakizaki, Y., Abe, K., Sakai, S., Browning, E.L., Li, X., Integrated Ocean Drilling Program Expedition 307 Scientists, 2007. Age constraints on the origin and growth history of a deep-water coral mound in the northeast Atlantic drilled during Integrated Ocean Drilling Program Expedition 307. Geology 35, 1051–1054. https://doi.org/10.1130/G23917A.1.

Khélifi, N., Sarnthein, M., Andersen, N., Blanz, T., Frank, M., Garbe-Schonberg, D., Haley, B.A., Stumpf, R., Weinelt, M., 2009. A major and long-term Pliocene intensification of the Mediterranean outflow, 3.5-3.3 Ma ago. Geology 37, 811–814. https://doi.org/10.1130/G30058A.1.

Khélifi, N., Sarnthein, M., Frank, M., Andersen, N., Garbe-Schönberg, D., 2014. Late Pliocene variations of the Mediterranean outflow. Mar. Geol. 357, 182–194. https://doi.org/10.1016/j.margeo.2014.07.006.

Li, H., Wang, Y., Zhu, W., Xu, Q., He, Y., Tang, W., Zhuo, H., Wang, D., Wu, J., Li, D., 2013. Seismic characteristics and processes of the Plio-Quaternary unidirectionally migrating channels and contourites in the northern slope of the South China Sea. Mar. Pet. Geol. 43, 370–380. https://doi.org/10.1016/j.marpetgeo.2012.12.010.

Liu, S., Hernández-Molina, F.J., Ercilla, G., Van Rooij, D., 2020. Sedimentary evolution of the Le Danois contourite drift systems (southern Bay of Biscay, NE Atlantic): A reconstruction of the Atlantic Mediterranean Water circulation since the Pliocene. Mar. Geol. 427, 106217. https://doi.org/10.1016/j.margeo.2020.106217.

Lisiecki, L.E., Raymo, M.E., 2005. A Pliocene-Pleistocene stack of 57 globally distributed benthic delta O-18 records. Paleoceanography 20, PA1003. https://doi.org/10.1029/2004PA001071.

Louwye, S., Foubert, A., Mertens, K., Van Rooij, D., THE IODP EXPEDITION 307 SCIENTIFIC PARTY, 2008. Integrated stratigraphy and palaeoecology of the Lower and Middle Miocene of the Porcupine Basin. Geol. Mag. 145, 321–344. https://doi.org/10.1017/S0016756807004244.

Lüdmann, T., Paulat, M., Betzler, C., Möbius, J., Lindhorst, S., Wunsch, M., Eberli, G.P., 2016. Carbonate mounds in the Santaren Channel, Bahamas: A current-dominated periplatform depositional regime. Mar. Geol. 376, 69–85. https://doi.org/10.1016/j.margeo.2016.03.013.

McCartney, M., Mauritzen, C., 2001. McCartney, M. S., Mauritzen, C. On the origin of the warm inflow to the Nordic Seas. Prog. Oceanogr. 51, 125-214. Prog. Oceanogr. 51, 125–214. https://doi.org/10.1016/S0079-6611(01)00084-2.

McDonnell, A., Shannon, P.M., 2001. Comparative Tertiary stratigraphic evolution of the Porcupine and Rockall basins. Geol. Soc. London Spec. Publ. 188, 323–344. https://doi.org/10.1144/GSL.SP.2001.188.01.19.

Mitchum, R.M.J., Vail, P.R., Sangree, J.B., 1977. Stratigraphic Interpretation of Seismic Reflection Patterns in Depositional Sequences. In: Payton, C.E. (Ed.), Seismic Stratigraphy: Applications to Hydrocarbon Exploration. The American Association of Petroleum Geologist, Tulsa, 26, pp. 117–133.

Mulder, T., Hassan, R., Ducassou, E., Zaragosi, S., Gonthier, E., Hanquiez, V., Marchès, E., Toucanne, S., 2013. Contourites in the Gulf of Cadiz: a cautionary note on potentially ambiguous indicators of bottom current velocity. Geo-Mar. Lett. 33, 357–367. https://doi.org/10.1007/s00367-013-0332-4.

Naylor, D., Shannon, P.M. (Eds.), 1982. Geology of Offshore Ireland and West Britain, Softcover reprint of the original 1st ed. 1982 edition. Springer, London.

New, A.L., Barnard, S., Herrmann, P., Molines, J.-M., 2001. On the origin and pathway of the saline inflow to the Nordic Seas: insights from models. Prog. Oceanogr. 48, 255–287. https://doi.org/10.1016/S0079-6611(01)00007-6.

Pearson, I., Jenkins, D.G., 1986. Unconformities in the Cenozoic of the North-East Atlantic. In: Summerhayes, C.P., Shackleton, N.J. (Eds.), North Atlantic Palaeoceanography. Geol. Soc. London Spec. Publ., pp. 79–86.

Pingree, R.D., Le Cann, B., 1989. Celtic and Armorican slope and shelf residual currents. Prog. Oceanogr. 23, 303–338. https://doi.org/10.1016/0079-6611(89)90003-7.

Pingree, R.D., Le Cann, B., 1990. Structure, strength and seasonality of the slope currents in the Bay of Biscay region. J. Mar. Biol. Assoc. U.K. 70, 857–885. https://doi.org/10.1017/S0025315400059117.

Raddatz, J., Rüggeberg, A., Margreth, S., Dullo, W.-C., 2011. Paleoenvironmental reconstruction of Challenger Mound initiation in the Porcupine Seabight, NE Atlantic. Mar. Geol. 282, 79–90. https://doi.org/10.1016/j.margeo.2010.10.019.

Rebesco, M., 2005. Sedimentary Environments: Contourites. In: Selley, R.C., Cocks, L.R.M., Plimer, I.R. (Eds.), Encyclopedia of Geology. Elsevier, Oxford, pp. 513–527. https://doi.org/10.1016/B0-12-369396-9/00497-4.

Rebesco, M., Wåhlin, A., Laberg, J.S., Schauer, U., Beszczynska-Möller, A., Lucchi, R.G., Noormets, R., Accettella, D., Zarayskaya, Y., Diviacco, P., 2013. Quaternary contourite drifts of the Western Spitsbergen margin. Deep-Sea Res., Part 1, Oceanogr. Res. Pap. 79, 156–168. https://doi.org/10.1016/j.dsr.2013.05.013.

Rebesco, M., Hernández-Molina, F.J., Van Rooij, D., Wåhlin, A., 2014. Contourites and associated sediments controlled by deep-water circulation processes: State-of-the-art and future considerations. Mar. Geol. 352, 111–154. https://doi.org/10.1016/j.margeo.2014.03.011.

Rice, A.L., Billett, D.S.M., Thurston, M.H., Lampitt, R.S., 1991. The institute of oceanographic sciences biology programme in the Porcupine Seabight: background and general introduction. J. Mar. Biol. Assoc. U.K. 71, 281–310. https://doi.org/10.1017/S0025315400051614.

Rodrigues, S., Hernández-Molina, F.J., Fonnesu, M., Miramontes, E., Rebesco, M., Campbell, D.C., 2022. A new classification system for mixed (turbidite-contourite) depositional systems: Examples, conceptual models and diagnostic criteria for modern and ancient records. Earth-Sci. Rev. 230, 104030. https://doi.org/10.1016/j.earscirev.2022.104030.

Schlitzer, R., 2021. Ocean Data View [WWW Document].

Stoker, M.S., Van Weering, T.C.E., Svaerdborg, T., 2001. A Mid- to Late Cenozoic tectonostratigraphic framework for the Rockall Trough. Geol. Soc. London Spec. Publ. 188, 411–438. https://doi.org/10.1144/GSL.SP.2001.188.01.26.

Stoker, M.S., Praeg, D., Hjelstuen, B.O., Laberg, J.S., Nielsen, T., Shannon, P.M., 2005. Neogene stratigraphy and the sedimentary and oceanographic development of the NW European Atlantic margin. Mar. Pet. Geol. 22, 977–1005. https://doi.org/10.1016/j.marpetgeo.2004.11.007.

Stow, D.A.V., 1982. Bottom currents and contourites in the North Atlantic. Bull. Inst. Geol. Bassin Aquitaine 31, 151–166.

Stow, D.A.V., Faugères, J.-C., Howe, J.A., Pudsey, C.J., Viana, A.R., 2002. Bottom currents, contourites and deep-sea sediment drifts: current state-of-the-art. Geol. Soc. London Mem. 22, 7–20. https://doi.org/10.1144/GSL.MEM.2002.022.01.02.

Stow, D.A.V., Faugères, J.-C., 2008. Chapter 13 Contourite Facies and the Facies Model. In: Rebesco, M., Camerlenghi, A. (Eds.), Developments in Sedimentology, Contourites. Elsevier, pp. 223–256. https://doi.org/10.1016/S0070-4571(08)10013-9.

Stow, D.A.V., Hernández-Molina, F.J., Llave, E., Bruno, M., García, M., Díaz del Rio, V., Somoza, L., Brackenridge, R.E., 2013. The Cadiz Contourite Channel: Sandy contourites, bedforms and dynamic current interaction. Mar. Geol. 343, 99–114. https://doi.org/10.1016/j.margeo.2013.06.013.

Thierens, M., Titschack, J., Dorschel, B., Huvenne, V.A.I., Wheeler, A.J., Stuut, J.B., O'Donnell, R., 2010. The 2.6 Ma depositional sequence from the Challenger cold-water coral carbonate mound (IODP Exp. 307): sediment contributors and hydrodynamic palaeo-environments. Mar. Geol. 271, 260–277. https://doi.org/10.1016/j.margeo.2010.02.021.

Toucanne, S., Soulet, G., Riveiros, N.V., Boswell, S.M., Dennielou, B., Waelbroeck, C., Bayon, G., Mojtahid, M., Bosq, M., Sabine, M., Zaragosi, S., Bourillet, J.-F., Mercier, H., 2021. The North Atlantic Glacial Eastern boundary current as a key driver for ice-sheet—amoc interactions and climate instability. Paleoceanogr. Paleoclimatol., 36. https://doi.org/10.1029/2020PA004068.

van Aken, H.M., 2000. The hydrography of the mid-latitude Northeast Atlantic Ocean: II: The intermediate water masses. Deep-Sea Res. I Oceanogr. Res. Pap. 47, 789–824. https://doi.org/10.1016/S0967-0637(99)00112-0.

Van Rooij, D., De Mol, B., Huvenne, V., Ivanov, M., Henriet, J.-P., 2003. Seismic evidence of current-controlled sedimentation in the Belgica mound province, upper Porcupine slope, southwest of Ireland. Mar. Geol. 195, 31–53. https://doi.org/10.1016/S0025-3227(02)00681-3.

Van Rooij, D., Blamart, D., Kozachenko, M., Henriet, J.-P., 2007. Small mounded contourite drifts associated with deep-water coral banks, Porcupine Seabight, NE Atlantic Ocean. Geol. Soc. Lond. Spec. Publ. 276, 225–244. https://doi.org/10.1144/GSL.SP.2007.276.01.11.

Van Rooij, D., Huvenne, V.A.I., Blamart, D., Henriet, J.-P., Wheeler, A., de Haas, H., 2009. The Enya mounds: a lost mound-drift competition. Int. J. Earth Sci. 98, 849–863. https://doi.org/10.1007/s00531-007-0293-9.

Van Rooij, D., Iglesias, J., Hernández-Molina, F.J., Ercilla, G., Gomez-Ballesteros, M., Casas, D., Llave, E., De Hauwere, A., Garcia-Gil, S., Acosta, J., Henriet, J.-P., 2010. The Le Danois Contourite Depositional System: Interactions between the Mediterranean Outflow Water and the upper Cantabrian slope (North Iberian margin). Mar. Geol. 274, 1–20. https://doi.org/10.1016/j.margeo.2010.03.001.

Van Rooij, D., Campbell, C., Rueggeberg, A., Wahlin, A., 2016. The contourite log-book: significance for palaeoceanography, ecosystems and slope instability. Mar. Geol. 378, 1–4. https://doi.org/10.1016/j.margeo.2016.05.018.

Vandorpe, T., Martins, I., Vitorino, J., Hebbeln, D., García, M., Van Rooij, D., 2016. Bottom currents and their influence on the sedimentation pattern in the El Arraiche mud volcano province, southern Gulf of Cadiz. Mar. Geol. 378, 114–126. https://doi.org/10.1016/j.margeo.2015.11.012.

Vandorpe, T., Delivet, S., Blamart, D., Wienberg, C., Bassinot, F., Mienis, F., Stuut, J.-B.W., Van Rooij, D., 2023. Palaeoceanographic and hydrodynamic variability for the last 47 kyr in the southern Gulf of Cádiz (Atlantic Moroccan margin): Sedimentary and climatic implications. Depos. Rec. 9, 30–51. https://doi/10.1002/dep2.212.

Verweirder, L., Van Rooij, D., White, M., Van Landeghem, K., Bossée, K, Georgiopoulou, A. 2021. Combined control of bottom and turbidity currents on the origin and evolution of channel systems, examples from the Porcupine Seabight. Mar. Geol. 442, 106639. https://doi.org/10.1016/j.margeo.2021.106639.

Verweirder, L., Van Rooij, D., Georgiopoulou, A., 2023. Margin processes sculpting a land-detached canyon-channel system: the Gollum Channel System in the Porcupine Seabight. Front. Earth. Sci. 11. https://doi.org/10.3389/feart.2023.1285171

Viana, A.R., Almeida, W., Nunes, M.C.V., Bulhões, E.M., 2007. The economic importance of contourites. Geol. Soc. Lond. Spec. Publ. 276, 1–23. https://doi.org/10.1144/GSL.SP.2007.276.01.01.

White, M., 2001. Hydrography and physical dynamics at the NE Atlantic margin that influence the deep water cold coral reef ecosystem. EU ACES-ECOMOUND internal report, Department of Oceanography, NUI, Galway.

White, M., 2007. Benthic dynamics at the carbonate mound regions of the Porcupine Sea Bight continental margin. Int. J. Earth Sci. 96, 1–9. https://doi.org/10.1007/s00531-006-0099-1.

Wilckens, H., Schwenk, T., Lüdmann, T., Betzler, C., Zhang, W., Chen, J., Hernández-Molina, F.J., Lefebvre, A., Cattaneo, A., Spieß, V., Miramontes, E., 2023. Factors controlling the morphology and internal sediment architecture of moats and their associated contourite drifts. Sedimentology 70, 1472–1495. https://doi.org/10.1111/sed.13093.

Wils, K., Wermersche, M., Van Rooij, D., Lastras, G., Lamy, F., Arz, H.W., Siani, G., Bertrand, S., Van Daele, M., 2021. Late Holocene current patterns in the northern Patagonian fjords recorded by sediment drifts in Aysén Fjord. Mar. Geol. 441, 106604. https://doi.org/10.1016/j.margeo.2021.106604.

2.8 Supplementary material

Table A.2.1. Identification and description of the seismic sub-units and higher-order sediment packages. The indicated thickness corresponds to the maximum thickness measured on the seismic profile represented in Fig. 2.5. The last column shows the sediment packages also observed at IODP site U1318 (Fig. 2.2).

Sub-units	Sediment package	Thickness (ms)	Description	Site U1318
U1-1	U1-1a	17	Youngest sub-unit of the contourite drift; high-amplitude and low-frequency horizons; the lower boundary is an erosive surface	√
	U1-1b	23	Set of high-amplitude and medium-frequency horizons; the upper and lower boundaries are erosive surfaces	√
	U1-1c	20	Low-amplitude and medium-frequency horizons	√
	U1-1d	15	High-amplitude and low-frequency horizons, with a high-amplitude horizon at the lower boundary	√
	U1-1e	26	High-frequency and medium-amplitude horizons; weakening of the amplitude towards the lower boundary	√
	U1-1f	19	Higher amplitude and high frequency at the upper boundary, set of high-to-lower-amplitude and low-frequency horizons	√
	U1-1g	19	High-amplitude and high-frequency horizons	
	U1-1h	6	Set of high-amplitude and low-frequency horizons	
	U1-1i	45	Medium amplitude at the upper boundary; set of higher-amplitude horizons towards the lower boundary; high-frequency horizons	
	U1-1j	11	Set of lower-amplitude and medium-frequency horizons; the lower boundary is an erosive surface	
U1-2	U1-2a	15	High-amplitude and low-frequency horizons; the upper and lower boundaries are erosive surfaces	
	U1-2b	15	High-amplitude and medium-frequency horizons; the upper boundary is an erosive surface	
	U1-2c	12	Medium-amplitude and low-frequency horizons	
	U1-2d	11	High-amplitude and medium-frequency horizons	
	U1-2e	12	High-amplitude and medium-frequency horizons; the lower boundary is an erosive surface	
	U1-2f	20	Low-to-medium-amplitude and medium-frequency horizons; the upper boundary is an erosive surface	
	U1-2g	22	High-amplitude and low-to-medium-frequency horizons	
	U1-2h	22	Medium-to-high-amplitude and low-frequency horizons	

Chapter 3 – Evaluation of present-day hydrodynamic processes associated to the Belgica Mound contourite drift, offshore Ireland

---

This chapter has been submitted as:

Matossian, A.O., Daly, E., Fennell, S., Shymbaliova, N., Vandorpe, T., White, M. and **Van Rooij, D.** Evaluation of present-day hydrodynamic processes associated to the Belgica Mound contourite drift, offshore Ireland. Deep Sea research Part I: Oceanographic Research Papers.

Abstract: The Belgica Mound Drift is a contourite drift located in the Porcupine Seabight, offshore Ireland, formed in association with cold-water coral mounds.

ROV imagery and bathymetry provided a close-up view of the seafloor, identifying multiple bedforms, including sinuous, linguoid and washed-out ripples as well as sediment waves. Three moorings equipped with current meters were deployed to better understand the spatial and temporal variations of the present-day hydrodynamic conditions over the drift moats and crest. Several velocity flows, ranging from 20 to 100 cm/s, were deduced from the interpretation of the bedforms and compared with the mooring-recorded flow values and character to evaluate the representativeness of the bedforms as a tool in the assessment of the strength and direction of bottom currents in deep environments. Both the tidally forced flows up to 50 cm/s, and the observed flow directions are consistent with the bedform estimation. While bedforms which require weaker bottom currents are currently formed during every tidal flow, the ripples created under stronger flows may be relic features formed during unrecorded peak flow events. This suggests that the drift and its moats are still being influenced by a strong hydrodynamic regime.

The spatial distribution of the bedforms suggests that the bottom-current velocities are extremely variable, partly supported by the measured currents. This is likely related to the local topography which may have a very small spatial scale impact on the bottom flows.

Keywords: tidal currents, small-scale bedforms, moorings, bottom currents, Porcupine Seabight

Authors contributions: The data acquisition and conceptualisation of the 2019/16 survey were made by D. Van Rooij. The acquisition of the mooring data was done by M. White, E. Daly and S. Fennell. The mooring data were processed by M. White. The acquisition of the ROV data was done by T. Vandorpe. The processing and analyses of the ROV data were made by A.O. Matossian under the supervision of T. Vandorpe, with the help of N. Shymbaliova. This chapter was written by A.O. Matossian, under the supervision of D. Van

Rooij, M. White, T. Vandorpe, E. Daly and S. Fennell. The figures were made by A.O. Matossian (apart from Fig. 3.3B, done by E. Daly).

3.1 Introduction

Hydrodynamic processes such as tides, bottom currents and internal waves shape the seafloor and enable the formation of erosional and depositional features (Besio et al., 2003). An example of these depositional features is represented by contourite drifts, occurring in shallow and deeper water settings ranging from hundreds of metres to several kilometres (Rebesco et al., 2014). On a smaller scale, hydrodynamic processes allow the development of bedforms that can give information about the strength, direction and variability of bottom currents (Hollister and Heezen, 1972; Kenyon and Belderson, 1973; Tucholke et al., 1985; Nelson et al., 1993; Wynn and Stow, 2002; Mulder et al., 2003; Masson et al., 2004; Hanquiez et al., 2007; Stow et al., 2009). However, due to a lack of thorough seafloor mapping and long-term hydrodynamic in-situ observations, little is known about bedform generation and dynamics in water depths beyond 100 m (Lo Iacono et al., 2020). Successful attempts, such as the bedform-velocity matrix developed by Stow et al. (2009), provide a first assessment of the present bottom-current velocities and their spatial variability based on the observed type of bedforms.

The Belgica Mound Drift (Matossian and Van Rooij, 2024) is an example of a deep-water small-scale contourite drift (36 km²; 500–800 m water depth) located in the Belgica Mound Province, along the eastern slope of the Porcupine Seabight, offshore Ireland (Fig. 3.1). The drift is enclosed by cold-water coral (CWC) mounds and was created as a result of Quaternary glacial–interglacial cycles and the related absence or presence of the Mediterranean Outflow Water (MOW) within the Porcupine Seabight (Matossian and Van Rooij, 2024). The formation of the drift is directly related to the interaction of the variable seabed topography with strong bottom currents, which are strengthened during interglacial periods and weakened during glacial periods. Additionally, these currents are crucial in the development of associated features, such as the CWC mounds (Van Rooij et al., 2003; Huvenne et al., 2009; Matossian and Van Rooij, 2024). The present-day area is affected by alongslope contour currents which are enhanced by trapped baroclinic diurnal tidal motions (White, 2007). Moreover, there is a local topographic intensification with the CWC mounds steering the bottom currents in their immediate surroundings (Van Rooij et al., 2007; Matossian and Van Rooij, 2024).

The Belgica Mound Province and more specifically the CWC mounds, such as the Challenger and Moira Mounds (Fig. 3.1B), have been thoroughly examined in the past using high-resolution side-scan sonar (Wheeler et al., 2005; Huvenne et al., 2005) and ROV imagery (Foubert et al., 2005). During these surveys, many different types of large-scale features, demonstrating active sediment transport, were identified such as striations, sand ribbons, barchan dunes, sediment waves and furrows (Foubert et al., 2005; Huvenne et al., 2005; Wheeler et al., 2005). The seafloor is typically made up of rippled sand with sediment waves and superimposed smaller-scale ripples representative of the general hydrodynamic conditions. According to Huvenne et al. (2005), the texture of the seafloor is rougher in the Belgica Mound Province than in the northern Porcupine Seabight areas, such as the Magellan and Hovland Mound Provinces. This is confirmed by Van Rooij et al. (2007) who indicated that the seafloor is composed of a coarse foraminiferal sand with moderate sorting and high sand

content. The Belgica Mound Province is characterised by an irregular bathymetry with steep slopes of 2 to 3° (Huvenne et al., 2005). Past ROV observations reported a large number of dropstones next to the CWC mounds, associated with scours and gravel patches. All those earlier observations confirm the existence of local strong bottom currents with the CWC mounds acting as obstacles and steering the currents in their immediate surroundings (Wheeler et al., 2005; Foubert et al., 2005, 2011). Although these studies were crucial for understanding the current hydrodynamic regime in the area, they do not provide detailed information about the processes further away from the CWC mounds, specifically in a contourite drift context.

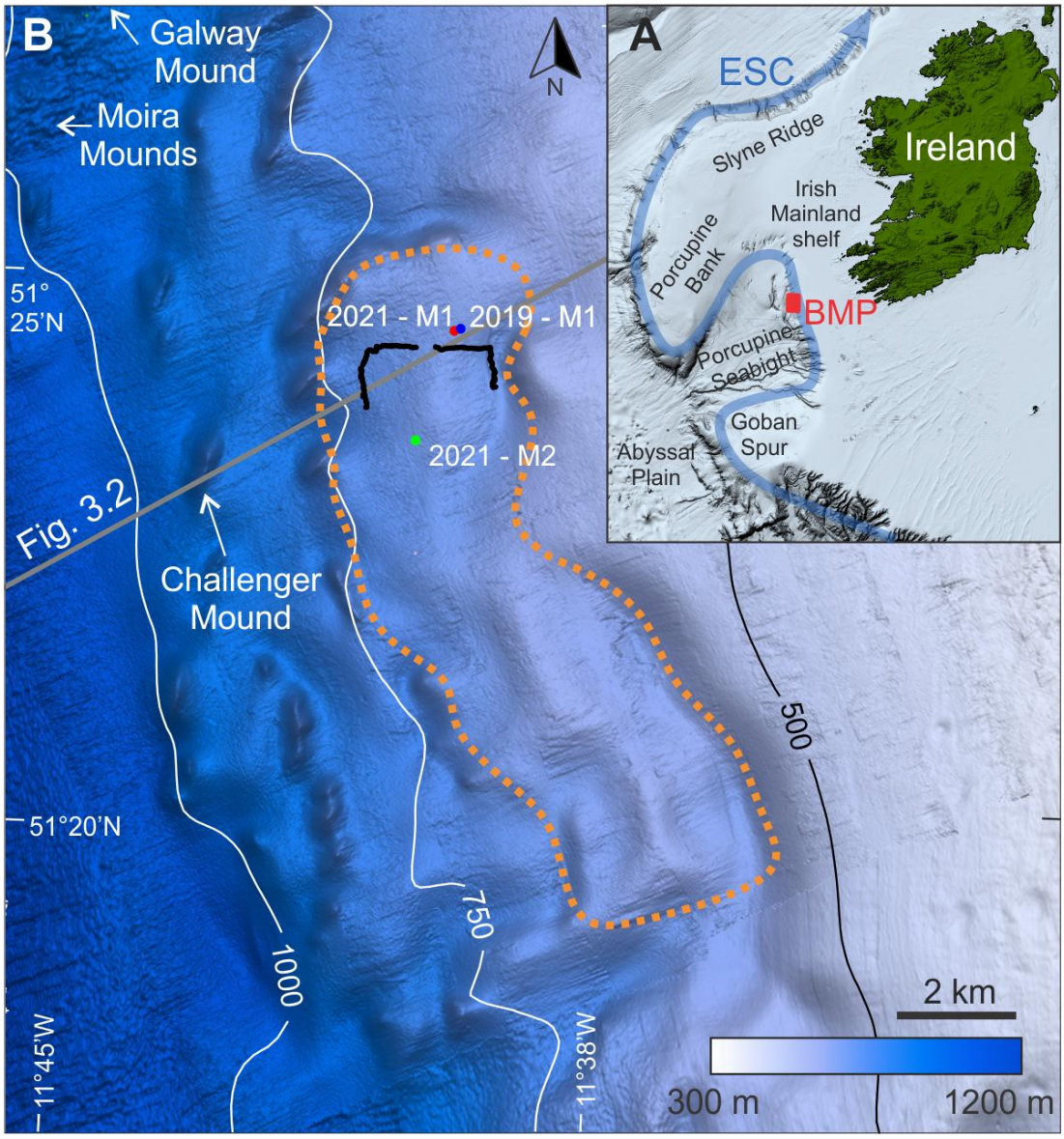

Figure 3.1. (A) Regional map with the location of the Belgica Mound Drift within the Belgica Mound Province (BMP) (red rectangle) in the Porcupine Seabight, offshore Ireland. ESC stands for the European Slope Current. (B) Map of the study area with 20 m resolution bathymetry data acquired during the RV Belgica 2022/18 survey and 25 m resolution data (INFOMAR, 2023) in the background. The orange dotted line shows the extent of the Belgica Mound Drift. The grey line represents the salinity

cross-section profile (Fig. 3.2). The mooring sites are circled in red, blue and green. The black line corresponds to the ROV track.

The latest seismic stratigraphy study of the contourite drift (Matossian and Van Rooij, 2024) suggests a heterogeneous depositional pattern, strongly influenced by the paleotopography and the CWC mounds. Strong alongslope bottom currents have been inferred in the moats, during the entire evolution of the drift, while the influence of the present-day hydrodynamic settings on the drift evolution remains difficult to entangle from seismic profiles alone. To improve comprehension of the lateral variability of the present-day bottom-current pattern, a higher resolution view of the drift and its moats, such as with ROV imagery, is required. Based on an accurate bedform distribution and the use of the matrix of Stow et al. (2009), the recent hydrodynamic regime influencing this contourite drift can be investigated, and the current spatial architectural dynamics of the Belgica Mound Drift can be assessed (Fig. 3.1B). The deployment of three moorings over the drift gives a great opportunity to define the temporal variability of the hydrodynamic regime on a very local level. Moreover, these moorings allow to illustrate the representativeness of bottom-current strengths and directions deduced from bedforms, by comparing them with the present-day recorded bottom currents.

Consequently, this study aims (1) to identify the seafloor features, such as the bedforms and the seafloor texture, through the ROV imagery; (2) to evaluate the strength, the direction and the spatial variability of the bottom currents through the interpretation of the ROV observations and (3) to assess the temporal variability of the present-day near-seabed hydrodynamic regime through the analysis of the mooring datasets and verify the representativeness of the deduced bottom currents.

3.2 Regional setting

3.2.1 Geographic setting

Located 200 km west of Ireland, on the western margin of the Irish Shelf, the Porcupine Seabight is a large basin (320 x 240 km) with a N–S trend (Fig. 3.1A) and water depth ranging from 350 m in the northern part to 3000 m in the southwest. The Irish Mainland Shelf borders this basin to the east, the Slyne Ridge and Porcupine Bank to the north, the Porcupine Ridge to the west and the Goban Spur to the south (Fig. 3.1A). The basin opens out into the Porcupine Abyssal Plain towards the southwest (Naylor and Shannon, 1982).

3.2.2 Hydrographic setting

Within the study area (500–900 m water depth), a seasonal thermocline in the vicinity of the Belgica Mound Drift can be observed at a depth of 50 to 70 m (White, 2007). From 0 to 600 m water depth, the warm and relatively saline Eastern North Atlantic Water (ENAW; 10–12°C; salinity range of 35.4–35.66) is present (Harvey, 1982; Rice et al., 1991; New et al., 2001; White, 2007). Between 600 and 800 m water depth, a permanent pycnocline separates the ENAW from the Mediterranean Outflow Water (MOW; 8-10°C; salinity > 35.5) (Pingree and Le Cann, 1990; Rice et al., 1991; White, 2007). From 800 to 1000 m water depth, a salinity maximum is observed, which corresponds to the core of the MOW. The MOW has impacted the hydrodynamic regime in the Porcupine Seabight both in the past and the present (Dorschel

et al., 2007; Huvenne et al., 2009). At present, the MOW flows steadily northwards from the Gibraltar Strait to the Porcupine Seabight (Iorga and Lozier, 1999; van Aken, 2000; McCartey and Mauritzen, 2001).

The general circulation in the Porcupine Seabight is cyclonic (White, 2007) and is influenced by the European Slope Current (Figs. 3.1A, 3.2B; 500–2000 m water depth; Toucanne et al., 2021), with at its shallower levels the northward-flowing Shelf-Edge Current (Pingree and Le Cann, 1989). Along the NE Atlantic margin, the Shelf-Edge Current (Fig. 3.2B) carries the upper part of the ENAW northward (Rice et al., 1991; New et al., 2001; White, 2007).

Along the NE Atlantic margin, there is an energy transfer from barotropic tides to baroclinic motions (Baines, 1974; White and Dorschel, 2010), including as examples, bottom trapped diurnal baroclinic waves and freely propagating semi-diurnal internal waves (White and Dorschel, 2010). Both these motions can be responsible for the amplification of bottom currents on the eastern flank of the Porcupine Seabight (Figs. 3.1, 3.2) (White, 2007). It has been evidenced by White et al. (2007) that the enhanced K_1 (diurnal) period baroclinic motions dominate the bottom-current strength and direction around the Belgica Mound Province relative to the M_2 (semi-diurnal) period tide. The trapped baroclinic motion can be rectified once it interacts with the seafloor, which allows the generation of a bottom current along the slope and a tidal (bottom) current. These alongslope bottom current and tidal current can be amplified under certain conditions (Huthnance, 1981; White and Dorschel, 2010), when a strong vertical density gradient, a permanent thermocline and a steep continental slope meet around the same water depth (600–800 m) (White, 2007; White and Dorschel, 2010). The local topography, including the CWC mounds, also plays a key role in the local variability and persistence of the bottom currents (White, 2007; Van Rooij et al., 2007). Associated to the Belgica Mound Drift area, the tidal current crosses the slope while the bottom current follows the slope northwards (White et al., 2007).

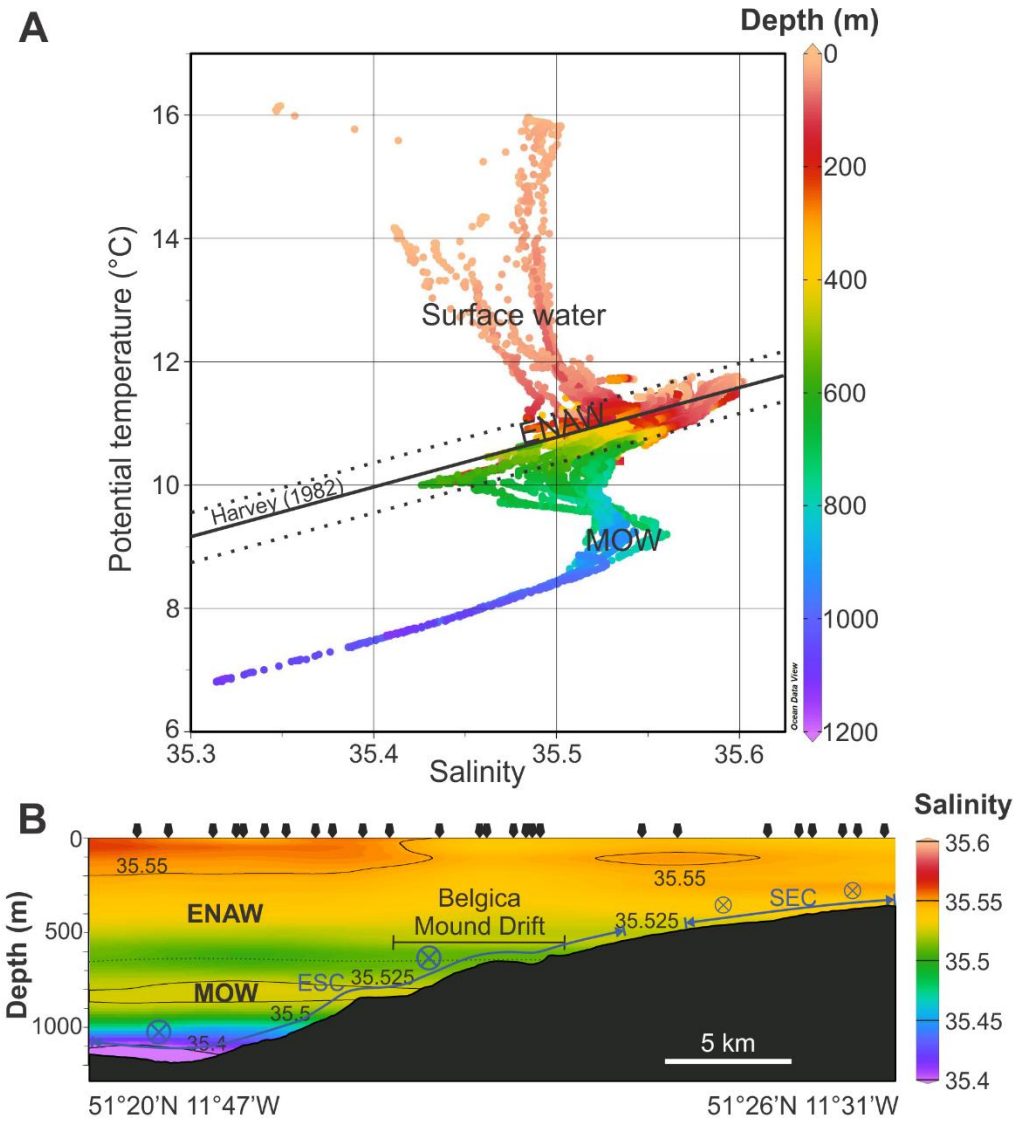

Figure 3.2. (A) Temperature - Salinity (T-S) diagram. The thick black line represents the characteristic T-S relationship of the ENAW as defined by Harvey (1982), while the dashed lines indicate a salinity variation of ±0.05 around this reference. (B) Salinity versus depth cross-section profile located over the study area (location: Fig. 3.1). A and B are based on CTD data (black arrows) from the World Ocean Database (Boyer et al., 2018) and were produced using Ocean Data View (Schlitzer, 2021). ENAW and MOW respectively stand for Eastern North Atlantic Water and Mediterranean Outflow Water. The dashed line shows the ENAW-MOW interface. The circled cross indicates the alongslope currents, European Slope Current (ESC) and Shelf-Edge Current (SEC), directed into the plane of the figure.

Mean persistent residual bottom currents, directed to the NW and thus following the continental slope, have been found to be between 1 and 7 cm/s (Pingree and Lecann, 1990; White, 2007; Dorschel et al., 2009). Rice et al. (1990) have recorded speeds rarely exceeding 15 cm/s at 1 m above the seabed. However, significantly higher instantaneous velocities, with a SW-NE orientation and associated with diurnal tides, were measured at the eastern edge of Porcupine Seabight, on the upper slopes and on top of Galway Mound (Fig. 3.1; Dorschel et al., 2007): Strong currents were measured, with peak velocities around 50 to 60 cm/s at 1 m above the seafloor (Dorschel et al., 2007). The observation of bedforms and current marks on

top of and between the Belgica mounds indicates however that occasional stronger bottom currents prevailed (Foubert et al., 2005; Huvenne et al., 2009). Several types of current-induced bedforms have been formerly identified on high-resolution side-scan imagery on the eastern slope of the Porcupine Seabight, with some of them indicating a peak south-north alongslope current of up to 120 cm/s (Chachkine and Akhmetzhanov, 1998; Kenyon et al., 1998; Wheeler et al., 2000; Foubert et al., 2011).

3.2.3 Geological setting

With a Middle to Late Jurassic failed rift structure and features made up of Precambrian rocks, deformed Upper Paleozoic strata, Mesozoic strata and a Cenozoic sediment cover on top, the bathymetry of the Porcupine Seabight demonstrates the complexity of the underlying geology (Naylor and Shannon, 1982). The basin is a deep sedimentary trough fault-bounded on its western and eastern margin and filled with post-rifts sediments with a thickness up to 10 km at its centre (Naylor and Shannon, 1982).

Several major margin-wide erosive Cenozoic events have been identified in the Porcupine Seabight (McDonnell and Shannon, 2001). The most recent event is related to the reintroduction of the MOW in the Porcupine Seabight during the Late Pliocene (Stow, 1982; Pearson and Jenkins, 1986; Van Rooij et al., 2003, 2009). It was responsible for the RD1 unconformity (Van Rooij et al., 2003), on top of which the CWC mounds and the Belgica Mound Drift started to form (Matossian and Van Rooij, 2024). The peculiar RD1 paleotopography, still visible in the present-day bathymetry, as well as the CWC mounds, strongly influence the local hydrodynamic conditions and play a role in the onset and development of the contourite drift. The contourite drift was formed under persistent alongslope bottom currents since the Pleistocene (Matossian and Van Rooij, 2024). At a larger scale, the evolution of the drift is related to the Pleistocene glacial and interglacial cycles (Matossian and Van Rooij, 2024). During interglacial periods, the MOW enters the Porcupine Seabight, increasing the bottom-current intensity, while during glacial periods, the MOW does not reach the basin, weakening the bottom currents (Huvenne et al., 2009; Raddatz et al., 2011) and allowing the sediment to accumulate on the drift (Matossian and Van Rooij, 2024). Since the lower Pliocene, the MOW is involved in the formation of large contourite depositional systems (Khélifi et al., 2009, 2014), which makes the Belgica Mound Drift one of the most distal contouritic expression of the MOW in the NE Atlantic Ocean.

3.3 Material and methods

Three moorings equipped with Aanderaa RCM7 current meters were used to assess the bottom-current regime (Table 3.1). In the course of the RV Belgica 2019/16 survey, a short-term fixed bottom mooring 2019-M1 (Table 3.1) was set up and placed on the crest of the drift (Fig. 3.1). Two additional long-term moorings were deployed (Table 3.1) within the Belgica Special Area of Conservation designation during the Irish Marine Institute survey CE21014 in 2021. Both moorings were disrupted by suspected trawling activity, leading to the loss of both near-seabed (< 10 m) current meters. While mooring 2021-M2 was deployed further south on the crest and recorded 20 days prior to experiencing a compass issue, 2021-M1 was deployed near the 2019 deployed mooring location and recorded for 6 months. The three deployed current meters were equipped with a Fenwall thermistor (temperature sensor). Vectors were

measured every 1/50th of the sampling interval (Table 3.1). Data were processed and quality controlled using instrument-specific calibration data provided by Aanderaa and appropriate magnetic declination. Measured current speed and direction were converted to east and north velocity components. A simple least squares tidal analysis was performed over the full available time series.

Table 3.1. Summary of the characteristics of the deployed moorings. Water depth was obtained through INFOMAR (2023) bathymetry (Fig. 3.1).

Mooring	Latitude	Longitude	Water depth	Height current meter	Start date	Recording period	Sampling interval
2019-M1	51°24'N	11°39'W	636 m	6 m	06/06/19	8 days	10 min
2021-M1	51°24'N	11°39'W	632 m	35 m	05/06/21	180 days	30 min
2021-M2	51°23'N	11°40'W	655 m	35 m	05/06/21	20 days	30 min

During the RV Belgica 2019/16 survey, one ROV-dive was carried out using the Flanders Marine Institute's (VLIZ) ROV *Zonnebloem* (SubAtlantic Cherokee observation type). The transect, located in the northern sector of the drift (5 km², 2.5 x 2 km; Fig. 3.1) is 3.4 km long and covers parts of three main morphological elements of the contourite drift: its western and eastern moats (1 km and 900 m long respectively) and a transect crossing the crest (1.5 km long).
A multibeam echosounder BlueView M900-2250 Dual Frequency Series operating at a frequency of 900 kHz was installed on the ROV to acquire high-resolution bathymetry. The vertical resolution of the data is approximately 5 cm. The BlueView has 130° field of view and sends out 768 beams at 900 kHz. The data were roll and pitch corrected using the compass of the ROV (TCM2.6) and positioning data were obtained every 2 seconds using an iXBlue GAPS USBL positioning device. Sound velocity data were collected by a ROV-mounted Sea&Sun 48M-CTD. The bathymetric data were recorded in real time using Qinsy (QPS). Due to the low update rate of the positioning data, the lack of a depth sensor and Kalman filter, the bathymetric data appear stepwise along-transect. The HD video data were gathered using a Luxus HD camera that faced downward. Along the track, the ROV flew no higher than 5 m above the seafloor. During the dive, the ship moved as slowly as possible (velocity < 1 knot) along the transect.

The processing of the ROV bathymetric data was performed with Qimera 2.6.2 (QPS). A sound velocity correction was applied on each sonar file using the collected CTD data and the outliers were manually removed. The analysis of the HD video and the mapping of the observed seafloor features have been carried out with ArcMap 10.7.1 coupled with the Full Motion Video module. Screenshots of the video frames were taken during the mapping.

Processed 25 m resolution bathymetric data (Fig. 3.1) were also made available by INFOMAR (2023) and downloaded from the INFOMAR Marine Data Download Portal. Higher resolution bathymetric data over the drift were acquired in 2022, using the Kongsberg EM 304 multibeam echosounder during the RV Belgica 2022/18 survey. The dataset has been processed with Qimera 2.6.2 (QPS) and exported with a 20 m resolution. The salinity data (Fig. 3.2) are based on CTD data from the World Ocean Database (Boyer et al., 2018) and were used for the identification of the water masses.

3.4 Results

3.4.1 Moorings

All current measurements showed similar characteristics for the bottom-current regime (Table 3.2). The 2021 data yielded comparable results (Fig. 3.3A; Table 3.2): Taking a smaller subset of the longer 2021-M1 dataset coinciding with the 2021-M2 dataset indicates that the shorter 2021-M2 data were representative of the longer time series during the coincident measurement period. Currents were dominated by across-slope tidal periodicity and smaller residual alongslope flows (Fig. 3.3A). The diurnal K_1 tide was the primary component of the tidally forced bottom currents observed in all the moorings (Fig. 3.3B).

Table 3.2. Summary statistics for the three deployed mooring. The residual current is computed using a time-averaging method with a 30-h averaging window.

Mooring	Speed (cm/s)	East (cm/s)	North (cm/s)	Residual current Direction (°) and speed (cm/s)
2019-M1				
Mean	20.5	-1.1	-3.7	196.0 and 3.8
Maximum	52.8	51.3	28.3	/
Minimum	0.6	-39.8	-26.7	/
2021-M1				
Mean	14.9	-0.9	4.6	348.6 and 4.7
Maximum	42.7	42.4	24.3	/
Minimum	1.1	-37.6	-18.4	/
2021-M2				
Mean	14.6	0.7	7.9	5.4 and 7.4
Maximum	42.1	40.7	23.9	/
Minimum	1.1	-29.7	-19.6	/

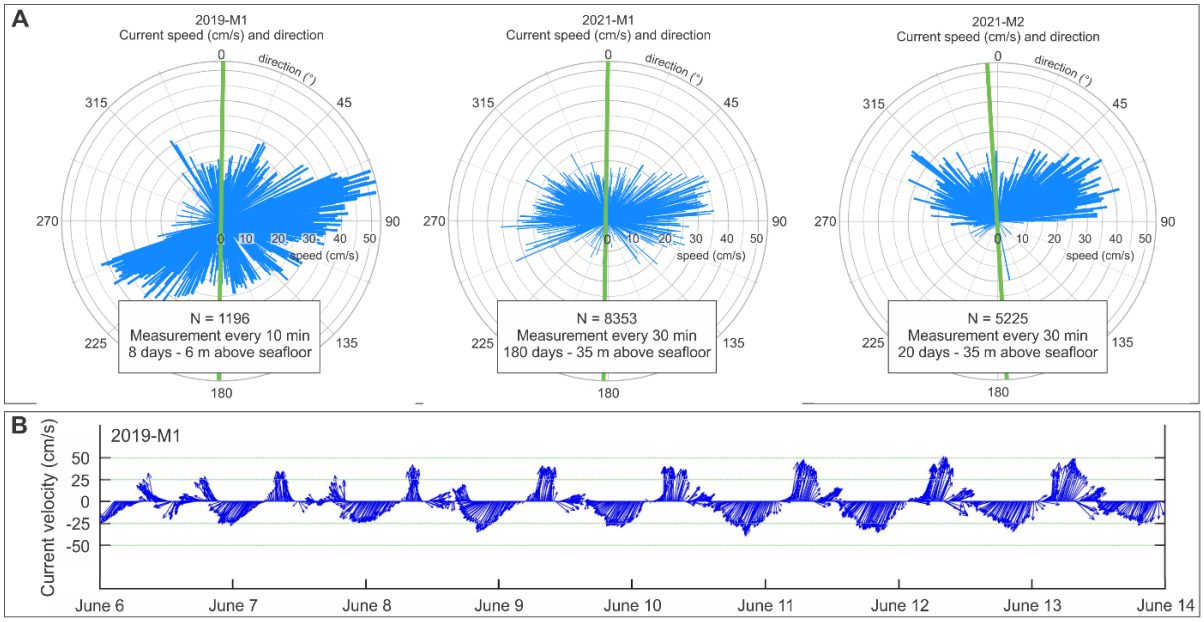

Figure 3.3. (A) Rose diagrams with the measured current speed (x axis) and direction from the three moorings (location: Fig. 3.1). The green bar shows the drift crest orientation. To make the figure clearer, only one measurement out of every ten is displayed for mooring 2021-M1. N corresponds to the number of measurements. (B) Results from mooring 2019-M1 (location: Fig. 3.1), with the current speed (cm/s) and direction at 6 m above the seafloor.

Peak tidally induced speeds were typically between 25 cm/s (neaps) to > 35 cm/s at spring tides, with a maximum speed of 40 cm/s (M1) and 42 cm/s (M2) respectively. Similarly, at both M1 and M2, mean flow speeds were similar (14.9 cm/s (M1) and 14.6 cm/s (M2, Table 3.2)) with M1 having a mean of 15.6 cm/s for the comparable M2 time period. Residual currents were directed alongslope and northward. At M1, there is a mean flow of 4.7 cm/s in direction 348.6˚N and at M2, 7.4 cm/s in direction 5.4˚N.

At the 2019-M1 location, characteristics are similar to the 2021 moorings with a tidally dominated across-slope bi-directional current (Fig. 3.3B) found in the short 8-day time period and a mean speed of 20 cm/s and maximum of 52.8 cm/s (Fig. 3.3A; Table 3.2). The residual flow of 3.8 cm/s is directed to the SW.

3.4.2 ROV bathymetry

Since the frequency of 900 kHz results in a 5 cm vertical resolution, the ROV bathymetric data are only suitable to describe bedforms exceeding 5 cm in height. Moreover, the update rate of the USBL positioning of the ROV and lack of Kalman filter caused steplike artefacts in the bathymetry data, which are visible as across-tracks lines on the bathymetry map (Fig. 3.4). Consequently, only across-track height differences exceeding 5 cm are reliable, as along-track height differences are most likely jumps in ROV latitude, longitude and/or altitude. Several NNW–SSE oriented sediment steps, with height differences of 5 to 40 cm, can be traced over 40 to 150 m along the western moat of the drift (Fig. 3.4, profile C-D).

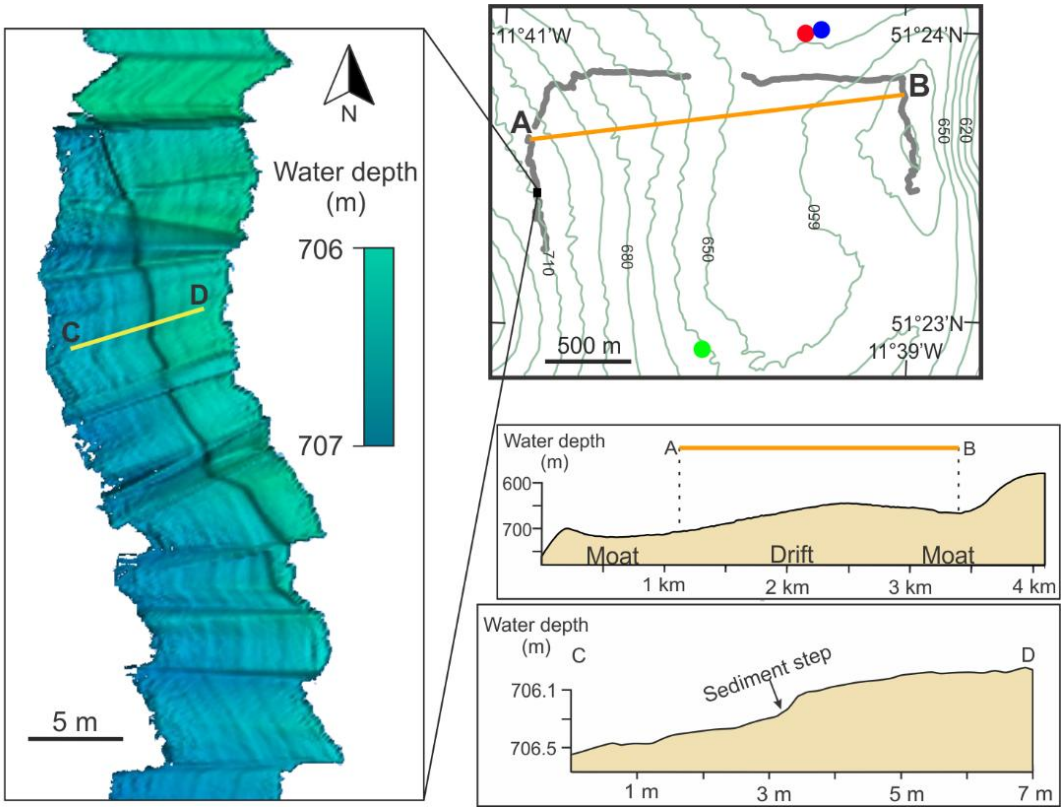

Figure 3.4. Bathymetric cross-section profile over the Belgica Mound Drift (A-B orange line), based on the 2022 bathymetric data (Fig. 3.1), and a small profile within the western moat (C-D yellow line), based on the 2019 ROV-acquired bathymetry. Given the presence of numerous along-track artefacts, only across-track height differences are considered. The mooring sites are represented by red (2021-M1), blue (2019-M1) and green (2021-M2) dots. The grey line corresponds to the ROV track.

3.4.3 ROV visual imagery

A variety of bedforms were observed over the crest and within the moats of the contourite drift. Following the bedform classification of Simon and Richardson (1966), as well as the bedform matrix of Stow et al. (2009), numerous features were observed and identified. They have been classified into five categories (Fig. 3.5, Table 3.3).

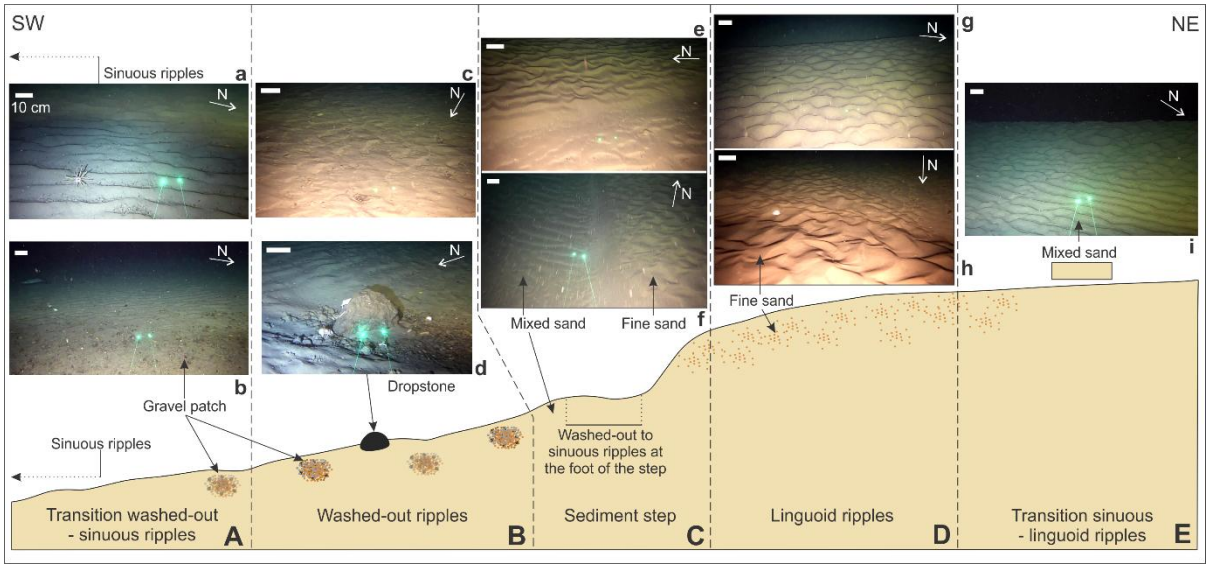

Figure 3.5. Schematic illustration (not to scale) of the observed ripple sequence on the western track, featuring images from the ROV dive. A 10 cm scale reference is shown by the white bar in the top left corner of each screenshot. The distance scale is only valid for the centre of the image. Screenshots of the video frames were extracted for illustrative purpose. The locations of the screenshots (indicated by lowercase letters) are shown on Fig. 3.6.

(1) Straight to sinuous ripples (Fig. 3.5A, Table 3.3) are asymmetrical with a short and steep lee side and a gentler stoss side. They are straight to undulatory crested. The associated texture of the seafloor is generally among the roughest encountered with pebble to cobble-size clasts and less sorted (biogenic) mixed sand, predominantly accumulating in the ripple troughs.

(2) Washed-out ripples (Fig. 3.5B, Table 3.3) are smaller compared to the straight to sinuous ripples, with a shorter lee side. They appear to be planed off. They are associated with irregular gravel patches visible in the trough of the ripples. These patches are composed of poorly sorted, coarser pebble to cobble-size clasts and some boulders.

(3) Linguoid ripples (Fig. 3.5D, Table 3.3) are asymmetrical with a steeper and shorter lee side compared to straight to sinuous ripples. They display a highly variable morphology with an irregular crescent-shaped crest. The seafloor texture is usually very fine and well-sorted with pale-coloured fine sand.

(4) Small-scale dropstones (Fig. 3.5B) are on average around 10 cm wide, but they can be up to 60 cm. Some are associated with scours and feature a gravel tail at the back. The gravel tails are 10 to 50 cm long and their orientations lie perpendicular to the surrounding ripple crests.

(5) Large-scale sediment steps (Fig. 3.5C, Table 3.3) are continuous straight ridges with an asymmetric profile. Their maximum height is 40 cm. They are ten to several tens of metres apart. They are characterised by a sharp, almost vertical drop. The steps are covered by smaller bedforms.

The observed ripple sequence is described in Fig. 3.5, ranging from deep (moat) to shallow (crest), in an upslope direction. Sinuous ripples (Fig. 3.5A) fade into washed-out ripples (Fig. 3.5B). Dropstones, as well as gravel patches are numerous in the washed-out ripple areas

(Fig. 3.5B). Washed-out to sinuous ripples are observed at the foot of the sediment step (Fig. 3.5C). These ripples are mostly observed perpendicular or oblique to the crest orientation of the step while the linguoid ripples on top have the same orientation (Fig. 3.5D). Sometimes, the ripples at the foot of the step are parallel to the step crest alignment (Figs. 3.6a, b). Further upslope, the linguoid ripples merge into straight to sinuous ripples (Fig. 3.5E). Straight to sinuous as well as linguoid ripples do not show any sign of erosion. The same sequence is observed in reverse on the eastern ROV track.

Table 3.3. Range of the dimensions of the different encountered bedforms.

Scale	**Bedform**	**Wavelength** ***(crest to crest distance)***	**Height/Amplitude** ***(trough to crest height)***
Small-scale	Straight to sinuous ripples	5 – 20 cm	2 – 5 cm
	Linguoid ripples	5 – 25 cm	2 – 5 cm
	Washed-out ripples	5 – 20 cm	> 1 cm
Large-scale	Sediment steps	10 – 50 m (western moat) 10 m (eastern moat)	10 – 40 cm

Based on the ROV visual imagery, the spatial distribution of the observed bedforms along the ROV track was plotted as sedimentary bedform maps (Fig. 3.6). These display the small and large-scale bedform distribution, as well as the texture of the seafloor.

The boundaries between the bedform areas generally feature a NNW–SSE orientation and their transition may be rather sharp. Most bedform areas are only a few metres wide in the moats, but on the drift crest, they can reach several tens of metres (Fig. 3.6d). The sediment steps are only located within the western and eastern moats of the drift (Figs. 3.6a, b, c, e, f). No steps were observed on the crest of the drift (Fig. 3.6d). They are typically 10 to 50 m apart in the western moat (Figs. 3.6a, b, c) and 10 m apart in the eastern moat (Fig. 3.6e), with an average NW–SE alongslope orientation. In total, 30 sediment steps have been observed along the ROV track: 13 in the eastern moat and 17 in the western moat, occurring between 658–712 m water depth. The ROV followed one sediment step for 150 m in the western moat (Fig. 3.6b), showing a rather straight crest line over the entire track. Washed-out ripples and linguoid ripples are more common in the western moat and sinuous ripples more often observed on the crest of the drift and in the eastern moat. Dropstones are commonly observed in the areas with the washed-out ripples (Figs. 3.6a, c) and on the crest of the drift (Fig. 3.6d).

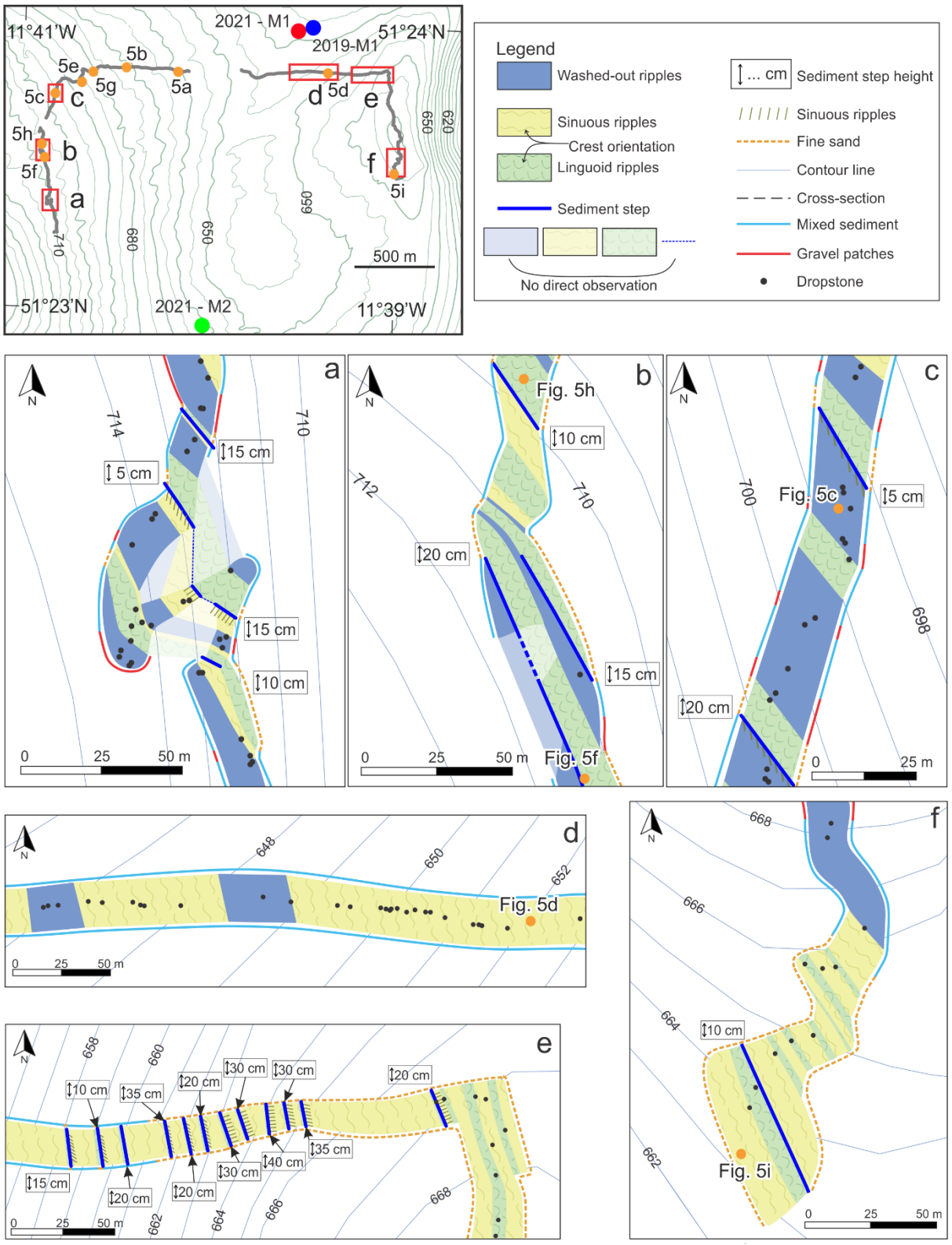

Figure 3.6. Sediment bedform maps (a to f, location see top left panel) zoomed from the seafloor map including various features observed using the ROV HD video data. The locations of the screenshots shown in Fig. 3.5 are marked by orange dots (5a to i).

3.5 Discussion

3.5.1 Present-day temporal variability of bottom currents

The measured bottom-current strength and direction (Fig. 3.3; Table 3.2) concur with what has been previously observed in the Belgica Mound Province through other direct measurements (White et al., 2007; Dorschel et al., 2007): The bottom currents are dominated by an intensified across-slope (W–E, SW–NE) diurnal tidal component with a weaker northward (alongslope) residual component. Measurements reported here are unique since, for the first time, several moorings yielded spatial and temporal information about the hydrodynamic regime over a relatively small contourite drift.

The 2021 moorings were affected by suspected trawling activity, resulting in the loss of near-seabed current meters. Only the current meters positioned at 35 m above the seafloor remained, reducing data completeness and limiting full comparison with the 2019 dataset. Additionally, differences in deployment year and recording period further limit the comparison between locations. Minor differences between the 2021 mooring data are likely due to the small-scale topographic variabilities in the vicinity of the measurements. The velocity readings for both current meters at 35 m above the seafloor in the north and south of the drift crest are similar (Table 3.2) and show weaker bottom currents than at 6 m above the seafloor (Fig. 3.3A). It is known that the bottom currents, mostly driven by trapped diurnal baroclinic waves, are enhanced near the seafloor within the northern section of the Belgica Mound Province (White, 2007). A weaker steering effect of the currents at 35 m, being further away from the local topography, i.e. CWC mounds and the drift topography, may be the reason for their W–E component, rather than the SW–NE orientation at 6 m above the seafloor (Fig. 3.3A). In other words, the closer to the seafloor, the more the currents show interaction with the variable seafloor topography. Consequently, the 2019-M1 data, collected at 6 m above the seafloor, would be more representative of the hydrodynamic regime on the drift, responsible for the formation of the bedforms, compared to the 2021 mooring data collected at 35 m above the seafloor.

This also suggests that the diurnal tidal components are amplified as found by White et al. (2007) and small-scale spatial variability is comparable to other locations within the Belgica Mound Province (Dorschel et al., 2007). The measured residual northward current combines both the alongslope bottom current generated by the trapped baroclinic motion (Huthnance, 1981; White and Dorschel, 2010) and the bottom current related to the European Slope Current (thermohaline circulation; Toucanne et al., 2021).

3.5.2 Sediment steps: dunes or waves?

One should be aware that the ROV visual imagery only represents a “snapshot” of the seabed morphology, displaying the seafloor features at the time of data collection. The presented dataset does not allow for the interpretation of the bedforms in terms of temporal variability. Since diurnal tidal currents are active in the area, acquisition of visual data 6 hours sooner or later could result in different sizes and/or orientations of the observed bedforms. It is assumed these are mobile bedforms, which is difficult to assess from this present dataset.

The large-scale features described as sediment steps (Figs. 3.5, 3.6) could correspond to two types of features based on their size (height differences up to 40 cm high), shape and distance between two features (between 10 and 50 m).

A similar ripple succession superimposed on larger scale features (crest height between 0.3 and 0.9 m and wavelengths of 3.5 to 5 m) was described by Stow et al. (2013) within the Cadiz Contourite Channel. According to their interpretation, the large-scale bedforms could be sinuous to crescent sediment waves and dunes, both with asymmetrical smaller-scale ripples on the stoss side (upstream) and a smooth lee side (downstream). Wynn et al. (2002) and Jiménez-Romero et al. (2022) also presented a similar sequence of ripples on top of, respectively, barchan dunes (crest height > 50 cm and 10–30 m wavelengths) and dunes. Barchan dunes have already been described in the Belgica Mound Province, NW of the study area (Wheeler et al., 2005). However, all observed sediment steps display a straight crest (Fig. 3.6), can at least be 150 m long and do not have a distinct dune shape.

A multitude of similar seabed features were also observed near the CWC mounds in the Belgica Mound Province through high-resolution side-scan sonar (Wheeler et al., 2005; Huvenne et al., 2005) and ROV imagery (Foubert et al., 2005). Here, the seafloor is typically made up of rippled sand with superimposed smaller-scale ripples on top of sediment waves (Foubert et al., 2005; Wheeler et al., 2005; Huvenne et al., 2005). These sediment waves were observed mainly in the vicinity of the Moira Mounds (NW of study area; Fig. 3.1). They are described as straight, long-crested (several hundreds of metres long), asymmetric, up to 50 cm high and with wavelengths of 15 to 20 m. Superimposed smaller-scale straight to linguoid ripples were also observed on top of those larger-scale bedforms (Foubert et al., 2005, 2011). The dimensions and shape of these features correspond to the described sediment steps (Figs. 3.5, 3.6), however, their lengths differ. The longest sediment step crest observed with the ROV was 150 m long and is possibly even longer.

Taking into account the description and interpretation made by Foubert et al. (2005, 2011), it is most likely the observed sediment steps can be interpreted as sediment waves. A deep-water sediment wave is defined as a large-scale depositional bedform generated by bottom currents (Wynn et al., 2000). These features usually have wavelengths of tens of metres to a few kilometres and heights of several metres. Therefore, the observed features could be interpreted as small-scale sediment waves with superimposed ripples. The main deviation from the definition is that the described sediment steps have steep, nearly vertical, lee sides (Figs. 3.4, 3.5) which may be due to erosional processes rather than strictly depositional processes. The straight to sinuous parallel to perpendicular ripples visible at the foot of the sediment waves (Fig. 3.5C) could be interference ripples, also known as ladderback ripples (Ramsay et al., 1989). Similar ripples (average wavelength of 7.7 cm and crest height of 1 cm) have been observed by Jiménez-Romero et al. (2022) in the trough of dunes on the Gulf of Cadiz. These ripples are often due to the refraction of oblique waves in coastal areas and highlight the presence of two current directions, either occurring simultaneously or successively (Ramsay et al., 1989). Although their origin in deeper environments is still not well understood (Jiménez-Romero et al., 2022), Stow et al. (2013) linked them to tidal currents, as observed in the area through the mooring data. The lee side of the sediment waves (Figs. 3.4, 3.5) could form an obstacle to the primary flow, i.e. the across-slope tidal current measured with the moorings. The lee side would modify the current speed and direction by refracting the current towards the NW (Fig. 3.7). This secondary refracted flow has the ability to erode the lee side of the sediment waves, changing the shape of the sediment waves and

making their lee side almost vertical. The secondary flow can also trigger the formation of straight to sinuous ripples at the foot of the sediment wave, with their crest oblique or even perpendicular to the crest orientation of the sediment wave (Fig. 3.5). The northward refracted flow could consequently play a role in the erosion of the lee side of the sediment waves and the local formation of small-scale bedforms.

3.5.3 Deduced bottom-current velocity and direction

Hydrodynamic processes are at work in the study area, as evidenced by the absence of degradation of the observed bedforms or the absence of bioturbations over the small-scale bedforms (Fig. 3.5). This either demonstrates that the bedforms are very recently formed or still actively developing. The observed bedforms can thus be used to assess the present-day hydrodynamic regime over the drift and be compared with the mooring data.

As both sediment waves and their superimposed ripples have the same crest orientation, it is reasoned that both are related to the same hydrodynamic processes. The alignment of the small-scale ripples and the sediment waves, with their NNW–SSE crests, indicates an across-slope flow direction perpendicular to the moats and drift orientation. On the eastern side of the drift crest, the inferred flow direction is towards ENE while on the western side, the flow direction is towards WSW (Fig. 3.7). These directions are consistent with the mooring observations and the direction of the across-slope tidal current. The residual alongslope northward current seems to have no direct influence on the bedform formation as no perpendicular ripples have been observed.

Flow velocities can be derived by examining the type of ripples, coupled with the seafloor texture, and using the matrix of Stow et al. (2009) (Table 3.4; Fig. 3.7). This matrix describes the flow velocities and the grain size needed to form different type of ripples. The grain size likely corresponds to coarse sand (Huvenne et al., 2005; Van Rooij et al., 2007) and is approximately 0.1 mm. The model of Stow et al. (2009) is an approximation, as the development of bedforms depends on several other physical parameters that were not taken into account in this interpretation, such as the fluid density, particle density, and sediment supply (Stow et al., 2009). The exact value of the flow responsible for a given type of bedform is difficult to evaluate, but the range of involved flow velocities can still be estimated using this model.

Table 3.4. Inferred flow velocities based on the ripple type. The washed-out ripples are not included in the Stow et al. (2009) bedform matrix. Baas and De Koning (1995) made an experiment with a grain size of 0.108 mm.

Ripple type	Inferred velocity range	Reference
Straight to sinuous	10 – 20 cm/s	Stow et al. (2009)
Linguoid	30 – 50 cm/s	Stow et al. (2009)
Washed-out	75 – 91 cm/s	Baas and De Koning (1995)
Sediment waves	75 –100 cm/s	Huvenne et al. (2005)
	50 – 120 cm/s	Soulsby (1997)

The across-slope tidal current, flowing up to 50 cm/s in a W or E direction as evidenced by the 2019-M1 mooring data (Fig. 3.3; Table 3.2), is strong enough to induce the sinuous and linguoid ripples (Table 3.4). The asymmetry of these ripples highlights their formation under one dominant flow direction. They could be created every tidal episode and the few

bioturbations observed in association with the straight to sinuous ripples could be formed and eroded after each tidal passing. Consequently, they only indicate the direction of the last tidal flow that has passed in the area. The straight to sinuous ripples are representative of the present-day hydrodynamic regime, in term of bottom-current velocities and directions, that are also recorded by the mooring data.

The origin of the washed-out ripples and the sediment waves (Table 3.4) cannot be explained solely by the flow velocities measured in the area (Fig. 3.3; Table 3.2; Pingree and Lecann, 1990; Rice et al., 1990; Roberts et al., 2005; White, 2007; Dorschel et al., 2009) as present currents are not stronger than 50 cm/s. Huvenne et al. (2005), Wheeler et al. (2005) and Foubert et al. (2011) mentioned that the large-scale features in the vicinity of the Moira Mounds may be related to not yet recorded peak flow events. Similarly, the sediment waves could not be shaped by the average diurnal tidal flow and could instead be related to peak flow events. As such, the sediment waves could be relict features formed by strong bottom currents occurring at any time since the last glacial period, possibly associated with a recent unrecorded peak flow event. The reintroduction of the MOW in a post-glacial Porcupine Seabight could be responsible for an amplification of the bottom-current strength and a transition into an environment with higher sediment mobilisation at the beginning of the current interglacial period (Huvenne et al., 2009; Raddatz et al., 2011). To better understand the processes responsible for the formation and mobilisation of these large-scale features, a more detailed investigation of the seafloor is required. In particular, confirming the identification of the sediment waves depends on accurately determining their dimensions. Without this information, it remains difficult to confirm their origin and evaluate the hydrodynamic conditions under which they formed.

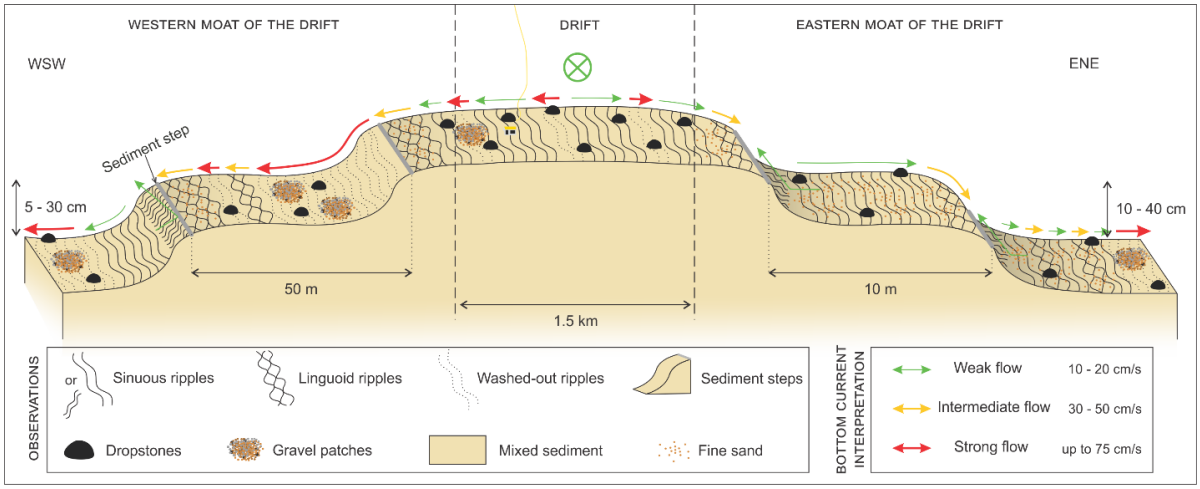

Figure 3.7. 3D sketch of an idealised cross-section profile (not to scale) over the crest and the western and eastern moats of the Belgica Mound Drift (northern sector). This shows the succession of the observed bedforms as well as the inferred current velocities and directions. The green arrows correspond to a weaker flow (10–20 cm/s), orange arrows to an intermediate flow (30–50 cm/s) and red arrows to a stronger flow (up to 75 cm/s). The circled cross indicates the residual northward (alongslope) current directed into the plane of the figure.

The wide variety of bedforms observed on the crest and within the moats of the drift indicates important spatial variations of the bottom-current velocity (Fig. 3.7), sometimes over a few

metres (Fig. 3.6). The NNW–SSE orientation of the boundaries between the bedform areas, which is parallel to slightly oblique to the bathymetric contours, reflects the importance of the local topography in the formation of these bedforms. The spatial variation of ripple patterns highlights the flow variation over the drift, with increased flow velocities on the drift moats enabling the daily formation of linguoid ripples (Fig. 3.7). The crest of the drift, even if no linguoid ripples have been observed there (Figs. 3.6, 3.7), is still under a dynamic regime allowing the formation of straight to sinuous ripples and even washed-out ripples during more intense hydrodynamic events. It is possible that the peak flow events were significantly more intense in the moats than over the drift, as the sediment waves are exclusively seen in the moats (Figs. 3.6, 3.7). During these post-last glacial peak events, the local topography, such as the drift and moat geometry and the CWC mounds, played a crucial role in local enhancement of the across-slope currents in the moats. While the drift was formed under the influence of an alongslope current since the Early Pleistocene (Matossian and Van Rooij, 2024), it is not presently the dominant current component influencing the drift and the moats. Indeed, nowadays, the across-slope tidal current plays a bigger role than the residual northward (alongslope) current. Numerous dropstones have also been observed by Huvenne et al. (2005), Foubert et al. (2005) and Wheeler et al. (2005) near the Moira Mounds. The presence of dropstones, with scours upstream and gravel patches downstream, confirms at least the occurrence of a post-last glacial highly dynamic flow regime eroding the seafloor in the Belgica Mound Province (Foubert et al., 2005; Huvenne et al., 2005; Wheeler et al., 2005) and a low sediment input in the present-day, preventing the moats to be filled in and the dropstones to be buried.

3.6 Conclusions

This work, focusing on the small-scale Belgica Mound Drift, has shown that bedforms, moorings and detailed analysis of ROV imagery yields valuable insights into the present-day hydrodynamic regime and its influence on the spatial and temporal drift evolution.

While the contourite drift was formed under persistent alongslope bottom currents since the Early Pleistocene (Matossian and Van Rooij, 2024), the present-day main flow directions are perpendicular to the drift crest, showing that the main oceanographic processes responsible for the formation of the drift are currently not playing a role in the evolution of the drift. Nevertheless, the Belgica Mound Drift and mostly its moats are still affected by a strong hydrodynamic regime, with depositional and erosional processes. The observed currents are enhanced closer to the seafloor, with recorded speeds up to 50 cm/s, whereas the velocities inferred from the bedforms range from 10 to 100 cm/s. The lowest inferred velocities are related to the recorded diurnal tidal flows and the highest linked to not yet recorded peak flow events, responsible for the formation of sediment waves. Defining the full extension of these sediment waves, which is still unknown from the ROV imagery, could give a better idea about the processes involved in their formation.

At a closer scale, the spatial variability of the bottom-current velocities is demonstrated by the spatial distribution of the bedforms that varies over a few metres. This is related to the local topography, such as the CWC mounds, the drift topography and the sediment waves deflecting and steering the bottom currents. As a result, the large-scale bedforms affect locally the bottom flows and the formation of small-scale ripples.

The hydrodynamic analysis relies on limited statistical treatment due to data loss and differences in deployment year and recording period, which constrain comparison between datasets. Additionally, this study does not include quantitative morphological reconstructions from ROV imagery, such as could be achieved through photogrammetry. However, the integrated approach still provides valuable insights. These limitations highlight opportunities for future research to build upon this foundation using more advanced methods. Although the conclusions are specific to the Belgica Mound Drift, the methodologies applied here can serve as a useful framework for investigating similar contourite systems in other deep-water environments.

Therefore, the identification of bedforms through the ROV imagery, in complement with mooring data, is an efficient method to investigate the spatial variations of the bottom currents in a deep environment and allows to comprehend their dynamic influence on the construction of a contourite drift.

Acknowledgements

This research was conducted in the framework of the FWO project DynaMOD (FWO grant 3G021719) and on the BOF extension BOF23/CDV/126. Ship time on RV Belgica was provided by BELSPO and RBINS-OD Nature. This study uses ROV *Zonnebloem* (previously ROV *Genesis*) provided by Flanders Marine Institute. We would like to thank Willem Versteeg and Robin Houthoofdt for their help with the ROV during the RV Belgica 2019/16 survey. The deployment of the 2021 moorings was kindly facilitated by the Marine Institute (Ireland) during the CE21014 weather buoy maintenance survey. We kindly acknowledge the two anonymous reviewers for their comments which improved the quality of this chapter.

3.7 References

Baas, J.H., 1994. A flume study on the development and equilibrium morphology of current ripples in very fine sand. Sedimentology 41, 185–209. https://doi.org/10.1111/j.1365-3091.1994.tb01400.x.

Baas, J.H., De Koning, H., 1995. Washed-out ripples: their equilibrium dimensions, migration rate, and relation to suspended-sediment concentration in very fine sand. J. Sediment. Res. 65, 431–435. https://doi.org/10.1306/D42680E5-2B26-11D7-8648000102C1865D.

Baines, P.G., 1974. The generation of internal tides over steep continental slopes. Philosophical Transactions of the Royal Society of London. Series A, Mathematical and Physical Sciences 277, 27–58. https://doi.org/10.1098/rsta.1974.0045.

Besio, G., Blondeaux, P., Brocchini, M., Vittori, G., 2003. Migrating sand waves. Ocean Dyn. 53, 232–238. https://doi.org/10.1007/s10236-003-0043-x

Boyer, T.P., Baranova, O.K., Coleman, C., García, H.E., Grodsky, A., Locarnini, R.A., Mishonov, A.V., Paver, C.R., Reagan, J.R., Seidov, D., Smolyar, I.V., Weathers, K.W., Zweng, M.M., 2018. In: Mishonov, A.V., Technical Editor (Eds.), World Ocean Database 2018, 87. NOAA Atlas NESDIS.

Chachkine, P., Akhmetzhanov, AM., 1998. Subbottom currents on the Porcupine Margin study by side-scan sonars. In: De Mol, B. (Ed.), Geosphere-biosphere coupling: Carbonate Mud Mounds and Cold Water Reefs. UNESCO, Paris, IOC Workshop Report 143, 30.

Dorschel, B., Hebbeln, D., Foubert, A., White, M., Wheeler A.J., 2007. Hydrodynamics and cold-water coral facies distribution related to recent sedimentary processes at Galway Mound west of Ireland. Mar. Geol. 244, 184–195. https://doi.org/10.1016/j.margeo.2007.06.010.

Dorschel, B., Wheeler, A.J., Huvenne, V.A.I., de Haas, H., 2009. Cold-water coral mounds in an erosive environmental setting: TOBI side-scan sonar data and ROV video footage from the northwest Porcupine Bank, NE Atlantic. Mar. Geol. 264, 218–229. https://doi.org/10.1016/j.margeo.2009.06.005.

Foubert, A., Beck, T., Wheeler, A.J., Opderbecke, J., Grehan, J., Klages, M., Thiede, J., Henriet, J.-P., Polarstern ARK-XIX/3a Shipboard Party, 2005. New view of the Belgica Mounds, Porcupine Seabight, NE Atlantic: Preliminary Results from the Polarstern ARK-XIX/3a ROV cruise. In: Freiwald, A., Roberts, J.M. (Eds.), Cold-Water Corals and Ecosystems. Springer, Heidelberg, pp. 403–415. https://doi.org/10.1007/3-540-27673-4_20.

Foubert, A., Huvenne, V.A.I., Wheeler, A.J., Kozachenko, M., Opderbecke, J., Henriet, J.-P., 2011. The Moira Mounds, small cold-water coral mounds in the Porcupine Seabight, NE Atlantic: Part B—Evaluating the impact of sediment dynamics through high-resolution ROV-borne bathymetric mapping. Mar. Geol. 282, 65–78. https://doi.org/10.1016/j.margeo.2011.02.008.

Hanquiez, V., Mulder, T., Lecroart, P., Gonthier, E., Marchès, E., Voisset, M., 2007. High resolution seafloor images in the Gulf of Cadiz, Iberian Margin. Mar. Geol. 246, 42–59. https://doi.org/10.1016/j.margeo.2007.08.002.

Hargreaves, P. M., 1984. The Distribution of Decapoda (Crustacea) in the open ocean and near-bottom over an adjacent slope in the northern North-East Atlantic Ocean during Autumn 1979. J. Mar. Biol. Assoc. U.K. 64, 829–857. https://doi.org/10.1017/S0025315400047275.

Harvey, J., 1982. θ-S relationships and water masses in the eastern North Atlantic. Deep-Sea. Res. I: Oceanogr. Res. Pap. 29, 1021–1033. https://doi.org/10.1016/0198-0149(82)90025-5.

Hollister, C.D., Heezen, B.C., 1972. Geologic effects of ocean bottom currents. In: Gordon, A.L. (Ed.), Studies in physical oceanography: Volume 2. Gordon and Breach, New York, pp. 37–66.

Huthnance, J.M., 1981. Waves and currents near the continental shelf edge. Prog. Oceanogr. 10, 193–226. https://doi.org/10.1016/0079-6611(81)90004-5.

Huvenne, V., Beyer, A., de Haas, H., Dekindt, K., Henriet J.-P., Kozachenko, M., Olu-Le Roy, K., Wheeler, A.J., TOBI/Pelagia 197, CARACOLE cruise participants, 2005. The seabed appearance of different coral bank provinces in the Porcupine Seabight, NE Atlantic: results from sidescan sonar and ROV seabed mapping. In: Freiwald, A., Roberts, J.M. (Eds.), Cold-Water Corals and Ecosystems. Springer, Heidelberg, pp. 535–569.

Huvenne, V.A.I., Van Rooij, D., De Mol, B., Thierens, M., O'Donnell, R., Foubert, A., 2009. Sediment dynamics and palaeo-environmental context at key stages in the Challenger cold-water coral mound formation: Clues from sediment deposits at the mound base. Deep-Sea Res. I Oceanogr. Res. Pap. 56, 2263–2280. https://doi.org/10.1016/j.dsr.2009.08.003.

INFOMAR, 2023. INFOMAR Marine Data Download Portal [WWW Document].

Iorga, M.C., Lozier, M.S., 1999. Signatures of the Mediterranean outflow from a North Atlantic climatology: 2. Diagnostic velocity fields. J. Geophys. Res. Oceans 104, 26011–26029. https://doi.org/10.1029/1999JC900204.

Jiménez-Romero, R., Fernandez-Salas, L.M., Palomino, D., Sanchez-Leal, R.F., Vila, Y., 2022. Discovering the Fine-Scale Morphology of the Gulf of Cádiz: An Underwater Imaging Analysis. J. Mar. Sci. Eng. 10, 651. https://doi.org/10.3390/jmse10050651.

Kenyon, N.H., Belderson, R.H., 1973. Bedforms of the Mediterranean undercurrent observed with sidescan sonar. Sediment. Geol. 9, 77–99. https://doi.org/10.1016/0037-0738(73)90027-4.

Kenyon, N.H., Ivanov, M.K., Akhmetzhanov, A.M., 1998. Cold water carbonate mounds and sediment transport on the north-east Atlantic margin. IOC Tech Ser 52, UNESCO, Paris.

Khélifi, N., Sarnthein, M., Andersen, N., Blanz, T., Frank, M., Garbe-Schönberg, D., Haley, B.A., Stumpf, R., Weinelt, M., 2009. A major and long-term Pliocene intensification of the Mediterranean outflow, 3.5-3.3 Ma ago. Geology 37, 811–814. https://doi.org/10.1130/G30058A.1.

Khélifi, N., Sarnthein, M., Frank, M., Andersen, N., Garbe-Schönberg, D., 2014. Late Pliocene variations of the Mediterranean outflow. Mar. Geol. 357, 182–194. https://doi.org/10.1016/j.margeo.2014.07.006.

Lo Iacono, C., Guillen, J., Guerrero, Q., Duran, R., Wardell, C., Hall, R.A., Aslam, T., Carter, G.D.O., Gales, J.A., Huvenne, V.A.I., 2020. Bidirectional bedform fields at the head of a submarine canyon (NE Atlantic). Earth Planet. Sci. Lett. 542, 116321. https://doi.org/10.1016/j.epsl.2020.116321.

Masson, D.G., Wynn, R.B., Bett, B.J., 2004. Sedimentary environment of the Faroe-Shetland Channel and Faroe Bank channels, NE Atlantic, and the use of bedforms as indicators of bottom current velocity in the deep ocean. Sedimentology 51, 1–35. http://10.1111/j.1365–3091.2004.00668.x.

Matossian, A. O., Van Rooij, D., 2024. Morphosedimentary evolution of the Belgica Mound Drift: Controls on contourite depositional system development in association with cold-water coral mounds. Mar. Geol 477, 107410. https://doi.org/10.1016/j.margeo.2024.107410.

McCartney, M., Mauritzen, C., 2001. On the origin of the warm inflow to the Nordic Seas. Prog. Oceanogr. 51, 125–214. https://doi.org/10.1016/S0079-6611(01)00084-2.

McDonnell, A., Shannon, P.M., 2001. Comparative Tertiary stratigraphic evolution of the Porcupine and Rockall basins. Geol. Soc. London Spec. Publ. 188, 323–344. https://doi.org/10.1144/GSL.SP.2001.188.01.19.

Mulder, T., Voisset, M., Lecroart, P., Le Drezen, E., Gonthier, E., Hanquiez, V., Faugères, J. C., Habgood, E., Hernández-Molina, F.J., Estrada, F., Llave-Barranco, E., Poirier, D., Gorini, C., Fuchey, Y., Voelker, A., Freitas, P., Lobo, S. F., Fernandez, L.M., Kenyon, N.H., Morel, J., 2003. The Gulf of Cadiz: An unstable giant contouritic levee. Geo-Mar. Lett. 23, 7–18. https://doi.org/10.1007/s00367-003-0119-0.

Naylor, D., Shannon, P.M., 1982. Geology of Offshore Ireland and West Britain, 1982 edition. Springer, London.

Nelson, C.H., Baraza, J., Maldonado, A., 1993, Mediterranean under current sandy contourites, Gulf of Cadiz, Spain. Sediment. Geol. 82, 103–131. http://doi.org/10.1016/0037–0738(93)90116-M.

New, A.L., Barnard, S., Herrmann, P., Molines, J.-M., 2001. On the origin and pathway of the saline inflow to the Nordic Seas: insights from models. Prog. Oceanogr. 48, 255–287. https://doi.org/10.1016/S0079-6611(01)00007-6.

Pearson, I., Jenkins, D.G., 1986. Unconformities in the Cenozoic of the North-East Atlantic. In: Summerhayes, C.P., Shackleton, N.J. (Eds.), North Atlantic Palaeoceanography. Soc. London Spec. Publ, Geol, pp. 79–86.

Pingree, R.D., Le Cann, B., 1989. Celtic and Armorican slope and shelf residual currents. Prog. Oceanogr. 23, 303–338. https://doi.org/10.1016/0079-6611(89)90003-7.

Pingree, R.D., Le Cann, B., 1990. Structure, strength and seasonality of the slope currents in the Bay of Biscay region. J. Mar. Biol. Assoc. U.K. 70, 857–885. https://doi.org/10.1017/S0025315400059117.

Raddatz, J., Rüggeberg, A., Margreth, S., Dullo, W.-C., 2011. Paleoenvironmental reconstruction of Challenger Mound initiation in the Porcupine Seabight, NE Atlantic. Mar. Geol. 282, 79–90. https://doi.org/10.1016/j.margeo.2010.10.019.

Ramsay, P.J.C., Cooper, A., Wright, C.I., Mason, T.R., 1989. The occurrence and formation of ladderback ripples in subtidal, shallow-marine sands, Zululand, South Africa. Mar. Geol. 86, 229–235.

Rebesco, M., Hernández-Molina, F.J., Van Rooij, D., Wåhlin, A., 2014. Contourites and associated sediments controlled by deep-water circulation processes: State-of-the-art and future considerations. Mar. Geol. 352, 111–154. https://doi.org/10.1016/j.margeo.2014.03.011.

Rice, A.L., Billett, D.S.M., Thurston, M.H., Lampitt, R.S., 1991. The institute of oceanographic sciences biology programme in the Porcupine Seabight: background and general introduction. J. Mar. Biol. Assoc. U.K. 71, 281–310. https://doi.org/10.1017/S0025315400051614.

Schlitzer, R., 2021. Ocean Data View [WWW Document].

Simons, D.B., Richardson, E.V., 1966. Resistance to Flow in Alluvial Channels. J. Hydraul. Eng. 86, 73–99. https://doi.org/10.3133/pp422J.

Soulsby, R.L., 1997. Dynamics of marine sands: a manual for practical applications. Thomas Telford, London.

Stow, D.A.V., 1982. Bottom currents and contourites in the North Atlantic. Bull. Inst. Geol. Bassin Aquitaine 31, 151–166.

Stow, D. A. V., Hernández-Molina, F.J., Llave, E., Sayago-Gil, M., Diaz del Rio, V., Branson, A., 2009. Bedform-velocity matrix: The estimation of bottom current velocity from bedform observations. Geology 37, 327–330. https://doi.org/10.1130/G25259A.1.

Stow, D.A.V., Hernández-Molina, F.J., Llave, E., Bruno, M., García, M., Díaz del Rio, V., Somoza, L., Brackenridge, R.E., 2013. The Cadiz Contourite Channel: Sandy contourites, bedforms and dynamic current interaction. Mar. Geol. 343, 99–114. https://doi.org/10.1016/j.margeo.2013.06.013.

Toucanne, S., Soulet, G., Riveiros, N.V., Boswell, S.M., Dennielou, B., Waelbroeck, C., Bayon, G., Mojtahid, M., Bosq, M., Sabine, M., Zaragosi, S., Bourillet, J.-F., Mercier, H., 2021. The North Atlantic Glacial Eastern boundary current as a key driver for ice-sheet—amoc interactions and climate instability. Paleoceanogr. Paleoclimatol., 36. https://doi.org/10.1029/2020PA004068.

Tucholke, B.E., Hollister, C.D., Biscaye, P., Gardner, W., 1985. Abyssal current character determined from sediment bedforms on the Nova Scotian continental rise. Mar. Geol. 66, 43–58. https://doi.org/10.1016/0025-3227(85)90022-2.

van Aken, H.M., 2000. The hydrography of the mid-latitude Northeast Atlantic Ocean: II: the intermediate water masses. Deep-Sea Res. I Oceanogr. Res. Pap. 47, 789–824. https://doi.org/10.1016/S0967-0637(99)00112-0.

Van Rooij, D., De Mol, B., Huvenne, V., Ivanov, M., Henriet, J.-P., 2003. Seismic evidence of current-controlled sedimentation in the Belgica mound province, upper Porcupine slope, southwest of Ireland. Mar. Geol. 195, 31–53. https://doi.org/10.1016/S00253227(02)00681-3.

Van Rooij, D., Blamart, D., Kozachenko, M., Henriet, J.-P., 2007. Small mounded contourite drifts associated with deep-water coral banks, Porcupine Seabight, NE Atlantic Ocean. Geol. Soc. Lond. Spec. Publ. 276, 225–244. https://doi.org/ 10.1144/GSL.SP.2007.276.01.11.

Van Rooij, D., Huvenne, V.A.I., Blamart, D., Henriet, J.-P., Wheeler, A., de Haas, H., 2009. The Enya mounds: a lost mound-drift competition. Int. J. Earth Sci. 98, 849–863. https://doi.org/10.1007/s00531-007-0293-9.

Wheeler, A.J., Bett, B.J., Billet, D.S.M., Masson, D.G., 2000. Very high resolution side-scan mapping of deep-water coral mounds: surface morphology and processes affecting growth. EOS Trans. 81, 48.

Wheeler, A.J., Kozachenko, M., Beyer, A., Foubert, A., Huvenne, V.A.I., Klages, M., Masson, D.G., Olu-Le Roy, K., Thiede, J., 2005. Sedimentary processes and carbonate mounds in the Belgica Mound province, Porcupine Seabight, NE Atlantic. In: Freiwald, A., Roberts, J.M. (Eds.), Cold-Water Corals and Ecosystems. Springer, Heidelberg, pp. 571–603. https://doi.org/10.1007/3-540-27673-4_28.

White, M., 2001. Hydrography and Physical Dynamics at the NE Atlantic Margin that Influence the Deep Water Cold Coral Reef Ecosystem. EU ACES-ECOMOUND Internal Report. Department of Oceanography, NUI, Galway.

White, M., 2007. Benthic dynamics at the carbonate mound regions of the Porcupine Sea Bight continental margin. Int. J. Earth Sci. 96, 1–9. https://doi.org/10.1007/ s00531-006-0099-1.

White, M., Roberts, J.M., van Weering, T., 2007. Do bottom-intensified diurnal tidal currents shape the alignment of carbonate mounds in the NE Atlantic?. Geo-Mar. Lett. 27, 391–397. https://doi.org/10.1007/s00367-007-0060-8.

White, M., Dorschel, B., 2010. The importance of the permanent thermocline to the cold water coral carbonate mound distribution in the NE Atlantic. Earth Planet. Sci. Lett. 296, 395–402. https://doi.org/10.1016/j.epsl.2010.05.025.

Wynn, R.B., Weaver, P.P.E., Ercilla, G., Stow, D.A.V, Masson, D.G., 2000. Sedimentary processes in the Selvage sediment-wave field, NE Atlantic: new insights into the formation of sediment waves by turbidity currents. Sedimentology 47, 1181–1197.

Wynn, R. B., Masson, D.G., Bett, B.J., 2002. Hydrodynamic significance of variable ripple morphology across deep-water barchan dunes in the Faroe-Shetland Channel. Mar. Geol. 192, 309–319. https://doi.org/10.1016/S0025-3227(02)00561-3.

Wynn, R.B., Stow, D.A.V., 2002. Classification and characterisation of deep-water sediment waves. Mar. Geol. 192, 7–22. https://doi.org/10.1016/S0025-3227(02)00547-9.

Chapter 4 – Elucidating sedimentary processes through near-seabed very high-resolution AUV mapping across a confined contourite drift

---

This chapter is ready to be submitted as:

Matossian, A.O., Boone, W., Langedock, K., Fourie, F. and **Van Rooij, D.** Elucidating sedimentary processes through near-seabed very high-resolution AUV mapping across a confined contourite drift. Sedimentology.

Abstract: Hydrodynamics and sediment dynamics are directly linked and shape the morphology of the ocean bottom. As direct measurements of bottom currents are limited, for example from moorings, the study of deep-water bedforms can offer fresh perspectives on spatial variability of local hydrodynamic processes.

To better understand the spatial variations of the hydrodynamic conditions over a contourite drift and establish its sediment dynamic evolution, deep-water bedforms formed over the drift and its moats were investigated, using AUV acquired high-resolution side-scan sonar imagery, interferometric bathymetry, and visual imagery.

Two sediment wave fields have been identified within, or close to, the moats of the drift. The sediment waves have superimposed ripples highlighting strong currents ranging from 20 to 75 cm/s. The orientation of the sediment waves and their superimposed ripples as well as the asymmetry of the sediment waves suggest a bi-directional across-slope current. This across-slope current would likely be a tidal current generated by a baroclinic motion enhanced in the depth range of a permanent thermocline, at the interface of two key water masses which is at the same depth as the two fields.

An alongslope current is also known in the area to be responsible for the formation of the drift throughout the Quaternary. This type of current is not directly observed in the bedforms but has been confirmed through in-situ current measurements from moorings. Other hydrodynamic processes, as across-slope currents, can shape a drift and its moats over time and form small-scale features, such as bedforms and sediment waves. The presented study shows that the associated features are crucial to develop greater insight into the local processes impacting small-scale drifts.

Keywords: Atlantic Ocean, Porcupine Seabight, seafloor mapping, contourite drift, bedforms, tidal current

Author contributions: The conceptualisation of the 2022/18 survey was made by A.O. Matossian and D. Van Rooij. The data acquisition was performed by W. Boone, K. Langedock

and F. Fourie. The pre-processing of the AUV data was made by K. Langedock. The processing was done by A.O. Matossian, under the supervision of K. Langedock. This chapter was written by A.O. Matossian, under the supervision of D. Van Rooij, W. Boone and K. Langedock. The figures were made by A.O. Matossian.

4.1 Introduction

The study of deep-water bedforms, such as sediment waves, can provide insights on the spatial variability of local hydrodynamic processes and their impact on associated features, especially in the absence of in-situ currents measurements from moorings. Sediment waves can be found throughout the oceans and in coastal areas (Heezen and Hollister, 1971; Ashley, 1990). They are large (tens of metres to a few kilometres wavelengths) undulating bedforms, formed by depositional processes linked to bottom currents on slopes and in mixed turbidite-contourite systems (Wynn et al., 2000; Wynn and Stow, 2002). There is a wide variety of sediment waves, in terms of environment, morphology and sediment composition, among which deep-water sediment waves. Wynn and Stow (2002) have classified deep-water sediment waves according to their formation mechanisms, linked to alongslope bottom currents, downslope turbidity currents, or a combination of both. A growing number of studies have also considered internal waves as an additional process at the origin of the sediment waves (Southard and Cacchione, 1972; Cacchione and Southard, 1974; Normark et al., 1980; Karl et al., 1986; Reeder et al., 2011; Ribó et al., 2016). Sediment waves generated by alongslope bottom currents can be found in association with contourite drifts, such as in the Rockall Trough (Howe, 1996; Masson et al., 2002). They are aligned obliquely to the contours and their crests are aligned perpendicularly or obliquely to bottom currents. Sediment wave fields formed by turbidity currents are associated with canyons or channels, like the Orinoco sediment wave field (Ercilla et al., 2002): Their crests are parallel to the contours. Intense turbulence close to the seafloor can be produced by internal waves breaking over the upper continental slope and the continental shelf, which produce local and strong bottom currents resuspending and transporting sediment (Southard and Cacchione, 1972; Cacchione and Wunsch, 1974; Normark et al., 1980; Bogucki and Redekopp, 1999; Ribbe and Holloway, 2001). The development of the asymmetry index (Knaapen, 2005), which is based on morphological characteristics and the shape of sediment waves, allows to assess their direction of migration, their formation mechanism, and dominant flow direction. Several examples of sediment waves generated by internal waves have been described, as on the continental slope of the Gulf of Valencia (Ribó et al., 2016), in the Gulf of Cadiz (Kenyon and Belderson, 1973), in the Browse Basin (Australia; Belde et al., 2015), and in the Messina Strait (Droghei et al., 2016). Internal waves can also have a tidal component that play a role in the enhancement of currents and the formation of the sediment waves, as stated by King et al. (2014) on the margin of the Barents Sea, Reiche et al. (2018) on the Israeli continental slope, and by Reeder et al. (2011), Ma et al. (2016) and Li et al. (2019) in the China Sea. Sediment waves induced by internal waves can also form on contourite drifts, as observed by Liu et al. (2019) in the Le Danois Bank region (Bay of Biscay).

Contourite drifts are sediment deposits produced by thermohaline-induced bottom currents flowing alongslope, i.e. contour currents (Rebesco et al., 2014). Though the energy of the geostrophic currents and their influence in shaping the seafloor are significant, associated

smaller-scale hydrodynamic processes and their effects are poorly understood (Rebesco et al., 2014). Large-scale contourite drifts (100 to 100000 km²) are observable from abyssal plains to continental margins. They are easily identifiable through bathymetric and seismic data (Rebesco et al., 2014). Conversely, smaller-scale drifts are frequently missed as they tend to be too small to be detected with standard methods from surface vessels. The use of high- to very high-resolution seismic and bathymetric surveys allowed the identification of smaller drifts, e.g. in the Porcupine Seabight (Matossian and Van Rooij, 2024), in fjord environments (Wils et al., 2021), in the Santaren Channel (Lüdmann et al., 2016), in the Lago Cardiel basin (Gilli et al., 2005), along the Norwegian continental slope (Rebesco et al., 2013), in the South China Sea (Li et al., 2013) and along the Moroccan margin (Vandorpe et al., 2023). These drifts can provide invaluable information about the local environmental conditions under which the sediment has been deposited while larger drifts tend to reflect the large-scale hydrodynamic processes, such as the thermohaline circulation (Rebesco et al., 2014). Furthermore, the study of these small drifts can be done at a very high vertical-resolution and with a dense spatial coverage. The use of seismic and bathymetric data can give a long-term indication of the average past hydrodynamic processes impacting the drift (Matossian and Van Rooij, 2024), while moorings and imagery of the seabed and its bedforms can improve comprehension of the present-day processes impacting the drift and help define the current sediment dynamics (Matossian et al., submitted). Moreover, a multidisciplinary approach allows to combine observations made at different temporal and spatial scales and resolutions and establish the limitations of each method.

The Belgica Mound Drift is a small-scale and deep-water contourite drift (36 km²; 500–800 m water depth) formed along the eastern margin of the Belgica Mound Province (Porcupine Seabight, offshore Ireland) by a contour current since the Early Pleistocene (Matossian and Van Rooij, 2024). Today, the area is known to be affected by trapped baroclinic tidal motion, enhancing bottom currents (White, 2007; White and Dorschel, 2010). Two types of bottom currents were measured via current meters from moorings deployed over the drift in 2019 and 2021 (Fig. 4.1; Matossian et al., submitted): an across-slope W–E tidal current and a residual northward bottom current. The tidal current and part of the residual current would be generated by the interaction of the trapped baroclinic motion with the seafloor (White and Dorschel, 2010; Matossian et al., submitted).

The vicinity of the Belgica Mound Drift (Fig. 4.1), i.e. the Belgica Mound Province, has been extensively studied in the past through high-resolution side-scan sonar (Wheeler et al., 2005; Huvenne et al., 2005) and ROV visual imageries (Foubert et al., 2005). Largescale features were observed, including sediment waves (Foubert et al., 2005; Huvenne et al., 2005; Wheeler et al., 2005). The sediment waves were described as straight, long-crested (several hundreds of metres long), asymmetric, up to 50 cm high with wavelengths of 15 to 20 m, fitting with the definition of Wynn and Stow (2002). In order to establish a better understanding of the lateral variability of the present-day current pattern and evaluate the activity of the drift system, ROV visual imagery had been acquired in 2019 over a transect of 3.4 km long in the northern sector of the drift (Fig. 4.1). On these imagery, numerous large-scale features, interpreted as sediment waves (10–50 m wavelengths and heights of maximum 40 cm) with superimposed centimetric ripples, have been observed (Matossian et al., submitted). This interpretation could not be confirmed due to the limited coverage of the ROV track and the 20 m resolution of the bathymetry data acquired from the research vessel, preventing to estimate their exact length. Autonomous underwater vehicles (AUV) have the ability to overcome these limitations. They

can operate close to the seafloor, enabling collection of ultra high-resolution bathymetric and photographic data that surface vessels cannot achieve at great depths due to signal attenuation and beam spreading (Wynn et al., 2014).

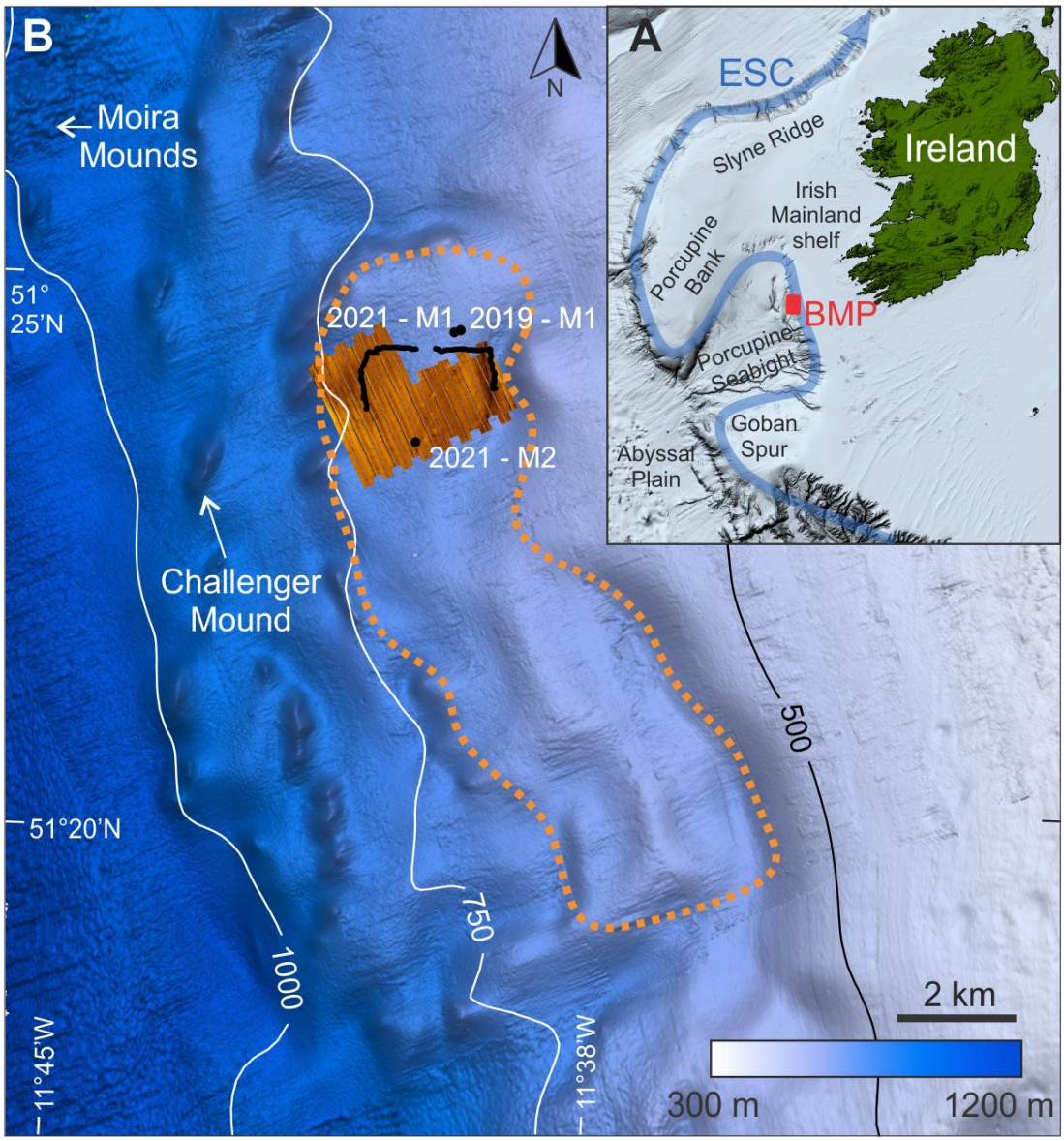

Figure 4.1. (A) Regional map with the location of the Belgica Mound Province (BMP; red rectangle) in the Porcupine Seabight, offshore Ireland. (B) Map of the Belgica Mound Drift (orange dotted line) with 20 m resolution bathymetry data acquired during the RV Belgica 2022/18 survey and 25 m resolution data (INFOMAR, 2023) in the background. The AUV-born dataset is indicated in overlay over the bathymetry. The black line corresponds to the ROV track and the black dots correspond to moorings deployed in 2019 and 2021 (Matossian et al., submitted).

This study uses AUV acquired very high-resolution side-scan sonar data from the northern sector of the Belgica Mound Drift with as goal to (1) investigate the large-scale bedforms and assess the presence sediment waves over the drift and its surroundings; (2) study the geometry of the large-scale features in order to determine the spatial variability of the hydrodynamic processes responsible for their formation; (3) establish a holistic view, integrating the large-scale bedforms, the drift and its surroundings as a dynamic system, and

decipher whether any of the present-day hydrodynamic processes still play a role in the sediment dynamic evolution of the drift.

4.2 Context

4.2.1 Geographic setting

The Porcupine Seabight is a large N–S trending basin located approximately 200 km west of Ireland, along the western edge of the Irish Shelf (Fig. 4.1). It spans about 320 by 240 km, with water depths ranging from 350 m in the north to 3000 m in the southwest. The basin is bordered by the Irish Mainland Shelf to the east, the Slyne Ridge and Porcupine Bank to the north, the Porcupine Ridge to the west, and the Goban Spur to the south (Fig. 4.1). To the southwest, it opens into the Porcupine Abyssal Plain (Naylor and Shannon, 1982).

4.2.2 Hydrographic setting

The study area ranges from 500 to 900 m water depth (Fig. 4.1) and is located at the interface between the Eastern North Atlantic Water (ENAW) and the Mediterranean Outflow Water (MOW) (White, 2007). The ENAW is a warm [10–12°C], salty [35.4–35.66] water mass that occurs from 0 to 600 m (Harvey, 1982; Rice et al., 1991; New et al., 2001; White, 2007). At a depth of roughly 700 m, a permanent pycnocline separates the MOW [8–10°C, salinity > 35.5] from the ENAW (Pingree and Le Cann, 1990; Rice et al., 1991; van Aken and Becker, 1996; White, 2007). Between 800 and 1000 m, a salinity maximum is observed, which corresponds to the MOW. Variability in occurrence of MOW has impacted the hydrodynamic regime in the Porcupine Seabight both in the past and the present. In the present day, the MOW, coming from the Mediterranean Sea, flows steadily northward from the Gibraltar Strait to the Porcupine Seabight (Iorga and Lozier, 1999; van Aken, 2000; McCartey and Mauritzen, 2001).

The general thermohaline circulation in the Porcupine Seabight is cyclonic (White, 2007) and is influenced by the European Slope Current (500–2000 m water depth; Toucanne et al., 2021). This current is the easternmost part of the upper branch of the Atlantic meridional overturning circulation (Huthnance et al., 2020; Toucanne et al., 2021). Along the NE Atlantic margin, the Shelf-Edge Current is above the European Slope Current (Fig. 4.1; Toucanne et al., 2021) and carries the upper part of the ENAW northward (Rice et al., 1991; New et al., 2001; White, 2007).

Along the NE Atlantic margin, there is an energy transfer from barotropic tides to baroclinic motions (Baines, 1974; White and Dorschel, 2010), including bottom trapped diurnal baroclinic waves and freely propagating semi-diurnal internal waves (White and Dorschel, 2010). Both these motions are baroclinic waves and can be responsible for the amplification of bottom currents on the eastern flank of the Porcupine Seabight (Figs. 4.1, 4.2) (White, 2007). It has been shown by White et al. (2007) that the enhanced K_1 (diurnal) period baroclinic motions dominate the bottom-current strength and direction around the Belgica Mound Province relative to the M_2 (semi-diurnal) period tide. The trapped diurnal tidal motion can be rectified when it interacts with the slope, allowing the generation of a bottom current along the slope as well as a tidal bottom current. The trapped baroclinic motion and the generated bottom currents are intensified around the permanent pycnocline (600–800 m) (White, 2007; White and Dorschel, 2010). The local topography, including the CWC mounds, plays also a key role

in the local variability and persistence of the bottom currents (White, 2007; Van Rooij et al., 2007), with the CWC mounds steering the bottom currents in their immediate surroundings (Van Rooij et al., 2007; Matossian and Van Rooij, 2024; Matossian et al., submitted). Associated to the Belgica Mound Drift area, the enhanced tidal bottom current is bi-directional and crosses the slope while the generated alongslope bottom current is uni-directional and follows the slope northwards (White et al., 2007; Matossian et al., submitted). Currents up to 50 cm/s have been recorded at 6 m above the seafloor over the crest of the drift (Fig. 4.1; Matossian et al., submitted).

The trapped diurnal baroclinic motion is enhanced near the bottom (Rhines, 1970) due to a resonance effect. This resonance frequency (f) is given by:

$$f = N\sin(\alpha)\sin(\gamma)$$

where N is the Brunt-Väisälä frequency, or buoyancy frequency (vertical density stratification N^2), α is the seafloor slope, and γ is the angle between the motion vector and the slope. The resonance is thus maximum where α, the vertical density stratification and γ are maximum. In the Belgica Mound Province, the measured peak values of Nsin(α) are at the permanent thermocline depth (600–800 m) (White, 2007), which fits with the water depth of the contourite drift.

4.2.3 Geological setting

The Belgica Mound Drift (Matossian and Van Rooij, 2024) is an elongated slope-parallel, mounded, and confined contourite drift located at water depths between 600 and 800 m. Oriented predominantly in a NNW–SSE direction and laterally confined E–W, its crest sits between 600 and 650 m water depth. Notably, the crest shifts from a north-south orientation in the northern sector to a NW–SE trend in the southern sector, allowing it to be subdivided into two distinct sectors. The drift lies within a complex seafloor setting, enclosed by conical cold-water coral (CWC) mounds, an escarpment, and surrounding moats. The drift extends approximately 10 km in length and 2.5 to 4 km in width, covering an area of 36 km².

The onset of the Belgica Mound Drift development is associated to an erosive event in the Late Pliocene, caused by the reintroduction of the MOW in the Porcupine Seabight (Stow, 1982; Pearson and Jenkins, 1986; McDonnell and Shannon, 2001; Van Rooij et al., 2003, 2009). This event formed the RD1 unconformity (Van Rooij et al., 2003), upon which CWC mounds started to form, followed by the onset of the Belgica Mound Drift during the Pleistocene (Matossian and Van Rooij, 2024). The RD1 paleotopography, still visible in current bathymetric data, along with the CWC mounds, continues to exert local control over hydrodynamic conditions, directly influencing the initiation and development of the drift.

The Belgica Mound Drift stands out as one of the most distal contouritic features influenced by the MOW in the NE Atlantic Ocean. Since the Pleistocene, the drift has been shaped by a persistent contour current (thermohaline-driven alongslope bottom current). This current also carved out moats flanking the drift (Matossian and Van Rooij, 2024). The thermohaline circulation remains active today and can be measured as part of a residual northward bottom current, including also the generated alongslope bottom current related to the trapped baroclinic motion (Matossian et al., submitted). Due to their interdependent geometries, the drift and its associated moats must be studied together (Wilckens et al., 2023). On a broader scale, the evolution of the drift is closely tied to Pleistocene glacial–interglacial cycles

(Matossian and Van Rooij, 2024). During interglacial periods, increased MOW inflow into the Porcupine Seabight enhances bottom-current strength, promoting erosion and shaping of the drift. In contrast, glacial periods see a retreat of the MOW from the Porcupine Seabight, triggering a weakening the bottom currents and allowing the sediment to accumulate (Huvenne et al., 2009; Raddatz et al., 2011; Matossian and Van Rooij, 2024). Since the lower Pliocene, the MOW has played a key role in the formation of large Contourite Depositional Systems along the NE Atlantic margin (Khélifi et al., 2009, 2014).

4.3 Material and methods

The study area, corresponding to the central part of the northern sector of the Belgica Mound Drift, is 2.5 x 3 km (Fig. 4.2A). It has been previously studied through ROV imagery (Matossian et al., submitted). The AUV investigation aimed to extend the ROV track towards the south and to visualise the surface of the drift at very high resolution.

Processed 25 m resolution bathymetric data used as background in Fig. 4.1 were made available by INFOMAR (2023) and downloaded from the INFOMAR Marine Data Download Portal. Higher resolution bathymetric data (Fig. 4.1) have been acquired in 2022 over the drift using the multibeam echosounder Kongsberg EM 304 during the RV Belgica 2022/18 survey. The dataset has been processed with Qimera 2.6.2 (QPS) and exported with a 20 m resolution.

Four AUV dives were carried out with AUV *Barabas* (Teledyne Gavia) from Flanders Marine Institute (VLIZ) over the Belgica Mound Drift during the cruise RV Belgica 2022/18, covering a total of 5 km². The objective of the first dive BMP01 (Table 4.1) was to cover a relatively large area at a lower resolution gathering low frequency (LF: 455 kHz) interferometric side-scan sonar data with the Klein 3500 at 100 m range, not covering nadir gaps (Table 4.2). The survey speed of 1.7 m/s and the sampling rate of 7812 Hz resulted in a sampling resolution of approximately 20 cm x 20 cm. The altitude above the seabed was 20 m, which was too high to collect visual imagery of seabed. During dives BMP02 and BMP03 (Table 4.1), the AUV flew 4 m above the seafloor, allowing for visual imagery to be co-registered. The Grasshopper GRAS-14S3M-C black and white camera was set to record with a frame rate of 3.75 FPS and a JPG quality of 75. Dive BMP04 (Table 4.1) focused on capturing features identified during dive BMP01 at a higher resolution and expanding the surveyed area. For capturing higher resolution, the side-scan sonar was set to 50 m range and a sampling rate of 31250 Hz, capturing both high frequency (HF: 900 kHz) side-scan data, LF side-scan data and 455 kHz interferometric bathymetry while flying at an altitude of 8 m (Table 4.2). The sampling resolution was approximately 5 cm (across track) x 10 cm (along track). During the second part of BMP04, the settings of BMP01 were copied and the original survey lines were extended. The AUV positioning was aided by an iXBlue GAPS Ultra-Short Baseline (USBL) system coupled to the shipboard GNSS (Kongsberg Seapath 380-R3). The side-scan sonar data were acquired in a raw SDF format containing separate channels for the HF side-scan data, LF side-scan data and raw interferometric data. The raw data were pre-processed along with the calibration file using the Klein Batch Processing V14.1, extracting readable bathymetry data. The raw navigation data were recorded by the iXBlue C3 Rovins at 100 Hz and post-processed separately for advanced trajectory computation using Delph INS software (Exail). The corrected navigation data were imported into the bathymetry and the side-scan

files with Navinjector Pro (Chesapeake Technology). The side-scan sonar data have been processed (empirical gain normalisation, de-stripe filter and nadir filter) using SonarWiz 7 (Chesapeake Technology). The bathymetry data were converted to XYZ files using SonarWiz 7 and subsequently processed with AutoClean (BeamworX 2023.1). The obtained resolution of the bathymetry is 50 cm and the side-scan sonar mosaics were exported at a grid cell resolution of 25 cm (Fig. 4.2).

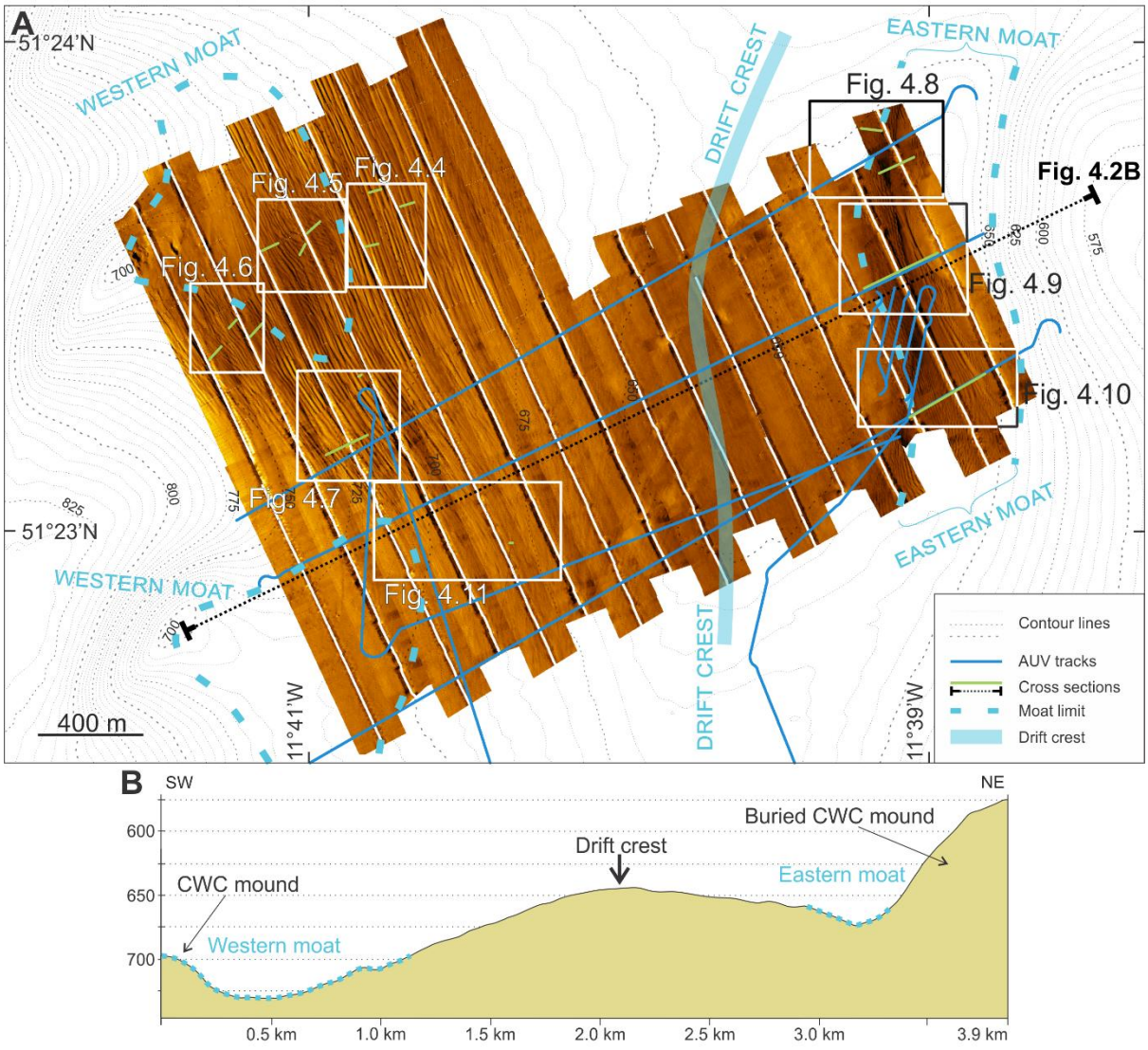

Figure 4.2. (A) Side-scan sonar mosaics (0.25 m resolution) over the northern sector of the Belgica Mound Drift, combining the low resolution surveys of both BMP01 and BMP04. The blue lines correspond to the AUV tracks during which seabed pictures were acquired (BMP02 and BMP03). (B) Cross-section over the drift and the moats. The moat extent is indicated by the blue dashed lines.

Table 4.1. Overview of the AUV dives during the RV Belgica 2022/18 survey. SSS stands for side-scan sonar.

Mission	Date	Duration (minutes)	Distance travelled (km)	Sensors
BMP01	06/08/22	342	32	SSS
BMP02	07/08/22	150	14.8	Camera (4 m)
BMP03	08/08/22	160	13.4	Camera (4 m)
BMP04	08/08/22	292	30.2	SSS

Table 4.2. AUV settings during the RV Belgica 2022/18 survey. SSS, HF and LF respectively stand for side-scan sonar, high frequency and low frequency.

Dive	BMP01 and BMP04	BMP02 and BMP03	BMP04
Survey altitude	20 m	4 m	8 m
SSS Mode	LF and Bathy	N/A	HF, LF and Bathy
SSS Range	100 m	N/A	50 m
SSS pulse length	8 ms	N/A	2 ms
Bathymetry (LF)	ON	N/A	ON
Camera	N/A	ON	N/A

The AUV visual imagery was loaded into QGIS (QGIS Association) and georeferenced by linking it to a CSV file containing the imagery coordinates, the calculated image size based on the altitude of the AUV and a seawater refraction index of 1.34 (Quan and Fry, 1995). The AUV side-scan sonar and bathymetry data were analysed with Global Mapper V25.0 (Blue Marble Geographics) and cross-section profiles have been produced using the Path Profile Tool. The larger view provided by the AUV side-scan sonar imagery allowed for a full observation of large-scale bedforms, with their dimensions, lengths and wavelengths, whereas the cross sections gave a detailed view of the shape of the lee and stoss sides, which were used to calculate the asymmetry index.

The asymmetry index (AI; Fig. 4.3) is based on the following formula (Knaapen, 2005):

$$\frac{(L_2 - L_1)}{L}$$

L_2 being the distance between the crest and the upslope trough, L_1, the distance between the crest and the downslope trough and L the wavelength (L_2 + L_1). It has been calculated for every large-scale bedform shown on the cross-section profiles. AI values between -0.2 and 0.2 correspond to symmetric bedforms, while values below and above that range indicate respectively upslope and downslope asymmetry. The asymmetry is an indicator of the direction of bedform migration and the direction of the dominant flow: The lee side is the downcurrent side, while the stoss side is the upcurrent side (Fig. 4.3).

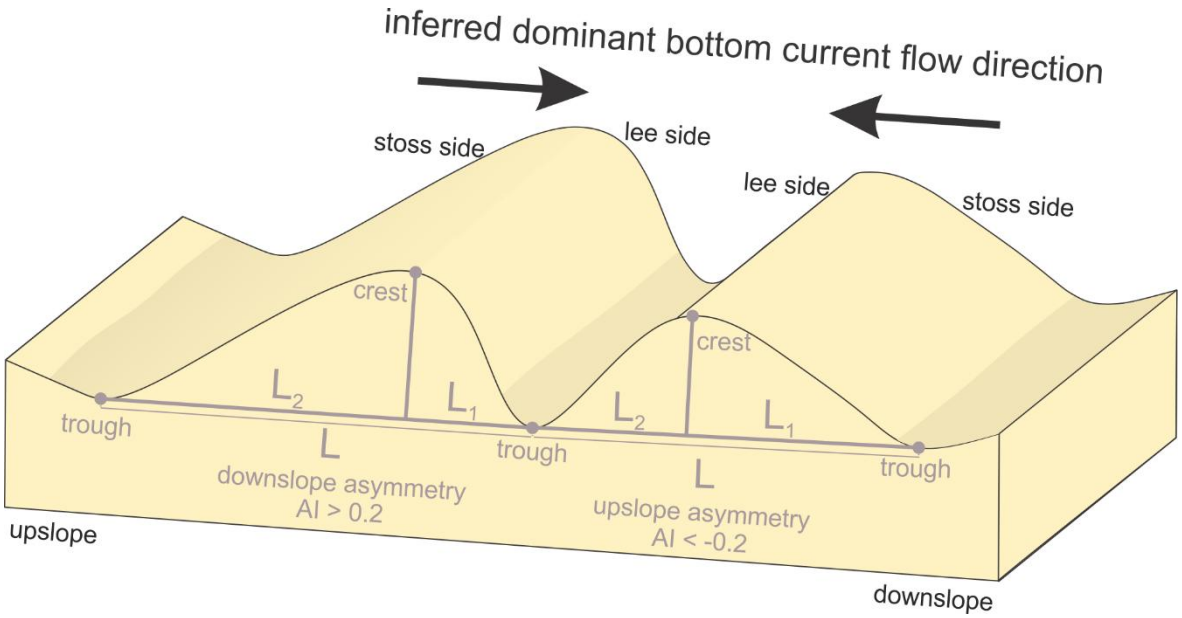

Figure 4.3. Schematic representation of two bedforms, with their geometric parameters and corresponding nomenclature. L: wavelength; L1 and L2: downslope and upslope wavelengths, respectively; AI: asymmetry index based on the formula of Knaapen (2005). The inferred dominant flow direction responsible for the creation of the bedform is indicated by the black arrows.

4.4 Results

Within the survey region, the slope gradient is 3–7° on the west of the crest and between 1 and 4° on the east of the crest (Fig. 4.2B). The identification of each moat is based, as primary criteria, on the changes of slope gradient. In absence of a clear brake of slope gradient on one of the sides of the moats, the edges of the moats have been defined at the same water depth (Fig. 4.2B). Three different moats were identified within the study area (Fig. 4.2A). These three moats are related to CWC mounds and RD1 paleobathymetry (Matossian and Van Rooij, 2024) and are thus spatially contained. Two are on the western side of the drift, upslope of two CWC mounds and cuvette-shaped. The limit of the moats takes into account the top of the CWC mounds (Fig. 4.2B). The third moat is continuous and located on the eastern side of the drift, downslope of a buried CWC mound. The limit of this moat is based on the change of slope at the foot of the buried CWC mound (Fig. 4.2B). All moats feature an alongslope orientation (Fig. 4.2A). The western moats are 900 m wide and 60 m deep (at least 1.1 km long), whereas the eastern moat is 500 m wide and 30 m deep (at least 1.8 km long).

Side-scan sonar imagery indicates the presence of two fields of large kilometric linear and elongated features at both extremities of the study area (Fig. 4.2A). These large-scale features are mainly asymmetrical (Figs. 4.4–4.10), with a gentle stoss side and a steeper and short lee side. These fields are both related to the moats of the drift and are spatially developed over limited areas, covering 2 km² of the surveyed area for the western field and 0.5 km² for the eastern field. No other similar large-scale elongated features have been observed outside of these two fields, on the drift and its crest (2.5 km², Fig. 4.2A). Only dropstones and bioturbations were scattered over the crest of the contourite drift, but numerous marks have

been identified (Fig. 4.11). These marks are straight, rectilinear and cross-cutting lines featuring a N–S elongation, with various levels of preservation, and can be up to one km long. They are a few centimetres deep and are predominantly present on the drift itself. They were identified as bottom otter trawling marks (Gerritsen, 2024).

4.4.1 Western field

The western field is situated between 680 and 765 m water depth. It is 2 km long and 1.5 km wide. It is located within and beyond one of the western moats of the drift, related to a buried CWC mound (Fig. 4.2A). Two main types of large-scale elongated features have been identified based on their crestline characteristics, both having similar wavelength range (between 5 and 35 m, average 15 m) and heights (between 10 and 50 cm, average 25 cm). The **first type** shows straight crestlines up to one km long (Figs. 4.4, 4.7) and covers most of the field (1.85 km²). Its crestline orientation is NNW–SSE, remains constant and thus is slightly oblique to the bathymetric contours. A gradual change of the shape of the straight features can also occur (Fig. 4.7), with a less developed stoss side and a flat and steep lee side. This was only observed near the southern limit of the field, also characterised by only downslope asymmetry (0.80–0.95). The **second type** is less spatially developed (0.06–0.07 km²) and displays crestlines shorter than 200 m with a minimum length of 10 m. The crestline either has a crescent-shaped (Fig. 4.5, section B) or a undulating pattern (Fig. 4.6), with a WNW–ESE orientation. The crescent-shaped elongated features (Fig. 4.5) are located in the cuvette-shaped centre of one of the western moats. Locally (Fig. 4.5, cross section C), the three types of symmetry can be found in a relatively small area of 6 m², with values ranging from -0.73 to 0.31.

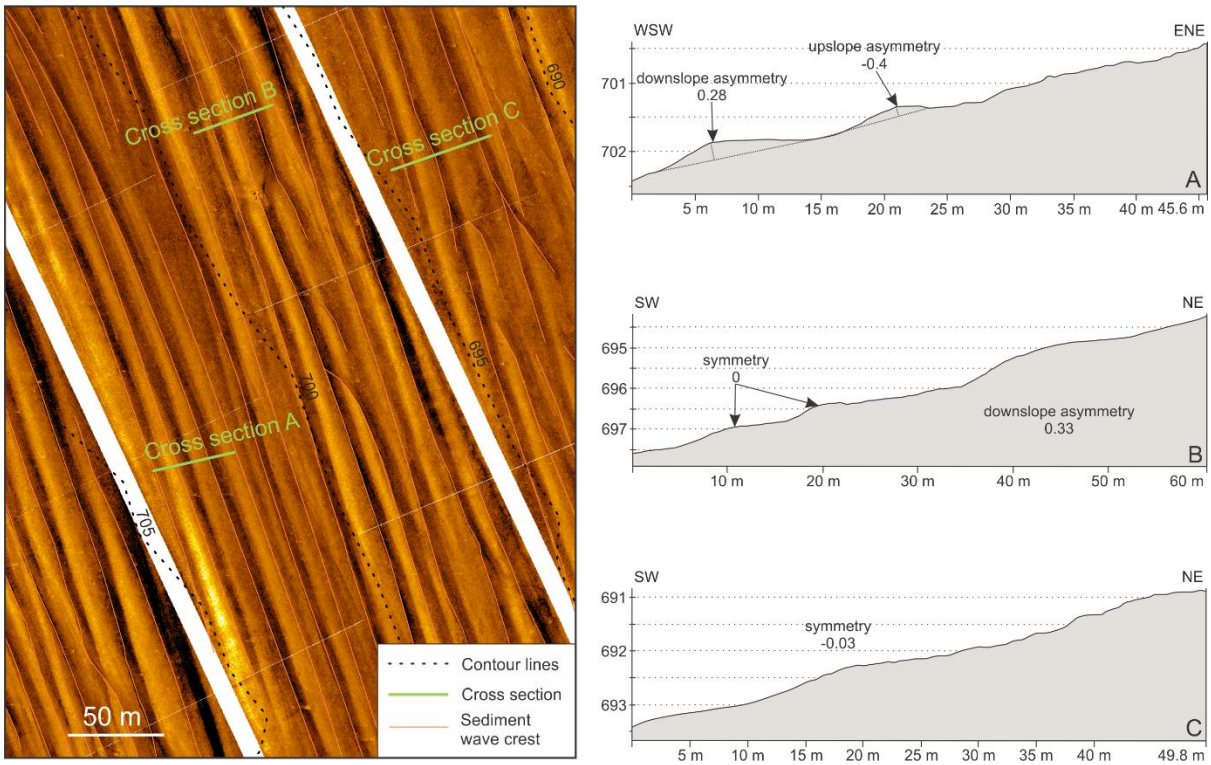

Figure 4.4. Zoom over the side-scan sonar mosaic (Fig. 4.2), with contour line indication every 5 m, and cross-section profiles (A, B and C), outside of the western moat. The AI is calculated for each large-scale feature visible on the cross sections.

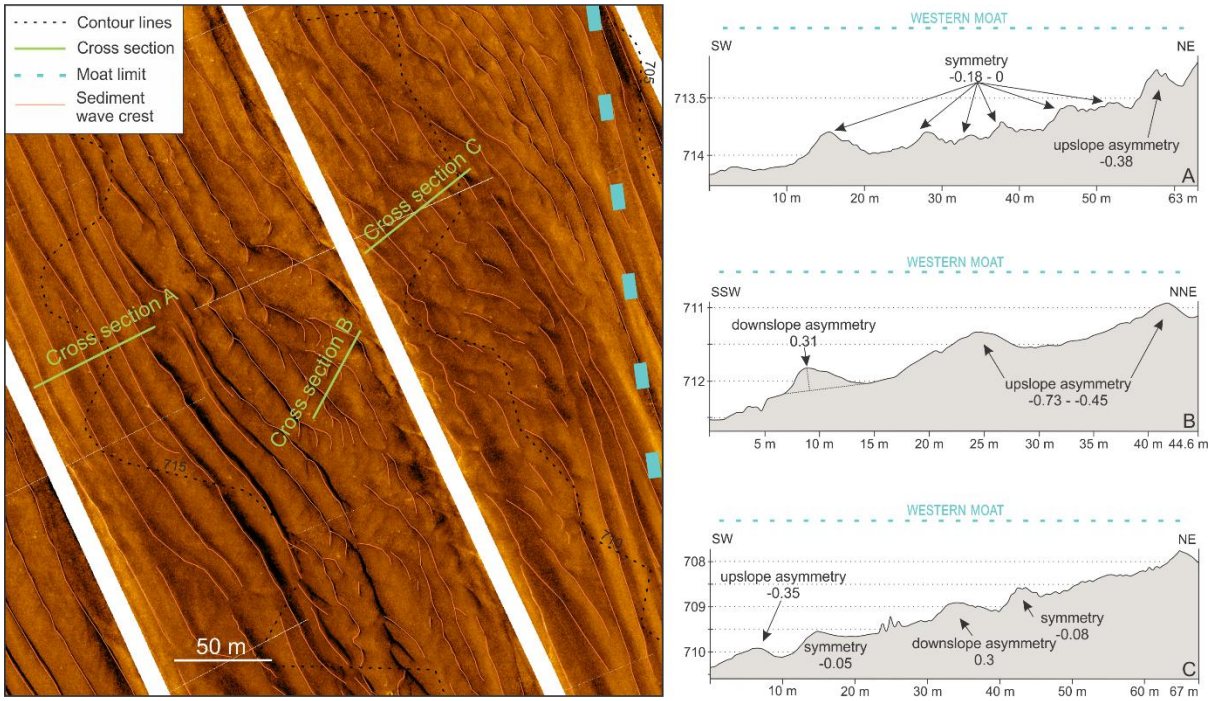

Figure 4.5. Zoom over the side-scan sonar mosaic (Fig. 4.2), with contour line indication every 5 m, and cross-section profiles (A, B and C), in the western moat. The blue dashed line shows the boundary of the moat. The AI is calculated for each large-scale feature visible on the cross sections.

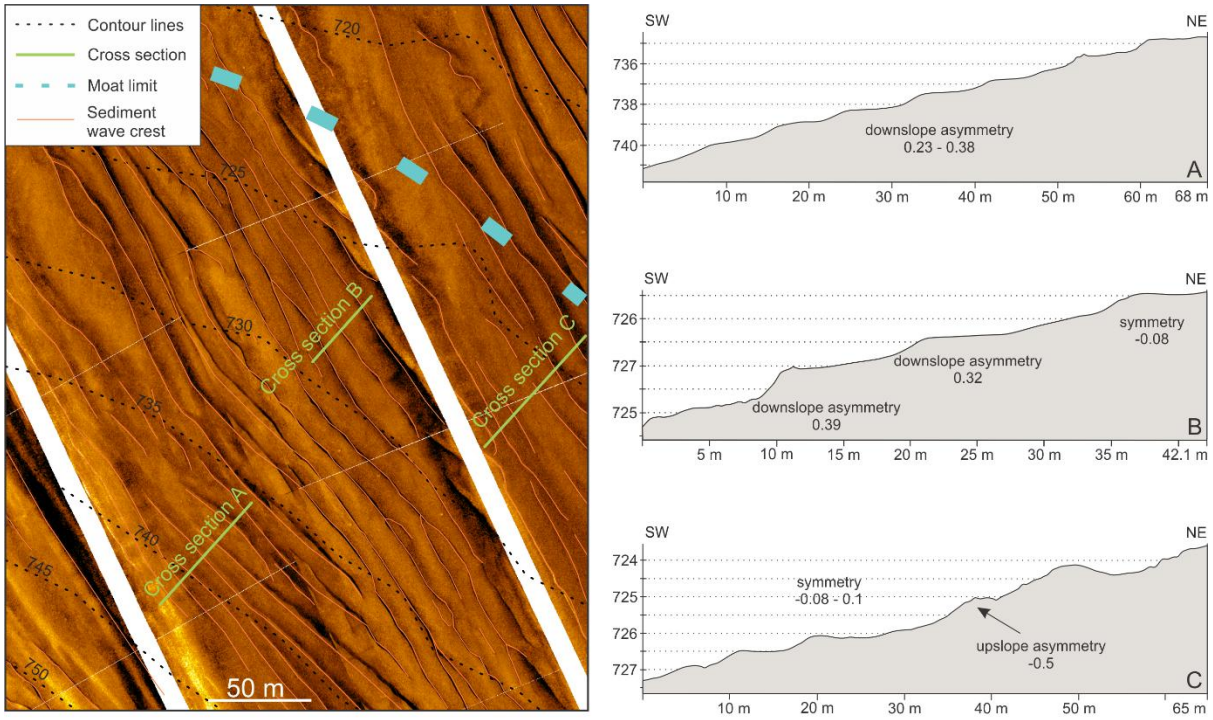

Figure 4.6. Zoom over the side-scan sonar mosaic (Fig. 4.2), with contour line indication every 5 m, and cross-section profiles (A, B and C), outside of the western moat. The blue dashed line shows the boundary of the moat. The asymmetry index (AI) is calculated for each large-scale feature visible on the cross sections.

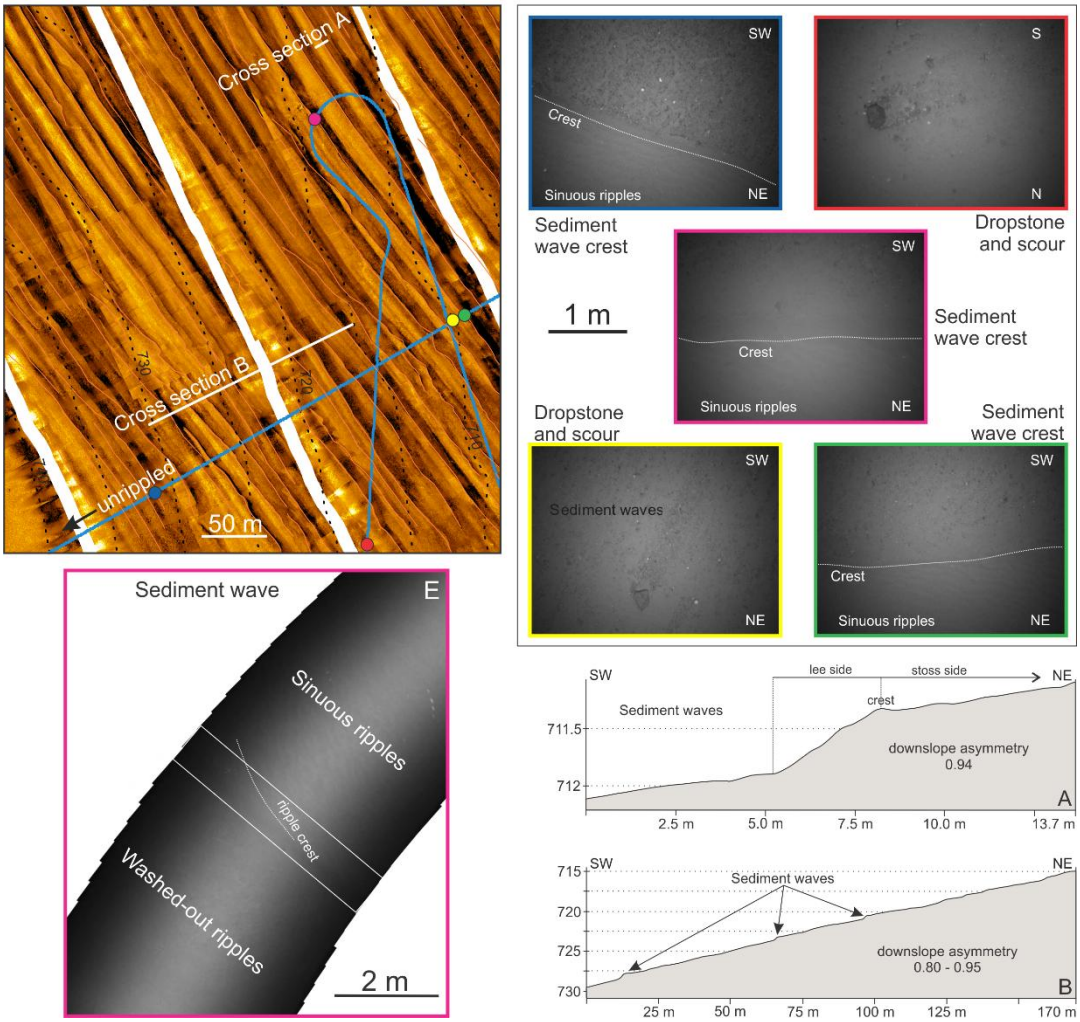

Figure 4.7. Zoom over the side-scan sonar mosaic (HF and LF; Fig. 4.2), with contour line indication every 5 m, and cross-section profiles (A and B), outside of the western moat. The AI is calculated for each large-scale feature visible on the cross sections. The location of each picture is shown by the coloured dots.

The large-scale features progressively fade away towards the south (Figs. 4.2, 4.7) and the east (Figs. 4.2, 4.4), with a progressive decrease of the height up to 10 cm (Fig. 4.4, cross section C). On the eastern limit, the wavelengths increase up to 35 m until the features fade away, with a crestline less easily identifiable (Fig. 4.4). The northern and western limits of the field cannot be inferred exactly as they occur outside the present dataset.

The only visual imagery available for this western moat field was acquired near the southern limit (Fig. 4.7). Two types of smaller-scale ripples superimposed on the large-scale features have been observed: straight to sinuous ripples and washed-out ripples, respectively on the stoss and lee sides of the downslope asymmetric large-scale features. Both smaller-scale ripples are on average a few centimetres high and have wavelengths comprised between 5 and 20 cm. The straight to sinuous ripples are asymmetrical with a short and steep lee side and a gentler stoss side. The washed-out ripples are smaller (minimum 1 cm high) straight to sinuous ripples, with a shorter lee side and a less well-defined crestline. They are associated with irregular gravel patches visible in the trough of the ripples. In the direct vicinity of the large-scale elongated feature crestlines, smaller-scale ripples tend to be oblique, with a

progressive change of orientation going further away from the crestline of the elongated features, until they are parallel. Scattered dropstones (around 10 cm wide) and related scours, as well as rare bioturbations have been also identified.

4.4.2 Eastern field

The eastern field has a water depth between 640 and 670 m, is 1.5 km long and 0.5 km wide. It is mainly located inside the eastern moat of the drift and is relatively constrained by topography, with a buried CWC mound to the east. The large-scale elongated features have a NNW–SSE crestline orientation, which is on average parallel to slightly oblique to the moat contours, but they do not exactly follow them (Figs. 4.2A, 4.8, 4.9, 4.10). The wavelengths are between 5 and 20 m (average 10 m) while the heights are between 10 and 30 cm (average around 20 cm). Also here, **two types** of large-scale features were observed, one with long straight crestline of up to 1 km long (0.23 km²) and the other with an undulating crestline (minimum 10 m long; 0.27 km²) (Figs. 4.8-4.10). The straight crestline features are surrounded to the west and east by the undulating features (Figs. 4.8–4.10). Some of these features can exhibit both types of crestlines (Fig. 4.10), with a progressive change from one type to another. There is a clear change of symmetry of the large-scale features between both flanks of the moat, with the features on the western flank being symmetric and downslope asymmetric (-0.14–0.63) and those on the eastern flank being symmetric and upslope asymmetric (-0.78–0.14) (Figs. 4.8, 4.9). This relation is reversed in the southern part of the field, with downslope asymmetry (0.04–0.66) on the east and upslope asymmetry (-0.84–0) on the western flank of the moat (Fig. 4.10). The large-scale elongated features displaying an upslope asymmetry mainly correspond to the straight crested features. The western and eastern boundaries of the field are covered by the present dataset, while the northern and southern boundaries extend outside of the study area.

The visual imagery allowed the identification of smaller-scale ripples superimposed on the large-scale features: linguoid ripples, straight to sinuous ripples and washed-out ripples. The smaller-scale ripples are on average a few centimetres high and have wavelengths comprised between 5 and 25 cm (Figs. 4.8–4.10). The linguoid ripples are asymmetrical with a steeper and shorter lee side. They display a highly variable morphology with an irregular crescent-shaped crest. The associated seafloor texture is usually very fine and well-sorted. The linguoid ripples are located near the crest, on the stoss side of the large-scale features, while sinuous ripples are on the lee side and on the stoss side, further away from the crestline of the features. Over a distance of less than 10 cm, two ripple types blend (Figs. 4.8–4.10). The crestlines of the ripples are on average parallel to the large-scale feature crestlines (Figs. 4.9, 4.10), except near the large-scale feature crestlines, where sinuous ripples tend to be oblique with a N–S orientation (Figs. 4.8, 4.9), or even perpendicular (NE–SW) (Fig. 4.8). The washed-out ripples are associated with coarser sediment and are only observed near the western and eastern boundaries of the field (Figs. 4.8–4.10). Further away outside of the moat and the field, the seafloor is coarser. Both sides of the moat are characterised by a 10–50 m wide area with washed-out ripples which disappear and leave the seafloor unrippled further away from the centre of the moat. Scattered dropstones (size up to 10 cm and wider; Figs. 4.8, 4.9) and related scours, as well as rare bioturbations (Fig. 4.8) have been also identified. The side-scan imagery sometimes also infers the presence of larger dropstones (at least 80 cm wide). They are usually located near the western boundary of the eastern moat, where no large-scale features are observed and where the seafloor is unrippled (Figs. 4.8–4.10).

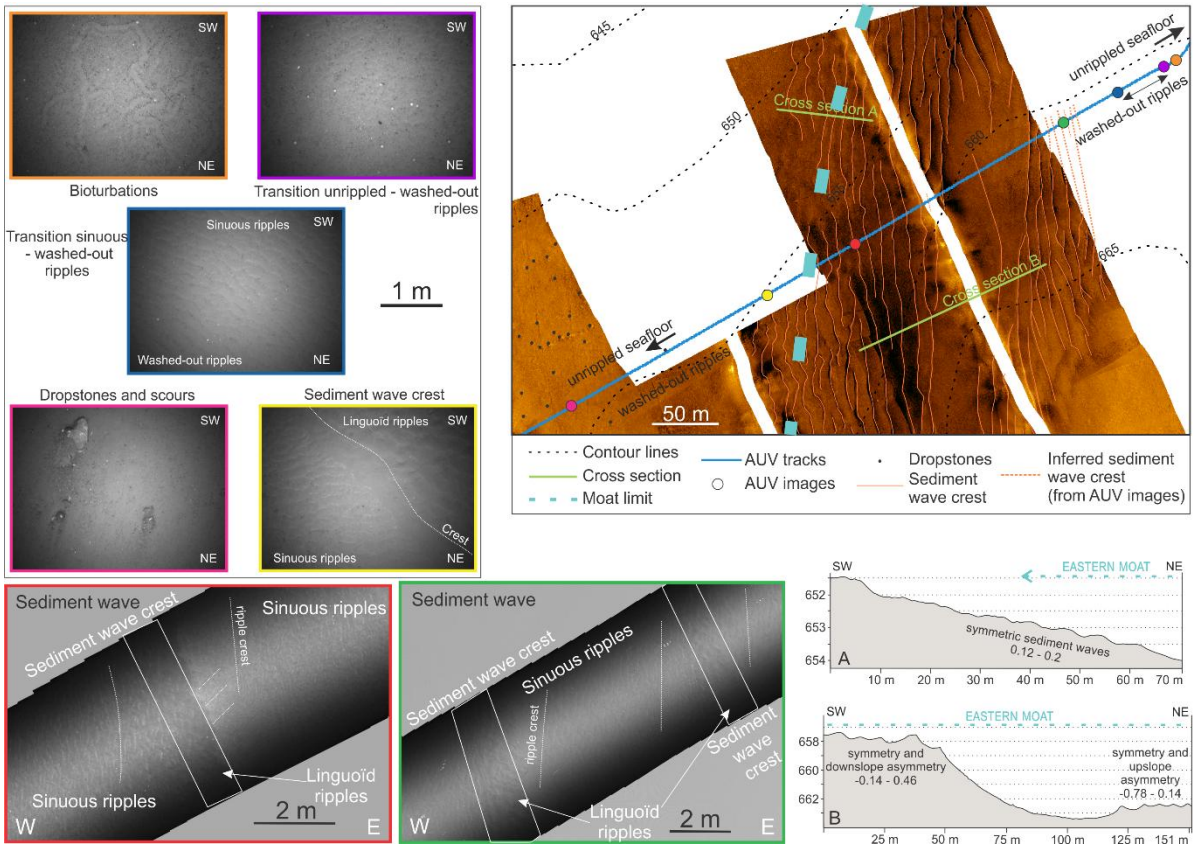

Figure 4.8. Zoom over the side-scan sonar mosaic (HF and LF; Fig. 4.2), with contour line indication every 5 m, and cross-section profiles (A and B), within the eastern moat. The blue dashed lines show the boundaries of the moats. The AI is calculated for each large-scale feature visible on the cross sections. The location of each picture is shown by the coloured dots.

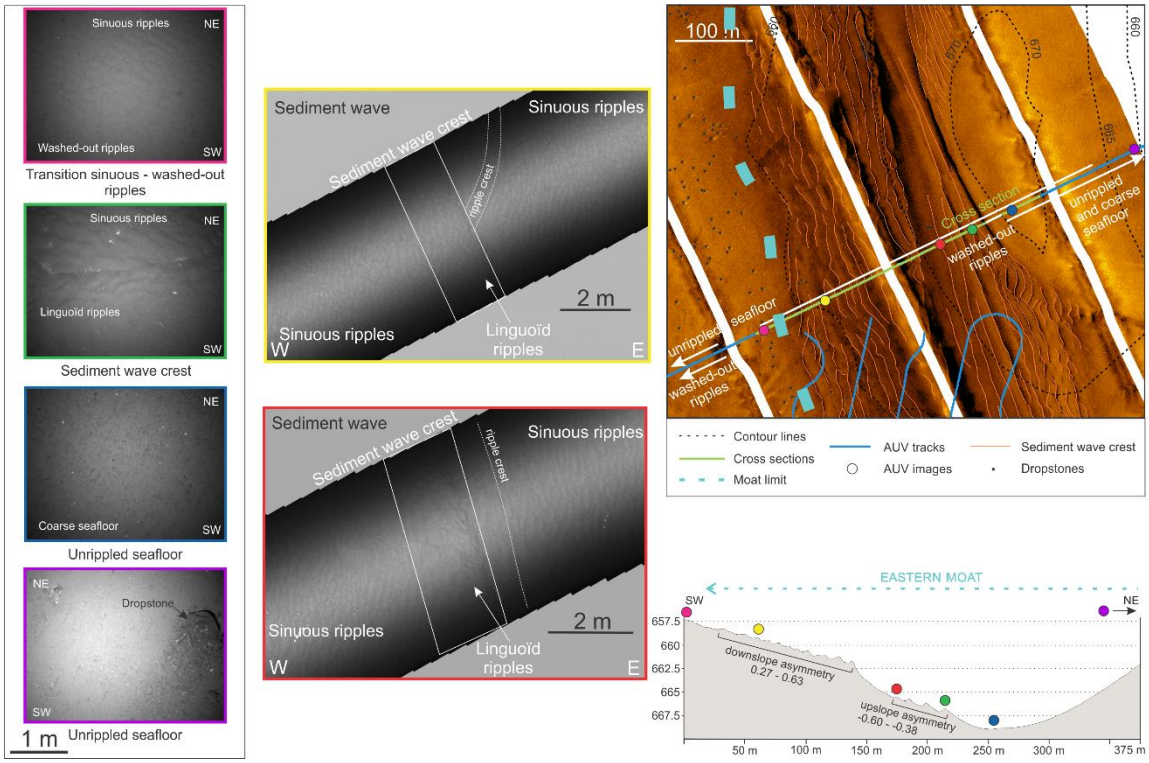

Figure 4.9. Zoom over the side-scan sonar mosaic (Fig. 4.2), with contour line indication every 5 m, and cross section profile, within the eastern moat. The blue dashed lines show the boundaries of the moats. The AI is calculated for each large-scale feature visible on the cross section. The location of each picture is shown by the coloured dots.

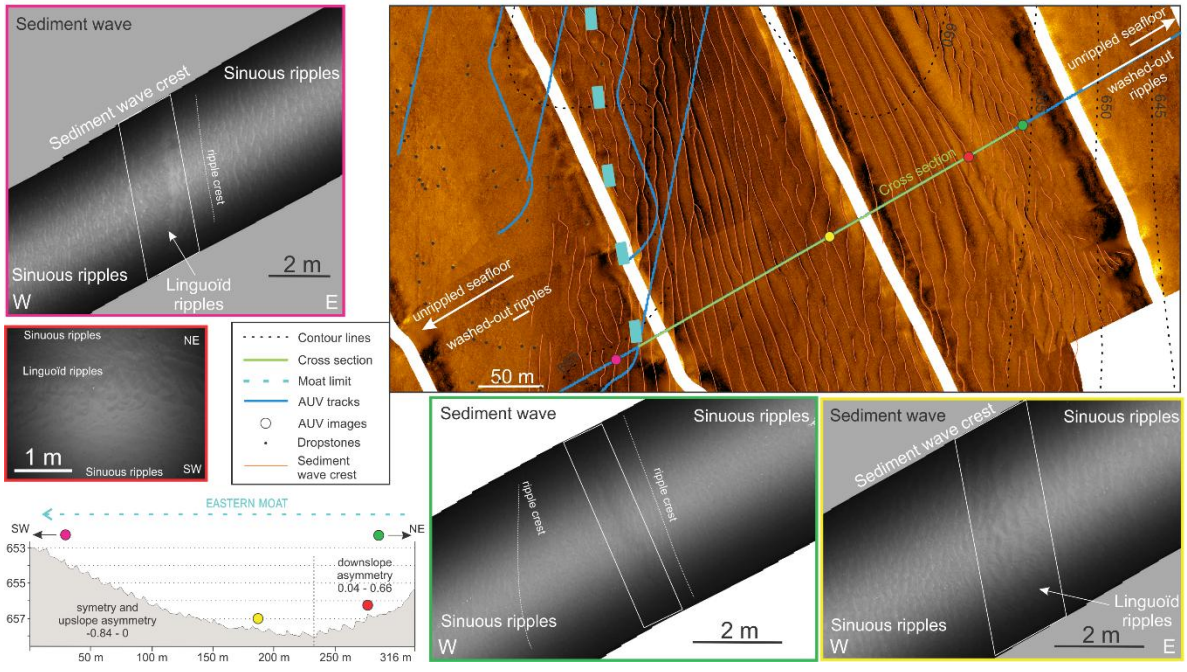

Figure 4.10. Zoom over the side-scan sonar mosaic (Fig. 4.2), with contour line indication every 5 m, and cross-section profile, within the eastern moat. The blue dashed lines show the boundaries of the moats. The AI is calculated for each large-scale feature visible on the cross section. The location of each picture is shown by the coloured dots.

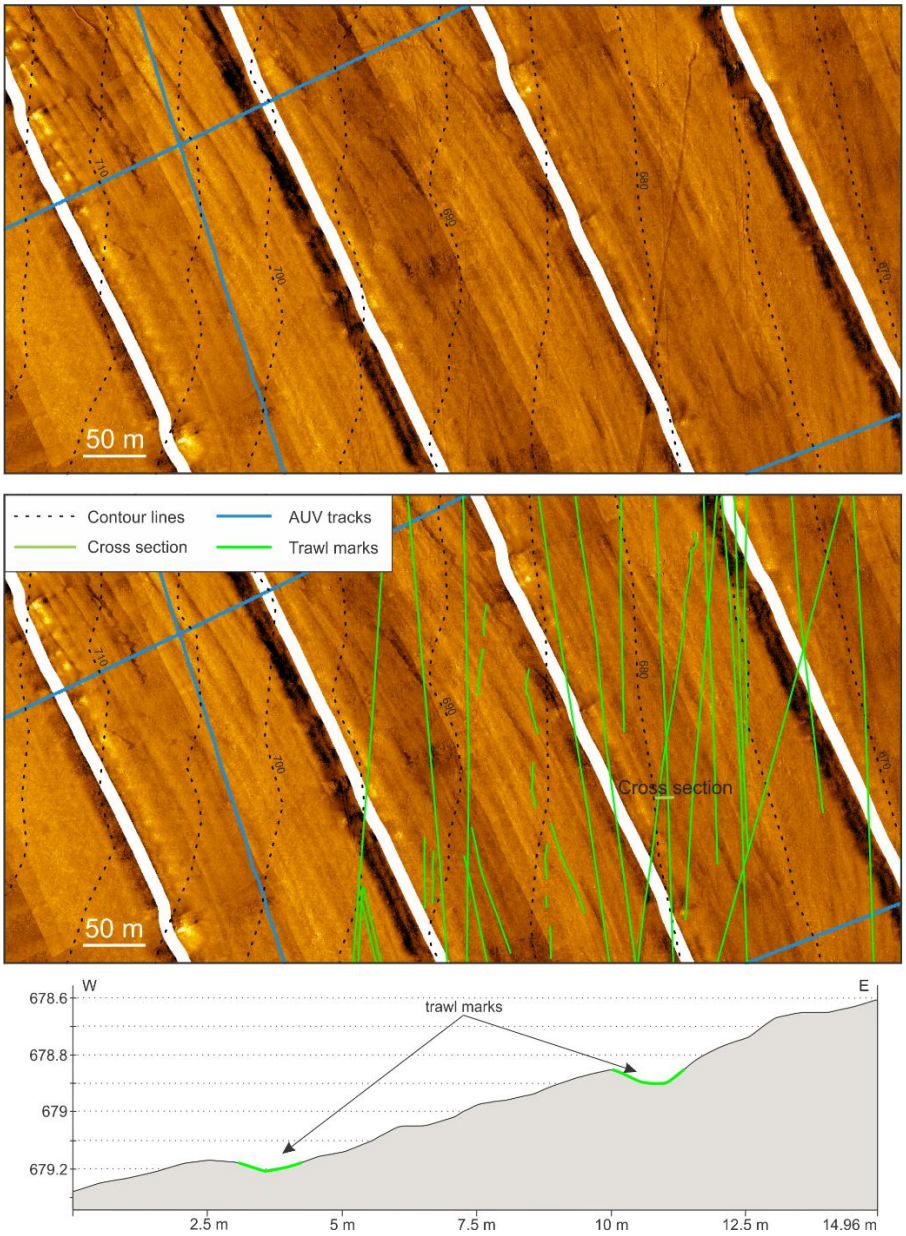

Figure 4.11. Zoom over the side-scan sonar mosaic (Fig. 4.2), with contour line indication every 5 m, and cross section showing the inferred seabed trawl marks.

4.5 Discussion

4.5.1 Large-scale elongated bedforms

4.5.1.1 Identification and classification

Matossian et al. (submitted) have encountered, through ROV imagery (Fig. 4.1), similar bedforms as the large-scale elongated features. Although their exact length was unknown, they have determined that they were possibly small-scale sediment waves with superimposed ripples. The precise dimensions of these features formed over a contourite drift are distinguishable through the high-resolution side-scan sonar and bathymetry (Figs. 4.2, 4.4–

4.10). The linear to undulating, for the majority kilometric, crestlines and wavelengths fit the broad definition of deep-water sediment waves by Wynn et al. (2000) and Wynn and Stow (2002): Sediment waves are large-scale (tens of metres to a few kilometres wavelengths) undulating bedforms, formed by depositional processes linked to bottom currents on slopes and in mixed turbidite-contourite systems. Furthermore, sediment waves have already been observed in the vicinity of the Moira Mounds (Fig. 4.1), situated to the NW of the drift (Foubert et al., 2005; Huvenne et al., 2005; Wheeler et al., 2005). They have been described as straight, long-crested (several hundreds of metres long), asymmetric, up to 50 cm high and with wavelengths of 15 to 20 m (Foubert et al., 2005, 2011), which corresponds to the characteristics of the sediment waves formed on the Belgica Mound Drift (wavelengths between 5 and 35 m, heights between 10 and 50 cm and several hundreds of metres to kilometric long crestlines). This would confirm the identification of Matossian et al. (submitted). Superimposed sediment waves at similar water depths, on similar slope gradients (0.5–2.8°) and with a height of 10 m are found in large-scale drifts close to the Le Danois Bank (Bay of Biscay) (Liu et al., 2019). Because of their small heights, the sediment waves were referred to as small-scale sediment waves (Liu et al., 2019). The sediment waves of the Belgica Mound Drift are smaller; hence they can be classified as small-scale sediment waves. Other than the ones observed by Liu et al. (2019), there are few examples of contourite drifts linked to superimposed sediment waves. This can be explained by the inability to observe features on the seafloor of these drifts due to a lack of high-resolution data.

4.5.1.2 Regional drivers of sediment wave development

There are three formation processes for the development of deep-water sediment waves: alongslope bottom current (Wynn and Stow, 2002), turbidity current (Wynn and Stow, 2002) or internal waves (Southard and Cacchione, 1972; Cacchione and Southard, 1974; Normark et al., 1980; Karl et al., 1986; Reeder et al., 2011; Ribó et al., 2016). Among these processes, the turbidity current seems to be unlikely as there is no evidence of dominating downslope currents in the vicinity of the Belgica Mound Drift. The presence of the contourite drift, observed through seismic data by Matossian and Van Rooij (2024), indicates the influence of a contour current, i.e. a thermohaline-driven alongslope bottom current (Rebesco et al., 2014). However, the sediment waves show a general NNW–SSE orientation which likely infers an across-slope (Prothero and Schwab, 1996; Knaapen, 2005) bi-directional ENE–WSW bottom currents being at the origin of the sediment waves. This current orientation would fit with the W–E tidal currents observed through moorings in the study area (Fig. 4.1; Matossian et al., submitted). The sediment waves would thus be related to tidal currents, known to result from the interaction between a trapped baroclinic motion with the seafloor. This motion, similar in term of process to internal waves but with a different period, is known in the area to be intensified at the pycnocline. Both sediment wave fields being at the same water depth as the ENAW–MOW interface, this enhanced motion has a direct impact on sediment dynamic of the fields. The trapped baroclinic motion and its tidal component have sufficient energy and potential to mobilise already-deposited sediment up and downslope in ripples and to overprint the contour current, as similarly observed Wu et al. (2023) on another contourite drift in the South China Sea. The type of sediment waves formed by trapped diurnal baroclinic motion (or semi-diurnal internal waves) is still poorly known, as these motions have variable intensity at a local scale. Therefore, there are not yet definitive criteria to recognise them (Pomar et al., 2012; Ribó et al., 2016).

As the potential mechanism for the formation of the sediment waves, being the tidal current, has also been recorded during recent mooring deployments (Matossian et al., submitted), it can be expected that the sediment waves are still active. It is, however, unknown when this process started and if the sediment waves are merely relict features, preserved by the present-day processes.

4.5.2 Spatial variability of the seabed sedimentary processes

The sediment waves and the superimposed ripples are often seen parallel with each other, with a NNW–SSE trend not following the local bathymetric contours (Figs. 4.12, 4.13). There are a few counterexamples of sediment waves with a NW–SE orientation at a very local scale in the western field (Fig. 4.5) and of superimposed small-scale ripples located in the direct vicinity of the sediment wave crest (Figs. 4.7–4.9, 4.13). The NNW–SSE bedform orientation infers ENE–WSW bottom currents being at the origin of both the sediment waves and the superimposed ripples (Figs. 4.13A, C). This orientation fits with the measured bi-directional W–E (across-slope) tidal currents (Matossian et al., submitted). At the drift scale, there are no bedforms that could have been formed as a result of the measured residual northward (alongslope) bottom current (White et al., 2007; Matossian et al., submitted), i.e. an uni-directional current combining the contour current (thermohaline circulation related to the European Slope Current) and the alongslope bottom current generated by the trapped baroclinic motion. The contour currents are typically renowned to be the primary factor controlling the initiation and evolution of contourite drifts (Rebesco et al., 2014). The absence of bedforms that could be formed by the contour current implies that this current, at the origin of the contourite drift and its moats (Matossian and Van Rooij, 2024), would consequently play a smaller role in the present-day active formation of the bedforms. Similar observations over a contourite drift in the northern South China Sea has been made by Wu et al. (2023): They highlighted that other hydrodynamic processes, like internal waves and tidal activities, can have a significant impact on the sediment remobilisation on a drift, stronger than the contour current that initiated the drift.

The sharp transitions between different types of superimposed ripples over a few metres (Figs. 4.8–4.10) suggest spatial variations in the current intensity on a plurimetric scale. Following the bedform-velocity matrix of Stow et al. (2009), inferred velocities range between 20 and 50 cm/s for the sinuous and linguoid ripples and up to 75 cm/s for the washed-out ripples (Baas and De Koning, 1995). Velocities up to 50 cm/s were recorded at 6 m above the seafloor of the drift (Matossian et al., submitted). The sinuous and linguoid ripples can be formed by the present-day recorded flow, while the washed-out ripples necessitate stronger and unrecorded flows to develop.

The bathymetry of the drift, the moats and the CWC mounds play also a role in the spatial variations of the local hydrodynamic processes shaping the sediment waves and their superimposed ripples.

4.5.2.1 Western sediment wave field

The CWC mounds are obstacles that can locally deviate the currents and intensify their strength (Van Rooij et al., 2003; Huvenne et al., 2009). The origin of the western moats was initially thought to be linked to the onset of drift in the Early Pleistocene, due to nearby outcropping CWC mounds deflecting the contour current (Matossian and Van Rooij, 2024). It

remains also possible that the alongslope current generated by the trapped baroclinic motion would have played a role in the onset of the drift and its moats, if such motion was already occurring in the area at that time. The enhancement of this motion relies on strong vertical density gradient (Rhines, 1970) partially related to the presence of the MOW. The introduction of the MOW in the Porcupine Seabight started during Pliocene (Stow, 1982; Pearson and Jenkins, 1986; McDonnell and Shannon, 2001; Van Rooij et al., 2003, 2009), it can thus be expected that the trapped baroclinic motion would be enhanced and the alongslope current would be generated by this motion since the drift onset (discussed below).

The almost circular shape of the western moats (Figs. 4.2, 4.12) would show that the CWC mounds deviate also the W–E tidal current, perpendicular to the measured residual northward bottom current. The residual current would be responsible for shaping the moats parallel to the contours while the W–E tidal flow would have widened the western moats on the eastern side of the CWC mounds, where the drift is entrapped and the sediment can be mobilised (Figs. 4.2, 4.12).

The western sediment wave field, located in and close by one of the western moats (Fig. 4.12), displays higher complexity in the sediment wave asymmetry and crestline direction than the eastern field. The NNW–SSE orientation of the sediment waves shows an association to the present-day recorded tidal current (Matossian et al., submitted). However, the asymmetry index does not allow to clearly define a dominant direction of this current in the field. At the centre of the moat (Fig. 4.5) and upslope (Fig. 4.4), there is no distinguishable spatial pattern for the asymmetry index. Based on Knaapen (2005), the direction of migration of the sediment waves is in the direction of the steepest slope (Fig. 4.3). The succession of downslope and upslope asymmetric sediment waves next to each other would show that there is not one primary direction (Knaapen, 2005) controlling the development of the observed sediment waves, but rather a bi-directional flow that can be linked to the tidal current. The change of types of sediment waves being either shorter with a crescent-shaped crestline (Fig. 4.5) or longer with a straight to undulating crestline (Figs. 4.4, 4.6, 4.7) could be related to local variations of the currents (Prothero and Schwab, 1996). The short sediment waves (Figs. 4.5, 4.12) display a NW–SE crestline, with a crescent shape suggesting stronger bi-directional current (Prothero and Schwab, 1996), with changes in the current direction in the vicinity of the CWC mound, in the cuvette-shaped centre of the moat. The change of crestline length and orientation indicates that the CWC mounds play a role in a local deflection of the current in their surroundings, as already observed by Van Rooij et al. (2003) and Huvenne et al. (2009) in the Belgica Mound Province. The cuvette-shaped moat could trap the tidal currents and trigger strong spatial variations of the current in the moat, forming the crescent-shaped sediment waves.

Outside of the moat, the sediment waves display a NNW–SSE orientation, demonstrating a W–E tidal current influence. However, here, the asymmetry index (Figs. 4.6, 4.7) clearly suggests a downslope asymmetry pattern, allowing to infer a dominant WSW to SW current direction. Out of the moats and further away from the CWC mounds, the tidal current can propagate freely and directly shape the sediment waves. The decreasing size of the sediment waves and the change of shape (Fig. 4.7) towards the southern limit of the field could be related to a weakening of the strength of the currents or a change of the sediment grain size (Stow et al., 2009).

4.5.2.2 Eastern sediment wave field

The origin of the eastern moat is related to the interaction of the contour current with the presence of a buried CWC mound developed over a kilometric escarpment (Matossian and Van Rooij, 2024). Similar to the western moat, it is possible that the alongslope current generated by trapped baroclinic motion would have also played a role in the shaping of the moats with a N–S orientation since the onset of the drift.

Apart from the extreme south and north (Fig. 4.10), the western limit of the sediment wave field corresponds to the western limit of the moat, while the eastern limit of the field is located within the moat. The eastern field is delimited at its boundaries by a 10–50 m broad zone of washed-out ripples on the west and east (Fig. 4.12), indicating strong currents up to 75 cm/s around the field. Such velocities have not yet been recorded through moorings (Huvenne et al., 2005; Wheeler et al., 2005; Foubert et al., 2011; Matossian et al., submitted). These velocities could be related to a local topographic acceleration or peak flow events, as stated by Huvenne et al. (2005), Wheeler et al. (2005) and Foubert et al. (2011) with the observation of large-scale features, such as sand ribbons, striations, furrows and barchan dunes near the Moira Mounds (Fig. 4.1), necessitating more than 100 cm/s to form.

The smaller wavelengths of the sediment waves in this eastern field could be related to a slower sediment mobilisation than in the western field, as demonstrated by Knaapen (2005). The NNW–SSE orientation of the sediment waves infers an across-slope tidal current also influencing this field. The change in the asymmetry index between both flanks of the moat (Figs. 4.8, 4.9, 4.12) suggests that the direction of the tidal current is converging towards the centre of the field: On the western side, the current is towards the ENE (downslope asymmetry) while on the eastern side, the current is towards the WSW (upslope asymmetry). To the south of the moat (Figs. 4.10, 4.12), the upslope asymmetry on the western side and the downslope asymmetry on the eastern side indicate an unidirectional WSW flow on both sides. In this region, the sediment waves seem to migrate out of the moat, directly on the drift, showing that the WSW tidal current is locally strong enough to transport sediment against the gravity-driven grain migration (Prothero and Schwab, 1996). It could be related to changes of the slope gradient of the moat. In the south, the flank slopes are less steep (0.2–3°), which could allow the tidal flow to overflow on the drift, while in the centre and towards the north, the tidal current is confined between steeper flanks (3–6°) of the moat. The straight crested sediment waves are primarily the ones that exhibit an upslope asymmetry. The straight crestlines, in contrast to the undulating sediment waves, show that the formation mechanism of the bedforms is under one dominant flow direction (Prothero and Schwab, 1996), which is consistent with the AI pattern seen on both sides of the eastern field.

The oblique to perpendicular superimposed ripples located on the lee side of the sediment waves (Figs. 4.9, 4.13B) could be ladderback ripples, also known as interference ripples (Ramsay et al., 1989). These ripples show the existence of two current directions, either concurrently or successively, and are frequently caused by the refraction of oblique waves in coastal areas (Ramsay et al., 1989). Despite the fact that their origin in deeper environments remains unclear (Jiménez-Romero et al., 2022), Stow et al. (2013) connected them to tidal currents. The lee side of large-scale bedforms can refract the flow, which can create straight to sinuous ripples, with their crest oblique or even perpendicular to the sediment wave crestline (Jiménez-Romero et al., 2022). Jiménez-Romero et al. (2022) have noted similar ripples in the trough of dunes on the continental slope of the Gulf of Cadiz, with an average wavelength

of 7.7 cm and a crest height of 1 cm. The lee side of the sediment waves could form an obstacle to a secondary flow, opposite to the dominant flow direction responsible for the formation of the sediment waves (Fig. 4.13B). Thus, the sediment waves themselves play also a role in the spatial variation of the bottom currents as seen by the change of types of superimposed bedforms.

4.5.2.3 Drift and moats

The dropstones are only discernible on the drift and upslope of the western side of the eastern field (Figs. 4.8–4.10). Their size (10 cm–1 m wide) prevents them from being transported away by currents weaker than 100 cm/s (Prothero and Schwab, 1996), unrecorded on the drift (Matossian et al., submitted). They are supposed to be noticeable everywhere on the drift and its moats, except if they are buried. The absence of any types of bedforms, the coarser sand cover and the dropstones on the drift as well as the fine sediment fraction discernible in the sediment wave fields evidence that the fine sediment fraction from the drift has been transported away. The winnowing of the fine fraction would prevent the formation of bedforms on the drift, as there would not be sufficient fine sediment on the drift that can be remobilised to form the ripples (Stow et al., 2009). The present-day predominance of the W–E bi-directional tidal current over the drift (Matossian et al., submitted) and its moats involves that the sediment is transported from the drift towards W and E, directly into the moats. The fine fraction would be trapped by the interaction of the tidal current and the moats topography, like the cuvette-shaped western moat (Fig. 4.5) and the elongated eastern moat with steep slopes (Figs. 4.8–4.10) and thus bury the dropstones. The fine sediment fraction can be resuspended and locally mobilised for the current formation of ripples within the moats (Stow et al., 2009). There would consequently be enough sediment to form the sediment waves and their superimposed ripples in and near the moats.

In the moat-drift system (Rebesco et al., 2014; Wilckens et al., 2023; Beelen and Wood, 2023), moats are related to alongslope processes (contour currents), with strong currents in the moats carrying the fine fraction away and weaker currents on the drift allowing the deposition of sediment over the drift. This is in contradiction with what is observed on the Belgica Mound Drift, with the winnowing of the fine fraction on the drift and the sediment trapped in the moats. Moreover, the formation of the sediment waves and their superimposed ripples as well as the shaping of the western moats by the tidal bi-directional currents over the contour current shows that a contourite drift can also be under the influence of secondary hydrodynamic processes. As stated by Rebesco et al. (2014), these processes and their influence on the drift formation/evolution are still poorly understood. As demonstrated for example by Miramontes et al. (2020) and Wu et al. (2023), local hydrodynamic processes such as internal waves or tides are important to consider to better understand the evolution of a drift. Studies focusing on associated processes would require multidisciplinary approaches with high-resolution datasets densely covering the drift.

The present-day dominance of the tidal current over the residual northward bottom current on the upper layer of the drift and its moats would show that there has been a change in the hydrodynamic processes occurring in the area since the onset of the contourite drift. The drift has been studied in detail through high-resolution reflection seismic data (Matossian and Van Rooij, 2024), which gives an idea of the average dominant hydrodynamic processes that happened during Quaternary. The drift and its moats started to form under the influence of the residual northward (alongslope) bottom current and the glacial and interglacial cycles during

Pleistocene (Matossian and Van Rooij, 2024). During interglacial periods, the sea-level rises (Van Rooij et al., 2009) allowing the MOW to enter into the Porcupine Seabight basin (Huvenne et al., 2009; Raddatz et al., 2011). The bottom-current intensity can then increase by the generation of bottom currents under the presence of the trapped baroclinic motion, enhanced at the ENAW–MOW interface (White, 2007; White and Dorschel, 2010). The strong alongslope currents can erode the sediment, winnow away the finer material and shape the moats with a N–S orientation. During glacial periods, the sea-level is lower (Van Rooij et al., 2009), preventing the MOW to reach the basin (Huvenne et al., 2009; Raddatz et al., 2011). Therefore, the trapped baroclinic motion and the bottom currents are weaker (Huvenne et al., 2009; Raddatz et al., 2011) which allows the muddy sedimentation to occur on the drift (Van Rooij et al., 2007; Matossian and Van Rooij, 2024). Several ice-rafting events have been recorded in the region, with the last one corresponding to the Last Glacial Maximum (Van Rooij et al., 2007). The observed dropstones could consequently be at the earliest from the Last Glacial Maximum. At the present interglacial period, the moats are mainly shaped by the W–E tidal current. Their morphologies trap the tidal current and prevent the sediment from leaving the moats. The sediment waves would accordingly be from this period, and at the latest formed during Holocene. The relatively small-size of the sediment waves would make it difficult to establish, even from high-resolution seismic data, if such features were formed during other interglacial periods.

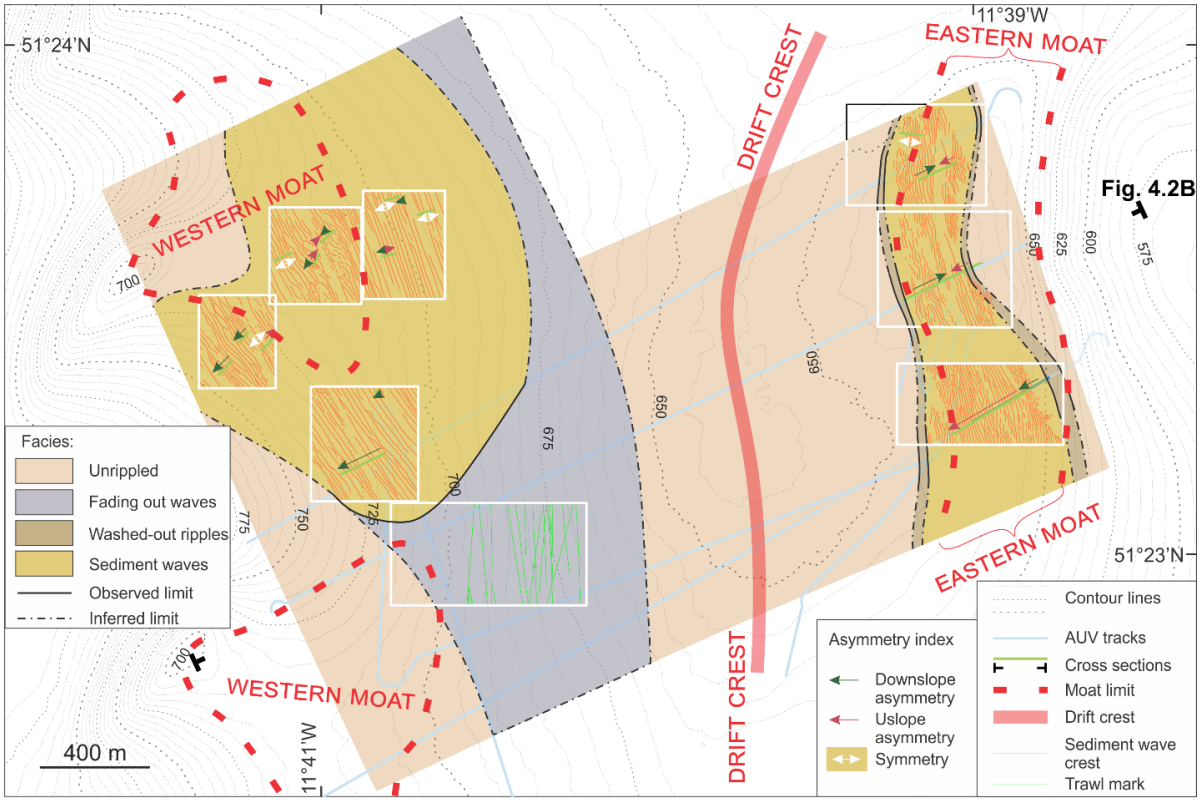

Figure 4.12. Morphosedimentary map over the area covered by the AUV side-scan sonar imagery.

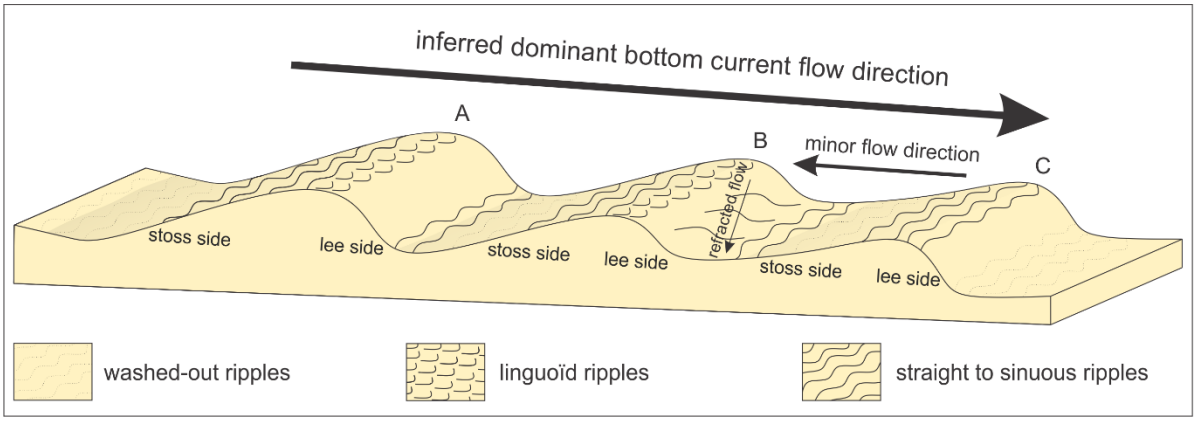

Figure 4.13. Schematic representation of the inferred sediment waves and their superimposed ripples. From the orientation of the crestline and the shape of the bedforms, the direction of the dominant current can be determined. (A) and (C) show superimposed ripples parallel to the crestline of the sediment wave. (B) displays ladderback ripples on the lee side of the sediment wave, highlighting the presence of a secondary flow opposite to the dominant flow.

4.6 Conclusions

The deployment of an AUV over the northern section of the Belgica Mound Drift overcame the limitations of surface vessels by enabling the collection of high-resolution bathymetric and photographic data, essential for understanding how present-day hydrodynamic processes influence the drift evolution.

The analyses of the AUV side-scan sonar, images and bathymetry allowed the validation of the identification of large-scale sediment waves with superimposed smaller-scale ripples over two fields in the northern sector of the contourite drift. The orientation of the sediment waves and their asymmetry allow to infer a bi-directional across-slope current, fitting with the interpretation of mooring data. This current corresponds to a W–E tidal current generated by a trapped baroclinic motion enhanced at the ENAW–MOW interface.

Sediment waves formed by trapped baroclinic motion (or internal waves) are still poorly known. Their characteristics can be broad, as the current at their origin can have variable intensities and directions at a local scale. Consequently, a good understanding of the local hydrodynamic processes is needed to define the origin of these features. At the scale of the drift, there are local variations of the tidal current due to bathymetry influence; the CWC mounds shape the moats while the moats can trap the current and the sediment. The sediment waves can also very locally deviate the current and impact the morphology of the superimposed small-scale bedforms.

While the drift and the moats were formed under the influence of an alongslope current, it is nowadays not the dominant current. The W–E bi-directional tidal current plays a bigger role in the evolution of the drift, with the lateral transport of the fine sediment fraction from the drift into the moats.

The small size of the sediment waves and their superimposed ripples makes them overlooked through seismic data or hull-mounted multibeam bathymetry, while they can be examined in

detail with near-seafloor high-resolution side-scan sonar imagery. The analysis of deep-water bedforms can provide new insights into local hydrodynamic processes occurring in a specific area, especially in the absence of long- or short-term in-situ measurements such as moorings. However, the mooring data and seabed imagery do not share the same temporal and spatial resolution, as the seabed imagery only gives an average stored signal. The addition of mooring data can help to confirm the interpretation from seabed imagery and get a full overview of the hydrodynamic processes, with their strength, direction and temporal variability.

Acknowledgements

This research was conducted in the framework of the FWO project “DynaMOD” (FWO grant 3G021719) and on the BOF extension BOF23/CDV/126. Ship time on RV Belgica was provided by BELSPO and RBINS-OD Nature. This study uses AUV *Barabas* from Flanders Marine Institute (VLIZ). We would also like to thank Vera Van Lancker (RBINS) for her help with the interpretation of the bedforms.

4.7 References

Ashley, G.M., 1990. Classification of large-scale subaqueous bedforms; a new look at an old problem. J. Sediment. Res. 60, 160–172.

Baas, J.H., De Koning, H., 1995. Washed-out ripples: their equilibrium dimensions, migration rate, and relation to suspended-sediment concentration in very fine sand. J. Sediment. Res. 65, 431–435. https://doi.org/10.1306/D42680E5-2B26-11D7-8648000102C1865D.

Baines, P.G., 1974. The generation of internal tides over steep continental slopes. Philos. Trans. R. Soc. Lond. Ser. A, Math. Phys. Sci. 277, 27–58. https://doi.org/10.1098/rsta.1974.0045.

Beelen, D., Wood, L.J., 2023. Predicting bottom current deposition and erosion on the ocean floor. Basin Res. 35, 1985–2009. https://doi.org/10.1111/bre.12788.

Belde, J., Back, S., Reuning, L., 2015. Three-dimensional seismic analysis of sediment waves and related geomorphological features on a carbonate shelf exposed to large amplitude internal waves, Browse Basin region, Australia. Sedimentology 62, 87–109. https://doi.org/10.1111/sed.12141.

Bogucki, D.J., Redekopp, L.G., 1999. A mechanism for sediment resuspension by internal solitary waves. Geophys. Res. Lett. 26, 1317–1320. https://doi.org/10.1029/1999GL900234.

Cacchione, D.A., Southard, J.B., 1974. Incipient sediment movement by shoaling internal gravity waves. J. Geophys. Res. 79, 2237–2242. https://doi.org/10.1126/science.1069803.

Cacchione, D.A., Wunsch, C., 1974. Experimental study of internal waves over a slope. J. Fluid Mech. 66, 223–239. https://doi.org/10.1017/S0022112074000164.

Droghei, R., Falcini, F., Casalbore, D., Martorelli, E., Mosetti, R., Sannino, G., Santoleri, R., Chiocci, F.L., 2016. The role of Internal Solitary Waves on deep-water sedimentary processes: the case of up-slope migrating sediment waves off the Messina Strait. Sci. Rep. 6, 36376. https://doi.org/10.1038/srep36376.

Ercilla, G., Alonso, B., Wynn, R.B., Baraza, J., 2002. Turbidity current sediment waves on irregular slopes: observations from the Orinoco sediment-wave field. Mar. Geol. 192, 171–187. https://doi.org/10.1016/S0025-3227(02)00554-6.

Foubert, A., Beck, T., Wheeler, A.J., Opderbecke, J., Grehan, J., Klages, M., Thiede, J., Henriet, J.-P., Polastern ARK-XIX/3a Shipboard Party, 2005. New view of the Belgica Mounds, Porcupine Seabight, NE Atlantic: Preliminary Results from the Polarstern ARK-XIX/3a ROV cruise. In: Freiwald, A., Roberts, J.M. (Eds.), Cold-Water Corals and Ecosystems. Springer, Heidelberg, pp. 403–415. https://doi.org/10.1007/3-540-27673-4_20.

Gerritsen, H.D., 2024. Atlas of Commercial Fisheries Around Ireland, fourth edition. Marine Institute, Ireland, 68 pp.

Gilli, A., Anselmetti, F.S., Ariztegui, D., Beres, M., McKenzie, J.A., Markgraf, V., 2005. Seismic stratigraphy, buried beach ridges and contourite drifts: the late Quaternary history of the closed Lago Cardiel basin, Argentina (49°S). Sedimentology 52, 1–23. https://doi.org/10.1111/j.1365-3091.2004.00677.x.

Harvey, J., 1982. θ-S relationships and water masses in the eastern North Atlantic. Deep-Sea Res. I: Oceanogr. Res. Pap. 29, 1021–1033.

Heezen, B.C., Hollister, C.D., 1971. The face of the deep. Oxford Univ. Press, New York, London, and Toronto, 659 pp.

Howe, J.A., 1996. Turbidite and contourite sediment waves in the northern Rockall Trough, North Atlantic Ocean. Sedimentology 43, 219–234. https://doi.org/10.1046/j.1365-3091.1996.d01-1.x.

Huthnance, J.M., 1981. Waves and currents near the continental shelf edge. Prog. Oceanogr. 10, 193–226. https://doi.org/10.1016/0079-6611(81)90004-5.

Huthnance, J.M., Inall, M.E., Fraser, N.J., 2020. Oceanic density/pressure gradients and slope currents. J. Phys. Oceanogr. 50, 1643–1654. https://doi.org/10.1175/JPO-D-19-0134.1.

Huvenne, V., Beyer, A., de Haas, H., Dekindt, K., Henriet J.-P., Kozachenko, M., Olu-Le Roy, K., Wheeler, A.J., TOBI/Pelagia 197, CARACOLE cruise participants, 2005. The seabed appearance of different coral bank provinces in the Porcupine Seabight, NE Atlantic: results from sidescan sonar and ROV seabed mapping. In: Freiwald, A., Roberts, J.M. (Eds.), Cold-Water Corals and Ecosystems. Springer, Heidelberg, pp. 535–569.

Huvenne, V.A.I., Van Rooij, D., De Mol, B., Thierens, M., O'Donnell, R., Foubert, A., 2009. Sediment dynamics and palaeo-environmental context at key stages in the Challenger cold-water coral mound formation: Clues from sediment deposits at the mound base. Deep-Sea Res. I Oceanogr. Res. Pap. 56, 2263–2280. https://doi.org/10.1016/j.dsr.2009.08.003.

Knaapen, M.A.F., 2005. Sandwave migration predictor based on shape information. J. Geophys. Res. 110, F04S11. https://doi.org/10.1029/2004JF000195.

INFOMAR, 2023. INFOMAR Marine Data Download Portal [WWW Document].

Iorga, M.C., Lozier, M.S., 1999. Signatures of the Mediterranean outflow from a North Atlantic climatology: 2. Diagnostic velocity fields. J. Geophys. Res. Oceans 104, 26011–26029. https://doi.org/10.1029/1999JC900204.

Jiménez-Romero, R., Fernandez-Salas, L.M., Palomino, D., Sanchez-Leal, R.F., Vila, Y., 2022. Discovering the Fine-Scale Morphology of the Gulf of Cádiz: An Underwater Imaging Analysis. J. Mar. Sci. Eng. 10, 651. https://doi.org/10.3390/jmse10050651.

Karl, H.A., Cacchione, D.A., Carlson, P.R., 1986. Internal-wave currents as a mechanism to account for large sandwaves in Navarinsky canyon head, Bering Sea. J. Sediment. Petrol. 56, 706–714. https://doi.org/10.1306/212F8A21-2B24-11D7-8648000102C1865D.

Kenyon, N.H., Belderson, R.H., 1973. Bedforms of the Mediterranean undercurrent observed with sidescan sonar. Sediment. Geol. 9, 77–99. https://doi.org/10.1016/0037-0738(73)90027-4.

Khélifi, N., Sarnthein, M., Andersen, N., Blanz, T., Frank, M., Garbe-Schönberg, D., Haley, B.A., Stumpf, R., Weinelt, M., 2009. A major and long-term Pliocene intensification of the Mediterranean outflow, 3.5-3.3 Ma ago. Geology 37, 811–814. https://doi.org/10.1130/G30058A.1.

Khélifi, N., Sarnthein, M., Frank, M., Andersen, N., Garbe-Schönberg, D., 2014. Late Pliocene variations of the Mediterranean outflow. Mar. Geol. 357, 182–194. https://doi.org/10.1016/j.margeo.2014.07.006.

King, E.L., Bøe, R., Bellec, V.K., Rise, L., Skarðhamar, J., Ferré, B., Dolan, M.F.J., 2014. Contour current driven continental slope-situated sandwaves with effects from secondary current processes on the Barents Sea margin offshore Norway. Mar. Geol. 353, 108–127. https://doi.org/10.1016/j.margeo.2014.04.003.

Ma, X.C., Yan, J., Hou, Y.J., Lin, F.L., Zheng, X.F., 2016. Footprints of obliquely incident internal solitary waves and internal tides near the shelf break in the northern South China Sea. J. Geophys. Res. Oceans 121, 8706–8719.

Masson, D.G., Howe, J.A., Stoker, M.S., 2002. Bottom-current sediment waves, sediment drifts and contourites in the northern Rockall Trough. Mar. Geol. 192, 215–237. https://doi.org/10.1016/S0025-3227(02)00556-X.

Matossian, A.O., Van Rooij, D., 2024. Morphosedimentary evolution of the Belgica Mound Drift: Controls on contourite depositional system development in association with cold-water coral mounds. Mar. Geol 477, 107410. https://doi.org/10.1016/j.margeo.2024.107410.

Matossian, A.O., Daly, E., Fennell, S., Shymbaliova, N., Vandorpe, T., White, M., Van Rooij, D. (submitted). Evaluation of present-day hydrodynamic processes associated to the Belgica Mound contourite drift, offshore Ireland. Deep-Sea Research I.

McCartney, M., Mauritzen, C., 2001. On the origin of the warm inflow to the Nordic Seas. Prog. Oceanogr. 51, 125–214. https://doi.org/10.1016/S0079-6611(01)00084-2.

McDonnell, A., Shannon, P.M., 2001. Comparative Tertiary stratigraphic evolution of the Porcupine and Rockall basins. Geol. Soc. London Spec. Publ. 188, 323–344. https://doi.org/10.1144/GSL.SP.2001.188.01.19.

Naylor, D., Shannon, P.M., 1982. Geology of Offshore Ireland and West Britain, 1982 edition. Springer, London, 161 pp.

New, A.L., Barnard, S., Herrmann, P., Molines, J.-M., 2001. On the origin and pathway of the saline inflow to the Nordic Seas: insights from models. Prog. Oceanogr. 48, 255–287. https://doi.org/10.1016/S0079-6611(01)00007-6.

Normark, W.R., Hess, G.R., Stow, D.A.V., Bowen, A.J., 1980. Sediment waves on the Monterey fan levee: a preliminary physical interpretation. Mar. Geol. 37, 1–18. https://doi.org/10.1016/0025-3227(80)90009-2.

Li, H., Wang, Y., Zhu, W., Xu, Q., He, Y., Tang, W., Zhuo, H., Wang, D., Wu, J., Li, D., 2013. Seismic characteristics and processes of the Plio-Quaternary unidirectionally migrating channels and contourites in the northern slope of the South China Sea. Mar. Pet. Geol. 43, 370–380. https://doi.org/10.1016/j.marpetgeo.2012.12.010.

Li, J., Li, W., Alves, T.M., Rebesco, M., Zhan, W., Sun, J., Mitchell, N.C., Wu, S., 2019. Different origins of seafloor undulations in a submarine canyon system, northern South China Sea, based on their seismic character and relative location. Mar. Geol. 413, 99–111. https://doi.org/10.1016/j.margeo.2019.04.007.

Liu, S., Van Rooij, D., Vandorpe, T., Gonzalez-Pola, C., Ercilla, G., Hernández-Molina, F.J., 2019. Morphological features and associated bottom-current dynamics in the Le Danois Bank region (southern Bay of Biscay, NE Atlantic): A model in a topographically constrained small basin. Deep-Sea Res. I: Oceanogr. Res. Pap. 149, 103054. https://doi.org/10.1016/j.dsr.2019.05.014.

Lüdmann, T., Paulat, M., Betzler, C., Möbius, J., Lindhorst, S., Wunsch, M., Eberli, G.P., 2016. Carbonate mounds in the Santaren Channel, Bahamas: a current-dominated periplatform depositional regime. Mar. Geol. 376, 69–85. https://doi.org/10.1016/j.margeo.2016.03.013.

Miramontes, E., Jouet, G., Thereau, E., Bruno, M., Penven, P., Guerin, C., Le Roy, P., Droz, L., Jorry, S.J., Hernández-Molina, F.J., Thiéblemont, A., Silva Jacinto, R., Cattaneo, A., 2020. The impact of internal waves on upper continental slopes: insights from the Mozambican margin (southwest Indian Ocean). Earth Surf. Process. Landforms 45, 1469–1482. https://doi.org/10.1002/esp.4818.

Pearson, I., Jenkins, D.G., 1986. Unconformities in the Cenozoic of the North-East Atlantic. In: Summerhayes, C.P., Shackleton, N.J. (Eds.), North Atlantic Palaeoceanography. Geol. Soc. London Spec. Publ., pp. 79–86.

Pingree, R.D., Le Cann, B., 1990. Structure, strength and seasonality of the slope currents in the Bay of Biscay region. J. Mar. Biol. Assoc. U.K. 70, 857–885. https://doi.org/10.1017/S0025315400059117.

Pomar, L., Morsilli, M., Hallock, P., Bádenas, B., 2012. Internal waves, an under-explored source of turbulence events in the sedimentary record. Earth Sci. Rev. 111, 56–81. https://doi.org/10.1016/j.earscirev.2011.12.005.

Prothero, D.R., Schwab, F., 1996. An Introduction to Sedimentary Rocks and Stratigraphy, Sedimentary Geology. W.H. Freeman and Company, New York, 575 pp.

Quan, X., Fry, E.S., 1995. Empirical equation for the index of refraction of seawater. Appl. Opt. 34, 3477–3480. https://doi.org/10.1364/AO.34.003477.

Raddatz, J., Rüggeberg, A., Margreth, S., Dullo, W.-C., 2011. Paleoenvironmental reconstruction of Challenger Mound initiation in the Porcupine Seabight, NE Atlantic. Mar. Geol. 282, 79–90. https://doi.org/10.1016/j.margeo.2010.10.019.

Ramsay, P.J.C., Cooper, A., Wright, C.I., Mason, T.R., 1989. The occurrence and formation of ladderback ripples in subtidal, shallow-marine sands, Zululand, South Africa. Mar. Geol. 86, 229–235.

Rebesco, M., Hernández-Molina, F.J., Van Rooij, D., Wåhlin, A., 2014. Contourites and associated sediments controlled by deep-water circulation processes: State-of-the-art and future considerations. Mar. Geol. 352, 111–154. https://doi.org/10.1016/j.margeo.2014.03.011.

Reeder, D.B., Ma, B.B., Yang, Y.J., 2011. Very large subaqueous sand dunes on the upper continental slope in the South China Sea generated by episodic, shoaling deepwater internal solitary waves. Mar. Geol. 279, 12–18. https://doi.org/10.1016/j.margeo.2010.10.009.

Reiche, S., Hübscher, C., Brenner, S., Betzler, C., Hall, J.K., 2018. The role of internal waves in the late Quaternary evolution of the Israeli continental slope. Mar. Geol. 406, 177–192. https://doi.org/10.1016/j.margeo.2018.09.013.

Rhines, P.B., 1970. Edge-, bottom- and Rossby waves. Geophys. Fluid Dyn. 1, 273–302.

Ribbe, J., Holloway, P.E., 2001. A model of suspended sediment transport by internal tides. Cont. Shelf Res. 21, 395–422. https://doi.org/10.1016/S0278-4343(00)00081-9.

Ribó, M., Puig, P., Munoz, A., Lo Iacono, C., Masqué, P., Palanques, A.L, Acosta, J., Guillén, J., Gómez Ballesteros, M., 2016. Morphobathymetric analysis of the large fine-grained sediment waves over the Gulf of Valencia continental slope (NW Mediterranean). Geomorphology 253, 22–37. https://doi.org/10.1016/j.geomorph.2015.09.027.

Rice, A.L., Billett, D.S.M., Thurston, M.H., Lampitt, R.S., 1991. The institute of oceanographic sciences biology programme in the Porcupine Seabight: background and general introduction. J. Mar. Biol. Assoc. U.K. 71, 281–310. https://doi.org/10.1017/S0025315400051614.

Southard, J.B., Cacchione, D.A., 1972. Experiments on bottom sediment movement by breaking internal waves. Shelf Sediment Transport: Process and Pattern. Dowden, Hutchinson and Ross, Inc., Stroudsburg, PA, 83–97.

Stow, D.A.V., 1982. Bottom currents and contourites in the North Atlantic. Bull. Inst. Geol. Bassin Aquitaine 31, 151–166.

Stow, D. A. V., Hernández-Molina, F.J., Llave, E., Sayago-Gil, M., Diaz del Rio, V., Branson, A., 2009. Bedform-velocity matrix: The estimation of bottom current velocity from bedform observations. Geology 37, 327–330. https://doi.org/10.1130/G25259A.1.

Stow, D.A.V., Hernández-Molina, F.J., Llave, E., Bruno, M., García, M., Díaz del Rio, V., Somoza, L., Brackenridge, R.E., 2013. The Cadiz Contourite Channel: Sandy contourites, bedforms and dynamic current interaction. Mar. Geol. 343, 99–114. https://doi.org/10.1016/j.margeo.2013.06.013.

Toucanne, S., Soulet, G., Riveiros, N.V., Boswell, S.M., Dennielou, B., Waelbroeck, C., Bayon, G., Mojtahid, M., Bosq, M., Sabine, M., Zaragosi, S., Bourillet, J.-F., Mercier, H., 2021. The North Atlantic Glacial Eastern boundary current as a key driver for ice-sheet—amoc interactions and climate instability. Paleoceanogr. Paleoclimatol. 36. https://doi.org/10.1029/2020PA004068.

van Aken, H.M., 2000. The hydrography of the mid-latitude Northeast Atlantic Ocean: II: the intermediate water masses. Deep-Sea Res. I Oceanogr. Res. Pap. 47, 789–824. https://doi.org/10.1016/S0967-0637(99)00112-0.

van Aken, H.M., Becker, G., 1996. Hydrography and through-flow in the north-eastern North Atlantic Ocean: the NANSEN project. Prog. Oceanogr. 38, 297–346. https://doi.org/10.1016/S0079-6611(97)00005-0.

Van Rooij, D., De Mol, B., Huvenne, V., Ivanov, M., Henriet, J.-P., 2003. Seismic evidence of current-controlled sedimentation in the Belgica mound province, upper Porcupine slope, southwest of Ireland. Mar. Geol. 195, 31–53. https://doi.org/10.1016/S0025-3227(02)00681-3.

Van Rooij, D., Blamart, D., Kozachenko, M., Henriet, J.-P., 2007. Small mounded contourite drifts associated with deep-water coral banks, Porcupine Seabight, NE Atlantic Ocean. Geol. Soc. Lond. Spec. Publ. 276, 225–244. https://doi.org/10.1144/GSL.SP.2007.276.01.11.

Van Rooij, D., Huvenne, V.A.I., Blamart, D., Henriet, J.-P., Wheeler, A., de Haas, H., 2009. The Enya mounds: a lost mound-drift competition. Int. J. Earth Sci. 98, 849–863. https://doi.org/10.1007/s00531-007-0293-9.

Vandorpe, T., Delivet, S., Blamart, D., Wienberg, C., Bassinot, F., Mienis, F., Stuut, J.-B. W., Van Rooij, D., 2023. Palaeoceanographic and hydrodynamic variability for the last 47kyr in the southern Gulf of Cadiz (Atlantic Moroccan margin): Sedimentary and climatic implications. Depositional Rec. 9, 30–51. https://doi/10.1002/dep2.212.

Wheeler, A.J., Kozachenko, M., Beyer, A., Foubert, A., Huvenne, V.A.I., Klages, M., Masson, D.G., Olu-Le Roy, K., Thiede, J., 2005. Sedimentary processes and carbonate mounds in the Belgica Mound province, Porcupine Seabight, NE Atlantic. In: Freiwald, A., Roberts, J.M. (Eds.), Cold-Water Corals and Ecosystems. Springer, Heidelberg, pp. 571–603. https://doi.org/10.1007/3-540-27673-4_28.

White, M., 2007. Benthic dynamics at the carbonate mound regions of the Porcupine Sea Bight continental margin. Int. J. Earth Sci. 96, 1–9. https://doi.org/10.1007/s00531-006-0099-1.

White, M., Roberts, J.M., van Weering, T., 2007. Do bottom-intensified diurnal tidal currents shape the alignment of carbonate mounds in the NE Atlantic?. Geo-Mar. Lett. 27, 391–397. https://doi.org/10.1007/s00367-007-0060-8.

White, M., Dorschel, B., 2010. The importance of the permanent thermocline to the cold water coral carbonate mound distribution in the NE Atlantic. Earth Planet. Sci. Lett. 296, 395–402. https://doi.org/10.1016/j.epsl.2010.05.025.

Wilckens, H., Schwenk, T., Lüdmann, T., Betzler, C., Zhang, W., Chen, J., Hernández-Molina, F.J., Lefebvre, A., Cattaneo, A., Spieß, V., Miramontes, E., 2023. Factors controlling the morphology and internal sediment architecture of moats and their associated contourite drifts. Sedimentology 70, 1472–1495. https://doi.org/10.1111/sed.13093.

Wu, L., Zhao, Y., Liu, Z., Ma, P., Zhang, Y., 2023. Sedimentary processes in the bottom boundary layer of a contourite drift in the northern South China Sea. Front. Mar. Sci. 10. https://doi.org/10.3389/fmars.2023.1217216.

Wils, K., Wermersche, M., Van Rooij, D., Lastras, G., Lamy, F., Arz, H.W., Siani, G., Bertrand, S., Van Daele, M., 2021. Late Holocene current patterns in the northern Patagonian fjords recorded by sediment drifts in Aysen Fjord. Mar. Geol. 441, 106604. https://doi.org/10.1016/j.margeo.2021.106604.

Wynn, R.B., Weaver, P.P.E., Ercilla, G., Stow, D.A.V and Masson, D.G., 2000. Sedimentary processes in the Selvage sediment-wave field, NE Atlantic: new insights into the formation of sediment waves by turbidity currents. Sedimentology 47, 1181–1197. https://doi.org/10.1046/j.1365-3091.2000.00348.x.

Wynn, R.B., Masson, D.G., Bett, B.J., 2002. Hydrodynamic significance of variable ripple morphology across deep-water barchan dunes in the Faroe-Shetland Channel. Mar. Geol. 192, 309–319. https://doi.org/10.1016/S0025-3227(02)00561-3.

Wynn, R.B., Huvenne, V., Le Bas, T.P., Murton, B.J., Connelly, D.P., Bett, B.J., Ruhl, H.A., Morris, K.J., Peakall, J., Parsons, D.R., Sumner, E.J., Darby, S.E., Dorrell, R.M., Hunt, J.E., 2014. Autonomous Underwater Vehicles (AUVs): Their past, present and future contributions to the advancement of marine geoscience. Mar. Geol. 352, 451–468. http://dx.doi.org/10.1016/j.margeo.2014.03.012.

Chapter 5 – Influence of a bottom trapped tidal baroclinic motion on the present-day hydrodynamic processes over a contourite drift

---

This chapter will be submitted for publication in a modified form:

Matossian, A.O., White, M., Ponsoni, L., Boone, W., Maier, C. and **Van Rooij, D.**

Abstract: The Belgica Mound Drift, a small (~36 km²) deep-water contourite drift located between 600 and 800 m water depth, is enclosed by cold-water coral mounds. It represents a baroclinically dominated and topographically steered hydrodynamic system. This study investigates the spatial and temporal variability of the present-day hydrodynamic regime both near the seafloor and within the water column. A high-resolution oceanographic dataset was acquired through the deployment of the glider *YOKO* from Flanders Marine Institute (VLIZ) equipped with CTD sensor and Acoustic Doppler Current Profiler (ADCP), supplemented by vessel-mounted ADCP measurements, CTD casts, and moorings equipped with current meters.

The obtained results highlight the effectiveness of gliders equipped with ADCP and CTD sensors in capturing high-resolution, three-dimensional water mass properties, with the identification of the ENAW and MOW (and their interface at a similar water depth as the drift), and documenting hydrodynamic processes across the drift. Among these processes, the trapped baroclinic motion is observed in all CTD profiles. This motion is characterised by a dominant diurnal K_1 tidal constituent. The stronger bottom currents (up to 50 cm/s) extending up to 100 m above the seafloor highlight the enhancement of this motion due to its interaction with the local steep topography and the presence of a water mass stratification. The bottom Ekman transport, which weakens and deflects the bottom currents close to the seafloor (up to 20 m), is a hydrodynamic process that has not been identified here before. Through the glider-mounted ADCP data, both processes can now be quantified.

This study underscores the value of integrating glider observations with traditional mooring and ship-based measurements to resolve large and small-scale oceanographic processes in deep-water environments.

Keywords: glider; moorings; enhanced bottom currents; tidal constituents; Ekman transport

Author contributions: The conceptualisation of the 2023/12 survey was made by A.O. Matossian and D. Van Rooij. The acquisition of the mooring data was done by M. White, E. Daly and S. Fennell. The mooring data were processed by M. White. The acquisition and the processing of the glider-mounted ADCP and CTD data, as well as the vessel mounted ADCP was done by L. Ponsoni, C. Maier and W. Boone. The interpretation of the mooring and glider

data was made by A.O. Matossian, under the supervision of M. White. The writing was performed by A.O. Matossian, under the supervision of D. Van Rooij. Figs. 5.4, 5.11, 5.14, 5.15 and 5.16 were provided by L. Ponsoni, C. Maier and W. Boone and modified by A.O. Matossian. The other figures were made by A.O. Matossian (Figs. 5.3, A.5.2 and A.5.3 were provided by S. Fennell and Fig. 5.5B was made by E. Daly).

5.1 Introduction

The Porcupine Seabight, located along the NE Atlantic margin, exhibits a complex hydrodynamic regime shaped by the interplay of large-scale oceanic circulation, baroclinic motions, tidal dynamics, and topographic features. The general circulation in the Porcupine Seabight is cyclonic (White, 2007) and largely driven by the European Slope Current (ESC) (500 - 2000 m water depth; Toucanne et al., 2021), which is an eastern boundary current flowing northward along the Atlantic margin and a component of the Atlantic Meridional Overturning Circulation (Huthnance et al., 2020; Toucanne et al., 2021). Close to the seafloor, the ESC is complemented by a stronger poleward flowing current generated by rectification processes of a trapped baroclinic motion (discussed below; Pingree and LeCann, 1990; White et al., 2007; Matossian et al., submitted). The water column is characterised by a summer seasonal thermocline between 50 and 70 m water depth (White, 2007), and a deeper permanent pycnocline at 700 m water depth that marks the interface between two water masses: the Eastern North Atlantic Water (ENAW) and the Mediterranean Outflow Water (MOW) (Pingree and Le Cann, 1990; White, 2007). The ENAW, occupying the upper 700 m, is a warm and saline water mass transported northward by the ESC (Toucanne et al., 2021) and the upper part of the ENAW is carried by the Shelf-Edge Current (Rice et al., 1991; New et al., 2001; White, 2007). Beneath it, the MOW forms a high-salinity core between 800 and 1000 m, originating from the Mediterranean Sea and flowing poleward through the Strait of Gibraltar towards the Porcupine Seabight (Iorga and Lozier, 1999; van Aken, 2000).

This circulation is modulated by tidal processes, which transfer energy from barotropic tides into baroclinic motions (Fig. A.5.1 in Supplementary material; Baines, 1974; White and Dorschel, 2010). Flows with surfaces of constant pressure (isobars) that are not parallel to surfaces of constant density (isopycnals) are known as baroclinic motions. These motions, generated by the interaction of a flow with topographic features, for example the edge of the continental slope (Garrett, 2003), are typical in stratified fluids. These baroclinic motions are driven by pressure gradients caused by horizontal density differences (Gill, 1982; Pedlosky, 1987). These baroclinic motions can manifest as freely propagating internal waves or as bottom trapped baroclinic waves. Both these motions can be responsible for the amplification of bottom currents on the eastern flank of the Porcupine Seabight, where these motions directly interact with the seafloor (White, 2007). The trapped baroclinic motions can be bottom intensified by resonance with the response of the density stratification to the motion. This resonance frequency (T_{res}) is given by (Rhines, 1970):

$$T_{res} = N\sin(\alpha)\sin(\gamma)$$

where N is the Brunt-Väisälä frequency, or buoyancy frequency (vertical density stratification N^2), α is the seafloor slope, and γ is the angle between the motion vector and the orientation of the continental slope. If the motion is directed across the slope, then sin(γ)=1 and the

maximum resonance frequency (or minimum wave period) would be where α and the vertical density stratification are also maximum (White, 2007; White and Dorschel, 2010).

The Belgica Mound Province (BMP) is located on the eastern margin of the Porcupine Seabight and is characterised by the occurrence of cold-water coral (CWC) mounds, including the Galway and Challenger Mounds (Van Rooij et al., 2003, 2007; Huvenne et al., 2009). Within this province, bottom-trapped baroclinic motions are particularly enhanced in the depth range of 600-800 m, which coincides with steeper slopes (2 to 3°; Huvenne et al., 2005), peak values of Nsin(α), the depth of the permanent pycnocline and the location of many CWC mounds (White, 2007; Van Rooij et al., 2007). The baroclinic motion is characterised by a diurnal tidal component. The motion can be trapped by the Coriolis force, i.e. laterally confined and deflected, in the vicinity of the topographic features that generate it. The trapping occurs when its period (~23.93 h) is longer than the inertial period (~15 h period in the BMP; Conway et al., 2019) 2π/f (Philips, 1966; Huthnance, 1981), where f, the local Coriolis parameter, depends on the rotational frequency of the Earth and increases with the latitude. The rectification of this motion by the Coriolis force leads to the generation of a persistent bottom current along the slope in the BMP (Huthnance, 1981; White, 2007; White and Dorschel, 2010). Several moorings have been deployed near the CWC mounds, such as the Galway Mound (Dorschel et al., 2007; White, 2007; White et al., 2007). The current meter data allowed to define the maximum intensification of the trapped baroclinic motions around 850 m water depth (White and Dorschel, 2010). Currents up to 50 cm/s were measured at the mound summit, with a mean of 16 cm/s (Dorschel et al., 2007), with a persistent residual (i.e. net flow excluding periodic components, such as tides) flow between 5-15 cm/s, directed to the NW and following the local contours (White et al., 2007). The diurnal tidal components of the trapped baroclinic motion were SW–NE orientated (White et al., 2007). The bottom tidal variability follows a strong spring-neap cycle (~13.6 days), with the diurnal K_1 tide (~23.93h period) dominating over the semi-diurnal M_2 tide (~12.42h) (Dorschel et al., 2007; White et al., 2007). The local complex topography, including the CWC mounds, plays a key role in the local variability and persistence of the bottom currents (Dorschel et al., 2007; White, 2007; Van Rooij et al., 2007), with the CWC mounds modifying local current patterns by steering and deflecting the flows (Van Rooij et al., 2007; Matossian and Van Rooij, 2024; Matossian et al., submitted).

The Belgica Mound Drift (Fig. 5.1) is a small-scale and deep-water contourite drift (36 km²; 600–800 m water depth) enclosed by CWC mounds. The drift has been studied through high-resolution seismic and bathymetric data which allowed to define that the drift was formed under the influence of an alongslope bottom current related to the thermohaline circulation (contour current) and that the CWC mounds steered the currents, directly influencing the onset and the evolution of the drift since Early Pleistocene (Matossian and Van Rooij, 2024). The study area lies precisely within the ENAW–MOW transition zone (Fig. 5.2), where the stratification and hydrodynamic regime are expected to be particularly intense (White, 2007; White et al., 2007; White and Dorschel, 2010). Associated to the Belgica Mound Drift area, enhanced diurnal baroclinic motion has been confirmed through mooring data. The measured bottom currents are dominated by an intensified across-slope (W–E, SW–NE) diurnal tidal component, induced by the trapped baroclinic motion, with a weaker northward residual alongslope component (White et al., 2007; Matossian et al., submitted). The measured residual northward current combines both the generated alongslope bottom current, related to the trapped baroclinic motion, and the contour current, related to the European Slope Current (Matossian et al., submitted). The across-slope tidal current, which forms small-scale

sediment waves and superimposed ripples, has been found to be the primary hydrodynamic process influencing the drift and its seafloor nowadays, according to the high-resolution side-scan sonar imagery of the drift (Matossian et al., in preparation).

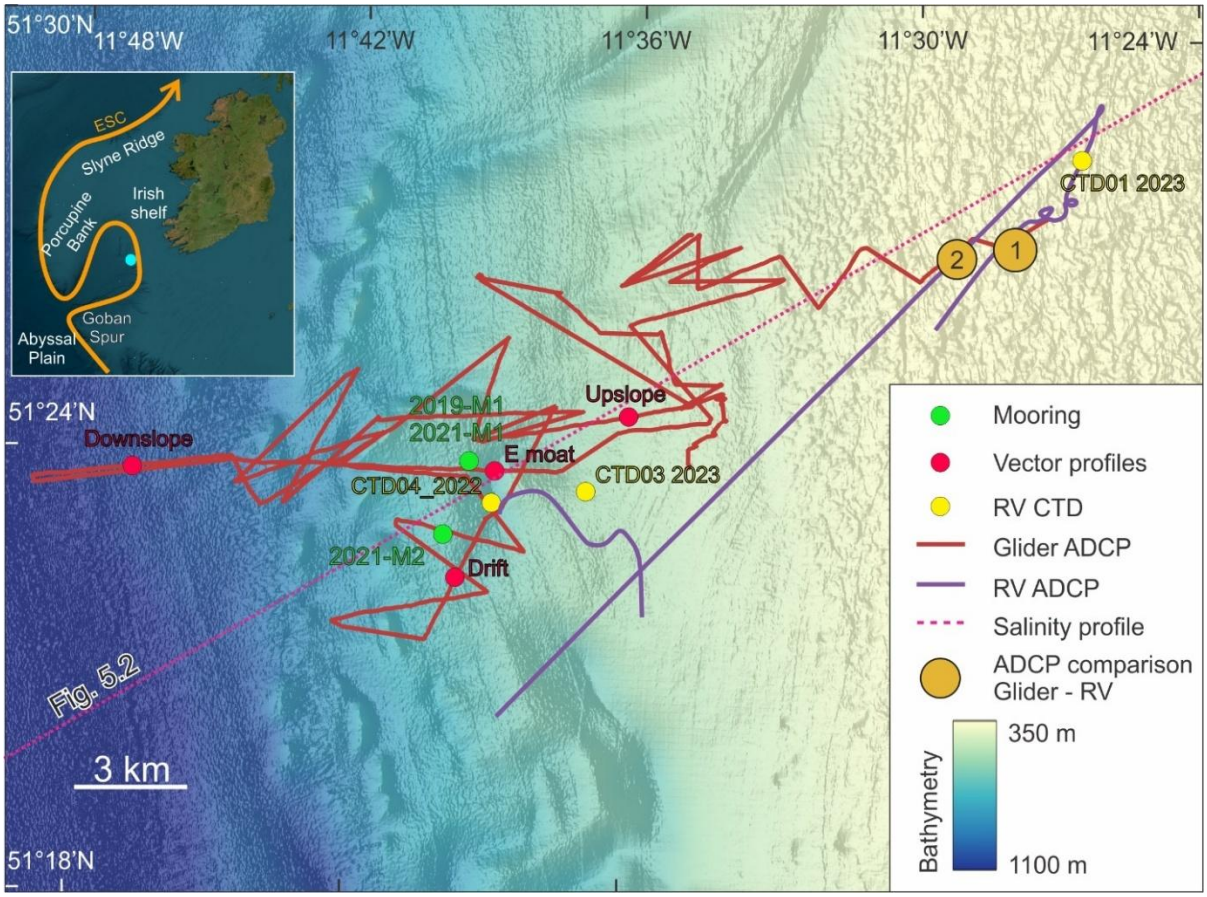

Figure 5.1. Map showing the location of the drift (blue dot on the top left panel), the glider track (red line) and the Belgica ADCP data (purple line). The orange line shows the circulation pattern of the European Slope Current (ESC; based on Toucanne et al., 2021). The moorings are indicated with the green dots, the CTD (from RV Belgica) are the yellow dots and the red dots represent the glider-mounted ADCP profiles (Downslope, Drift, E moat and Upslope) used in Figs. 5.11, 5.12, 5.13 and 5.14. The orange dots (1 and 2) show the two locations used to compare the vessel-mounted ADCP with the glider-mounted ADCP (Fig. 5.7). The pink dotted line represents the location of the salinity profile (Fig. 5.2).

Recent studies (Liu et al., 2019; Miramontes et al., 2020; Wu et al., 2023) have shown that local hydrodynamic processes, as the baroclinic motions, can play a critical role in the evolution and sediment dynamics of contourite drifts. In the northern South China Sea, Wu et al. (2023) highlighted that such processes can exert a stronger influence on sediment remobilisation than the initial formation mechanisms of the drift itself (i.e. alongslope bottom current). These findings align with the observations of Miramontes et al. (2020), who emphasised the significance of incorporating local hydrodynamic conditions when assessing drift evolution. Understanding these local processes requires a multidisciplinary approach supported by high-resolution and spatially extensive datasets that can capture the complex interplay between sediment dynamics and near-bottom hydrodynamics. Three moorings have been deployed directly on the crest of the Belgica Mound Drift to monitor near-seafloor

hydrodynamics (Matossian et al., submitted). Given the significant influence of local topography on current variability, it is essential to extend this investigation to areas surrounding the drift, both upslope and downslope, as well as within its associated moats, where sediment waves were observed (Matossian et al., in preparation). This broader spatial assessment is crucial for developing a comprehensive understanding of the hydrodynamic regime governing the evolution of contourite drifts.

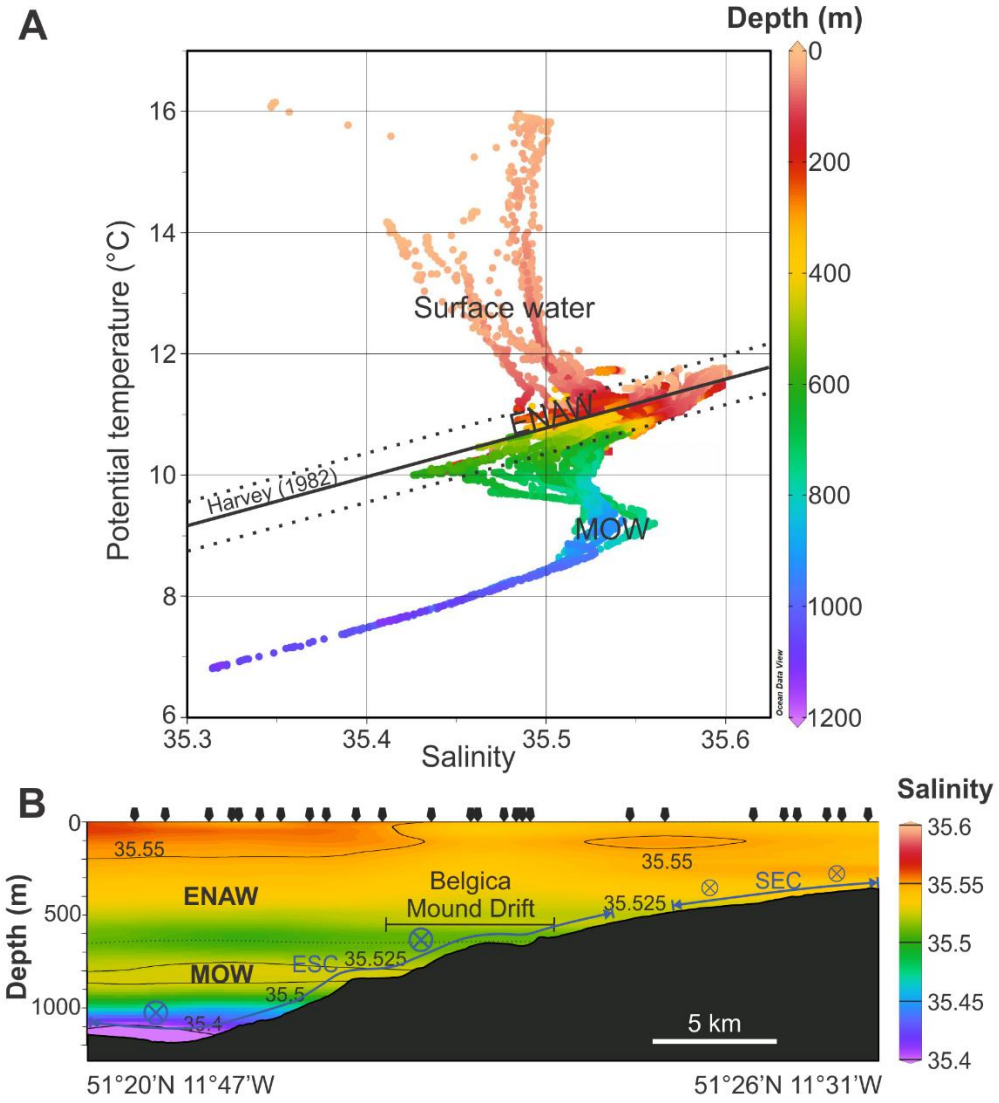

Figure 5.2. (A) Temperature – salinity (T-S) diagram. The thick black line represents the characteristic T-S relationship of the ENAW as defined by Harvey (1982), while the dashed lines indicate a salinity variation of ±0.05 around this reference. (B) Salinity versus depth cross-section profile located over the study area (location: Fig. 5.1). A and B are based on CTD data (black arrows) from the World Ocean Database (Boyer et al., 2018) and were produced using Ocean Data View (Schlitzer, 2021). ENAW and MOW respectively stand for Eastern North Atlantic Water and Mediterranean Outflow Water. The dashed line shows the ENAW-MOW interface. The circled cross indicates the alongslope currents, European Slope Current (ESC) and Shelf-Edge Current (SEC), directed into the plane of the figure.

The Belgica Mound Drift is a prime example of a baroclinically-dominated, topographically steered deep-sea hydrodynamic system that can be easily covered with high-resolution oceanographic data. The oceanographic properties were investigated to grasp more fully the

spatial (x, y and z) and temporal variations of these hydrodynamic processes around and over the drift within the same time frame. This study focuses on evaluating the spatial and temporal variability of the present-day hydrodynamic regime close to the seabed but also in the water column, as well as acquiring a better understanding of the enhancement of the bottom currents near the seafloor.

5.2 Context

5.2.1 Geographic and geological settings

Situated about 200 km west of Ireland on western margin of the Irish Shelf, the Porcupine Seabight is a broad, N–S oriented basin measuring roughly 320 by 240 km (Fig. 5.1). Water depths range from 350 m in its northern region to 3000 m in the southwest. The basin is enclosed by several features: the Irish Mainland Shelf lies to the east, the Slyne Ridge and Porcupine Bank to the north, the Porcupine Ridge to the west, and the Goban Spur to the south (Fig. 5.1). Toward the southwest, the basin gradually opens into the deeper Porcupine Abyssal Plain (Naylor and Shannon, 1982).

The Belgica Mound Drift, as described by Matossian and Van Rooij (2024), is a slope-parallel mounded, elongated contourite drift, confined within a complex topographic setting at depths between 600 and 800 m. Bounded by conical CWC mounds, an escarpment and flanking moats, the drift measures approximately 10 km in length and 2.5 to 4 km in width, covering a total area of 36 km². It is elongated in the NNW-SSE direction and confined in the W-E direction. The crest is located with a depth range between 600 and 650 m, with a noticeable change of orientation from N-S in the north to NW-SE in the south. The drift can thus be divided into two sectors: the northern and the southern sectors.

The onset of the contourite drift generation happened after an erosive event, which occurred due to the reintroduction of the MOW in the Porcupine Seabight (Stow, 1982; Pearson and Jenkins, 1986; McDonnell and Shannon, 2001; Van Rooij et al., 2003, 2009). It was responsible of the RD1 unconformity (Van Rooij et al., 2003), on top of which the CWC mounds formed and later on, during Pleistocene, the Belgica Mound Drift was deposited (Matossian and Van Rooij, 2024). The peculiar RD1 paleotopography, still discernible in the present-day bathymetry, as well as the CWC mounds strongly influence at a local scale the hydrodynamic conditions and play a role in the onset and development of the contourite drift. Since the Pleistocene, a contour current (Matossian and Van Rooij, 2024), and potentially the alongslope bottom current produced by the trapped baroclinic motion (Matossian et al., in preparation), have driven the formation of the drift. Both currents can be measured through moorings nowadays on the drift as a residual northward (alongslope) bottom current (Matossian et al., submitted). Moats, also produced by the residual current, can be observed alongside the drift (Matossian and Van Rooij, 2024; Matossian et al., in preparation). As the geometries of a drift and its moats are interdependent, they cannot be studied separately (Wilckens et al., 2023). On a broader temporal scale, the evolution of the drift reflects the glacial–interglacial dynamics of the Pleistocene (Matossian and Van Rooij, 2024). During interglacial periods, the MOW is present within the Porcupine Seabight, intensifying bottom currents, similar as those today. In contrast, during glacial periods, the MOW does not reach the basin, weakening the bottom currents (Huvenne et al., 2009; Raddatz et al., 2011) and

allowing the sediment to accumulate on the drift (Matossian and Van Rooij, 2024). Since the lower Pliocene, the MOW is involved in the formation of large Contourite Depositional Systems all along the NE Atlantic margin (Hernández-Molina et al., 2006, 2014; Khélifi et al., 2009, 2014).

5.2.2 Current circulation

The European Slope Current (ESC) is a poleward eastern boundary current that represents the easternmost segment of the upper branch of the Atlantic Meridional Overturning Circulation (Huthnance et al., 2020). It can be seen from the Iberian margin to the Faroe-Shetland Channel. (Huthnance et al., 2020; Toucanne et al., 2021). The ESC is driven by the steepness of the NE Atlantic margin, large-scale meridional density gradients (Pingree and Le Cann, 1990; Friocourt et al., 2007, 2008; Toucanne et al., 2021) and by the wind forcing driving geostrophic circulation towards the slope (Huthnance, 1984; Friocourt et al., 2007; Marsh et al., 2017; Depuydt et al., 2024). This current plays a key role in ocean circulation and climate regulation (Hall and Bryden, 1982; Trenberth et al., 2019; Toucanne et al., 2021). For instance, the MOW relies on the ESC to be carried northward (Fig. 5.1) along the NE Atlantic margin (Booth and Ellett, 1983; Huthnance, 1986; Pingree and Le Cann, 1989; Toucanne et al., 2021).

5.3 Methods

In order to map the bottom currents over the Belgica Mound Drift and its surroundings in high resolution, the glider *YOKO* from Flanders Marine Institute (VLIZ) was deployed supplemented with vessel-mounted ADCP measurements, conductivity, temperature and depth (CTD) casts and moorings.

5.3.1 Moorings

The bottom current regime over the drift was evaluated by deploying several moorings equipped with Aanderaa RCM7 (Fig. A.5.2 in Supplementary material) and RCM9 (Fig. A.5.3 in Supplementary material) recording current meters (Table 5.1).

Table 5.1. Summary of the characteristics of the deployed moorings.

Mooring	Latitude	Longitude	Water depth (m)	Height current meter (m above seabed)	Start date	Record-ing period	Sampling rate
2019-M1	51°24'N	11°39'W	636	6	06/06/19	8 days	10 min
2021-M1	51°24'N	11°39'W	632	6	Lost (trawling activity)		
				35	05/06/21	180 days	30 min
2021-M2	51°23'N	11°40'W	655	6	Lost (trawling activity)		
				35	05/06/21	20 days	30 min
2021-M3	51°22'N	11°40'W	668	6	Not recovered (no response)		
				35			
				70			

A short-term fixed bottom mooring 2019-M1 (Table 5.1), assembled with a RCM9 current meter, was installed on the crest of the drift (Fig. 5.1) during the RV Belgica 2019/16 survey. Three long-term moorings were also deployed (Table 5.1) within the Belgica Special Area of Conservation designation during the Irish Marine Institute survey CE21014 in 2021. They aimed to better understand the local variations of the bottom currents over the drift, over a longer period. Trawling activity affected the 2021-M1 and 2021-M2 moorings (Figs. 5.1, 5.3) and near-seabed current meters (RCM9) were lost. 2021-M1 was deployed close to the 2019 mooring location and recorded for 6 months, 2021-M2 was deployed in the south on the crest and recorded 20 days before encountering a compass issue while 2021-M3 was located further south and did not respond during recovery. The three deployed current meters were equipped with a Fenwall thermistor (temperature sensor). Vectors were measured every 1/50th of the sampling interval (Table 5.1). Instrument-specific calibration data provided by Aanderaa and appropriate magnetic declination for the year were used to calibrate and perform quality control of the data. Measured speed and direction were converted to east and northerly velocity components. A simple least squares tidal analysis was performed over the full available time series.

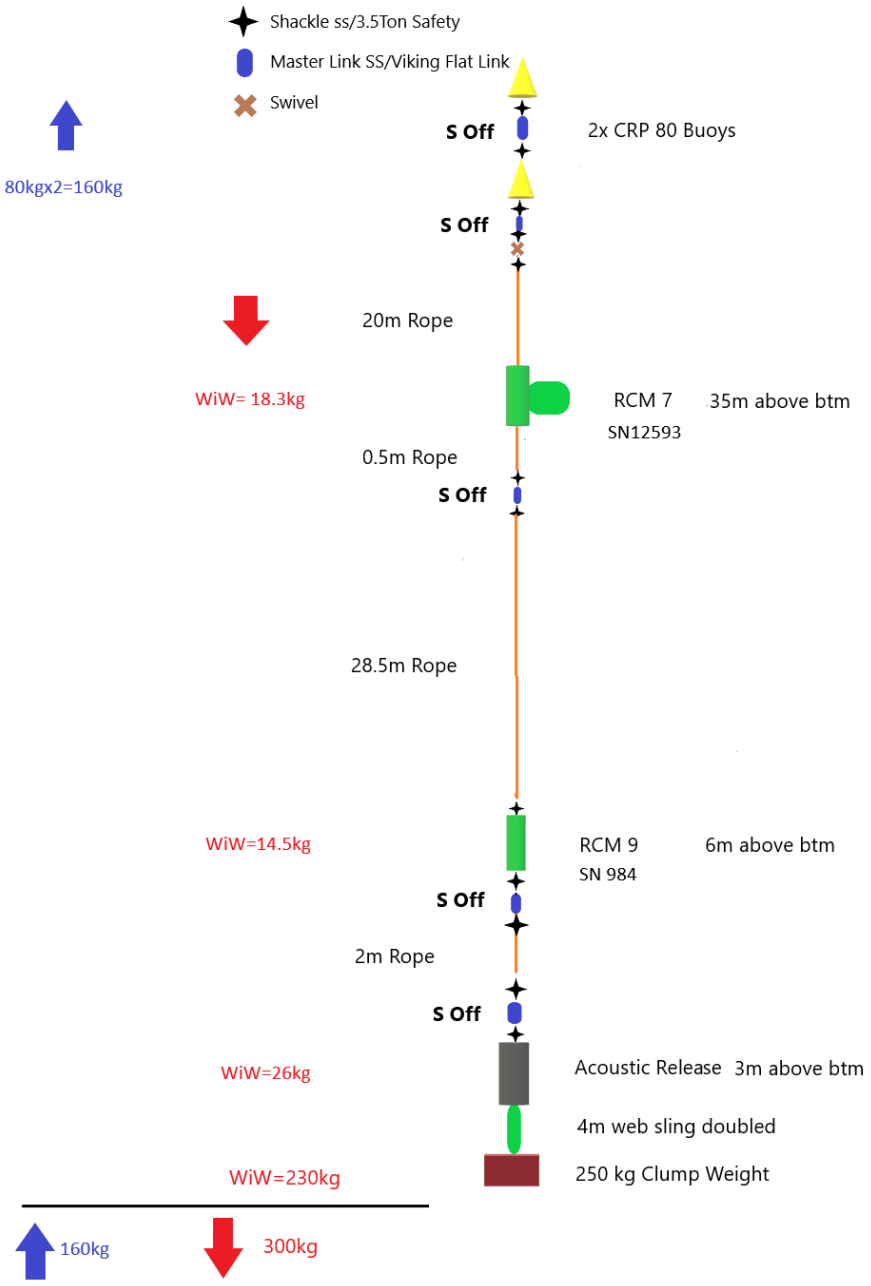

Figure 5.3. Mooring layout of the 2021-M1 mooring (Fennell, pers. comm.). WiW stands for "weight in water" and S off for "shackle off".

5.3.2 CTD and vessel-mounted ADCP

A total of 3 CTD casts were acquired with a Seabird 19-Plus sensor (Table 5.2). One cast was taken in 2022 over the Belgica Mound Drift, during the RV Belgica 2022/18 survey, and the two others were taken in 2023, upslope of the drift (Fig. 5.1), during the RV Belgica 2023/12 survey. The figures related to the CTD data were produced using Ocean Data View (Schlitzer, 2023). Additionally, ADCP measurements were running before and during the 2023 CTD casts as well as the glider deployment and recovery using the hull-mounted Teledyne RDI Ocean Surveyor 75 kHz ADCP and Teledyne RDI Workhorse Mariner 600 kHz ADCP (Fig. 5.1). The ADCP profiles were processed via CODAS toolbox (Hummon, 2025).

Table 5.2. Summary of the characteristics of the CTD casts.

CTD	Latitude	Longitude	Depth (m)	CTD depth (m)	Remark
B2218-CTD-04	51°23’ N	11°40’ W	687	652	Belgica Mound Drift
B2312-CTD-01	51°28’ N	11°26' W	283	273	IODP 307 U1318
B2312-CTD-03	51°24’ N	11°37’ W	534	518	

5.3.3 Glider

During the RV Belgica 2023/12 survey, the VLIZ ocean glider *YOKO* (SeaExplorer SEA010) was deployed around the Belgica Mound Drift for a five-day mission. The glider was equipped with an ADCP (Nortek AD2CP-Glider 1000 kHz) for the current velocities and depth from bottom; CTD (RBR Legato); chlorophyll-a (470 nm) and backscatter (700 nm) (ECO Puck FLBBCD – EXP) and dissolved oxygen (JFE Rinko AROD-FT). The sampling frequencies were 0.5 Hz for the ADCP measurements and 1 Hz for all the other sensors. The ADCP was configured with a blanking distance of 0.5 m, a cell size of 2 m and a total number of cells of 15. The glider was piloted from Ostend, Belgium and collected high-resolution ADCP and CTD profiles across the drift system, encompassing upslope, drift and downslope regions, reaching seafloor or depths of up to 1000 m (Fig. 5.4). Data were gathered continuously during both the descent and ascent phases of each dive. The glider completed approximately 50 dives, resulting in around 100 vertical profiles. One CTD profile was collected during each descent and ascent, while multiple ADCP short-range profiles, with a vertical range of 30.5 m, were recorded throughout both phases.

The ADCP data were processed using Python and the gliderad2cp toolbox (Queste, 2024). After processing, the ADCP data produced one representative velocity profile per ascent and descent. The CTD profiles were post-processes and organised as NetCDF files by the Python-based toolbox PyGlider (PyGlider team, 2022). To cross-compare data acquired from the vessel and glider, two CTD casts (Table 5.2) and a few vessel-mounted ADCP profiles acquired from the RV Belgica were used to validate the glider CTD and ADCP data. The CTD and ADCP glider figures were produced using Ocean Data View (Schlitzer, 2023), Python (Python Software Foundation) and Grapher (Golden Software). Near-seafloor vectors were computed by averaging the deepest measurements over 3 m from each ADCP profile. Consequently, each dive provided two vectors close to the seafloor, closely matched in both time and space: one preceding the bottom detection and one just after, when the glider started its ascent.

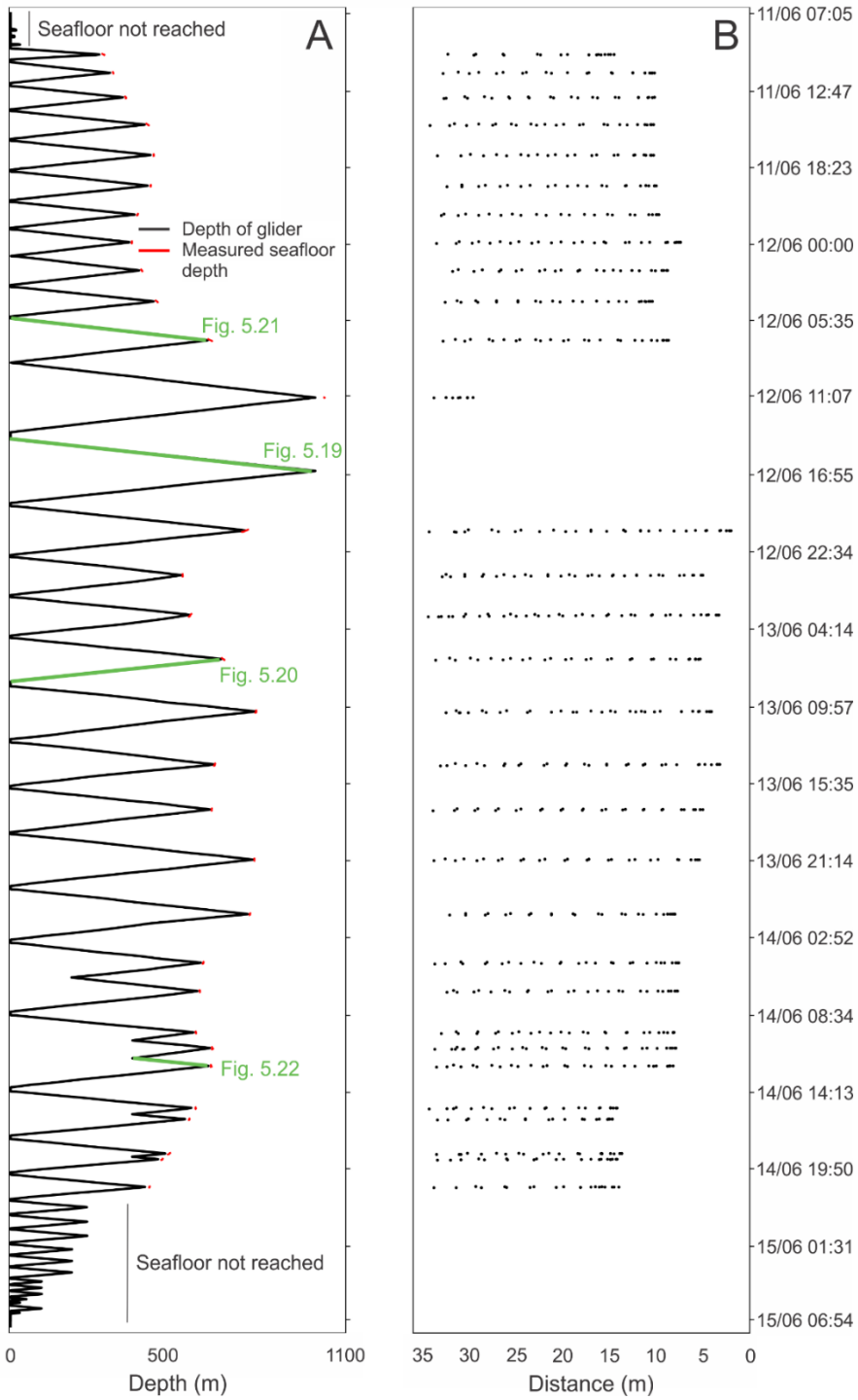

Figure 5.4. (A) Depth of the glider during each dive (black) and corresponding seafloor measured depth (red). (B) Distance between the glider and the seafloor.

5.3.4 Supporting datasets

Processed 25 m resolution bathymetric data (Fig. 5.1) were downloaded from the INFOMAR Marine Data Download Portal. In 2022, during the RV Belgica 2022/18 survey, higher resolution bathymetric data over the drift were obtained using the Kongsberg EM 304 multibeam echosounder. Qimera 2.6.2 (QPS) was used to process the dataset, exported with

a 20 m resolution. The salinity data (Fig. 5.2) are based on CTD data from the World Ocean Database (Boyer et al., 2018).

5.4 Results

5.4.1 Moorings

All current measurements exhibit similar characteristics in the near-seafloor flow regime (Table 5.3). The 2021 mooring data, only recovered from the 35 m M1 and M2 moorings, demonstrate comparable results (Fig. 5.5A; Table 5.3): A subset of the longer M1 dataset aligns well with the M2 dataset, suggesting that the shorter M2 data are representative of the longer time series (Figs. 5.6, 5.7).

Table 5.3. Summary statistics for the three deployed mooring. The mean direction and speed are derived from the East and North components.

Mooring	Speed (cm/s)	East (cm/s)	North (cm/s)	Mean vector Direction (°) & speed (cm/s)
2019-M1				
Mean	20.5	-1.1	-3.7	196 & 3.8
Maximum	52.8	51.3	28.3	/
Minimum	0.6	-39.8	-26.7	/
2021-M1				
Mean	14.9	-0.9	4.6	348.6 & 4.7
Maximum	42.7	42.4	24.3	/
Minimum	1.1	-37.6	-18.4	/
2021-M2				
Mean	14.6	0.7	7.9	5.4 & 7.9
Maximum	42.1	40.7	23.9	/
Minimum	1.1	-29.7	-19.6	/

The bottom-current speed and direction at all three moorings (Fig. 5.6) revealed a dominant across-slope diurnal tidal component and a smaller alongslope residual components (Fig. 5.5A). In the 2021-M2 mooring (Fig. 5.6C), a semi-diurnal constituent is also apparent.

Rotary spectral and tidal analyses (Fig. 5.8) identified the diurnal K_1 tide (23.93 h period; Parker, 2007) with the diurnal O_1 tide (25.82 h period; Parker, 2007) and semi-diurnal M_2 tide (12.42 h period; Parker, 2007) as the primary and secondary tidal constituents respectively, dominating the bottom currents at all moorings. At the 2021-M1 mooring (Fig. 5.8B), the diurnal O_1 tide was significant. The three tidal constituents have their major tidal ellipse axis directed across slope, with orientation and amplitudes of K_1=88˚, 15.3 cm/s, M_2=113˚, 6.9 cm/s and O_1=82˚, 7.7 cm/s, respectively. The K_1 component is characterised by a strongly elongated, anti-clockwise rotary tidal ellipse (from the 2021-M1 timeseries), with M_2 and O_1 having clockwise rotary motion. All mooring based temperature timeseries (Fig. 5.7) show an asymmetrical pattern, with rapid temperature decrease correlated with upslope flow, followed by more gradual increase linked to downslope flows.

At the 2021 locations, peak tidal current speeds typically range from 25 cm/s during neap tides to over 35 cm/s during spring tides, with maximum speeds reaching 40 cm/s at M1 and 42 cm/s at M2. At both sites, the K_1 tidal current ellipses are orientated across the main slope. Mean flow speeds are comparable at M1 (14.9 cm/s) and M2 (14.6 cm/s; Table 5.3), with M1 having a mean of 15.6 cm/s during the same time period covered by the M2 dataset.

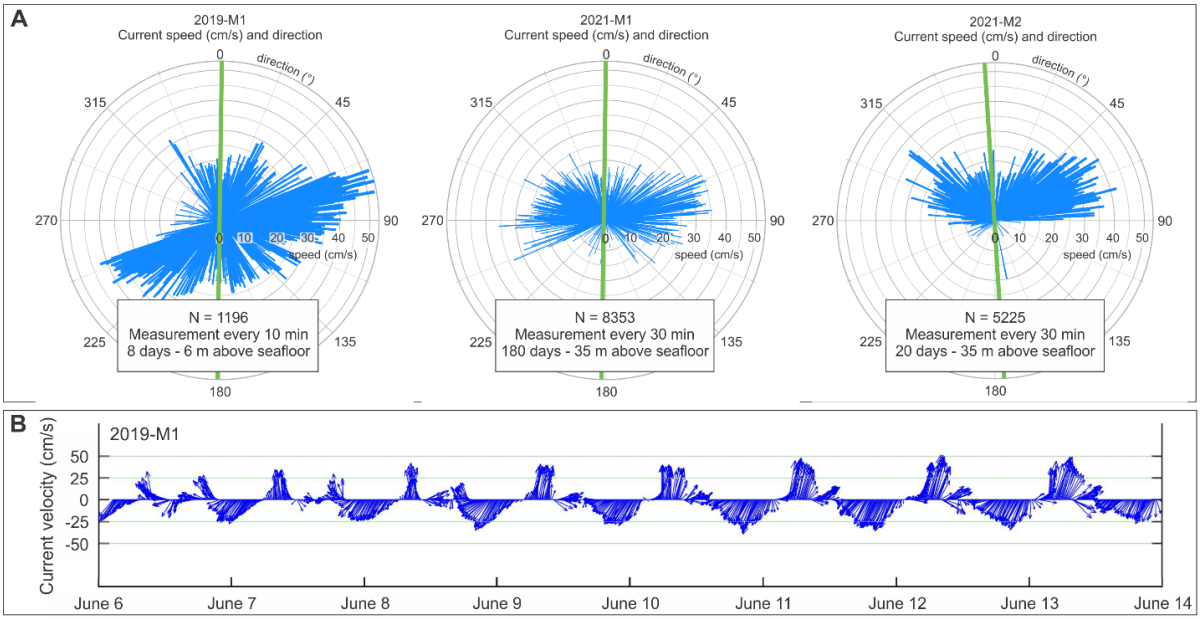

Figure 5.5. (A) Rose diagrams with the measured current speed (x axis) and direction from the three moorings (Fig. 5.1). The green bar shows the drift crest orientation. To make the figure clearer, only one measurement out of every ten is displayed for mooring 2021-M1. N corresponds to the number of measurements. (B) Results from mooring 2019-M1 (Fig. 5.1), with the current velocities (cm/s) at 6 m above the seafloor.

Residual currents at both locations are directed along the slope and poleward (Fig. 5.6), with M1 exhibiting a mean residual flow of 4.7 cm/s in direction 348.6˚N and M2 showing 7.9 cm/s in direction 5.4˚N. A pronounced spring-neap cyclicity (~13.6 days, Mf=327 h) is evident in the 2021-M1 dataset (Fig. 5.9). At the 2019-M1 site, similar flow characteristics can be observed during the shorter 8-day deployment. The current is dominated by a bi-directional tidal component oriented across-slope (Fig. 5.5B), with a mean speed of 20 cm/s and a peak speed of 52.8 cm/s (Fig. 5.5A; Table 5.3). The residual flow is weaker, averaging 3.9 cm/s and directed to the SW (Figs. 5.5A, 5.6).

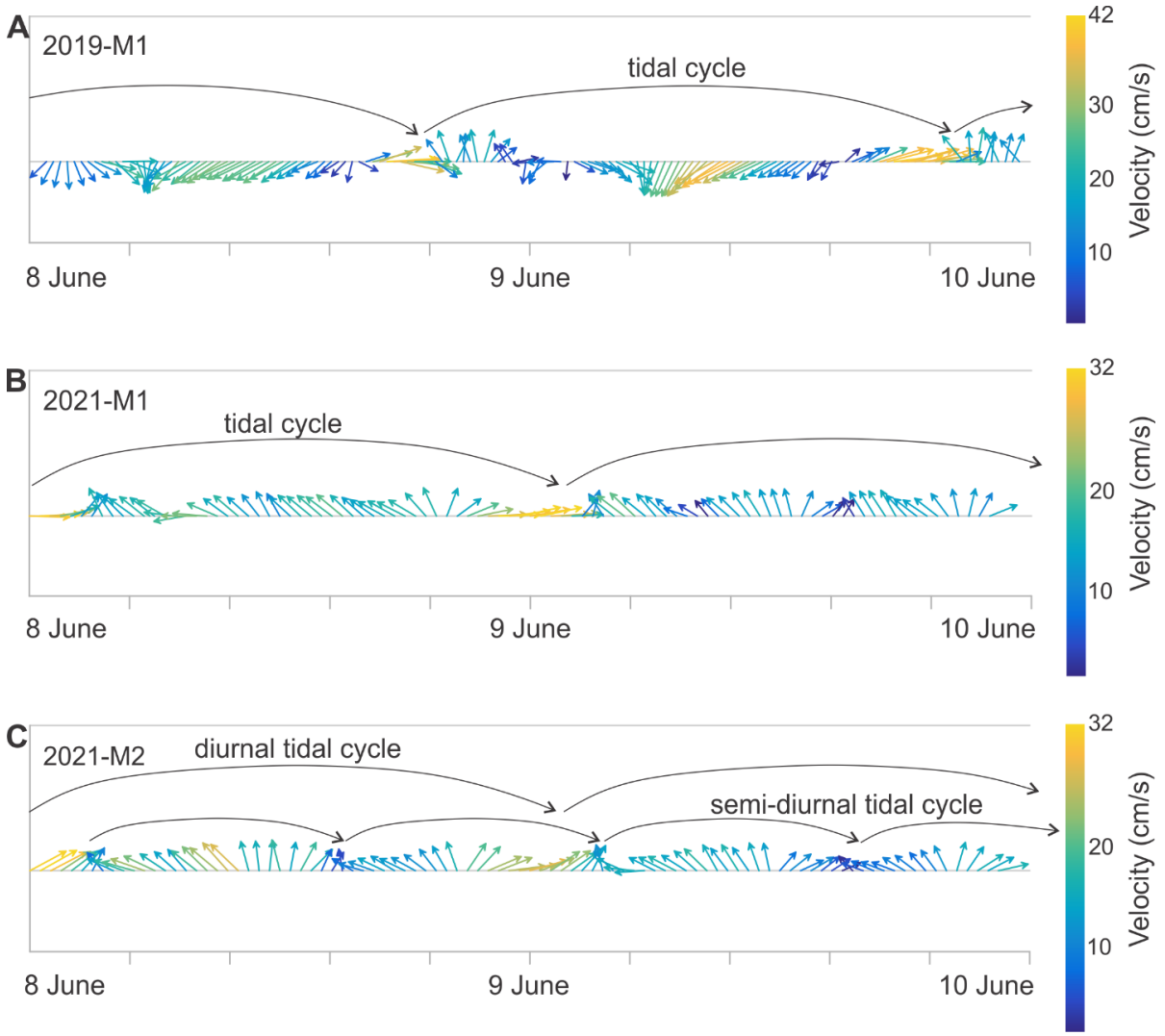

Figure 5.6. Bottom-current velocities (cm/s) from (A) mooring 2019-M1 (6 m above seafloor), (B) 2021-M1 (35 m above seafloor) and (C) 2021-M2 (35 m above seafloor) over two selected days, being exactly the same days for the 2021 moorings (B and C), but in 2019 for mooring 2019-M1 (A). The arrow represents the diurnal and semi-diurnal tidal period.

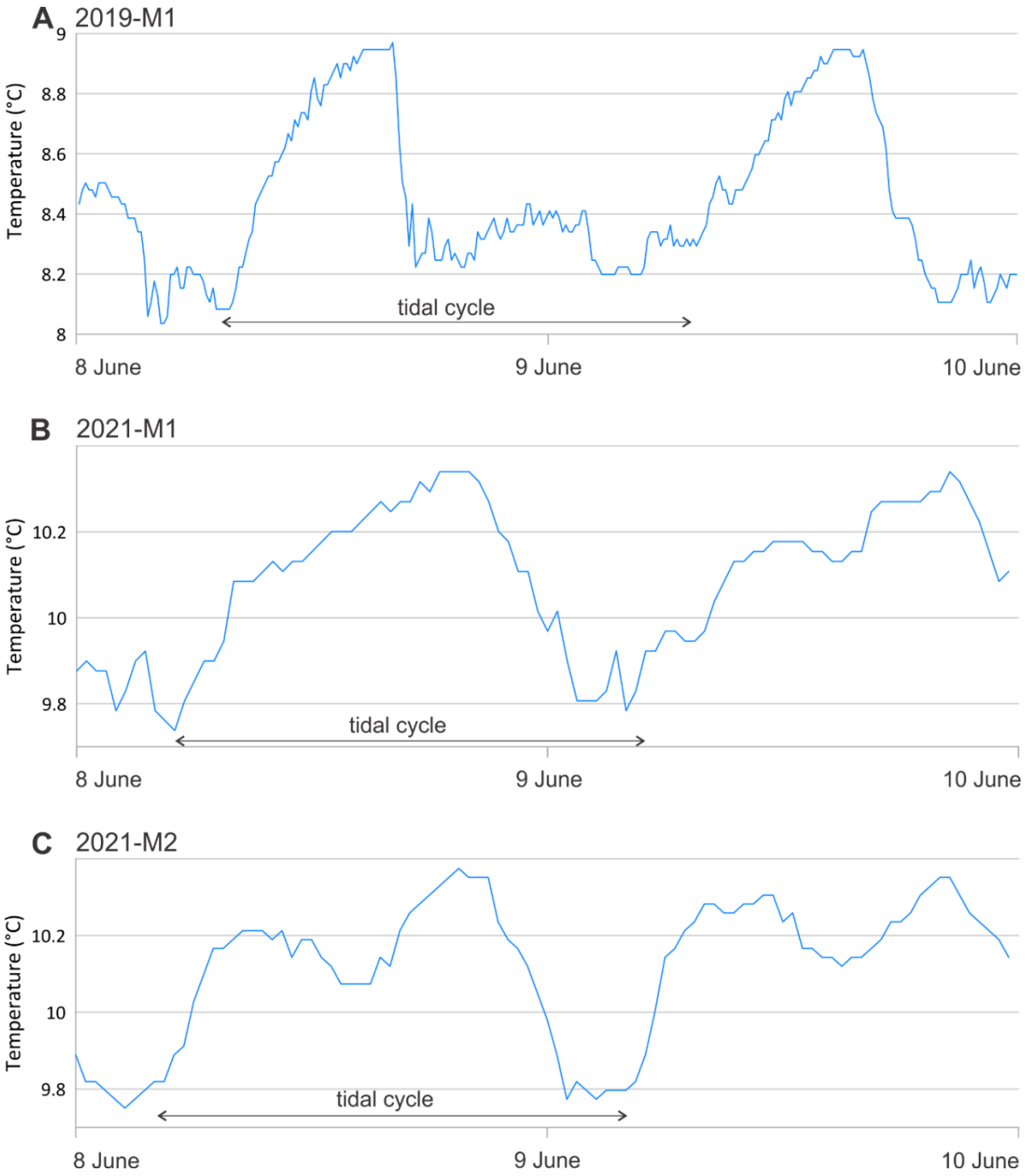

Figure 5.7. Evolution of the temperature measured by the moorings over 2 days in (A) 2019 (6 m above the seafloor) and (B and C) 2021 (35 m above the seafloor). The arrow represents the diurnal tidal period.

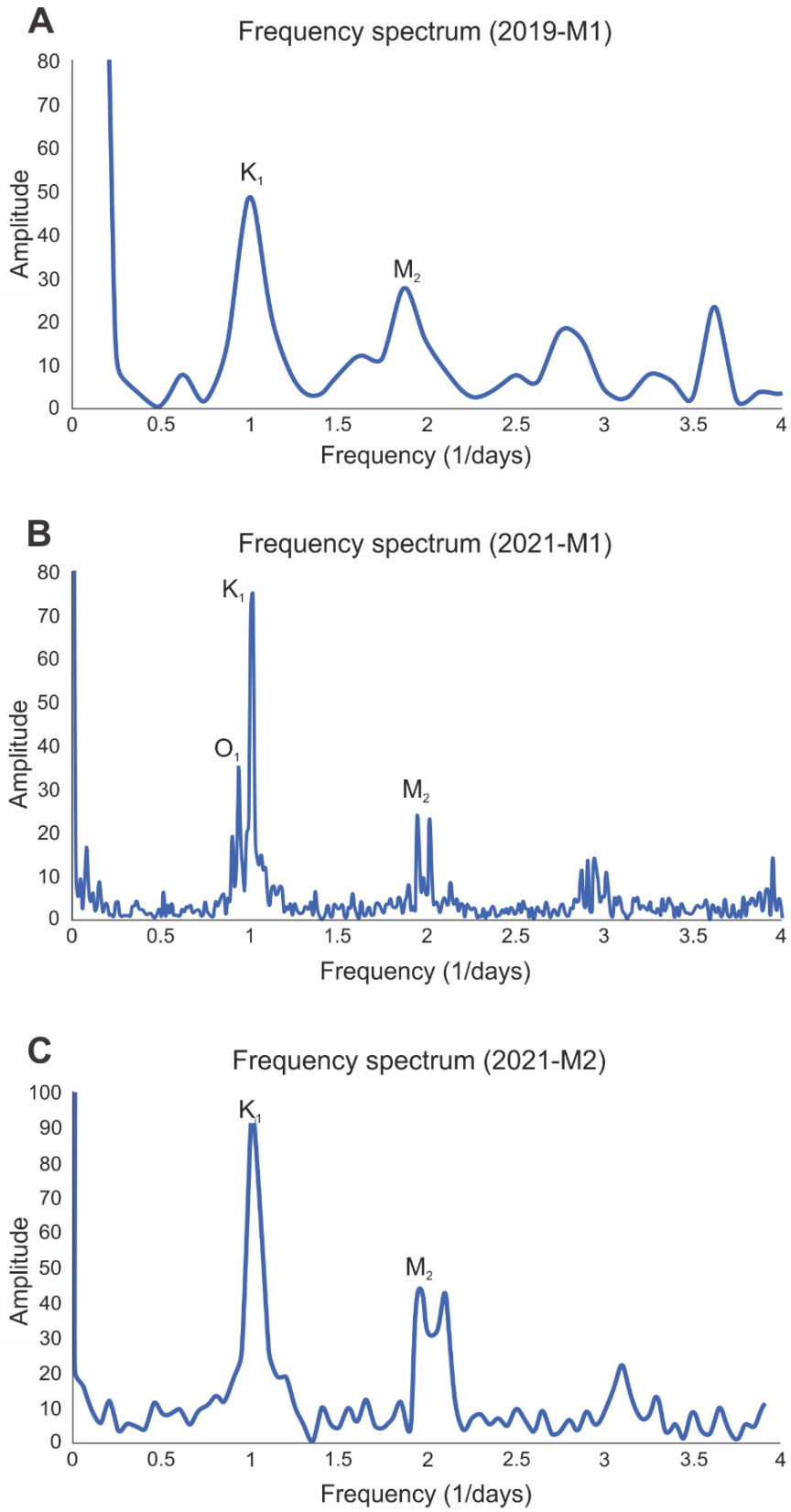

Figure 5.8. Frequency spectra based on the tidal analysis for the (A) 2019 mooring, (B) 2021-M1 and (C) 2021-M2. K_1, M_2 and O_1 are tidal constituents (periodic waves).

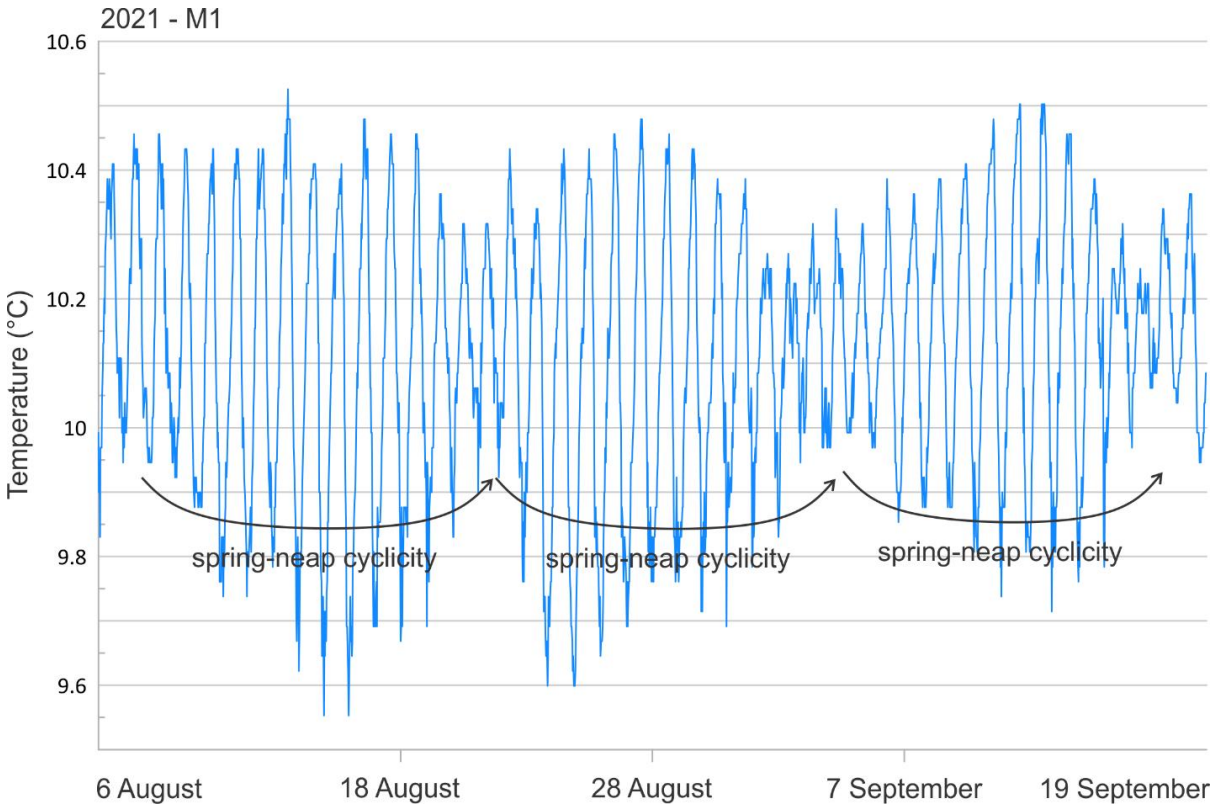

Figure 5.9. Temperature records for the 2021-M1 mooring, from 6/08 to 19/09 and located 35 m above the seafloor, revealing a clear spring-neap cycle in the measurements.

5.4.2 CTD

To validate the glider-mounted CTD data, one of the profiles was compared with a nearby vessel-mounted CTD cast (Fig. 5.10). Both were collected on the same day, within less than two hours apart. Whereas the temperature profiles only showed slight deviations, the salinity values, however, differed significantly, with the vessel-mounted CTD cast showing much greater variability. This discrepancy is most likely attributed to a malfunctioning conductivity sensor, since all casts from the RV Belgica 2023 survey exhibited anomalous salinity values.

Figure 5.11 presents all CTD profiles recorded by the glider. A vertical variability can be observed at the seasonal thermocline depth (Fig. 5.11C). Deeper, a ~24 h cyclicity can be observed throughout the temperature, salinity and oxygen concentration variations, with at least four apparent cycles occurring between 11/06 and 15/06. This cyclicity shows a maximum positive amplitude around 300 m water depth, while the maximum negative amplitude is near 800 m water depth. Temperature values range from 16°C at the surface to 9°C at ~1000 m water depth. At the depth of the Belgica Mound Drift, temperatures are around 10°C. Salinity varies between 35.48 and 35.68, decreasing gradually with depth until the wave-affected zone, below which salinity increases again. Oxygen concentration peaks at ~340 µmol/L and the chlorophyll-a concentrations reach up to 1.75 mg/m^3, both occurring between 50 and 70 m water depth.

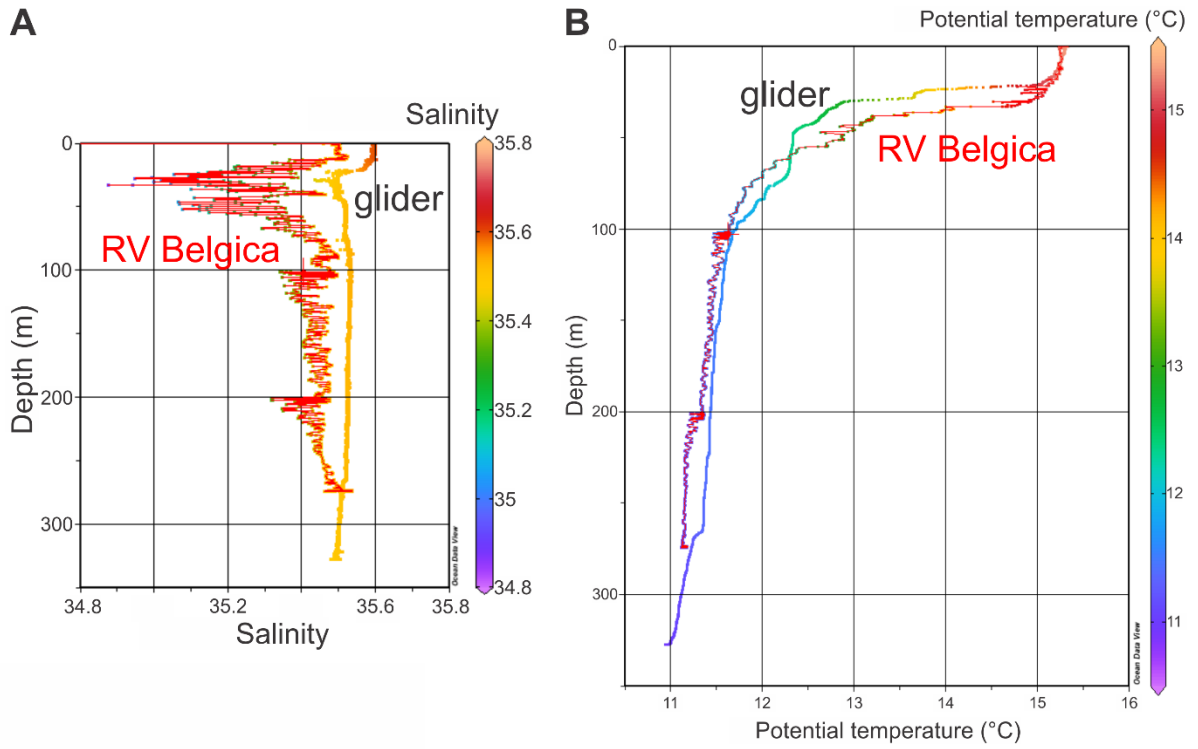

Figure 5.10. Comparison between a CTD cast, salinity (A) and temperature (B), from RV Belgica (in red; CTD1 11/06/23 09h50; Fig. 5.1) and a nearby glider profile collected later the same day (11/06/23 11h30). The figure was produced using Ocean Data View (Schlitzer, 2023).

Two distinct water masses can be identified in the glider dataset (Figs. 5.12, 5.13): the Eastern North Atlantic Water (ENAW) and the Mediterranean Outflow Water (MOW). The surface water (0-100 m) is characterised by temperatures above 12°C and a broad range of salinity values (Fig. 5.13). Below 100 m water depth, T-S points cluster to form the ENAW signature, with a temperature between 10-12°C and salinity ranging from 35.45 to 35.6. The lower boundary of the ENAW lies around 700 m water depth. Beneath this, increasing salinity indicates the presence of the MOW, which is marked by a temperature between 9-10°C and salinity from 35.5 to 35.6, reaching peak salinity values near 1000 m water depth.

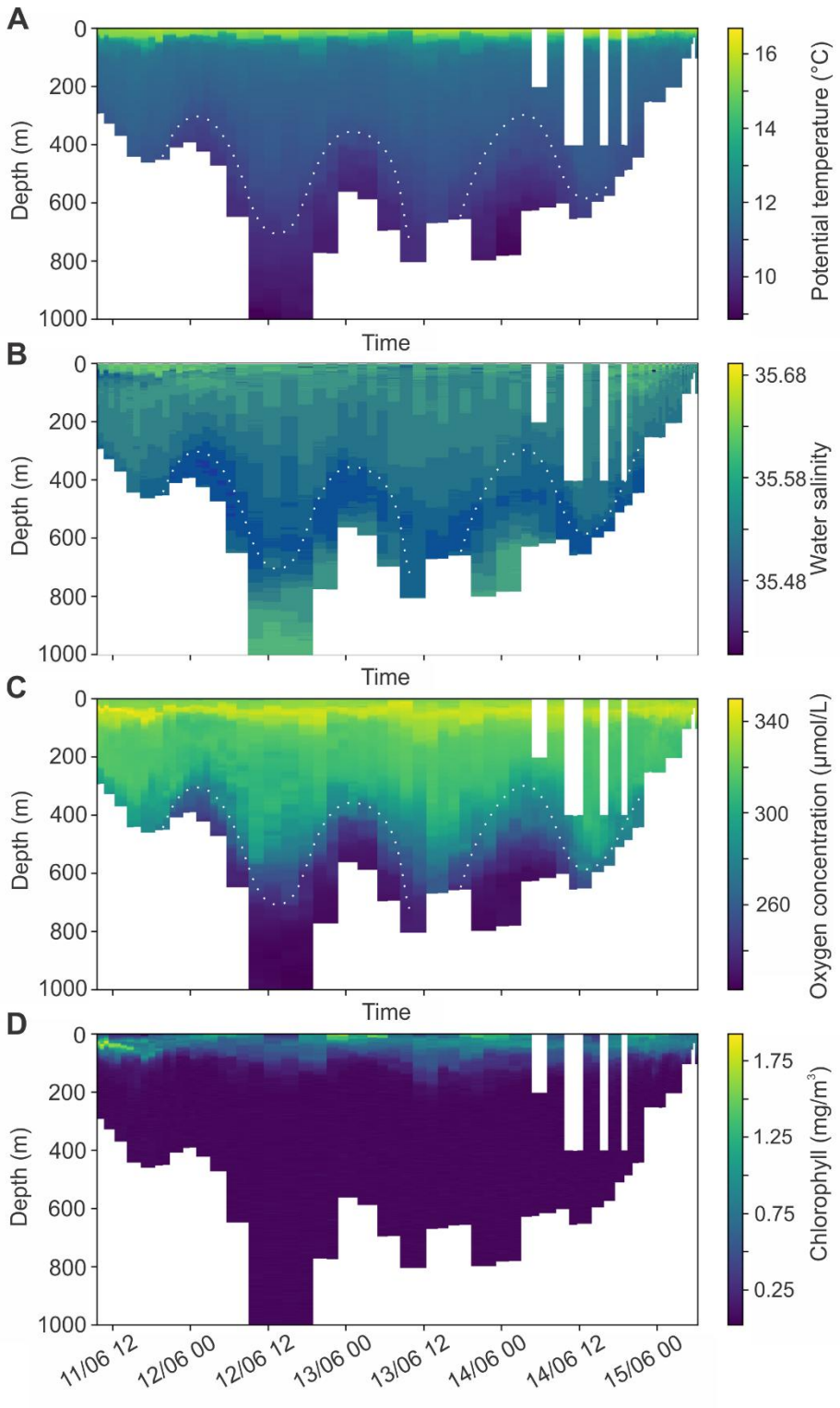

Figure 5.11. Glider-mounted CTD data for all 50 profiles. (A) Potential temperature. (B) Water salinity. (C) Oxygen concentration. (D) Chlorophyll. The white rectangles in the data correspond to sections where the glider did not reach the sea surface, due to limitations in its minimal survey depth at those locations. The white dotted lines highlight the sinusoidal pattern.

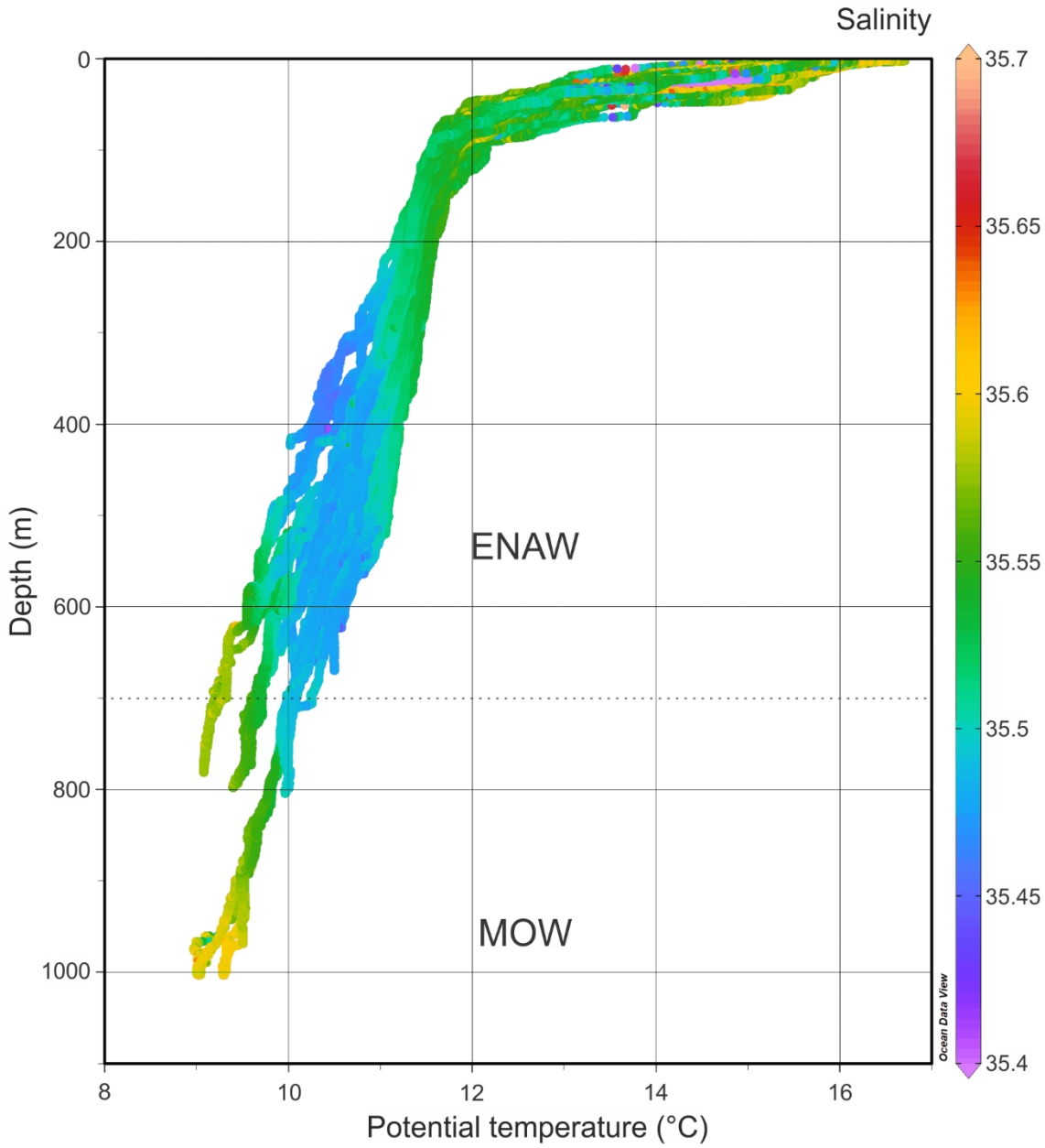

Figure 5.12. Plot of the potential temperature and salinity (colour scale) for all glider CTD profiles. ENAW: Eastern North Atlantic Water. MOW: Mediterranean Outflow Water. The figure was produced using Ocean Data View (Schlitzer, 2023).

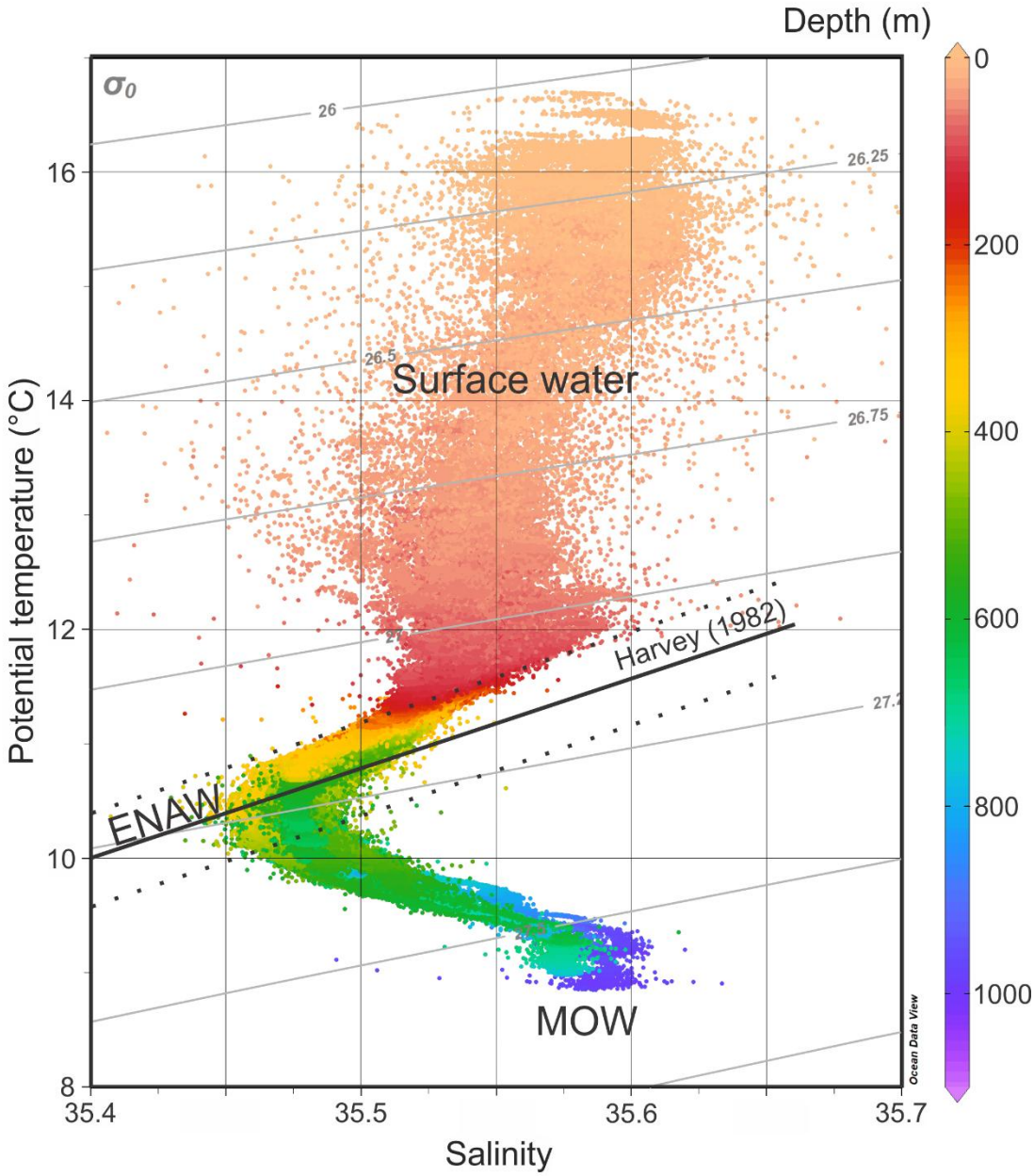

Figure 5.13. Temperature - Salinity (T-S) diagram from the glider-mounted CTD profiles. The colour scale corresponds to the water depth (m). The grey lines show the potential density anomaly (kg/m^3). The thick dark line represents the characteristic T-S relationship of the ENAW as defined by Harvey (1982), while the dashed lines indicate a salinity variation of ±0.05 around this reference. ENAW: Eastern North Atlantic Water. MOW: Mediterranean Outflow Water. The figure was produced using Ocean Data View (Schlitzer, 2023).

5.4.3 ADCP

Vessel-mounted ADCP data (Fig. 5.14) were compared with selected glider-mounted ADCP measurements in two locations (Figs. 5.1, 5.15). At location 1 (Figs. 5.1, 5.15A), there is an overlap of the magnitude and zonal (eastern component) velocity curves, but notable differences are observed in the meridional (northern component) velocity and the angle

(direction). These discrepancies are likely due to the temporal gap between the datasets: The vessel-mounted ADCP measurements were taken several hours before the glider's, during which the meridional velocity shifted from negative to positive, as shown in Fig. 5.14A.

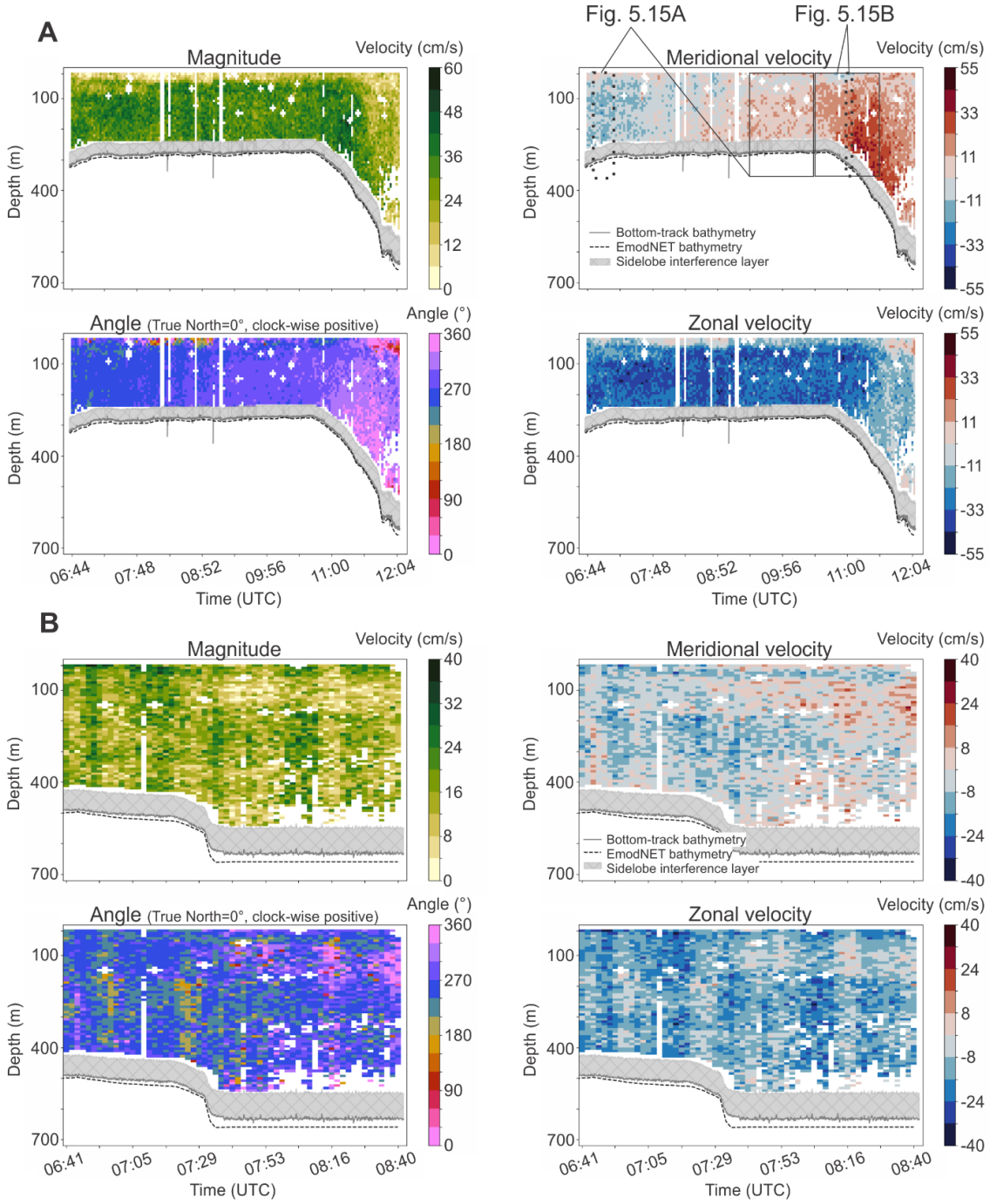

Figure 5.14. Vessel-mounted ADCP (OS75BB) measurements (Fig. 5.1). (A) 11/06/23. In the meridional velocity profile, the solid rectangles and dotted rectangles represent the glider-mounted ADCP and vessel-mounted ADCP measurements, respectively, used for the inter-comparison (Fig. 5.15). (B) 15/06/23.

In contrast, location 2 (Figs. 5.1, 5.15B) displays a clear overlap of all curves, which can be attributed to the simultaneous data collection - vessel-mounted ADCP from 10:59 to 11:04 and glider-mounted ADCP from 10:30 to 11:30 (Fig. 5.14A). Based on this comparison, the glider-mounted ADCP data are considered validated in location 2.

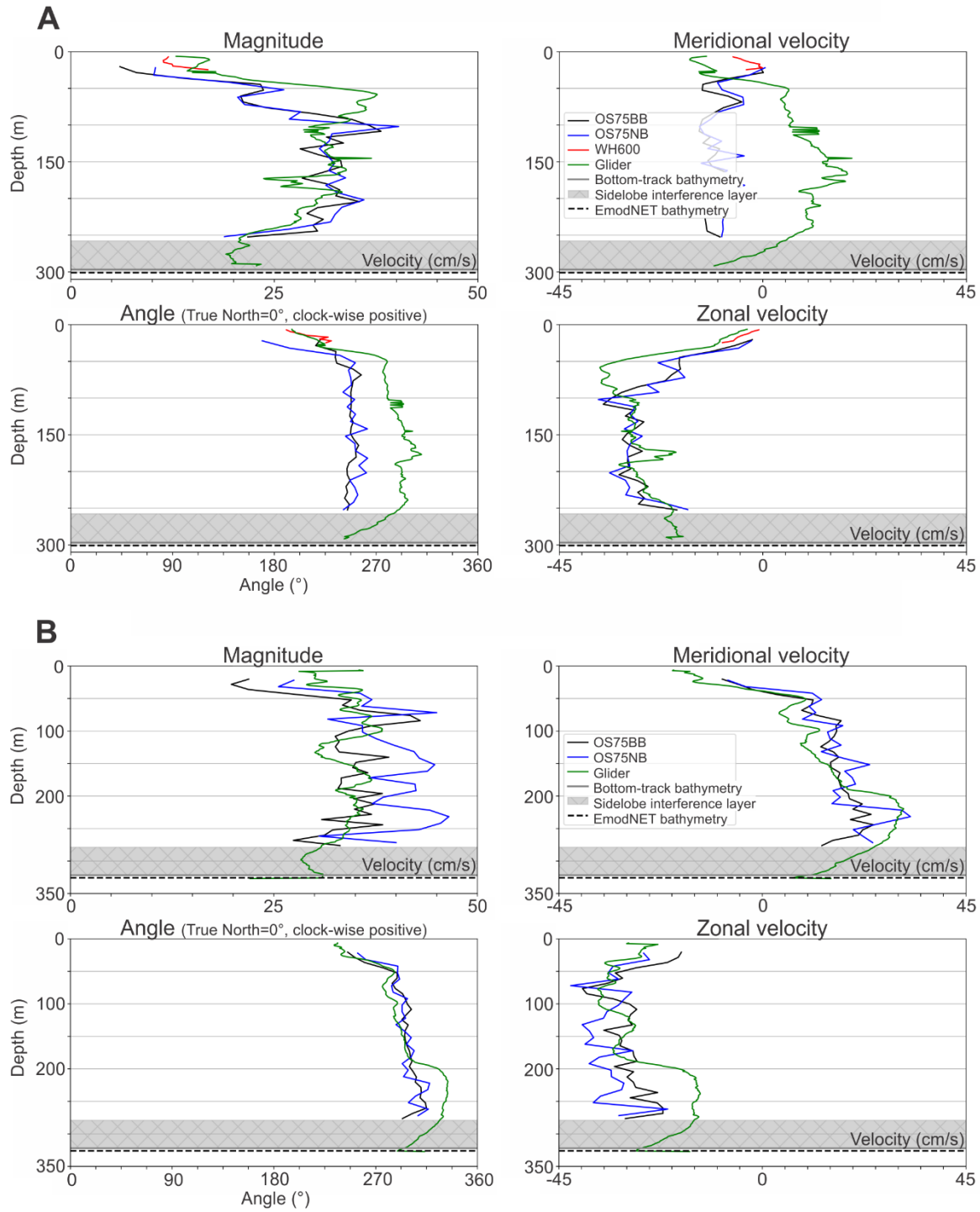

Figure 5.15. Inter-comparison between vessel-mounted (OS75BB, OS75NB and WH600) and glider-mounted ADCPs. (A) Location 1 (Fig. 5.1) with 9 vessel-mounted ADCP profiles (11/06/23 from 06:55 to 07:06) compared to 2 glider-mounted ADCP profiles (11/06/23 from 09:25 to 10:28). (B) Location 2 (Fig. 5.1) with 5 vessel-mounted ADCP profiles (11/06/23 from 10:59 to 11:04) compared to 2 glider-mounted ADCP profiles (11/06/23 from 10:30 to 11:30).

Figure 5.16 shows the eastern (Fig. 5.16A) and northern (Fig. 5.16B) velocity components from the glider-mounted ADCP. In the eastern component, there are alternating shifts between positive (white circles in Fig. 5.16A) and negative velocities following cycles of 24 h: The positive values correspond to an upslope flow towards E while negative values show a

downslope flow towards W. Notably, two ascending glider profiles recorded strong eastward velocities reaching up to 95 cm/s near the seafloor. The northern component displays less distinct periodicity, with a predominance of positive values, indicating persistent northward flow. Depth-dependent variations are noticeable, with stronger northward flows concentrated near the seafloor, between 400-600 m and even more pronounced fluctuations occurring from 650 to 800 m water depth.

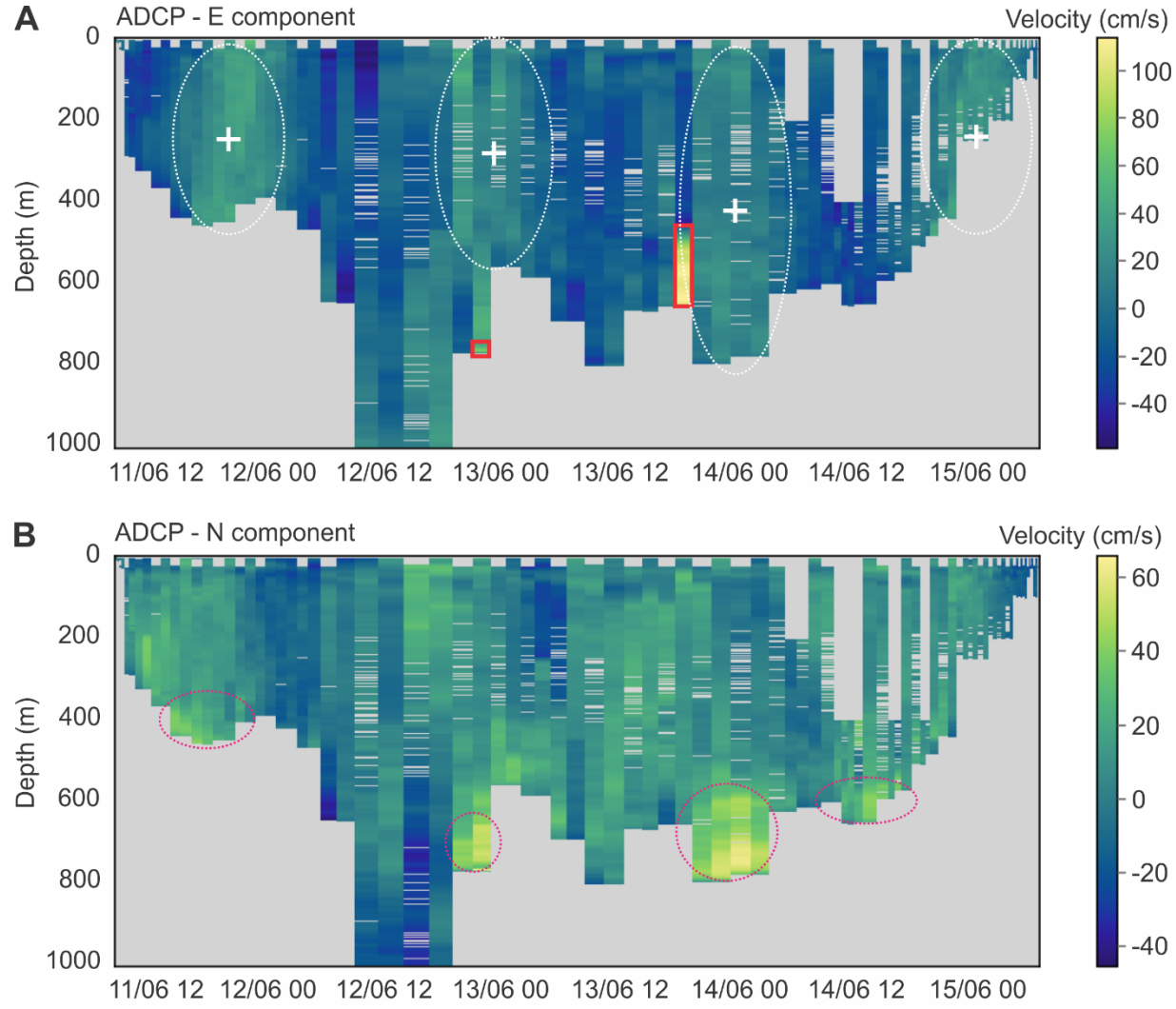

Figure 5.16. Glider-mounted ADCP measurements for all 50 profiles. (A) Eastern velocity component, with two outliers (red) and white circles representing positive velocities. (B) Northward velocity component with pink circles showing the bottom enhancement.

For each glider-mounted ADCP profile (Fig. 5.16), the deepest measurements were averaged over a 3 m interval to estimate the speed and direction of the bottom currents. Current vectors were calculated on this 3 m interval and plotted on a map (Fig. 5.17). All vectors recorded from the beginning of the glider survey until 11 June at 11h25, and from 14 June at 21h10 until the end of the survey, were excluded, as they correspond to measurements taken too far from the seafloor (Fig. 5.4A). Two vectors displayed peak velocities of 68 and 95 cm/s, which were stronger than those recorded by the moorings over the drift and in the literature. These two outlier values were removed from the map (Fig. 5.17) but remain apparent in Fig. 5.16. Additionally, the immediately preceding diving profiles indicated lower current velocities (Fig.

5.16). When the outliers are excluded, flow speeds range from 3 to 55 cm/s, with an average of 25,6 cm/s, aligning well with the 2019 mooring data collected 6 m above the seafloor. The vectors are not synchronised in time. As a result, the differences in vector direction and speed in Fig. 5.17 reflect a combination of both spatial and temporal changes.

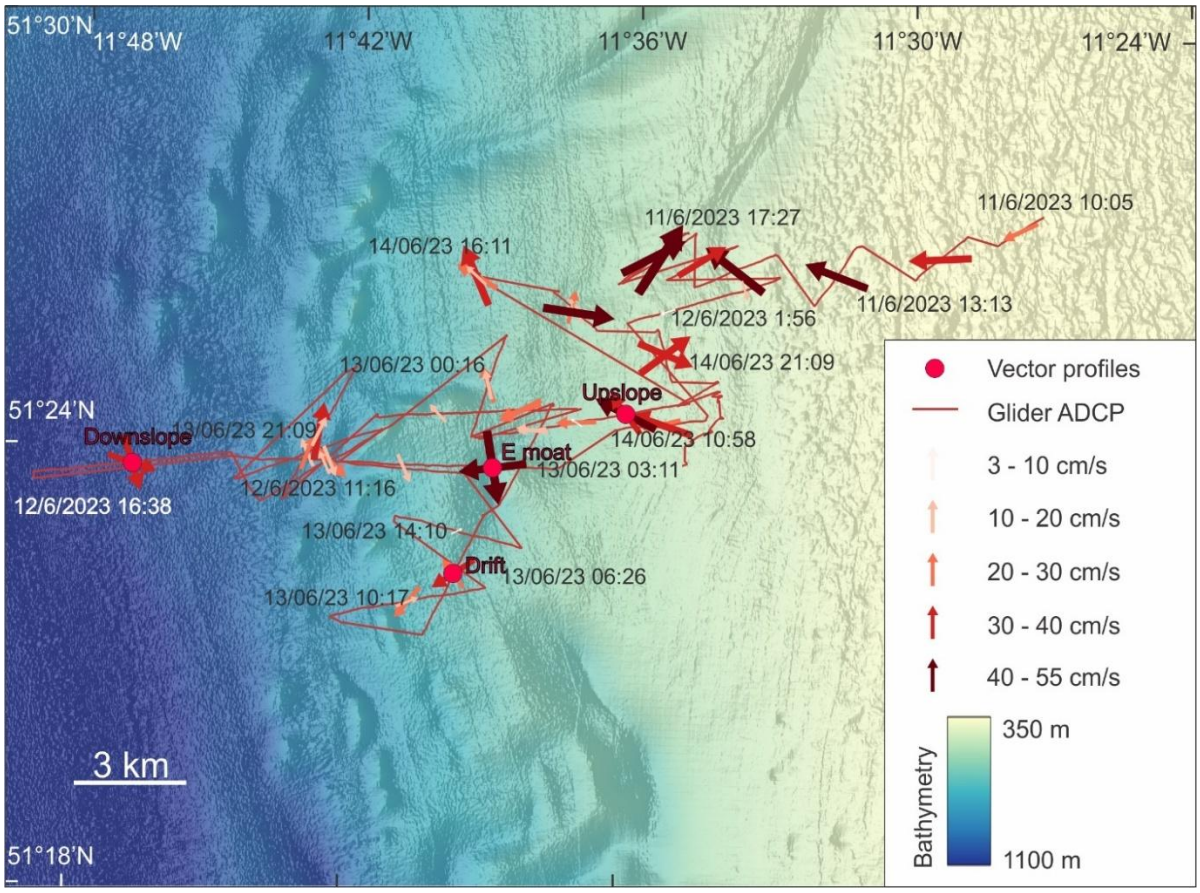

Figure 5.17. Vectors showing the bottom (3 m average above seafloor) current direction and speed along the glider track, from diving and ascending profiles. The vectors are not aligned in time.

To better observe the temporal variations in the bottom currents recorded by the glider, the vectors were plotted over time (Fig. 5.18). Diurnal tidal fluctuations in current direction can be observed, similar to those observed in the mooring data (Fig. 5.6). However, the dominant diurnal tidal pattern is less distinct, as the glider was not fixed in one location in contrast to the moorings, making it more difficult to isolate temporal changes from spatial variations.

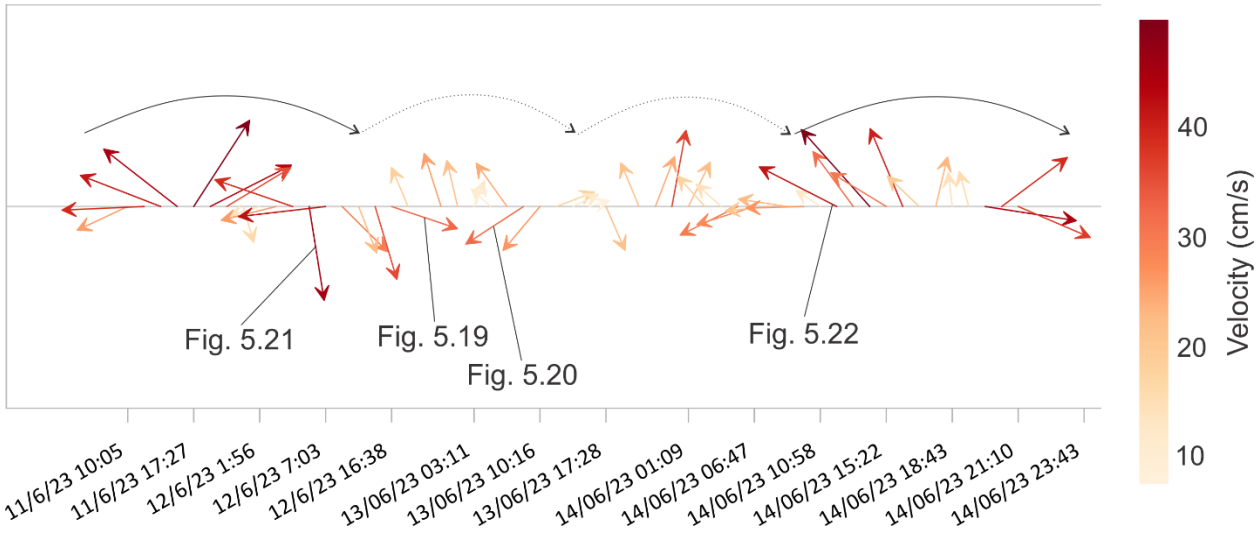

Figure 5.18. Vectors aligned in time and showing the bottom (3 m average above seafloor) current velocities, with diving and ascending profiles. The black arrows show the tidal periodicity.

Table 5.4. Summary statistics for the four glider-mounted ADCP profiles.

Profile	Maximal speed (cm/s)	Minimal speed (cm/s)	Mean vector direction (°) and speed (cm/s)	Water depth (m)
Downslope 12/06 13h49-16h38	38.4	2.2	72.8, 10.6	1003
Drift 13/06 06h26-08h05	40.7	9.9	281.0, 19.1	695
Moat 12/06 05h29-08h05	53.7	5.5	250.0, 20.0	648
Upslope 14/06 11h44-12h17	46.2	18.1	259.0, 23.9	651

In order to assist the visualisation of the spatial variations in the ADCP measurements, four representative glider profiles were selected (Figs. 5.1, 5.4, 5.18): downslope of the drift (the deepest glider profile; Fig. 5.19), on the drift (Fig. 5.20), in the eastern moat of the drift (Fig. 5.21), and upslope of the drift (Fig. 5.22). For each profile, current vectors (Table 5.4) were calculated at each measurement point and displayed through the water column. Additionally, separate plots showing only current speed as a function of water depth were produced. In all profiles, current velocity abruptly increases with depth by a factor 1.5 to 4 in the 100 m above the seafloor. It is in the 100 m above the seafloor that the recorded flow is the strongest and reached the maximum recorded speed values (Table 5.4) and it is on the drift and in the moat that the factor is the biggest. In three of the four profiles (downslope, drift and upslope), current velocity decreases again within the 20 to 5 m near the seafloor by a factor 0.55 to 0.85. This is near the seafloor, in the moat profile, that the strongest flow was recorded, up to 53.7 cm/s. In this profile (Fig. 5.21), no reduction of the strength of the flow was observed near the seafloor.

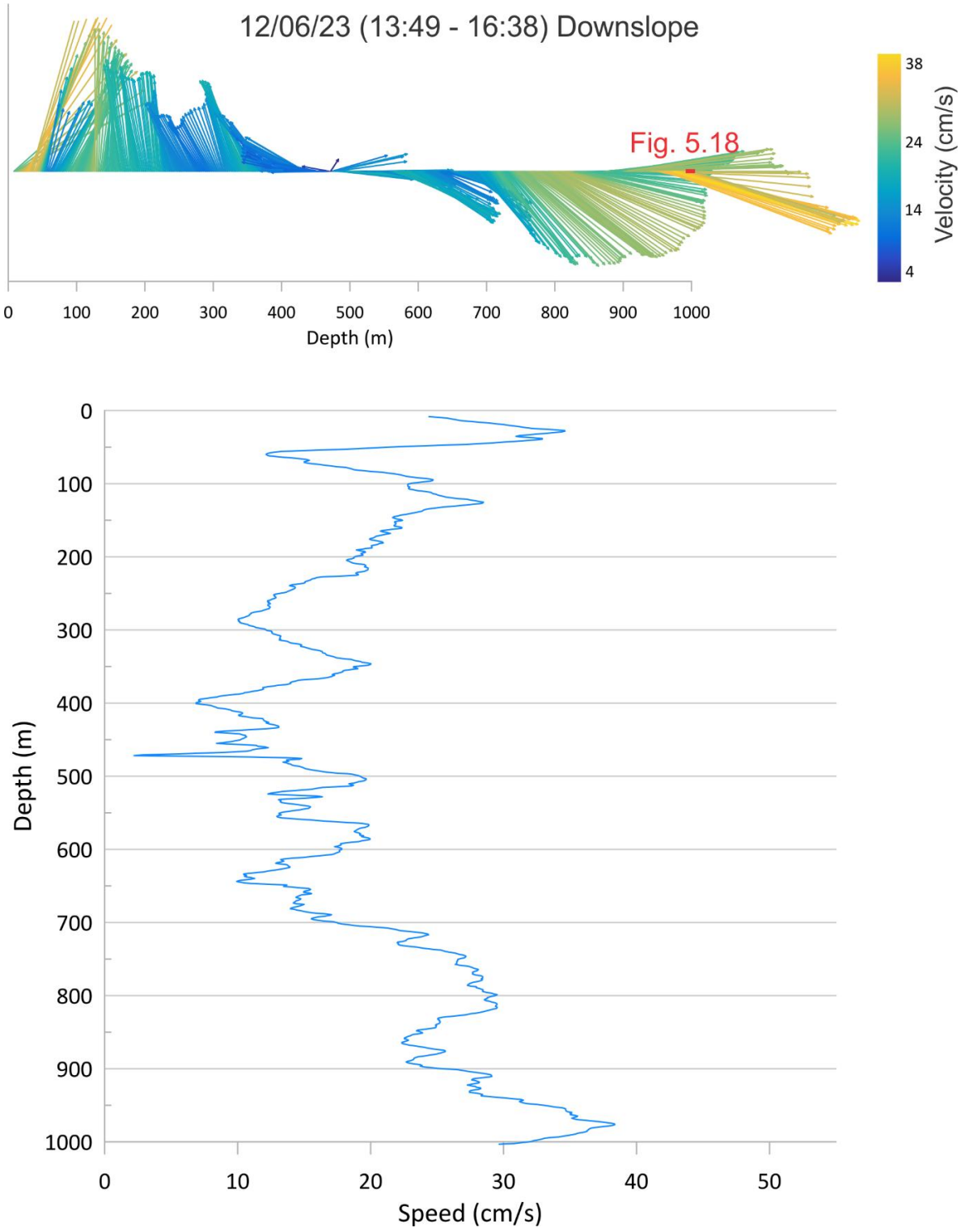

Figure 5.19. Single glider-mounted ADCP profile (Figs. 5.1, 5.4, 5.17), located downslope of the drift. It shows the current direction and speed in the water column and close to the seafloor. Diving profile, 12/06/23 13:49 - 16:38.

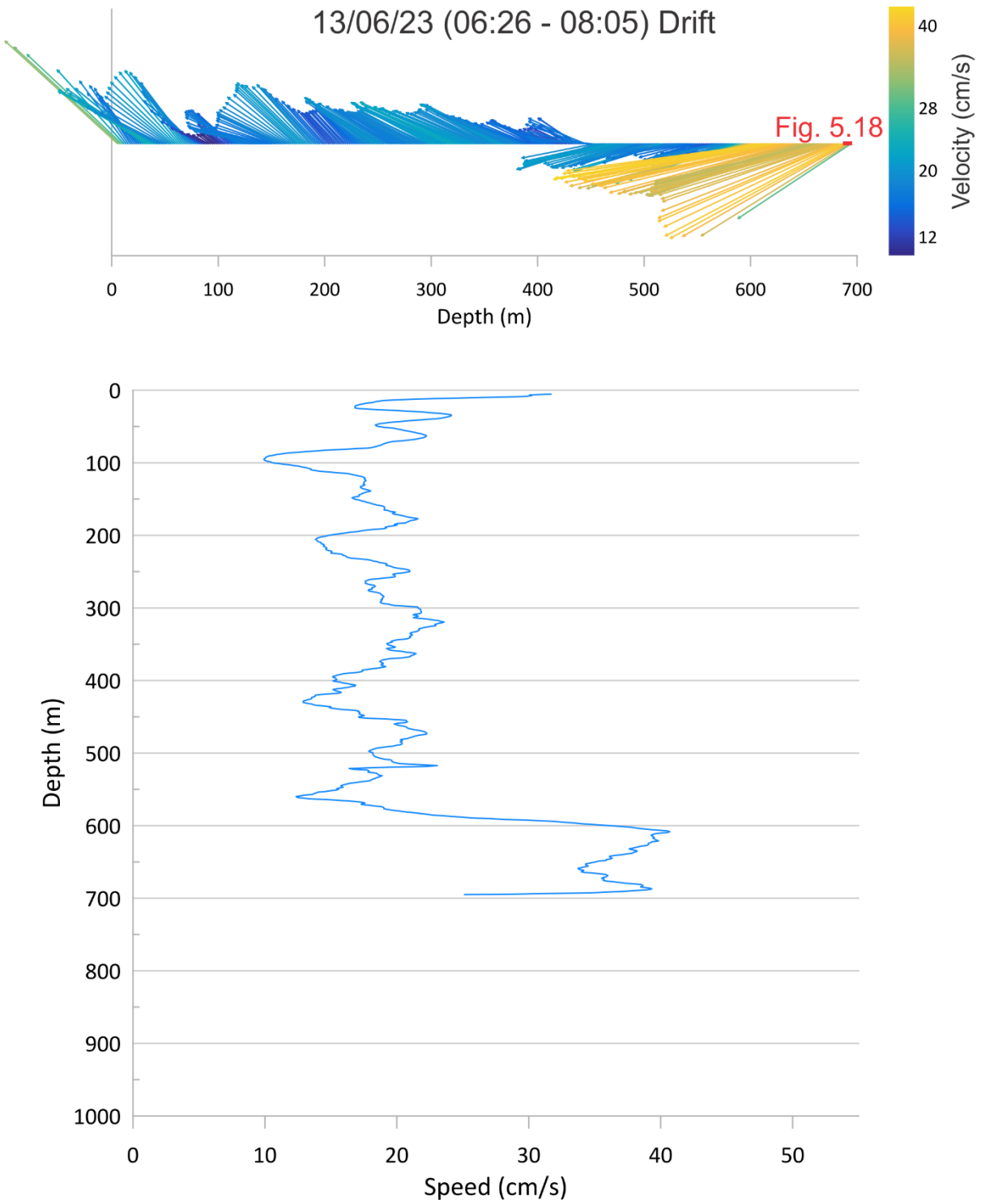

Figure 5.20. Single glider-mounted ADCP profile (Figs. 5.1, 5.4, 5.17), located on the drift. It shows the current direction and speed in the water column and close to the seafloor. Ascending profile, 13/06/23 06:26 - 08:05.

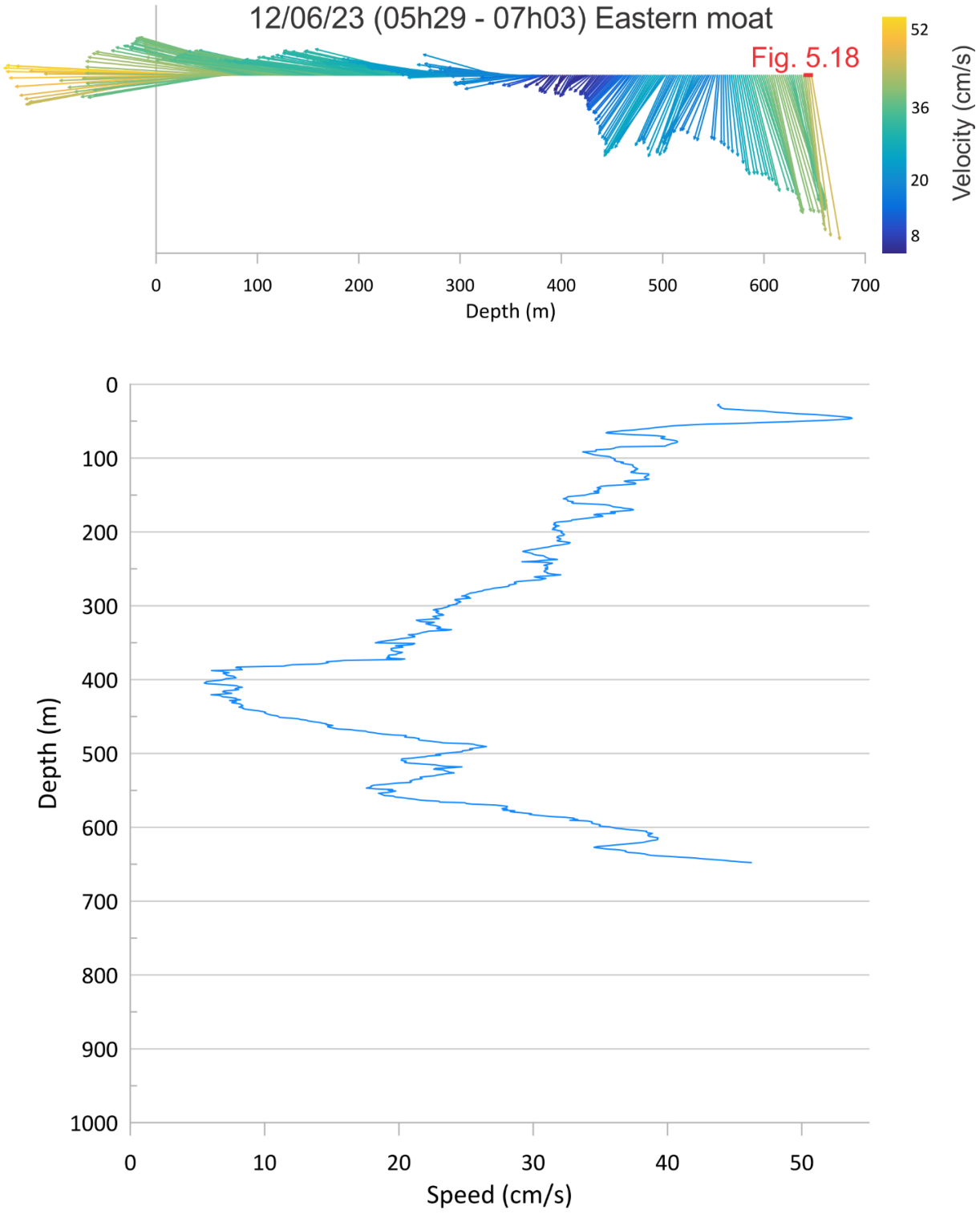

Figure 5.21. Single glider-mounted ADCP profile (Figs. 5.1, 5.4, 5.17), located in the eastern moat of the drift. It shows the current direction and speed in the water column and close to the seafloor. Diving profile, 12/06/23 05:29 - 07:03.

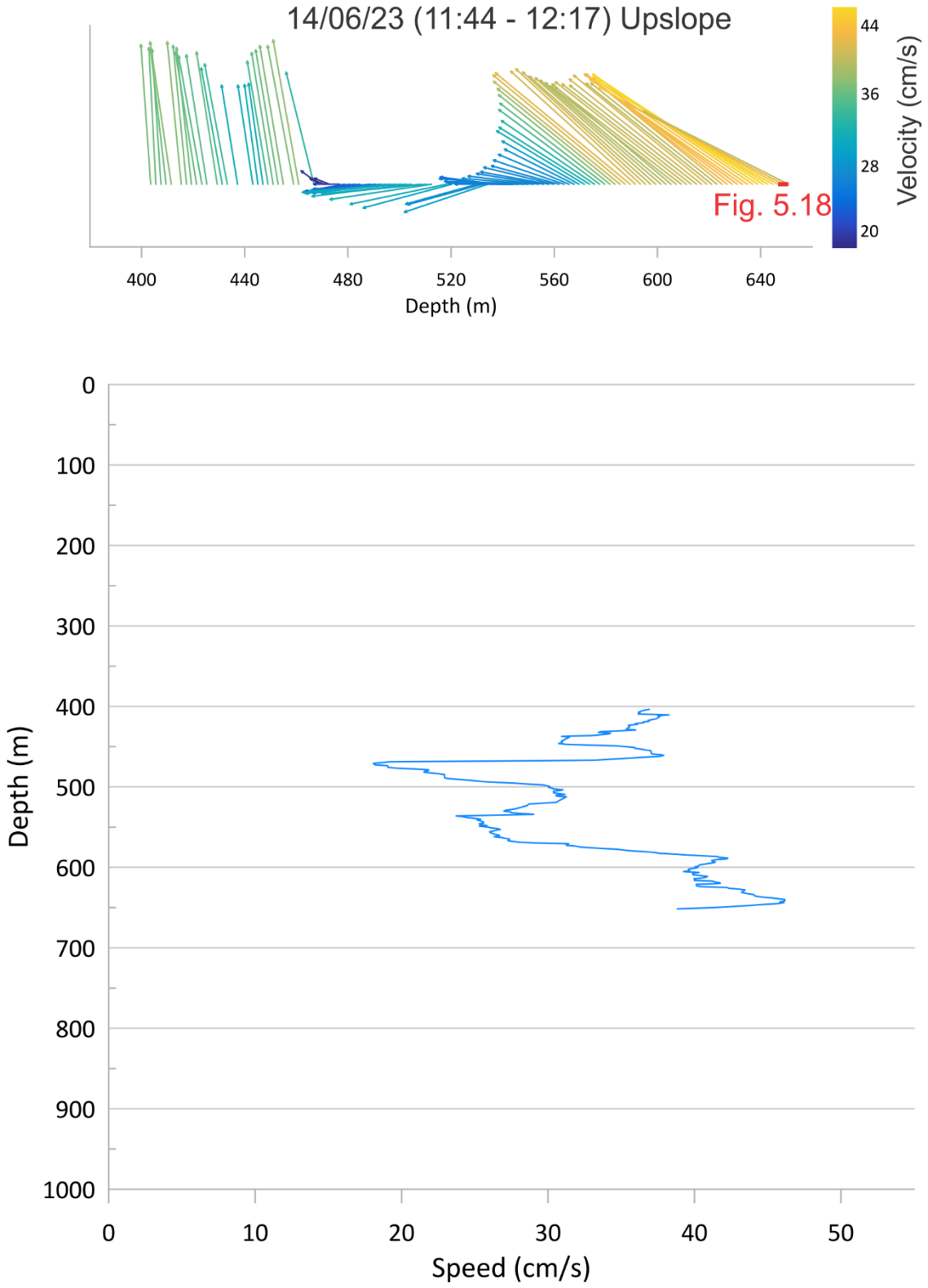

Figure 5.22. Single glider-mounted ADCP profile (Figs. 5.1, 5.4, 5.17), located upslope of the drift. It shows the current direction and speed in the water column and close to the seafloor. Diving profile, 14/06/23 11:44 - 12:17.

5.5 Discussion

5.5.1 Water column stratification

The glider CTD profiles reveal two distinct water masses: the ENAW and the MOW. The ENAW has a temperature between 10-12°C and salinity ranging from 35.45 to 35.6, while the MOW exhibits a temperature between 9-10°C and salinity from 35.5 to 35.6. The boundary between these two water masses is located around 700 m depth, with a salinity peak marking the core of the MOW around 1000 m depth (Figs. 5.12, 5.13). These observations align with the findings of Harvey (1982) and van Aken and Becker (1996), who documented similar characteristics for both water masses (Fig. 5.13). The ENAW in the NE Atlantic typically shows a salinity of 35.4 at 10°C and 35.66 at 12°C, with a ±0.05 variation in salinity (Fig. 5.13) around the curve presented by Harvey (1982). The MOW, on the other hand, has a temperature ranging from 8 to 10°C and salinity above 35.5, as observed on the southern slope of the Porcupine Bank (van Aken and Becker, 1996). The MOW is typically found below 600 m depth and is characterised by the highest salinity in the NE Atlantic, particularly between 900 and 1150 m (Harvey, 1982).

A distinct diurnal oscillation is observed in the temperature, salinity and oxygen concentration (Fig. 5.11). This sinusoidal pattern matches the expected period of the trapped baroclinic motion, i.e. around 24 h as previously observed in the Belgica Mound Province by White (2007), White et al. (2007) and White and Dorschel (2010). Based on Fig. 5.11, it appears that the trapped baroclinic motion would occur over a depth of approximately 500 m. From literature, the precise vertical scale of this motion remains uncertain. Further investigation is needed to accurately determine the vertical scale of this motion in the water column. One approach could involve comparing the calculated density profile (derived from glider data) with the theoretical depth at which this density is typically found, helping to estimate the vertical displacement caused by the motion.

The observed asymmetry in temperature fluctuations (Fig. 5.7) further supports the presence of the trapped tidal baroclinic motion and its interaction with the topography. Specifically, the sharp temperature drops during the shorter upslope flow contrasts with the more gradual increases during the longer downslope flow. The upslope flows (towards E for 2021 moorings or NE for 2019-M1) exhibit higher velocities than the downslope flows (Fig. 5.6). This pattern is associated with the movement of colder and deeper water during upslope flow. This has been often observed for freely propagating baroclinic motion on slopes (e.g. White,1994; Lorke et al., 2005) and also for diurnal tidal motions on the slopes of the Rockall Bank (Mienis et al., 2007). The trapped motion affects at least 35 m above the seafloor, as evidenced by the motion observable through the temperature measurements from the three moorings (Fig. 5.7).

5.5.2 Trapped baroclinic motion and its influence on the bottom currents

The measured bottom-current strength and direction (Figs. 5.5, 5.6; Table 5.3) are consistent with previous observations from the Belgica Mound Province based on direct measurements (White et al., 2007; Dorschel et al., 2007). These currents are primarily driven by a diurnal tidal component moving across the slope (W-E), with a weaker residual component flowing northward along the slope. Minor discrepancies between the mooring data likely reflect small-

scale variations in local topography near the measurement sites. Velocity readings from the current meters positioned 35 m above the seafloor, both north and south of the drift crest, are comparable (Table 5.3), and notably weaker than those recorded at 6 m above the seafloor (Fig. 5.5A). This vertical difference suggests a reduced steering influence from topographic features, such as CWC mounds and drift structures. As a result, currents at 35 m show a predominantly W-E flow, while those closer to the seafloor follow a more SW-NE orientation due to increased interaction with the complex bottom topography. These findings indicate that the diurnal tidal components are amplified and modulated by a spring-neap tidal cycle, aligning with patterns identified in earlier studies (White et al., 2007; Dorschel et al., 2007). Additionally, the observed small-scale spatial variability mirrors patterns found elsewhere in the Belgica Mound Province (Dorschel et al., 2007).

The eastern velocity component of the glider-mounted ADCP measurements (Fig. 5.16A) shows distinct 24 h shifts between positive (upslope) and negative (downslope) velocity flows. These fluctuations can be associated with the W-E diurnal tidal component (Figs. 5.5, 5.6) of the trapped baroclinic motion. On average, the northern velocity component displays a persistent northward flow (Fig. 5.16B). This is also evident in the mooring data (Figs. 5.5, 5.6) with the measured residual northward current, which combines the alongslope bottom current, generated by the rectification of the trapped baroclinic motion by the Coriolis force near the seafloor (Huthnance, 1981; White, 2007; White and Dorschel, 2010), and the contour current (Matossian et al., submitted). The stronger currents near the seafloor (Fig. 5.16B), from 400 up to 800 m water depth, can be attributed to the interaction of the trapped baroclinic motion with the seafloor topography. Notably, the northward flow intensifies between 650 and 800 m, particularly during tidal upslope flows, when the eastern velocity component becomes positive. While the velocities may also be enhanced below 800 m, the glider's deeper dives occurred during a tidal change, when downslope flows were present, potentially masking further enhancements. The dynamics of trapped baroclinic motion suggest that the intensity of the flow is maximised when $N\sin(\alpha)$ reaches its peak, where N is the Brunt-Väisälä frequency, or buoyancy frequency (vertical density stratification N^2) and α is the slope angle of the seafloor (Rhines, 1970; White, 2007; White and Dorschel, 2010). According to White et al. (2007) and White and Dorschel (2010), this enhancement is most pronounced near a water depth of approximately 850 m in the Belgica Mound Province, where the values of $N\sin(\alpha)$ are maximised (Fig. 5.23). This depth coincides with the region where there is the ENAW–MOW interface and where the continental margin steepens, contributing to stronger baroclinic motion. The contourite drift is located between 600 and 800 m water depth and would thus be under the influence of the enhanced trapped baroclinic motion. At approximately 850 m water depth, where the baroclinic motion is most enhanced, the corresponding minimum wave period has been defined by White et al. (2007). This period is approximately 25 h, which closely aligns with the diurnal component of the trapped baroclinic motion observed in the data (Figs. 5.5-5.7, 5.11, 5.16, 5.18).

The sharp increase in speed at 100 m above the seafloor across all glider profiles (Figs. 5.19-5.22) indicates the interaction between the enhanced trapped baroclinic motion and the seafloor, which affects the bottom currents. This effect is most pronounced on the drift and in the eastern moat, where the strongest recorded flow reached 53.7 cm/s. In the profiles, except for the eastern moat (Fig. 5.21), a weakening in current speed from 20 to 5 m near the seafloor suggests friction with the seafloor. The region between the seafloor and up to 5 to 20 m above it likely represents the bottom boundary layer (or bottom Ekman layer). White and Dorschel (2010) also noted the potential presence of a 10 m thick frictional layer in the area.

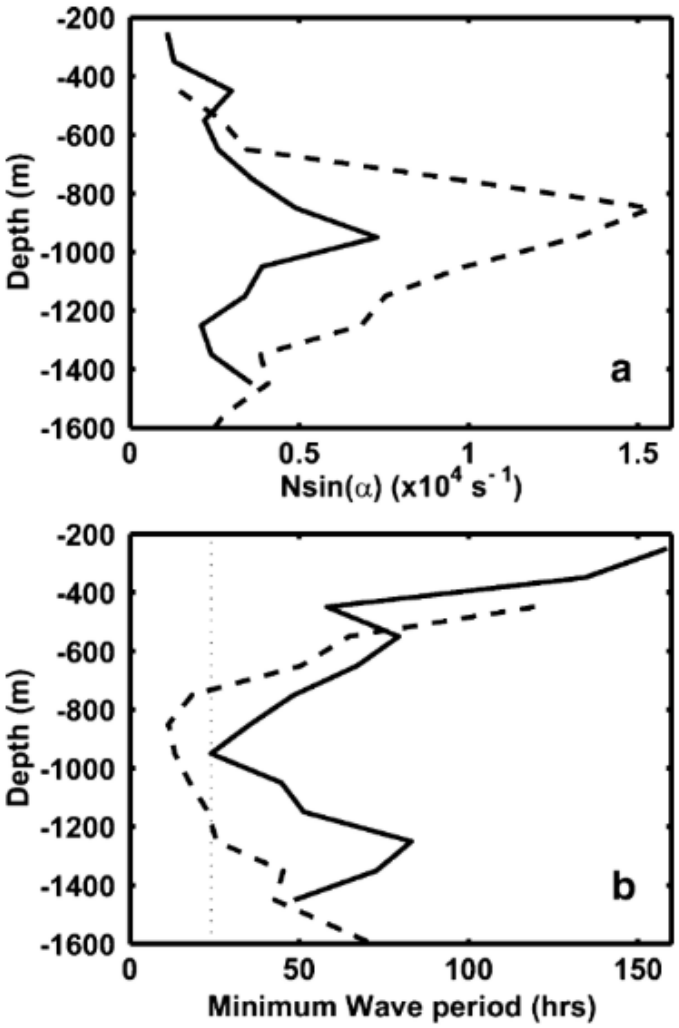

Figure 5.23. (a) Vertical profiles of Nsin(α) with depth and (b) vertical profiles of the minimum wave period of the baroclinic motion for the Belgica (solid line) and the Logachev (dashed line; Rockall Bank) mound provinces (from White et al., 2007). A 25 h period is indicated by the dotted line in b.

This layer can be impacted by the bottom Ekman transport, which results from the combined effect of the Coriolis force and bottom friction. In the Northern Hemisphere, this transport is directed to the right of the stress (Ekman, 1905). For the bottom Ekman layer, the stress acts opposite to the flow, causing the transport to be directed to the left of the flow (Taylor and Sarkar, 2008). The bottom Ekman transport is considered as a possible mechanism for lateral sediment transfer across the moat-drift system (Hernández-Molina et al., 2014; Yin et al., 2024). Flume-tank experiments by Wilckens et al. (2023) further support this, showing that a transverse flow is necessary to transport sediment from the moat onto the drift. While the primary flow in the drift-moat system is the contour current (Rebesco et al., 2014), a secondary flow is required to transport the sediment toward the drift (Wilckens et al., 2023). Due to friction near the seafloor, the alongslope current is deflected to the left (W), facilitating the deposition of sediment on the drift. However, no distinct bottom boundary layer was observed in the eastern moat profile (Fig. 5.21), even if the glider went up to 8 m above the seafloor in this

region (Fig. 5.4). This absence of a bottom boundary layer suggests that sediment transfer from the moat to the drift may not currently be occurring. The steep flanks of the N-S moat may also contribute to trapping the flow within the moat, thereby preventing the generation of Ekman transport to the left. Wilckens et al. (2023) suggested that once the moat forms, the secondary flow (in this case, the bottom Ekman transport) may become confined to the moat. The role of the bottom Ekman transport in the deflection of bottom currents remains challenging to isolate, as tidal signals also influence current patterns. The effects of friction and the deflection of bottom currents are likely to be influenced by local topography, which may explain the variability observed across different areas of the drift.

5.6 Conclusions

The sedimentary processes active on the Belgica Mound Drift are driven by complex hydrodynamic regime. It lies at the depth range of the ENAW–MOW interface, where the trapped tidal baroclinic motion is enhanced over at least 100 m above the seafloor. The interaction of this motion with the seafloor topography allows the generation of two bottom currents: (1) the across-slope tidal current (up to 50 cm/s) with a dominant K_1 tidal constituent and characterised by enhanced upslope flows, and (2) the alongslope bottom current (which is part of the residual northward current). The bottom Ekman transport, influencing the bottom currents over up to 20 m above the seafloor, could also play a role in the local variations of the currents and on the sedimentary processes occurring on and around the drift.

This study demonstrates the value of high-resolution glider data for investigating bottom currents and the water column, offering essential insights into the hydrodynamic regime driving sedimentary processes over contourite drifts. Gliders equipped with ADCPs, with their broad spatial and temporal coverage, provide a distinct advantage over moorings equipped with current meters, which typically offer data from a single point. This expanded coverage allows for a better detection of local variations of large motions, such as the baroclinic motions, and helps identify small-scale processes like the bottom Ekman layer, which can be directly quantified. The estimation of the relative phase with respect to the K_1 tidal period (Figs. 5.6, 5.18-5.22) as well as defining the vertical scale of the trapped baroclinic motion through the study of the vertical density displacement is crucial for a better characterisation of the trapped tidal baroclinic motion. A detailed investigation into the bottom Ekman layer and its influence on the bottom-current variability still needs to be carried out to grasp more fully the present-day sediment transport dynamic over the drift and its moats.

Acknowledgements

This research was conducted in the framework of the FWO project DynaMOD (FWO grant 3G021719) and on the BOF extension BOF23/CDV/126. Ship time on RV Belgica was provided by BELSPO and RBINS-OD Nature. This study uses the glider *YOKO* provided by Flanders Marine Institute. We would like to thank Willem Versteeg, Thomas Vandorpe and Hannelore Theetaert for their help with the glider during the RV Belgica 2023/12 survey. The deployment of the 2021 moorings was kindly facilitated by the Marine Institute (Ireland) during the CE21014 weather buoy maintenance survey. We would also like to thank Eoghan Daly and Sheena Fennell for their help with the mooring deployment and data processing.

5.7 References

Aanderaa Instruments, 2000. Recording current meter RCM7 & RCM8. Self-contained instruments for recording speed, direction, temperature, pressure and conductivity of ocean currents. Data sheet D 197. https://epic.awi.de/45145/11/RCM7.pdf.

Aanderaa Instruments, 2001. RCM9. A unique Recording Current Meter for use in the sea and in freshwater featuring the Mark II DOPPLER CURRENT SENSOR DCS 3920. Data sheet D 328. https://epic.awi.de/45145/1/RCM9.pdf.

Baines, P.G., 1974. The generation of internal tides over steep continental slopes. Philos. Trans. R. Soc. Lond. Ser. A, Math. Phys. Sci. 277, 27–58.

Bearman, G., 1989. Ocean Circulation, The Open University, Pergamon Press Ltd, Oxford, England.

Booth, D.A., Ellett, D.J., 1983. The Scottish continental slope current. Cont. Shelf Res. 2, 127–146. https://doi.org/10.1016/0278-4343(83)90012-2.

Boyer, T.P., Baranova, O.K., Coleman, C., García, H.E., Grodsky, A., Locarnini, R.A., Mishonov, A.V., Paver, C.R., Reagan, J.R., Seidov, D., Smolyar, I.V., Weathers, K.W., Zweng, M.M., 2018. In: Mishonov, A.V., Techincal Editor (Eds.), World Ocean Database 2018, 87. NOAA Atlas NESDIS.

Conway, J.P., Bodeker, G.E., Waugh, D.W., Murphy, D.J., Cameron, C., Lewis, J., 2019. Using project Loon superpressure balloon observations to investigate the inertial peak in the intrinsic wind spectrum in the midlattitude stratosphere. J. Geophys. Res. Atmos. 124, 8594–8604. https://doi.org/10.1029/2018JD030195.

Depuydt, P., Toucanne, S., Barras, C., Le Houedec, S., Mojtahid, M., 2024. Last Glacial - Holocene variability of the European Slope Current, NE Atlantic. Palaeogeogr., Palaeoclimatol., Palaeoecol. 633, 111884. https://doi.org/10.1016/j.palaeo.2023.111884.

Dorschel, B., Hebbeln, D., Foubert, A., White, M., Wheeler A.J., 2007. Hydrodynamics and cold-water coral facies distribution related to recent sedimentary processes at Galway Mound west of Ireland. Mar. Geol. 244, 184–195. https://doi.org/10.1016/j.margeo.2007.06.010.

Ekman, V.W., 1905. On the influence of the Earth's rotation on ocean currents. Arkiv för Matematik, Astronomi och Fysik 2, 1–53.

Friocourt, Y., Levier, B., Speich, S., Blanke, B., Drijfhout, S.S., 2007. A regional numerical ocean model of the circulation in the Bay of Biscay. J. Geophys. Res. Oceans 112, C09008. https://doi.org/10.1029/2006jc003935.

Friocourt, Y., Drijfhout, S., Blanke, B., 2008. On the dynamics of the slope current system along the West European Margin. Part I: Analytical calculations and numerical simulations with steady-state forcing. J. Phys. Oceanogr. 38, 2597–2618. https://doi.org/10.1175/2008jpo3744.1.

Garrett, 2003. Internal tides and ocean mixing. Science 301, 1858–1859. https://doi.org/10.1126/science.1090002.

Gill, A.E., 1982. Atmosphere-Ocean Dynamics, Academic Press.

Hall, M.M., Bryden, H.L., 1982. Direct estimates and mechanisms of ocean heat transport. Deep Sea Research Part A. Oceanogr. Res. Pap. 29, 339–359. https://doi.org/10.1016/0198-0149(82)90099-1.

Harvey, J., 1982. θ-S relationships and water masses in the eastern North Atlantic. Deep-Sea. Res. I: Oceanogr. Res. Pap. 29, 1021–1033. https://doi.org/10.1016/0198-0149(82)90025-5.

Hernández-Molina, F.J., Llave, E., Stow, D.A.V., García, M., Somoza, L., Vázquez, J.T., Lobo, F.J., Maestro, A., Díaz del Río, V., Leon, R., Medialdea, T., Gardner, J., 2006. The contourite depositional system of the Gulf of Cadiz: a sedimentary model related to the bottom current activity of the Mediterranean outflow water and its interaction with the continental margin. Deep Sea Res. Part II Top. Stud. Oceanogr. 53, 1420–1463. https://doi.org/10.1016/j.dsr2.2006.04.016.

Hernández-Molina, F.J., Stow, D.A.V., Alvarez-Zarikian, C.A., Acton, G., Bahr, A., Balestra, B., Ducassou, E., Flood, R., Flores, J.-A., Furota, S., Grunert, P., Hodell, D., Jimenez-Espejo, F., Kim, J.K., Krissek, L., Kuroda, J., Li, B., Llave, E., Lofi, J., Lourens, L., Miller, M., Nanayama, F., Nishida, N., Richter, C., Roque, C., Pereira, H., Sanchez Goni, M.F., Sierro, F.J., Singh, A.D., Sloss, C., Takashimizu, Y., Tzanova, A., Voelker, A., Williams, T., Xuan, C., 2014. Onset of Mediterranean outflow into the North Atlantic. Science 344, 1244–1250. https://doi.org/10.1126/science.1251306.

Hummon, J., 2025. CODAS ADCP Processing. https://currents.soest.hawaii.edu/docs/adcp_doc/codas_doc/index.html

Huthnance, J.M., 1981. Waves and currents near the continental shelf edge. Prog. Oceanogr. 10, 193–226. https://doi.org/10.1016/0079-6611(81)90004-5.

Huthnance, J.M., 1986. The Rockall slope current and shelf-edge processes. Proceedings of the Royal Society of Edinburgh. Section B: Biological Sciences 88, 83–101. https://doi.org/10.1017/s0269727000004486.

Huthnance, J.M., Inall, M.E. and Fraser, N.J., 2020. Oceanic density/pressure gradients and slope currents. J. Phys. Oceanogr. 50, 1643–1654. https://doi.org/10.1175/JPO-D-19-0134.1.

Huvenne, V., Beyer, A., de Haas, H., Dekindt, K., Henriet J.-P., Kozachenko, M., Olu-Le Roy, K., Wheeler, A.J., TOBI/Pelagia 197, CARACOLE cruise participants, 2005. The seabed appearance of different coral bank provinces in the Porcupine Seabight, NE Atlantic: results from sidescan sonar and ROV seabed mapping. In: Freiwald, A., Roberts, J.M. (Eds.), Cold-Water Corals and Ecosystems. Springer, Heidelberg, pp. 535–569.

Huvenne, V.A.I., Van Rooij, D., De Mol, B., Thierens, M., O'Donnell, R., Foubert, A., 2009. Sediment dynamics and palaeo-environmental context at key stages in the Challenger cold-water coral mound formation: Clues from sediment deposits at the mound base. Deep-Sea Res. I Oceanogr. Res. Pap. 56, 2263–2280. https://doi.org/10.1016/j.dsr.2009.08.003.

INFOMAR, 2023. INFOMAR Marine Data Download Portal [WWW Document].

Iorga, M.C., Lozier, M.S., 1999. Signatures of the Mediterranean outflow from a North Atlantic climatology: 2. Diagnostic velocity fields. J. Geophys. Res. Oceans 104, 26011–26029. https://doi.org/10.1029/1999JC900204.

Liu, S., Van Rooij, D., Vandorpe, T., Gonzalez-Pola, C., Ercilla, G., Hernández-Molina, F.J., 2019. Morphological features and associated bottom-current dynamics in the Le Danois Bank region (southern Bay of Biscay, NE Atlantic): A model in a topographically constrained small basin. Deep-Sea Res. I: Oceanogr. Res. Pap. 149, 103054. https://doi.org/10.1016/j.dsr.2019.05.014.

Lorke, A., Peeters, F., Wüest, A., 2005. Shear-induced convective mixing in bottom boundary layers on slopes. Limnol. Oceanogr. 50, 1612–1619. https://doi.org/10.4319/lo.2005.50.5.1612.

Marsh, R., Haigh, I.D., Cunningham, S.A., Inall, M.E., Porter, M., Moat, B.I., 2017. Large-scale forcing of the European Slope Current and associated inflows to the North Sea. Ocean Science 13, 315–335. https://doi.org/10.5194/os-13-315-2017.

Matossian, A.O., Van Rooij, D., 2024. Morphosedimentary evolution of the Belgica Mound Drift: Controls on contourite depositional system development in association with cold-water coral mounds. Mar. Geol 477, 107410. https://doi.org/10.1016/j.margeo.2024.107410.

Matossian, A.O., Daly, E., Fennell, S., Shymbaliova, N., Vandorpe, T., White, M., Van Rooij, D., submitted. Evaluation of present-day hydrodynamic processes associated to the Belgica Mound contourite drift, offshore Ireland. Deep-Sea Research. I.

Matossian, A.O., Boone, W., Langedock, K., Fourie, F., Van Rooij, D., in preparation. Elucidating sedimentary processes through near-seabed very high-resolution AUV mapping across a confined mounded drift. Sedimentology.

McDonnell, A., Shannon, P.M., 2001. Comparative Tertiary stratigraphic evolution of the Porcupine and Rockall basins. Geol. Soc. London Spec. Publ. 188, 323–344. https://doi.org/10.1144/GSL.SP.2001.188.01.19.

Mienis, F., De Stigter, H.C., White, M., Duineveld, G., De Haas, H., Van Weering, T.C.E., 2007. Hydrodynamic controls on cold-water coral growth and carbonate-mound development at the SW and SE Rockall Trough Margin, NE Atlantic Ocean. Deep-Sea Res. I Oceanogr. Res. Pap. 54, 1655–1674. https://doi.org/10.1016/j.dsr.2007.05.013.

Miramontes, E., Jouet, G., Thereau, E., Bruno, M., Penven, P., Guerin, C., Le Roy, P., Droz, L., Jorry, S.J., Hernández-Molina, F.J., Thiéblemont, A., Silva Jacinto, R., Cattaneo, A., 2020. The impact of internal waves on upper continental slopes: insights from the Mozambican margin (southwest Indian Ocean). Earth Surf. Process. Landforms, 45, 1469–1482. https://doi.org/10.1002/esp.4818

Naylor, D., Shannon, P.M., 1982. Geology of Offshore Ireland and West Britain, 1982 edition. Springer, London.

New, A.L., Barnard, S., Herrmann, P., Molines, J.-M., 2001. On the origin and pathway of the saline inflow to the Nordic Seas: insights from models. Prog. Oceanogr. 48, 255–287. https://doi.org/10.1016/S0079-6611(01)00007-6.

Parker, B.B., 2007. Tidal analysis and prediction, Silver Spring, MD, NOAA NOS Center for Operational Oceanographic Products and Services.

Pearson, I., Jenkins, D.G., 1986. Unconformities in the Cenozoic of the North-East Atlantic. In: Summerhayes, C.P., Shackleton, N.J. (Eds.), North Atlantic Palaeoceanography. Soc. London Spec. Publ, Geol, pp. 79–86.

Pedlosky, J., 1987. Geophysical Fluid Dynamics, Springer-Verlag.

Phillips, O.M., 1966. The Dynamics of the Upper Ocean. CUP Archive.

Pingree, R.D., Le Cann, B., 1989. Celtic and Armorican slope and shelf residual currents. Prog. Oceanogr. 23, 303–338. https://doi.org/10.1016/0079-6611(89)90003-7.

Pingree, R.D., Le Cann, B., 1990. Structure, strength and seasonality of the slope currents in the Bay of Biscay region. J. Mar. Biol. Assoc. U.K. 70, 857–885. https://doi.org/10.1017/S0025315400059117.

PyGlider team, 2022. PyGlider: Convert glider data to NetCDF. https://pyglider.readthedocs.io/en/latest/.

Queste, B., 2024. Gliderad2cp. https://github.com/bastienqueste/gliderad2cp.

Rebesco, M., Hernández-Molina, F.J., Van Rooij, D., Wåhlin, A., 2014. Contourites and associated sediments controlled by deep-water circulation processes: State-of-the-art and future considerations. Mar. Geol. 352, 111–154. https://doi.org/10.1016/j.margeo.2014.03.011.

Rhines, P.B., 1970. Edge-, bottom- and Rossby waves. Geophys. Fluid Dyn., 1, 273–302.

Rice, A.L., Billett, D.S.M., Thurston, M.H., Lampitt, R.S., 1991. The institute of oceanographic sciences biology programme in the Porcupine Seabight: background and general introduction. J. Mar. Biol. Assoc. U.K. 71, 281–310. https://doi.org/10.1017/S0025315400051614.

Schlitzer, R., 2023. Ocean Data View [WWW Document].

Stow, D.A.V., 1982. Bottom currents and contourites in the North Atlantic. Bull. Inst. Geol. Bassin Aquitaine 31, 151–166.

Taylor, J.R., Sarkar, S., 2008. Stratification effects in a bottom Ekman layer. J. Phys. Oceanogr. 38, 2535–2555. https://doi.org/10.1175/2008JPO3942.1.

Toucanne, S., Soulet, G., Riveiros, N.V., Boswell, S.M., Dennielou, B., Waelbroeck, C., Bayon, G., Mojtahid, M., Bosq, M., Sabine, M., Zaragosi, S., Bourillet, J.-F., Mercier, H., 2021. The North Atlantic Glacial Eastern boundary current as a key driver for ice-sheet-amoc interactions and climate instability. Paleoceanogr. Paleoclimatol., 36. https://doi.org/10.1029/2020PA004068.

Trenberth, K.E., Zhang, Y., Fasullo, J.T., Cheng, L., 2019. Observation-based estimates of global and basin ocean meridional heat transport time series. Journal of Climate 32, 4567–4583. https://doi.org/10.1175/jcli-d-18-0872.1.

van Aken, H.M., 2000. The hydrography of the mid-latitude Northeast Atlantic Ocean: II: the intermediate water masses. Deep-Sea Res. I Oceanogr. Res. Pap. 47, 789–824. https://doi.org/10.1016/S0967-0637(99)00112-0.

van Aken, H.M., Becker, G., 1996. Hydrography and through-flow in the north-eastern North Atlantic Ocean: the NANSEN project. Prog. Oceanogr. 38, 297–346. https://doi.org/10.1016/S0079-6611(97)00005-0.

Van Rooij, D., De Mol, B., Huvenne, V., Ivanov, M., Henriet, J.-P., 2003. Seismic evidence of current-controlled sedimentation in the Belgica mound province, upper Porcupine slope, southwest of Ireland. Mar. Geol. 195, 31–53. https://doi.org/10.1016/S00253227(02)00681-3.

Van Rooij, D., Blamart, D., Kozachenko, M., Henriet, J.-P., 2007. Small mounded contourite drifts associated with deep-water coral banks, Porcupine Seabight, NE Atlantic Ocean. Geol. Soc. Lond. Spec. Publ. 276, 225–244. https://doi.org/ 10.1144/GSL.SP.2007.276.01.11.

Van Rooij, D., Huvenne, V.A.I., Blamart, D., Henriet, J.-P., Wheeler, A., de Haas, H., 2009. The Enya mounds: a lost mound-drift competition. Int. J. Earth Sci. 98, 849–863. https://doi.org/10.1007/s00531-007-0293-9.

White, M., 1994. Tidal and subtidal variability in the sloping benthic boundary layer. J. Geophys. Res. Oceans 99, 7851–7864. https://doi.org/10.1029/93JC03211.

White, M., 2007. Benthic dynamics at the carbonate mound regions of the Porcupine Sea Bight continental margin. Int. J. Earth Sci. 96, 1–9. https://doi.org/10.1007/ s00531-006-0099-1.

White, M., Roberts, J.M., van Weering, T., 2007. Do bottom-intensified diurnal tidal currents shape the alignment of carbonate mounds in the NE Atlantic?. Geo-Mar. Lett. 27, 391–397. https://doi.org/10.1007/s00367-007-0060-8.

White, M., Dorschel, B., 2010. The importance of the permanent thermocline to the cold water coral carbonate mound distribution in the NE Atlantic. Earth Planet. Sci. Lett. 296, 395–402. https://doi.org/10.1016/j.epsl.2010.05.025.

Wilckens, H., Eggenhuisen, J.T., Adema, P.H., Hernández-Molina, F.J., Silva Jacinto, R., Miramontes, E. 2023. Secondary flow in contour currents controls the formation of moat-drift contourite systems. Commun. Earth Environ. 4, 316. https://doi.org/10.1038/s43247-023-00978-0.

Wu, L., Zhao, Y., Liu, Z., Ma, P., Zhang, Y., 2023. Sedimentary processes in the bottom boundary layer of a contourite drift in the northern South China Sea. Front. Mar. Sci. 10. https://doi.org/10.3389/fmars.2023.1217216.

Yin, S.R., Hernández-Molina, F.J., Mejías, M.B., Zhao, Y., Manley, T., Manley, P.L., Li, J., 2024. Bottom Ekman transport drives transverse flows to shape contourite moat and

drift systems. Earth Planet. Sci. Lett. 643, 118926. https://doi.org/10.1016/j.epsl.2024.118926.

Supplementary material

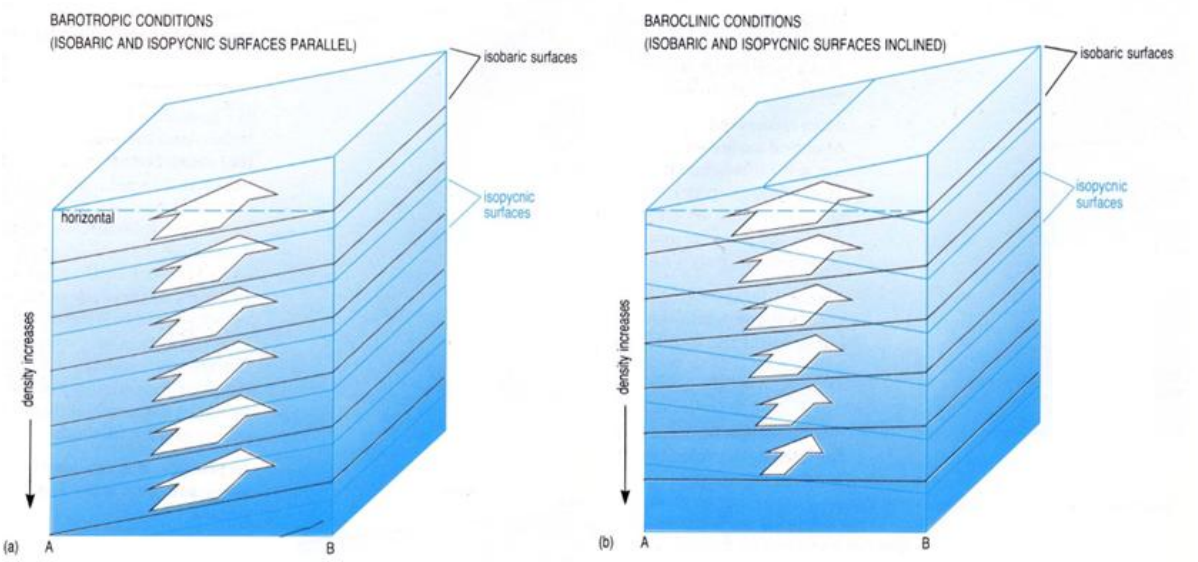

Figure A.5.1. Barotropic (left) and baroclinic (right) conditions (from Bearman, 1989). (Left) Isopycnic (surfaces of constant density) and isobaric (surfaces of constant pressure) surfaces are parallel in barotropic flows while in baroclinic flows (right) surfaces intersects.

Figure A.5.2. Recording current meter (RCM7) before deployment (Fennell, pers. comm.). The RCM7 is a rotor current meter consisting of a vane to define the flow direction and a recording unit with a rotor (to measure the speed), a magnetic compass and a Fenwall thermistor (temperature sensor). Optional sensors (conductivity and pressure) can be used (Aanderaa Instruments, 2000).

Figure A.5.3. Recording current meter (RCM9) before deployment (Fennell, pers. comm.). The RCM9 consists of a recording unit equipped with an Acoustic Doppler Current Sensor (to measure the speed and direction of the flow) and a Fenwall thermistor (temperature sensor). Optional sensors (conductivity, turbidity, pressure and oxygen) can be used (Aanderaa Instruments, 2001).

Chapter 6 – Conclusions and outlooks

This chapter discusses the main results achieved within the PhD thesis and places them in the context of the broader sedimentological and paleoceanographic framework of the Belgica Mound Province. The discussion is organised into three parts. The first section focuses on the spatial and temporal variability of the Belgica Mound Drift, examining its evolution from the pre-drift stage to its present-day configuration. This includes an interpretation of the paleoceanographic changes inferred from the present-day hydrodynamic regime. The morphology of the drift and its moats, through the interpretation of the seismic dataset, allows to extrapolate the bottom-current dynamics across the evolution of the drift, including its onset, after the Middle Pleistocene Transition and its present-day stage. The second section addresses the use of a multi-method approach, assessing the complementary nature of the applied methods, their respective spatial and temporal resolutions, and the insights each has provided into the development of the drift. This part also reflects on methodological limitations. The final section outlines the perspectives for future research, suggesting potential directions that could enhance the understanding of the Belgica Mound Drift as well as contourite drift systems in general. Some of these perspectives can be pursued with existing data, while others would benefit from new data acquisition or technological advances.

6.1 Spatial and temporal variability of the Belgica Mound Drift

Despite their scientific value, small-scale contourite drifts remain under-investigated. Refining the diagnostic criteria of contourite drifts and particularly the characteristics of the bottom currents responsible for their formation is essential for accurately identifying contourite drifts. Contourite drifts are typically associated with contour currents (Rebesco et al., 2014; Van Rooij et al., 2016; Nicholson et al., 2024). However, it is now clear from the Belgica Mound Drift and other recent studies (Liu et al., 2019; Miramontes et al., 2020; Wu et al., 2023), that additional processes such as across-slope tidal currents, play an important role in the evolution of contourite drifts. Research during the past two decades highlighted that the small-scale drifts are highly sensitive to local hydrodynamic conditions such as the enhancement of currents that are more complex to apprehend than regional alongslope thermohaline circulation (Rebesco et al., 2014). As seen through this work, moats and bedforms associated with these drifts can provide valuable information on present-day local sediment dynamic and bottom-current variability, as evidenced by AUV and ROV-based studies (Chapters 3 and 4).

Through pseudo-3D seismic stratigraphic analysis of the Belgica Mound Drift, its spatial and temporal evolution was reconstructed. High-resolution data from AUV and ROV imagery

provide detailed insight into the recent and present-day sedimentary evolution of the drift (Chapters 3 and 4). Meanwhile, the present-day hydrodynamic regime is better constrained using data from moorings, glider-based ADCP and CTD measurements (Chapter 5). Questions that could not be resolved during the early seismic-based study (Chapter 2), such as the precise hydrodynamic mechanisms and their influence on shaping the drift, can now be addressed using the integrated dataset. Together, these datasets offer a comprehensive and holistic view of both the development of the drift and the hydrodynamic conditions that have influenced it throughout the Quaternary. In particular, processes such as locally enhanced trapped baroclinic motions appear to be critical. This improved understanding of present-day dynamics allows to more confidently extrapolate past environmental conditions and better constrain the parameters required for drift formation and maintenance over geological timescales.

The conceptual model presented in Figure 6.1 builds on the results presented in Chapter 2 and displays the evolution of the Belgica Mound Drift from its onset till the present day. This model includes updated interpretations of the present-day drift morphology, moats, and associated features, which were not fully captured in the seismic dataset (Fig. 2.10) as well as the past hydrodynamics inferred from the present-day processes (Chapter 5).

6.1.1 Evolutionary stages of the Belgica Mound Drift

6.1.1.1 Pre-drift stage

During the Pliocene, prior to the onset of cold-water coral (CWC) mound growth and the initiation of the contourite drift, the RD1 erosive event significantly impacted the eastern slope of the Porcupine Seabight. This event sculpted a distinct paleotopography, locally marked by steep escarpments, with the RD1 unconformity deeply incising into units U2 and U3 (Fig. 2.9A). This irregular topography remains visible in present-day bathymetry (Fig. 2.4) and plays a key role in deflecting and enhancing bottom currents, contributing to their erosive nature. The formation of the RD1 topography is attributed to strong and persistent contour currents (thermohaline-driven bottom currents; Fig. 2.10A), likely triggered by the reintroduction of the Mediterranean Outflow Water (MOW) in the NE Atlantic (Stow, 1982; Pearson and Jenkins, 1986; Van Rooij et al., 2003) by the European Slope Current (ESC; thermohaline circulation from 500 to 2000 m water depth; Toucanne et al., 2021). It can also be inferred that the trapped diurnal baroclinic motion, observed in the present-day datasets (Chapter 5), may have also played a role prior to the onset of the drift and especially during the RD1 event. This type of motion arises from the interaction of a flow with topographic features, such as the continental slope (Garrett, 2003). In the Belgica Mound Province, the interaction of this trapped baroclinic motion against the continental slope generates both a diurnal tidal bottom current and a northward alongslope bottom current (Chapters 3 and 5; White, 2007). For such trapped motion to be sustained and enhanced, strong stratification is required (following $N\sin(\alpha)\sin(\gamma)$; Rhines, 1970; Chapter 5). The arrival of the dense and saline MOW flowing below the Eastern North Atlantic Water (ENAW) (Chapter 5) in the Porcupine Seabight would have likely strengthened the stratification and enhanced this motion, contributing to strong bottom currents during RD1 event and erosion of the seafloor.

Khélifi et al. (2014) identified a significant reduction in the MOW strength between 2.95 Ma and 2.65 Ma, coinciding with the onset of the Northern Hemisphere Glaciation, i.e. major ice sheet formation in the Northern Hemisphere, marking a global climatic transition from warm to

cyclical glacial–interglacial periods. The sea level decrease during the first glacial period would have restricted Atlantic–Mediterranean exchanges, diminishing the MOW production and thermohaline circulation, and thereby weakening the bottom currents, i.e. the contour current and bottom currents (triggered by the trapped baroclinic motion, also weakened without the MOW), in the Porcupine Seabight, effectively terminating the RD1 event. Later, during the following interglacial period, renewed inflow of MOW by the ESC likely reinvigorated the trapped baroclinic motion and the bottom-current activity, creating favourable hydrodynamic conditions for the onset of CWC mounds (Huvenne et al., 2009; Raddatz et al., 2011), around 2.7 Ma, in the Late Pliocene (Kano et al., 2007). These bottom currents, steered and enhanced by the presence of the CWC mounds, initiated the formation of the drift (Fig. 2.9) and shaped the associated moats (Fig. 2.4) (Van Rooij et al., 2003; Huvenne et al., 2009). The contourite drift probably started to form between 2.1 and 1.7 Ma, as attested by the deposition of sandy contourites at IODP site U1316 at the foot of the Challenger Mound during this timeframe (Huvenne et al., 2009) and thus earlier than the start of deposition at IODP site U1318 (1.24 Ma; Kano et al., 2007).

Following the RD1 erosive event in the Pliocene, the slopes in the area were steeper than today (Fig. 2.9A), likely amplifying the effect of the trapped baroclinic motion (following Nsin(α); Rhines, 1970; Chapter 5). According to White et al. (2007) and White and Dorschel (2010), this enhancement is nowadays strongest around 850 m water depth in the Belgica Mound Province (Fig. 5.23). This depth coincides with the region where there is currently the ENAW–MOW interface and where the continental margin steepens. While the precise depth of the ENAW–MOW interface during the Quaternary remains uncertain, it likely varied in response to glacial–interglacial sea-level fluctuations and shifting depth of water mass boundaries. It is reasonable to propose that currents, generated by the interaction of the trapped baroclinic motion with the continental slope, were active and enhanced near the seafloor during Pliocene, RD1 event and throughout the Quaternary, influencing sediment transport and the long-term development of features like the CWC mounds, the Belgica Mound Drift and its moats.

6.1.1.2 Onset of drift formation

The first drift deposits were formed in the central area of the southern sector (Fig. 2.9B), with the start of deposition of the oldest sub-unit of the drift U1-2 (Chapter 2), followed by the central part of the northern sector (Fig. 6.1). The two centres evolved independently and were initially separated by a non-depositional area (Fig. 2.9B). Differences in morphology and elongation between the two centres appear to reflect variations in circulation patterns. The southern centre, characterised by its elongated shape (Fig. 2.9B), is associated with SE–NW oriented alongslope currents, flowing along both the western and eastern moats. In contrast, the northern centre exhibits a more circular shape (Fig. 2.9B), likely influenced by a more complex hydrodynamic setting. Here, deflection of the alongslope bottom currents by the presence of CWC mounds likely led to localised current acceleration, impeding deposition in their direct vicinity and deposition between both centres. This configuration suggests the presence of a local circulation cell trapped in the northern centre, influenced by topographic constraints, as the CWC mounds and RD1 paleotopography (Fig. 2.9B). Stratigraphic features (Chapter 2) within U1-2 such as unconformities, irregular horizons, and variable growth orientations of the drift, combined with the mixed morphology of the moats, point to an unstable current regime: The bottom currents likely fluctuated in intensity, alternately causing erosion of sub-unit U1-2 or enabling deposition. The sediment input (discussed below) would also play a role, with

potential non-depositional periods due to strong currents or no input at all. This regime could be related to the Early Pleistocene equivalent of glacial and interglacial periods, characterised by the short duration obliquity-cycles of 41 ky (Lisiecki and Raymo, 2005). A gradual decrease of the alongslope current intensities and diminishing strength of the local circulation cell are evidenced by the increasing sediment input near the mounds and in the moats of the drift, where deposition became more prominent.

The dominant alongslope bottom current, interpreted as the main hydrodynamic process from the seismic dataset (Fig. 2.10B), would likely result from the combined influence of the contour current (bottom current related to the ESC) and the alongslope bottom current generated by the rectification of the trapped baroclinic motion against the slope by the Coriolis force. This hydrodynamic configuration fully resembles the averaged present-day conditions, with a residual northward current measured by the moorings deployed on the drift (Chapters 3 and 5) and is consistent with observations made by Pingree and LeCann (1990) and White et al. (2007). In addition to the residual current, tidal across-slope currents (Chapters 3 and 5) and Ekman transport (Chapter 5) were potentially active as well. These transverse flows may have had a strong influence on sediment dynamics, transporting sediment from the moats on the drift and allowing its deposition on the drift.

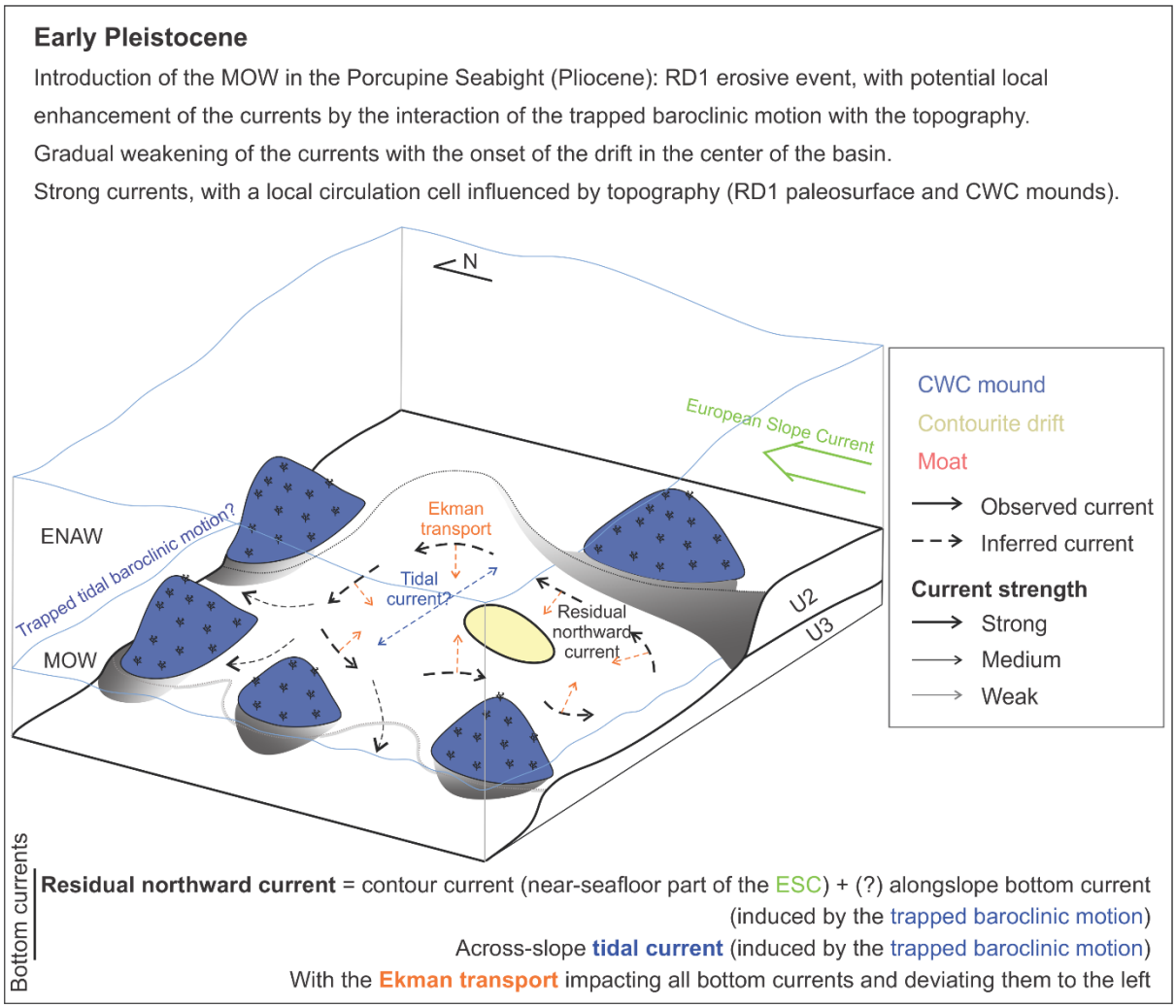

Figure 6.1. Conceptual model of the onset of the Belgica Mound Drift during Early Pleistocene.

6.1.1.3 Post-Middle Pleistocene Transition

In contrast to sub-unit U1-2, sub-unit U1-1 exhibits a more uniform growth style (Fig. 2.5). This contrasting stratigraphic architecture between sub-units U1-1 and U1-2 reflects significant paleoceanographic changes during the Pleistocene, with a shift toward more stable, deposition-dominated conditions, with reduced current intensity and increased sediment input across the drift. This shift would fit with the early phase of the Middle Pleistocene Transition (MPT). The MPT marked a shift to 100 ky eccentricity-driven glacial cycles, leading to longer global cooling, ice volume growth and sea-level fall periods (Lisiecki and Raymo, 2005; Berends et al., 2021), inducing reduced MOW outflow (Hernández-Molina et al., 2008), weaker bottom currents, and increased sediment supply (Van Rooij et al., 2007; Huvenne et al., 2009). These conditions favoured large sediment input and sedimentation, burying the CWC mounds (Figs. 2.5–2.8) which resulted in their decline (Hebbeln et al., 2016). Increased sediment input would have also allowed the burial of some moats (Figs. 2.5, 2.6, 2.8), while the rest of the moats (Fig. 2.7) remain active along the escarpment (eastern moat) and CWC mounds (western moats) due to local current enhancement, further supporting a dominant residual northward directed flow (Fig. 2.10C), as a combination of the contour current (related to the ESC) and the alongslope bottom current (related to the trapped baroclinic motion).

Given the general northward circulation associated with the ESC, it can be expected that one of the sources of terrigenous sediment in the Belgica Mound Drift originates from the south, particularly from systems such as the Gollum channels. These channels are known to have acted as conduits for turbidity currents transporting sediment downslope from the shelf (Verweirder et al., 2021, 2023). This would have been the case in the early Quaternary when the channels were shallower, allowing the alongslope current to flow into them and transport away the sediment from the turbidity current (Verweirder, pers. comm.). It can also be expected that there would be sediment coming from the wider shelf during interglacial periods and ice-rafted debris (IRD) from the British-Irish Ice Sheet during glacial periods, as demonstrated by Van Rooij et al. (2007), who identified six ice-rafting events during the last 100000 years in the Porcupine Seabight.

The oceanographic circulation inferred for the Dansgaard-Oeschger interstadials and stadials during the last glacial period (Toucanne et al., 2021) can be extrapolated to previous glacial periods (Fig. 6.2). During the last glacial period, the Atlantic meridional overturning circulation (AMOC) was still active (Weber et al., 2007; Pöppelmeier et al., 2020) but weaker (Weber et al., 2007; Vettoretti and Peltier, 2013; Du et al., 2020) and shifted towards south due to the continental ice-sheets altering wind patterns (Keffer et al., 1988; Löfverström et al., 2014). The Glacial eastern Boundary Current (Fig. 6.2), the glacial version of the ESC, which is the easternmost part of the upper branch of the AMOC, is driven by the steepness of the NE Atlantic margin, large-scale meridional density gradients (Pingree and Le Cann, 1990; Friocourt et al., 2007, 2008; Toucanne et al., 2021) and by the wind forcing driving geostrophic circulation towards the slope (Friocourt et al., 2007; Marsh et al., 2017; Depuydt et al., 2024). During Dansgaard-Oeschger interstadials, the ESC continued to flow through the Porcupine Seabight, whereas during Dansgaard-Oeschger stadials, the flow weakened and did not pass through the Porcupine Seabight (Fig. 6.4; Toucanne et al., 2021). During glacial periods (Fig. 6.3), lowered sea levels restricted the exchange between the Atlantic Ocean and the Mediterranean Sea, reducing MOW production (Rogerson et al., 2006; Rogerson et al., 2012; Khélifi et al., 2014) and even preventing it from reaching the Porcupine Seabight (Van Rooij et al., 2007).

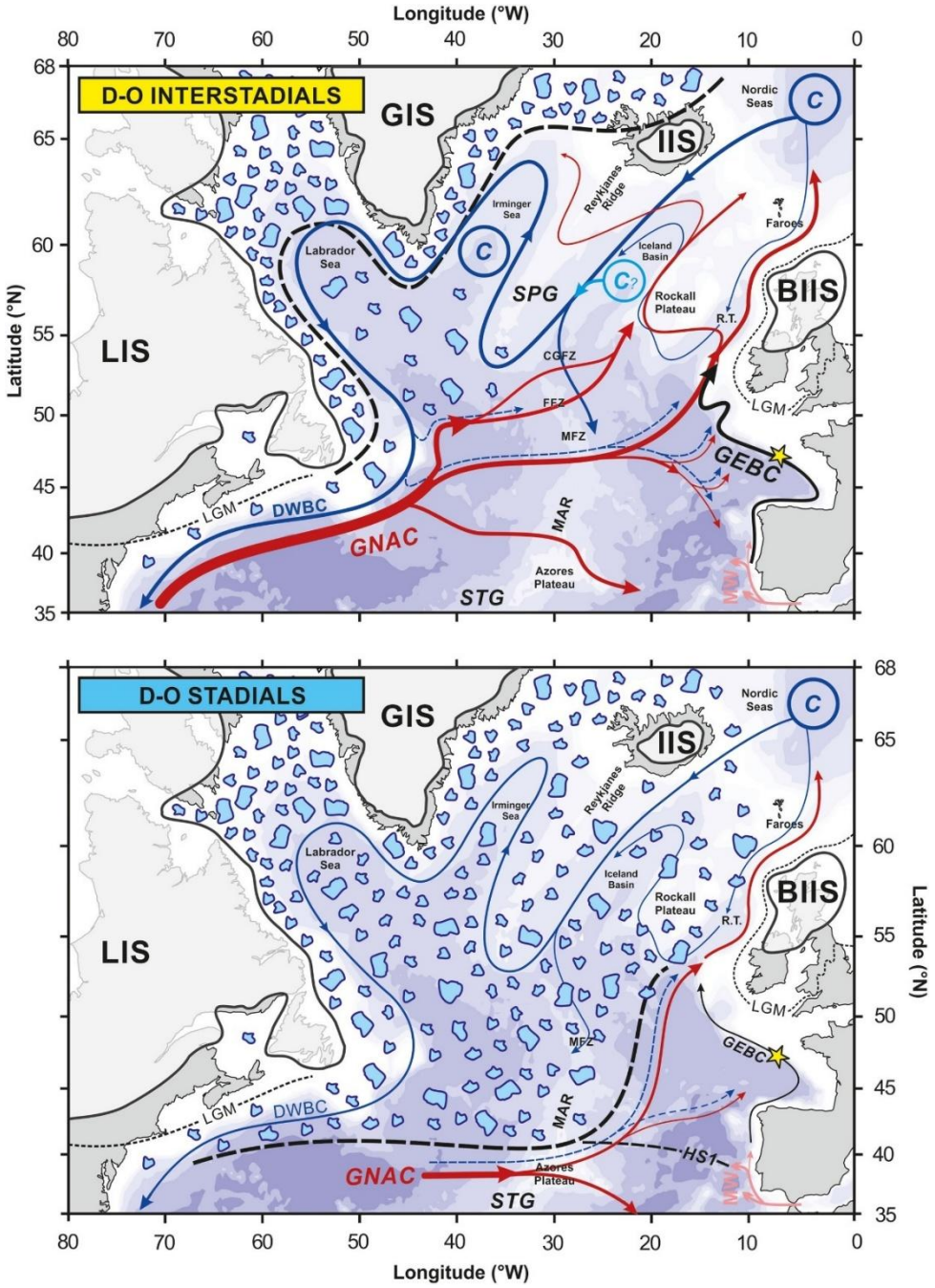

Figure 6.2. Schematic representation of the North Atlantic circulation during Dansgaard-Oeschger interstadials (A) and stadials (B) of Marine Isotope Stage 3 (from Toucanne et al., 2021). The Glacial Eastern Boundary Current (GEBC) is considered the glacial analogue of the modern European Slope Current and is shown with black arrows.

The absence of the MOW led to a weakening of the density contrasts along the slope that could weaken the trapped baroclinic motion and the Glacial eastern Boundary Current, even preventing it from entering the Porcupine Seabight during colder phases. Consequently, the currents along the continental slope were also weakened, which favoured sediment deposition and fine sediments coming from the Gollum channels and carried northward by the weaker Glacial Eastern Boundary Current, as well as the sediment dispersing freely over the shelf. The resulting deposit would be a muddy contourite with IRD (Van Rooij et al., 2007).

Conversely, during interglacial periods (Fig. 6.4), rising sea levels re-established stronger Atlantic–Mediterranean exchange, enhancing MOW outflow into the NE Atlantic (Hernández-Molina et al., 2011), until it reaches the Porcupine Seabight (Van Rooij et al., 2007), allowing to enhance the trapped baroclinic motion and the ESC. The increased bottom-current activity during these times intensified erosion and sediment redistribution, shaping the contourite drift systems such as the Belgica Mound Drift (Chapter 2). The bottom currents would winnow the sediment deposited during glacial periods, leaving coarser fraction and resulting in silty to sandy contourites on the seafloor (Van Rooij et al., 2007).

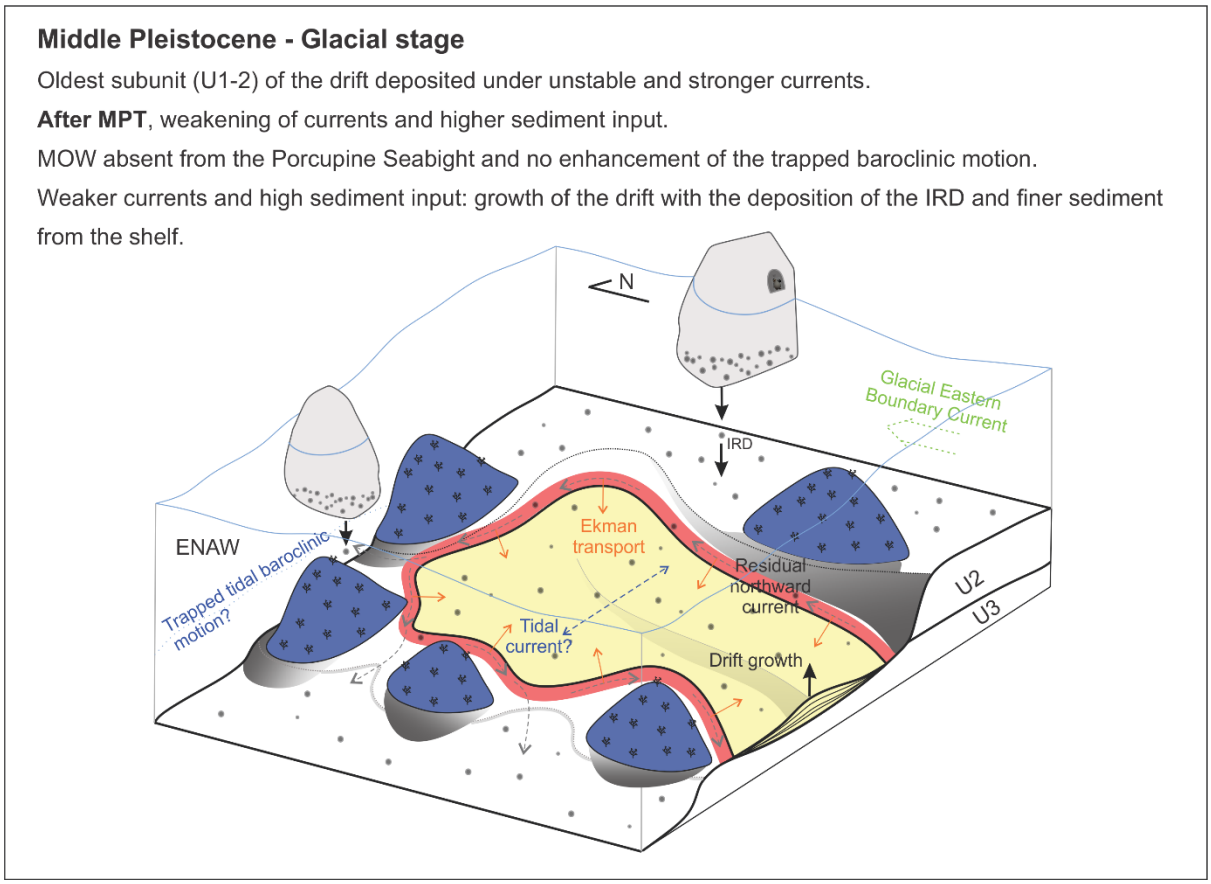

Figure 6.3. Conceptual model of the Belgica Mound Drift, during glacial phases after the Middle Pleistocene Transition (legend in Fig. 6.1). IRD stands for ice-rafted debris.

Middle Pleistocene - Interglacial stage

Environment under the MOW influence: potential enhancement of the currents by the interaction of the trapped baroclinic motion with the topography.

Medium strength currents and low sediment input from the shelf.

Shaping of the moats by the residual current and winnowing of the sediment by the bottom currents, leaving coarser sediment on the drift.

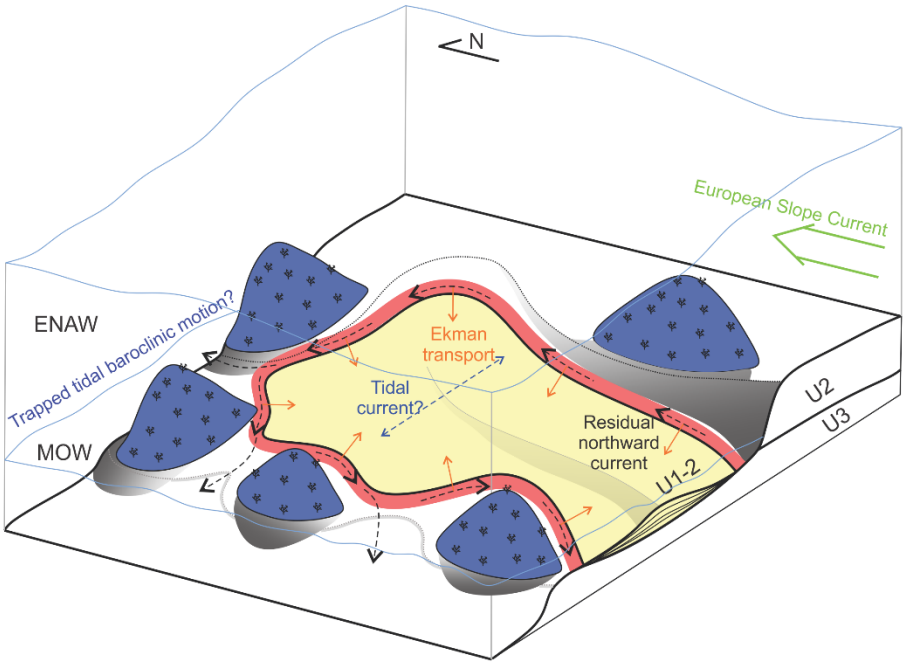

Figure 6.4. Conceptual model of the Belgica Mound Drift during interglacial phases after the Middle Pleistocene Transition (legend in Fig. 6.1).

6.1.2 Present-day processes of the Belgica Mound Drift

6.1.2.1 Present-day development of the Belgica Mound Drift

In recent times, the ESC has shown a noticeable weakening throughout the Holocene, likely linked to a long-term reduction in the latitudinal density gradient, influenced by changes in insolation and the strength of the subpolar gyre (Depuydt et al., 2024).

The study of moats adjacent to the Belgica Mound Drift provides crucial insights into present-day sediment dynamics that would be missed by focusing on the drift alone. While traditional models (e.g. Wilckens et al., 2023a; Beelen and Wood, 2023) associate moats with erosional or non-depositional processes due to persistent bottom currents along the moat's axis, new high-resolution AUV (Chapter 4) and glider (Chapter 5) data show a different picture: Across-slope or across-axis tidal currents can shape the moats and dominate the drift (Fig. 6.5). Through the evolution of the drift, there is a clear shift in the dominant current regime: From northward alongslope currents that initially shaped the drift and moats to W-E tidal currents that dominate current sediment dynamics and shape the moats (Chapter 4).

The measured residual northward bottom current (Chapter 3; Fig. 6.5) is a combination of the ESC and the alongslope bottom current generated by the interaction of the enhanced trapped

baroclinic motion with the seafloor (Chapters 3 and 5). This interaction also generates strong across-slope tidal bottom currents (Chapter 3). Both currents as well as the trapped baroclinic motion have been observed through the mooring and glider data, particularly through ADCP and CTD measurements (Chapter 5). These data reveal current intensification up to 100 m above the seafloor. Additionally, a bottom Ekman layer has been inferred within the lowest 5 to 20 m of the water column (Chapter 5), where currents are slowed down and redirected due to the combined effects of Coriolis force and friction with the seafloor. For the bottom Ekman layer, the stress acts opposite to the flow, causing the transport to be directed to the left of the flow (Taylor and Sarkar, 2008). The bottom Ekman transport is proposed as a mechanism for lateral sediment transfer from the moats to drift (Yin et al., 2024). In the classical moat-drift model (Rebesco et al., 2014; Wilckens et al., 2023a; Beelen and Wood, 2023), a secondary across-slope flow is necessary to supply sediment to the drift (Wilckens et al., 2023b), with the Ekman layer playing a key role by deflecting currents westward. Determining the exact influence of the Ekman transport on the bottom currents over the drift and its surroundings remains difficult, as they are a combination of alongslope bottom currents and across-slope tidal currents. In addition, local seafloor topography strongly influences how bottom friction and current deflection interact, contributing to the observed hydrodynamic variability across the drift-moat system. However, in the eastern moat, no distinct bottom boundary layer has been observed (Fig. 5.21), suggesting that sediment transfer from moat to drift may currently be inactive. The steep topography of the N-S oriented moat flanks may confine the flow and inhibit the formation of a lateral transport layer. Wilckens et al. (2023b) proposed that once a moat is established, secondary flows (like the Ekman transport) may become trapped within it.

Nowadays, the sediment input through the Gollum channels (Verweirder et al., 2023) and coming directly from the shelf is evaluated as minimal, preventing accumulation on the drift. Instead, sediment from the Last Glacial Maximum (26,5–19 ky BP; Mix et al., 2001; Clark et al., 2009) is being reworked. The sediment waves and ripples observed in both western and eastern moats (Fig. 4.2) suggest active sediment reworking occurring in the moats (Fig. 6.5). The orientation of these bedforms corresponds with the observed tidal currents, supporting interpretations based on their morphology. In contrast, the absence of bedforms on the drift, with a rougher seafloor texture and numerous dropstones (Chapters 3 and 4), indicate that fine fraction has been winnowed from the drift, likely by the tidal currents. The removal of the fine fraction would prevent the formation of bedforms on the drift, as there would not be sufficient fine sediment that can be remobilised to form the ripples (Stow et al., 2009). Instead, the fine fraction is transported laterally into the moats, where it becomes trapped due to the interaction between the tidal currents and the morphology of the moats, like the cuvette-shaped western moat (Fig. 4.5) and the elongated eastern moat with steep slopes (Figs. 4.8-4.10). Glider data confirm that current strengths are similar over both the drift and the moats (Chapter 5), allowing for resuspension and localised redistribution of fine sediments within the moats. These processes can lead to ongoing ripple formation and the burial of dropstones. This dynamic is not fully in line with the standard drift-moat system model (Rebesco et al., 2014; Wilckens et al., 2023a; Beelen and Wood, 2023), which assumes deposition on the drift and erosion or non-deposition in the moats. Additionally, local variations in hydrodynamic processes are observed even between moats just a few kilometres apart, influenced by topography, the presence of the CWC mounds, and tidal current interaction. With the AUV side-scan sonar, it is easier to observe the difference between the western and eastern moats. In the case of the western moat, its shape rather shows an influence of the tidal currents,

interacting with the CWC mound, over the residual northward current, probably influencing it since its formation.

Holocene (present-day conditions)

Sub-unit U1-1 deposited under weaker and more stable currents (main drift growth stage after Middle Pleistocene).

Environment under the MOW influence: enhancement of the currents by the interaction of the trapped baroclinic motion with the topography up to 100 m above seafloor.

Measured across-slope tidal current with a residual northward (alongslope) current.

Shaping of the W moats by the interaction of the tidal current with the CWC mounds. The moat shape traps the current and finer sediment, allowing the formation of sediment waves in the moats.

Finer sediment carried away from the drift into the moats by the tidal current, leaving coarser sediment on the drift and preventing the formation of bedforms.

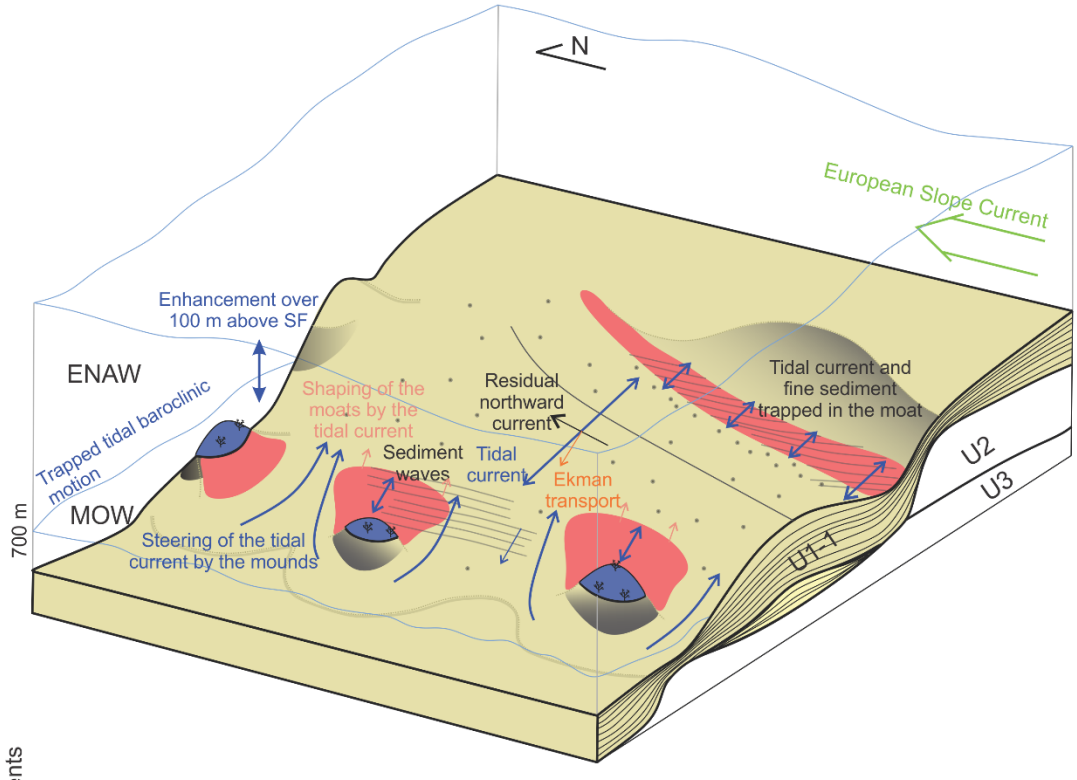

Bottom currents

Residual northward current = contour current (near-seafloor part of the ESC) + alongslope bottom current (induced by the trapped baroclinic motion)

Across-slope **tidal current** (induced by the trapped baroclinic motion)

With the **Ekman transport** impacting all bottom currents and deviating them to the left

Figure 6.5. Conceptual model of the Belgica Mound Drift, present-day situation, after the deposition of sub-unit U1-1 (legend in Fig. 6.1).

The complexity of this small-scale contourite drift and its moats is not represented by their youngest phase, but is inherited from their initiation phase, with the combined effect of RD1 paleotopography and CWC mounds on the deflection of bottom currents. Importantly, without examining the moats, the shift in dominant current regimes, from initial residual northward current to present-day tidal currents, would have gone unnoticed. This case demonstrates that contourite drifts are influenced not only by large-scale thermohaline-induced bottom currents

(contour currents), but also by local associated hydrodynamic processes, including tides and baroclinic motions. As noted by Rebesco et al. (2014), these associated processes and their impact on drift formation and evolution remain poorly understood. Capturing these dynamics requires integrated, high-resolution datasets that densely cover both the drift and its surrounding features, emphasising the need for multidisciplinary approaches in future contourite research.

6.1.2.2 Sediment waves, past and present-day activity

It is difficult to establish when the sediment wave formation began, since the vertical resolution of seismic data does not allow to detect similar (40 cm high) or larger sediment waves in the past stages of the drift, while the present-day imagery data are limited in temporal resolution (snapshot) and do not allow to define if the sediment waves are still mobile.

The onset of sediment wave development is closely linked to the nature and initiation of the hydrodynamic processes responsible for their formation. Based on AUV imagery, the orientation of the sediment waves suggests they are generated by tidal currents resulting from the interaction of trapped baroclinic motions with the seafloor. Bottom Ekman transport, occurring within the bottom boundary layer, may also contribute to the sediment wave formation. As proposed by King et al. (2014), Ekman transport could serve as a secondary mechanism that retains sand locally within the sediment wave field and may influence the sediment wave asymmetry. However, glider-mounted ADCP data (Fig. 5.21) do not show a reduction in bottom-current strength within the eastern moat of the drift, implying a potential absence of Ekman transport in this moat. Consequently, sediment wave formation in the eastern moat is likely solely driven by tidal currents. From the current dataset, it remains challenging to determine the dominant tidal direction influencing sediment wave development. The presence of both downslope and upslope asymmetries (Fig. 4.12) indicates that two alternating tidal directions are at play, as confirmed by mooring data (Chapter 5). The tidal component of the trapped baroclinic motion possesses enough energy to remobilise previously deposited sediments upslope and downslope, forming sediment waves and thus overriding the residual northward bottom current. Consequently, these sediment waves would probably form when the tidal currents are occurring in the area, depending also on the sediment availability. Given that trapped baroclinic motions would have persisted throughout the Quaternary in the Porcupine Seabight region (see 6.1.1.1), it is plausible that similar sediment waves formed repeatedly during this period. These features may also develop directly on the drift, and not only in the moats, when finer sediment was present. They may still be preserved in the sub-units of the drift but are not observable due to their limited size and the vertical resolution of the seismic data. Sediment availability would be the main limiting factor for sediment wave formation in and around the drift, as glider-mounted ADCP data reveal comparable bottom-current intensities across the drift and within the moats (Chapter 5).

In the northern sector of the drift, there is a spatial overlap between the ROV and AUV tracks (Fig. 4.1). Both datasets show sediment wave crests with similar spacing and orientation, confirming that the features identified in the ROV imagery correspond to the sediment waves detected via the AUV side-scan sonar. While the ROV imagery provides a limited, close-up view (metric scale), the AUV side-scan sonar captures the full extent of the sediment waves (kilometric scale). However, due to potential positioning offsets between the 2019 ROV and

2022 AUV surveys, it is difficult to determine whether the sediment waves have migrated during this period.

To evaluate whether the sediment waves remain active and how they migrated, such as with changes in direction as reported by Ribó et al. (2016), two strategies can be proposed: (1) time-series analysis involving repeat side-scan sonar surveys and recalculation of the asymmetry index, or (2) acquire sub-bottom seismic profiles (SBP) over the sediment waves. While several SBP profiles have been collected along the AUV tracks in 2022, none of them were conclusive due to no penetration of the signal below the seafloor. High-resolution SBP data (e.g. AUV-born 3.5 kHz) could reveal the internal sediment wave structures, allowing to verify if there is any asymmetry in the uppermost layer of the sediment waves (Migeon et al., 2000; Masson et al., 2002; Cartigny et al., 2011), and potentially constrain the thickness of the mobile sediment layer within the moats. It could also allow to better characterise these sediment waves formed under the influence of a trapped diurnal baroclinic motion, improving the understanding of sediment wave formation under such motion. Furthermore, the sediment waves produced by the tidal component of the trapped diurnal baroclinic motion are not yet well characterised, largely due to the spatial variability (depth and lateral) in this motion intensity (Chapter 5). As a result, diagnostic criteria to distinguish these sediment waves are currently lacking (Pomar et al., 2012; Ribó et al., 2016). A more comprehensive characterisation of these sediment waves, especially through high-resolution SBP data, is therefore essential. This dataset could also help identify the dominant tidal constituents involved in sediment wave development and assess changes in current direction over time (discussed below).

6.2 Multi-method approach in contourite investigations

A combination of methods, including reflection seismic data (Chapter 2), multibeam bathymetry (Chapter 2), current meters (Chapters 3 and 5), glider-based CTD and ADCP measurements (Chapter 5), and AUV (Chapter 4) and ROV (Chapter 3) imagery, was used in this study to capture the spatial and temporal variability of deep-water sediment dynamic and related hydrodynamic processes. Each technique offers unique insights, varying in resolution and spatial coverage (Table 6.1), highlighting the importance of a multidisciplinary approach to fully capture, at every scale, the complexity of dynamic systems, such as small-scale contourite drifts.

The seismic dataset used in this study was acquired using a SIG sparker source in combination with a single-channel SIG surface streamer (Chapter 2). This acquisition setup offered an optimal balance between penetration depth and vertical resolution, achieving a maximum penetration of approximately 400 m. This allowed for full imaging of the drift body (seismic unit U1) and of the underlying units (U2 and U3). The vertical resolution of ~1.5 m enabled a detailed subdivision of U1, capturing its internal architecture in detail. Among the various types of seismic sources available, the sparker was chosen as the best compromise for this study. While sub-bottom profilers like TOPAS can provide higher vertical resolution, their limited penetration would not have been sufficient to visualise the entire thickness of the drift. For this work, deeper penetration was necessary, as the goal was to resolve the complete stratigraphy of the drift, not just its uppermost part. The sparker source was the best option, offering both adequate penetration depth and vertical resolution. Furthermore, the seismic

survey was conducted with a dense network of closely spaced lines (maximum 450 to 900 m in between), which significantly enhanced the spatial resolution of the data. A sparse grid of profiles might have been sufficient to identify the presence of a drift deposit and define its main units, but the dense coverage employed here enabled a much more refined characterisation (Table A.2.1). This coverage allowed for a pseudo-3D reconstruction of the drift (Fig. 2.9), revealing not only its overall geometry but also small-scale spatial variations. This level of detail makes it possible to investigate the lateral heterogeneity of the drift, improving the understanding of the depositional processes and paleoceanographic conditions that controlled its formation. This dataset allowed to map the architecture of the drift and its moats, capturing average bottom-current trends, particularly an alongslope flow shaping the large-scale features in a N–S direction. This method, however, smoothed out the sediment waves and smaller scale bedforms that directly record local hydrodynamic processes. As a result, seismic surveys reveal the averaged paleocurrents but not the specific oceanographic processes, such as the trapped baroclinic motion.

Table 6.1. Summary of the different methods used in this thesis. The symbols "+" "++" and "+++" indicate low, medium and high levels, respectively.

Method	Spatial resolution	Temporal resolution	Coverage	Use
Reflection seismic	++	++	+++	Temporal and spatial variation of past sedimentary processes
Multibeam echosounder (shipborne)	+	Snapshot	+++	Spatial variation of present-day sedimentary processes
Current meters (moorings)	+	+++	+	Temporal variation of present-day hydrodynamic processes
Glider (CTD and ADCP)	+++	++	+++	Temporal and spatial variation of present-day hydrodynamic processes
ROV (visual imagery)	+++	Snapshot	++	Spatial variation of present-day sedimentary processes
AUV (side-scan sonar, visual imagery and bathymetry)	+++		+++	

The ROV and AUV data complement one another, with ROV visual imagery offering high-resolution observations of bedforms along a single track, while AUV-mounted side-scan sonar allows for broader spatial mapping of identified features such as the sediment waves (see 6.1.2.2). Importantly, the absence of observable features in ROV and AUV imagery does not imply the absence of active processes across the drift system. Moreover, the visual imagery taken along a track, like with the ROV and the AUV, cannot be considered as representative of the entire drift, as there is a spatial variability in seafloor features even over short distances. Another limitation is the difficulty to establish if the bedforms have moved as the available datasets represent single-time observations. While the ROV data suggest that small-scale bedforms may be mobile during each tidal flow, this assumption cannot be confirmed without repeated surveys or time-series data. Nevertheless, where direct current measurements (moorings or ADCP) are unavailable, the bedforms can serve as a proxy for assessing spatial

variability in the bottom hydrodynamic regime, especially in contrasting environments such as a drift and its adjacent moats.

Regarding the moorings, they were deployed on the drift and not in the moats, where sediment waves predominantly occur. Without direct measurements in the moats, an uncertainty remained whether currents could exceed those over the drift, which could have explained why the ripples and sediment waves form specifically in the moats. However, previous studies (Dorschel et al., 2007; White and Dorschel, 2010) recorded maximum bottom currents near mounds up to 50 cm/s, hinting a similar strong topographic steering effect and not indicating higher bottom currents than those recorded by the moorings (2019 and 2021; Chapters 3 and 5). The glider dataset played a crucial role in assessing the broader-scale oceanographic processes influencing the drift system. Equipped with both CTD and ADCP sensors, the glider provided high-resolution, spatially continuous profiles of water column properties and current velocities across the drift and its surroundings. This allowed for a more comprehensive evaluation of the spatial variability of the bottom current than moorings could provide. The glider-based ADCP data confirmed the mooring data taken over the drift by showing similar current magnitudes over both drift and moats. Notable differences with the moorings were the direct observation of the enhancement of the trapped baroclinic motion and the identification of the bottom Ekman layer (Figs. 5.19, 5.20, 5.22) and its absence from the eastern moat (Fig. 5.21).

6.3 Perspectives and recommendations

Despite the progress achieved through the work presented above, several questions remain unresolved. The following section outlines proposals for further analysis of the existing dataset, as well as suggestions for additional data collection that could help advance the development of the contourite-moat model as well as the research of small-scale contourite drifts and their associated sedimentary and hydrodynamic processes.

A better characterisation of the trapped baroclinic motion and its exact dimensions, including its vertical scale in the water column, is needed and could be done through a supplementary analysis of the glider CTD and ADCP dataset (Chapter 5). One approach could involve comparing the calculated density profile (derived from glider-mounted CTD data) with the theoretical depth at which densities are typically found, helping to estimate the vertical displacement caused by the motion. The estimation of the relative phase of the tidal component of this motion with respect to the K_1 tidal period is crucial for a better characterisation of the trapped tidal baroclinic motion.

A more detailed investigation of the bottom Ekman transport and its influence on the bottom-current variability is still required to improve the understanding of the present-day and bottom sediment transport dynamics over the drift and its associated moats. The existing glider dataset offers a valuable resource for such investigation. Alternatively, the deployment of additional moorings, equipped with downward-looking ADCPs positioned at least 20 m above the seafloor, could provide crucial data. These moorings could be placed both on the drift and within the moats. Notably, the eastern moat appears to be a suitable location for deployment, as glider-recorded velocities there were comparable to those observed on the drift, and side-scan sonar imagery from the AUV revealed no evidence of trawling activity within the moats.

This suggests a lower risk of mooring removal by fishing vessels compared to the drift area (Chapter 5, Table 5.1). Such a setup would enable a more robust evaluation of the bottom Ekman layer's role in modulating bottom currents and the deflection associated with Ekman transport near the seafloor.

Another important future research is the reconstruction of paleohydrodynamic variability, with the aim of improving the understanding of the past oceanographic processes that have influenced the formation and evolution of the contourite drift and its associated moats. While seismic data provide valuable insight into the average flow characteristics, such as relative strength and direction during the main developmental phases of the drift, they do not capture small-scale processes or high-temporal-resolution variability. A three-dimensional morphodynamic numerical model (Zhang et al., 2016) can be used to address this gap. Building on the current understanding of modern hydrodynamic and sedimentary processes and the already acquired datasets, such a model could be used to reconstruct past flow regimes and assess how glacial–interglacial oceanographic changes have shaped sediment dynamics over time. The availability of high-resolution geophysical datasets provides a solid basis for model calibration and validation, thereby enabling a more comprehensive evaluation of the relative influence of key driving forces throughout the drift's development.

An additional prospect would be to determine whether the sediment waves observed in the moats are currently active or represent only relict features formed under past, more vigorous hydrodynamic conditions. Understanding this distinction is crucial for reconstructing sediment transport dynamics and bottom-current variability over time. To achieve this, new side-scan sonar coverage of the northern sector would allow for time-series analysis capable of detecting changes in sediment wave morphology. Additionally, further investigation is needed to assess whether the southern sector of the drift, which appears to have developed under different environmental conditions, is governed by distinct present-day hydrodynamic and sedimentary processes. This hypothesis is supported by previous seismic observations with the steep, kilometric N–S escarpment associated with the RD1 event, which bounds the drift to the east and may influence local sediment dynamics and current behaviour within the eastern moat. Acquiring side-scan sonar data over the southern sector would help to test this hypothesis.

Monitoring of trawling activity, together with the observation of the sediment waves using newly acquired side-scan sonar data from the AUV, could also be undertaken. The Belgica Mound Drift, located within the Belgica Mound Province, is designated as a Special Area of Conservation. Consequently, activities impacting the seafloor, including trawling, are prohibited without a permit in this area. However, evidence from the 2021 moorings recovered by fishermen, as well as from the 2022 side-scan sonar data, indicates that trawling activity is still occurring within this protected region. Based on the current side-scan sonar dataset, it remains difficult to determine when these trawl marks were formed or how long such features persist on the seafloor.

A complementary objective would be to strengthen the link between seismic stratigraphy and the lithological and chronological framework of the study area. For this purpose, it would be essential to define the sediment nature and source on the drift and within its moats from its onset until the present day. The acquisition of long sediment cores (minimum 20 m and maximum 150 m) through drilling (MeBo) would provide critical ground-truth data. When combined with chronological data, these records would support the development of an age model, facilitating the recognition of glacial–interglacial cycles and enhancing the temporal

resolution of paleoceanographic reconstructions. Such work would also allow testing the hypothesis proposed by Van Rooij et al. (2003), which suggests that muddy contourites were deposited during glacial periods and sandy contourites during interglacial periods. Given the significant resources required for a drilling campaign, research efforts could be strategically focused on the existing 80 m cores from IODP Expedition 307 Site U1318. Although this site is located upslope and outside the main drift body and thus does not capture sediments from the initial stages of drift development, it does record the youngest sub-units of the drift (Fig. 2.2). Despite this limitation, the cores offer valuable material for detailed study. High-resolution grain-size analysis and XRF core scanning could be applied to evaluate the Zr/Al proxy for bottom-current strength, as proposed by Bahr et al. (2014), thereby contributing to the reconstruction of recent hydrodynamic conditions.

Unlike large-scale drifts that tend to reflect regional oceanographic processes, small-scale drifts capture the local hydrodynamic processes, making these drifts particularly valuable archives for high-resolution paleoceanographic reconstructions (Rebesco, 2005; Rebesco et al., 2014). However, accurately reconstructing past processes from the drift morphology requires a detailed understanding of the present-day sediment dynamic and oceanographic processes shaping the morphology of small-scale contourite drifts. This study advances the understanding of small-scale contourite drifts by providing a detailed, multidisciplinary analysis of the local sedimentary and present-day hydrodynamic processes that shape them. By integrating moorings, glider-based ADCP and CTD data, AUV and ROV imagery, and seismic data, this work has revealed the influence of secondary processes, such as trapped baroclinic motions, on bottom dynamics and drift-moat sediment transfer. This study demonstrates that moats and bedforms associated with small-scale contourite drifts offer valuable insights into present-day local sediment dynamics and bottom-current variability.

6.4 References

Bahr, A., Jiménez-Espejo, F.J., Kolasinac, N., Grunert, P., Hernández-Molina, F.J., Röhl, U., Voelker, A.H.L., Escutia, C., Stow, D.A.V., Hodell, D., Alvarez-Zarikian, C.A., 2014. Deciphering bottom current velocity and paleoclimate signals from contourite deposits in the Gulf of Cádiz during the last 140 kyr. Geochem., Geophys., Geosyst. 15, 3145–3160. https://doi.org/10.1002/2014GC005356.

Beelen, D., Wood, L.J., 2023. Predicting bottom current deposition and erosion on the ocean floor. Basin Res. 35, 1985–2009. https://doi.org/10.1111/bre.12788.

Berends, C.J., Köhler, R., Lourens, L.J., Wal, R.S.W., 2021. On the cause of the Mid-Pleistocene transition. Rev. Geophys. 59. https://doi.org/10.1029/2020RG000727.

Cartigny, M.J.B., Postma, G., van den Berg, J.H., Mastbergen, D.R., 2011. A comparative study of sediment waves and cyclic steps based on geometries, internal structures and numerical modeling. Mar. Geol. 280, 40–56.https://doi.org/10.1016/j.margeo.2010.11.006.

Clark, P. U., Dyke, A. S., Shakun, J. D., Carlson, A. E., Clark, J., Wohlfarth, B., Mitrovica, J. X., Hostetler, S. W., and McCabe, A. M., 2009. The Last Glacial Maximum. Science 325, 710–714. https://doi.org/10.1126/science.1172873.

Depuydt, P., Toucanne, S., Barras, C., Le Houedec, S., Mojtahid, M., 2024. Last Glacial - Holocene variability of the European Slope Current, NE Atlantic. Palaeogeogr., Palaeoclimatol., Palaeoecol. 633, 111884. https://doi.org/10.1016/j.palaeo.2023.111884.

De Mol, B., Van Rensbergen, P., Pillen, S., Van Herreweghe, K., Van Rooij, D., McDonnell, A., Huvenne, V., Ivanov, M., Swennen, R., Henriet, J.P., 2002. Large deep-water coral banks in the Porcupine Basin, southwest of Ireland. Mar. Geol. 188, 193–231. https://doi.org/10.1016/S0025-3227(02)00281-5.

Dorschel, B., Hebbeln, D., Foubert, A., White, M., Wheeler A.J., 2007. Hydrodynamics and cold-water coral facies distribution related to recent sedimentary processes at Galway Mound west of Ireland. Mar. Geol. 244, 184–195. https://doi.org/10.1016/j.margeo.2007.06.010.

Du, J., Haley, B.A., Mix, A.C., 2020. Evolution of the Global Overturning Circulation since the Last Glacial Maximum based on marine authigenic neodymium isotopes. Quat. Sci. Rev. 241, 106396. https://doi.org/10.1016/j.quascirev.2020.106396.

Friocourt, Y., Levier, B., Speich, S., Blanke, B., Drijfhout, S.S., 2007. A regional numerical ocean model of the circulation in the Bay of Biscay. Journal of Geophysical Research: Oceans 112, C09008. https://doi.org/10.1029/2006jc003935.

Friocourt, Y., Drijfhout, S., Blanke, B., 2008. On the dynamics of the slope current system along the West European Margin. Part I: Analytical calculations and numerical simulations with steady-state forcing. Journal of Physical Oceanography 38, 2597–2618. https:// doi.org/10.1175/2008jpo3744.1.

Garrett, 2003. Internal tides and ocean mixing. Science 301, 1858–1859. https://doi.org/10.1126/science.1090002.

Grant, W.D., Madsen, O.S., 1979. Combined wave and current interaction with a rough bottom. J. Geophys. Res. 84, 1797–1808.

Hebbeln, D., Van Rooij, D., Wienberg, C., 2016. Good neighbours shaped by vigorous currents: Cold-water coral mounds and contourites in the North Atlantic. Mar. Geol. 378, 171–185. https://doi.org/10.1016/j.margeo.2016.01.014.

Hernández-Molina, F.J., Iglesias, J., Van Rooij, D., Ercilla, G., Gomez-Ballesteros, M., Casas, D., Llave, E., 2008. The Le Danois Contourite Depositional System: an exceptional record of the MOW circulation off the North Iberian margin. Geo-Temas 10, 535–538.

Hernández-Molina, F.J., Serra, N., Stow, D.A.V., Llave, E., Ercilla, G., Van Rooij, D., 2011. Along-slope oceanographic processes and sedimentary products around the Iberian margin. Geo-Mar. Lett. 31, 315–341. https://doi.org/10.1007/s00367-011-0242-2.

Huvenne, V.A.I., Van Rooij, D., De Mol, B., Thierens, M., O'Donnell, R., Foubert, A., 2009. Sediment dynamics and palaeo-environmental context at key stages in the Challenger cold-water coral mound formation: Clues from sediment deposits at the mound base. Deep-Sea Res. I Oceanogr. Res. Pap. 56, 2263–2280. https://doi.org/ 10.1016/j.dsr.2009.08.003.

Kano, A., Ferdelman, T.G., Williams, T., Henriet, J.-P., Ishikawa, T., Kawagoe, N., Takashima, C., Kakizaki, Y., Abe, K., Sakai, S., Browning, E.L., Li, X., Integrated Ocean Drilling Program Expedition 307 Scientists, 2007. Age constraints on the origin and growth history of a deep-water coral mound in the northeast Atlantic drilled during Integrated Ocean Drilling Program Expedition 307. Geology 35, 1051–1054. https://doi.org/10.1130/G23917A.1.

Keffer, T., Martinson, D.G., Corliss, B.H., 1988. The position of the Gulf Stream during Quaternary glaciations. Science 241, 440–442. https://doi.org/10.1126/science.241.4864.440.

Khélifi, N., Sarnthein, M., Frank, M., Andersen, N., Garbe-Schönberg, D., 2014. Late Pliocene variations of the Mediterranean outflow. Mar. Geol. 357, 182–194. https://doi.org/10.1016/j.margeo.2014.07.006.

King, E.L., Bøe, R., Bellec, V.K., Rise, L., Skarðhamar, J., Ferré, B., Dolan, M.F.J., 2014. Contour current driven continental slope-situated sandwaves with effects from secondary current processes on the Barents Sea margin offshore Norway. Mar. Geol., 353, 108–127. https://doi.org/10.1016/j.margeo.2014.04.003.

Lisiecki, L.E., Raymo, M.E., 2005. A Pliocene-Pleistocene stack of 57 globally distributed benthic delta O-18 records. Paleoceanography 20, PA1003. https://doi.org/10.1029/2004PA001071.

Löfverström, M., Caballero, R., Nilsson, J., Kleman, J., 2014. Evolution of the large-scale atmospheric circulation in response to changing ice sheets over the last glacial cycle. Clim. Past 10, 1453–1471. https://doi.org/10.5194/cp-10-1453-2014.

Masson, D. G., Howe, J.A. and Stoker, M.S. (2002) Bottom-current sediment waves, sediment drifts and contourites in the northern Rockall Trough. Mar. Geol. 192, 215–237. https://doi.org/10.1016/S0025-3227(02)00556-X.

Marsh, R., Haigh, I. D., Cunningham, S. A., Inall, M. E., Porter, M., Moat, B.I., 2017. Large-scale forcing of the European Slope Current and associated inflows to the North Sea. Ocean Science 13, 315–335. https://doi.org/10.5194/os-13-315-2017.

Mellor, G., 2004. Users guide for a three-dimensional, primitive equation, numerical ocean model. Technical Report, Princeton University.

Migeon, S., Savoye, B., Faugeres, J.-C., 2000. Quaternary development of migrating sediment waves in the Var deep-sea fan: distribution, growth pattern, and implication for levee evolution. Sediment. Geol. 133, 265–293. https://doi.org/10.1016/S0037-0738(00)00043-9.

Mix, A. C., Bard, E., and Schneider, R., 2001. Environmental processes of the ice age: land, oceans, glaciers (EPILOG). Quaternary Sci. Rev. 20, 627–657, https://doi.org/10.1016/S0277-3791(00)00145-1, 2001.

Nicholson, U., Stow, D. A. V., Brackenridge, R. E., Miramontes, E., Wåhlin, A. (2024). Introduction: Special issue on bottom currents and contourites: Processes, products and impact. Mar. Geol., 469, Article 107237. https://doi.org/10.1016/j.margeo.2024.107237.

Pearson, I., Jenkins, D.G., 1986. Unconformities in the Cenozoic of the North-East Atlantic. In: Summerhayes, C.P., Shackleton, N.J. (Eds.), North Atlantic Palaeoceanography. Geol. Soc. London Spec. Publ., pp. 79–86.

Pingree, R.D., Le Cann, B., 1990. Structure, strength and seasonality of the slope currents in the Bay of Biscay region. J. Mar. Biol. Assoc. U.K. 70, 857–885. https://doi.org/10.1017/S0025315400059117.

Pöppelmeier, F., Blaser, P., Gutjahr, M., Jaccard, S.L., Frank, M., Max, L., Lippold, J., 2020. Northern-sourced water dominated the Atlantic Ocean during the Last Glacial Maximum. Geology 48, 826–829. https://doi.org/10.1130/g47628.1.

Raddatz, J., Rüggeberg, A., Margreth, S., Dullo, W.-C., 2011. Paleoenvironmental reconstruction of Challenger Mound initiation in the Porcupine Seabight, NE Atlantic. Mar. Geol. 282, 79–90. https://doi.org/10.1016/j.margeo.2010.10.019.

Rebesco, M., Hernandez-Molina, F.J., Van Rooij, D., Wåhlin, A., 2014. Contourites and associated sediments controlled by deep-water circulation processes: State-of-the-art and future considerations. Mar. Geol. 352, 111–154. https://doi.org/10.1016/j.margeo.2014.03.011.

Rhines, P.B., 1970. Edge-, bottom- and Rossby waves. Geophys. Fluid Dyn., 1, 273–302.

Ribó, M., Puig, P., Munoz, A., Lo Iacono, C., Masqué, P., Palanques, A.L, Acosta, J., Guillén, J. and Gómez Ballesteros, M., 2016. Morphobathymetric analysis of the large fine-grained sediment waves over the Gulf of Valencia continental slope (NW Mediterranean). Geomorphology, 253, 22–37. https://doi.org/10.1016/j.geomorph.2015.09.027.

Rice, A.L., Billett, D.S.M., Thurston, M.H., Lampitt, R.S., 1991. The institute of oceanographic sciences biology programme in the Porcupine Seabight: background and general introduction. J. Mar. Biol. Assoc. U. K. 71, 281–310. https://doi.org/10.1017/S0025315400051614.

Rogerson, M., Rohling, E.J., Weaver, P.P.E., 2006. Promotion of meridional overturning by Mediterranean-derived salt during the last deglaciation. Paleoceanography 21, PA4101. https://doi.org/doi:10.1029/2006PA001306.

Rogerson, M., Rohling, E.J., Bigg, G.R., Ramirez J., 2012. Paleoceanography of the Atlantic-Mediterranean exchange: Overview and first quantitative assessment of climatic forcing. Rev. Geophys. 50. https://doi.org/10.1029/2011rg000376.

Stow, D.A.V., 1982. Bottom currents and contourites in the North Atlantic. Bull. Inst. Geol. Bassin Aquitaine 31, 151–166.

Stow, D. A. V., Hernandez-Molina, F.J., Llave, E., Sayago-Gil, M., Diaz del Rio, V., Branson, A., 2009. Bedform-velocity matrix: The estimation of bottom current velocity from bedform observations. Geology 37, 327–330. https://doi.org/10.1130/G25259A.1.

Toucanne, S., Soulet, G., Riveiros, N.V., Boswell, S.M., Dennielou, B., Waelbroeck, C., Bayon, G., Mojtahid, M., Bosq, M., Sabine, M., Zaragosi, S., Bourillet, J.-F., Mercier, H., 2021. The North Atlantic Glacial Eastern boundary current as a key driver for ice-sheet-amoc

interactions and climate instability. Paleoceanogr. Paleoclimatol. 36. https://doi.org/10.1029/2020PA004068.

Van Rooij, D., De Mol, B., Huvenne, V., Ivanov, M., Henriet, J.-P., 2003. Seismic evidence of current-controlled sedimentation in the Belgica mound province, upper Porcupine slope, southwest of Ireland. Mar. Geol. 195, 31–53. https://doi.org/10.1016/S00253227(02)00681-3.

Van Rooij, D., Blamart, D., Kozachenko, M., Henriet, J.-P., 2007. Small mounded contourite drifts associated with deep-water coral banks, Porcupine Seabight, NE Atlantic Ocean. Geol. Soc. Lond. Spec. Publ. 276, 225–244. https://doi.org/ 10.1144/GSL.SP.2007.276.01.11.

Van Rooij, D., Huvenne, V.A.I., Blamart, D., Henriet, J.-P., Wheeler, A., de Haas, H., 2009. The Enya mounds: a lost mound-drift competition. Int. J. Earth Sci. 98, 849–863. https://doi.org/10.1007/s00531-007-0293-9.

Van Rooij, D., Iglesia, J., Hernández-Molina, F.J., Ercilla, G., Gomez-Ballesteros, M., Casas, D., Llave, E., De Hauwere, A., Garcia-Gil, S., Acosta, J., Henriet, J.-P., 2010. The Le Danois Contourite Depositional System: Interactions between the Mediterranean Outflow Water and the upper Cantabrian slope (North Iberian margin). Marine Geology 274, 1–20. https://doi.org/10.1016/j.margeo.2010.03.001.

Van Rooij, D., Campbell, C., Rueggeberg, A., Whalin, A., 2016. The Contourite Log-Book: significance for Palaeoceanography, Ecosystems and Slope Instability. Mar. Geol. 378, 1–4. https://doi.org/10.1016/j.margeo.2016.05.018.

Verweirder, L., Van Rooij, D., White, M., Van Landeghem, K., Bossée, K, Georgiopoulou, A. 2021. Combined control of bottom and turbidity currents on the origin and evolution of channel systems, examples from the Porcupine Seabight. Mar. Geol. 442, 106639. https://doi.org/10.1016/j.margeo.2021.106639.

Verweirder, L., Van Rooij, D., Georgiopoulou, A., 2023. Margin processes sculpting a land-detached canyon-channel system: the Gollum Channel System in the Porcupine Seabight. Front. Earth. Sci. 11. https://doi.org/10.3389/feart.2023.1285171.

Vettoretti, G., Peltier, W.R., 2013. Last Glacial Maximum ice sheet impacts on North Atlantic climate variability: The importance of the sea ice lid. Geophys. Res. Lett. 40, 6378–6383. https://doi.org/10.1002/2013gl058486.

Weber, S.L., Drijfhout, S.S., Abe-Ouchi, A., Crucifix, M., Eby, M., Ganopolski, A., Murakami, S., Otto-Bliesner, B., Peltier, W.R., 2007. The modern and glacial overturning circulation in the Atlantic Ocean in PMIP coupled model simulations. Clim. Past 3, 51–64. https://doi.org/10.5194/cp-3-51-2007.

White, M., 2007. Benthic dynamics at the carbonate mound regions of the Porcupine Sea Bight continental margin. Int. J. Earth Sci. 96, 1–9. https://doi.org/10.1007/ s00531-006-0099-1.

White, M., Roberts, J.M., van Weering, T., 2007. Do bottom-intensified diurnal tidal currents shape the alignment of carbonate mounds in the NE Atlantic?. Geo-Mar. Lett. 27, 391–397. https://doi.org/10.1007/s00367-007-0060-8.

White, M., Dorschel, B., 2010. The importance of the permanent thermocline to the cold water coral carbonate mound distribution in the NE Atlantic. Earth Planet. Sci. Lett. 296, 395–402. https://doi.org/10.1016/j.epsl.2010.05.025.

Wilckens, H., Schwenk, T., Lüdmann, T., Betzler, C., Zhang, W., Chen, J., Hernández-Molina, F.J., Lefebvre, A., Cattaneo, A., Spieß, V., Miramontes, E., 2023a. Factors controlling the morphology and internal sediment architecture of moats and their associated contourite drifts. Sedimentology 70, 1472–1495. https://doi.org/10.1111/sed.13093.

Wilckens, H., Eggenhuisen, J.T., Adema, P.H., Hernández-Molina, F.J., Silva Jacinto, R., Miramontes, E. 2023b. Secondary flow in contour currents controls the formation of moat-drift contourite systems. Commun. Earth Environ. 4, 316. https://doi.org/10.1038/s43247-023-00978-0.

Wu, L., Zhao, Y., Liu, Z., Ma, P., Zhang, Y., 2023. Sedimentary processes in the bottom boundary layer of a contourite drift in the northern South China Sea. Front. Mar. Sci. 10. https://doi.org/10.3389/fmars.2023.1217216.

Yin, S.R., Hernández-Molina, F.J., Mejías, M.B., Zhao, Y., Manley, T., Manley, P.L., Li, J., 2024. Bottom Ekman transport drives transverse flows to shape contourite moat and drift systems. Earth Planet. Sci. Lett. 643, 118926. https://doi.org/10.1016/j.epsl.2024.118926.

Zhang, W., Hanebuth, T.J.J., Stöber, U., 2016. Short-term sediment dynamics on a meso-scale contourite drift (off NW Iberia). Mar. Geol. 378, 81–100. https://doi.org/10.1016/j.margeo.2015.12.006.